UNIVERSITY
OF TASMANIA

Milky Way Halo Objects, IC 4499 and the Large Magellanic Cloud

Warren Hankey

Submitted in total fulfilment of the requirements
of the degree of Doctor of Philosophy

October 24, 2014

School of Physics
The University of Tasmania

The work described in this thesis is that of the candidate alone, except where otherwise acknowledged in the text. The observations of IC 4499 at the AAT were carried out by my supervisor Dr. Andrew A. Cole but the candidate was responsible for the reduction process and all subsequent analysis. The IC 4499 material in this thesis was published in the *Monthly Notices of the Royal Astronomical Society*, volume 411, pages 1536 to 1546, March 2011, with the candidate as first author and with Dr. Cole as co-author contributing part of the discussion. MNRAS hold the copyright for that content, and access to the material should be sought from the journal. The remaining non published content of the thesis may be made available for loan and limited copying and communication in accordance with the Copyright Act 1968. The Monte Carlo Markov Chain program to estimate the velocity dispersion and mass in IC 4499 was scripted in *R* by Dr. Simon Wotherspoon. The candidate substantially adapted the code and methodology to the larger problem of estimation of LMC rotation model parameters. LMC target selection, field plate setup, sky-fibre, and guide star placement were all carried out by the candidate, Dr. Cole travelled to the AAT to assist with the final LMC observations. Reduction and analysis of the LMC data is that of the candidate alone. Dr. Cole performed a calibration check of the LMC metallicity results and Appendix D is entirely his work. Thanks to Dr. Cole for encouragement, discussions and assistance. Observations at the Mount Pleasant radio telescope supporting the JAXA Selene Moon mission resulted in a co-author credit in *Radio Science*, volume 45, number 2, April 2010. Travel support for observing was provided by the Anglo-Australian Observatory (AAO). The AAO was funded by the British and Australian governments. Thanks to AAT support astronomer Dr. Rob Sharp and night assistant Winston Campbell for their assistance during the observing run.

Warren Hankey

Abstract

Two Galactic halo objects are studied spectroscopically, the far-Southern Galactic globular cluster IC 4499 and the Large Magellanic Cloud. Radial velocity and metallicity measurements from the near-infrared calcium triplet obtained with the AAOmega spectrograph are analysed and discussed in the context of Milky Way and halo evolution.

Several hundred red giant stars were observed in and around IC 4499. 43 targets were identified as cluster members based on velocity and abundance, by far the largest spectroscopic sample of IC 4499 giants ever studied. The mean heliocentric radial velocity of the cluster was determined to be $31.5 \pm 0.4\,\mathrm{km\,s^{-1}}$, and the most likely central velocity dispersion found to be $2.5 \pm 0.5\,\mathrm{km\,s^{-1}}$. This gave a dynamical mass estimate for the cluster of $93 \pm 37 \times 10^3\,M_\odot$. No evidence for cluster rotation was seen down to a sensitivity amplitude of $\approx$1 $\mathrm{km\,s^{-1}}$. The cluster metallicity was found to be [Fe/H] $= -1.52\ \pm 0.12$ on the Carretta-Gratton scale; this is in agreement with some earlier estimates but carries significantly higher precision. The radial velocity of the cluster, previously highly uncertain, is consistent with membership in the Monoceros tidal stream but also with a halo origin. The horizontal branch morphology of the cluster is slightly redder than average for its metallicity, but it is not unusually young compared to other clusters of the halo.

Radial velocities were obtained for 585 giant stars in the Large Magellanic Cloud central bar region, the most extensive, high quality spectroscopic sample to date of late-type stars in the crowded central galaxy. Metallicity has also been estimated for 240 stars. The data were calibrated by contemporary radial velocity results from the same instrument. The velocity sample is Gaussian distributed about $259\,\mathrm{km\,s^{-1}}$ with a dispersion of $24\,\mathrm{km\,s^{-1}}$. A systemic velocity for the LMC of $255 \pm 5\,\mathrm{km\,s^{-1}}$ is estimated which is lower than previous estimates. Disk plane velocities are consistent with a rotating disk galaxy. Monte Carlo simulations are made of parameters for a disk rotation model having a maximum velocity of $79 \pm 18\,\mathrm{km\,s^{-1}}$ before asymmetric drift correction. A mean metallicity of [Fe/H] = -0.36 dex and a metallicity distribution function were found consistent with previous estimates, confirming the bar is slightly more metal-rich than the disk. The bar stars are rotating with the disk making the bar kinematically indistinguishable from the disk galaxy. No evidence is found for streaming motions along the bar nor a counter-rotating population. The bar is not an unexpected feature in a thick disk with instability induced by tidal interaction with the Small Magellanic Cloud.

Contents

List of Figures

List of Tables

Some velvet morning when I'm straight
I'm gonna open up your gate
And maybe tell you 'bout Phaedra
And how she gave me life
And how she made it in

Lee Hazlewood (1929-2007)

1 Constructing Galaxies

1.1 Laying Foundations

The problem of galaxy construction is one of the most important challenges facing astronomy. The modern paradigm of hierarchical structure formation around dark matter (DM) needs to be reconciled with observations. While simulations of a DM dominated universe recreate large scale structure very well, they fail to reproduce structure on galactic scales, the so-called "missing satellites" problem (Klypin et al. 1999; Moore et al. 1999). Clues to the formation of the Galaxy are to be found in the stellar populations of Milky Way (MW) halo objects.

Stellar populations retain chemical traces and dynamical imprints of their formation environment. Detailed views of stellar populations are only possible in the MW and nearby Local Group (LG). The oldest stars in the MW halo are early universe fossils whose age is equivalent to the look back time of the furthest visible galactic objects. Near-infrared calcium triplet spectroscopy of red giant branch (RGB) stars allows detailed kinematic and abundance measurements of these distant stellar populations. They represent a detailed local archaeological record of the evolution of the Galaxy.

The easily observable MW and halo objects naturally inform our understanding of the cosmos. This study of the halo objects globular cluster (GC) IC 4499 and the Large Magellanic Cloud (LMC) galaxy, observes locations of structure building at scales where DM simulations fail. Universal galactic structural evolution in the context of a Λ cold dark matter (ΛCDM) cosmology can be illuminated by observing the interactions between satellites and their host MW Galaxy. In this thesis stellar populations within these halo objects were searched for dynamical and chemical clues to the construction of the MW Galaxy and halo.

Interactions between galaxies affect their structural evolution over much shorter time scales than the age of the universe. Gravity is the force that creates structure and order from scattered elements on galactic scales, even as entropy increases. Tiny quantum fluctuations in the Big Bang, seen as minute temperature variations in the cosmic microwave background, rapidly inflated to homogeneously fill all of space-time with the seeds of galaxies (Bennett et al.

2013). The gravity of DM appears necessary to fill these seeds with baryonic matter and sustain galactic structure.

Ancient halo GCs with homogenous populations were created in conditions that existed at the birth of the Galaxy. Along with the halo dwarf galaxies they show structural evolution and devolution by accretion at a variety of scales. This evolution of smaller objects has occurred within the sphere of influence of the massive MW. IC 4499 was an understudied member of the halo GC population, whose odd characteristics promised new insights into halo history.

The Magellanic system is a disk galaxy with a substantial dwarf satellite and attendant globular clusters, almost a scale model of the MW, but with important differences, such as the lack of a halo and bulge. The LMC is in a state of disturbance with hierarchical structure formation occurring through accretion, as well as star formation driven by close range interactions with the Small Magellanic Cloud (SMC) or MW. In this thesis stellar velocity information from spectroscopy was used to analyse the internal dynamics of two MW halo objects, IC 4499 and the LMC. Internal effects on stellar tracers give clues to the larger scale causal interactions. Spectroscopic metallicity reveals ages and evolutionary patterns in halo objects. Implications for LG dynamic evolution and structural feedback were examined in light of our findings.

ΛCDM models have successfully described the structure of the large scale universe, but fail on the galaxy and dwarf galaxy scale (Klypin et al. 1999; Moore et al. 1999; Klypin et al. 2002; Moore et al. 2006). Disk galaxies need smooth gas flows to form and the excess of small structures predicted by ΛCDM tend to disrupt the smooth conditions (Moore et al. 1999). In fact the excess of small structure is not observed (Klypin et al. 1999; Boylan-Kolchin et al. 2010). The study of halo objects can address cosmological questions of structural evolution at the galactic scale.

The outer regions of the MW and the halo are where kinematic traces of accretion and remnants of hierarchical structure formation are easier to find (Johnston et al. 1996; Helmi 2008). In the Galactic bulge for example, time would have erased most evidence where the dynamical timescales are short. Velocity dispersion in Baade's window is $\sim 120\,\mathrm{km\,s^{-1}}$ (Morrison and Harding 1993). The outer MW potential is where evidence of ancient structures can still be observed. Multi-object Ca II spectroscopy can provide large samples of stellar tracers in these populations. In this study statistical techniques applied to observed samples allowed estimation of global parameters for IC 4499 and the LMC galaxy.

1.2 Building Blocks in a ΛCDM Universe

Early authors surmised that the the galaxy simply collapsed quickly ($\leq 1\,\mathrm{Gyr}$) from a single proto-cloud of primeval material in a top-down formation scenario (Eggen et al. 1962) . The inner halo condensed before the outer halo and should show a metallicity gradient, rich to poor, from the inside out. Later studies revealed there was no abundance gradient in the outer halo like that seen in the

inner MW disk (Searle and Zinn 1978). The complicated nature of kinematics and abundances in the Galactic halo pointed to a more convoluted formation history involving accretion (Freeman and Bland-Hawthorn 2002). The concept arose of the construction of the galaxy from a variety of objects and sources, the bottom-up formation of the Searle-Zinn paradigm.

There are problems with the hierarchical formation theory. Only a fraction of the Galactic halo can be attributed to fragments (Geisler et al. 2007). There remains a general uniformity of age, dynamics and abundance amongst an old halo population which contrasts with a younger halo population (Mackey and van den Bergh 2005). The old halo objects also display the Oosterhoff dichotomy in RR Lyrae periodicity, whereas the dwarf population, the LMC and young halo do not (Catelan 2009a). This indicates that not all the halo is accreted from fragments, as the old halo seems to share some kind of common heritage. Many young halo GCs are associated with accretion sites (Mackey and van den Bergh 2005) If age is the second parameter of horizontal branch (HB) morphology, then an age gradient is evident from the halo down to the central bulge (Lee 1992).

We propose that the formation of the Galaxy may well be described jointly by both the top-down and bottom-up paradigms. Some of the Galaxy followed the Eggen et al. (1962) top-down scenario becoming the bottom layer for a complex and evolving hierarchical accretion process. A relatively rapid homogenous collapse of a proto-cloud or collision of proto-clouds formed the bulge at the same time as the old halo including the GCs. This structure was to be later supplemented by a long accretion and amalgamation process of the satellite dwarf galaxy substructure.

The hierarchical bottom-up structure building process can be observed continuing now at $z = 0$ in the LG. The Magellanic clouds are interacting with themselves, driving tidal star formation and accretion processes (Harris and Zaritsky 2009). In addition the MW itself is somehow affecting the LMC-SMC as they in turn are accreted onto an even larger structure (Weinberg 1995, 2000). Many other dwarf galaxy objects are only just now accreting on the MW, others have long since been disrupted beyond recognition, leaving streams of stars wrapped around the MW disk (Morrison et al. 2000).

Detailed metallicity analysis of α-elements show the Sagittarius (Sgr) dwarf and other dwarfs along with the LMC and SMC form a group distinct from the MW halo (Chou et al. 2009). They exhibit a range of metallicities showing a history of slow star formation throughout their history and early enrichment . None of the satellites share a common star formation history (SFH) (Mateo 1998; Geisler et al. 2007), which shows that there was no homogenous single galactic formation event for these objects. Their uniqueness suggests the satellites formed in isolation from the more homogenous metal-poor MW old halo objects such as the globular clusters (McConnachie 2012). The dwarf galaxies show complex, unique and on-going sporadic star formation histories, indicating once again that the MW halo is in a constant state of interaction, accretion and disruption.

Unlike other dwarf galaxies in the MW halo, the LMC at about $10^{10} M_{\odot}$

(Besla et al. 2010; van der Marel et al. 2002), it is a substantial fraction, near 1%, of the MW mass. It represents a category midway between dwarf galaxies and large spirals. There is active star formation in the LMC, more so than other dwarf satellite galaxies in the MW halo (Harris and Zaritsky 2009). The LMC appears more metal rich than the rest of the MW halo and probably formed in isolation from the MW. Modern proper motion studies suggest the LMC-SMC have only recently interacted with the MW, perhaps on their first orbit of the MW (Besla et al. 2011).

The number of large LMC type satellites observed around MW L_* type galaxies agree with simulations of galaxy formation based on ΛCDM models of the universe (Tollerud et al. 2011; Robotham et al. 2012) While Magellanic-type satellites are commonly observed, the LMC is bluer than most satellite galaxies which tend to be redder for their luminosity (Tollerud et al. 2011).. This may indicate that the LMC is just beginning to interact with the MW, triggering current star formation, while halo quenching of star formation has not yet occurred.

Simulations of formation in a ΛCDM universe show many more DM sub-haloes around the central DM galaxy potential than are observed and amount to 5-10% of the virial mass of the central potential (Macciò et al. 2006). This is referred to as the missing satellites problem (Klypin et al. 1999). ΛCDM simulations appear to mimic sub-structure of galaxy clusters, but fail at the galactic level. Re-ionisation in the early universe stopping condensation of baryons in the DM sub-haloes has been proposed as a method of suppressing the formation of satellite galaxies (Macciò et al. 2006; Moore et al. 2006).

The LMC formed a little later than the earliest objects and didn't experience the re-ionisation suppression. The lack of a LMC halo is an analogue of the MW missing satellite problem. If there were LMC sub-haloes they too would have been suppressed and if any did survive they have been accreted. The number of satellites looks to be a function of host mass size which rapidly goes towards zero for a LMC size galaxy, as there may be cut-off mass for baryon accretion in DM sub-haloes (Klypin et al. 1999).

Old stars in the halo contain a fossil record of accretion processes in the MW halo and at least 10% are remnants of a satellite population that has been accreted (Starkenburg et al. 2009). The Sgr dwarf spheroidal (dSph) galaxy is the best demonstrated example of accretion by the MW of a satellite (Ibata et al. 1994). High resolution spectroscopy has been able to identify the disparate elements of the accretion process. M54, Terzan 7, Terzan 8 and Arp 2 have been identified as members of the remnant tidal stream by chemical tagging (Da Costa and Armandroff 1995). Other GC Sgr stream candidates include Whiting 1 (Carraro et al. 2007) and Palomar 12 (Cohen 2004).

The dSph/dwarf elliptical (dE) MW satellite galaxies exhibit a substantial mass to light ratio showing that they do form within DM sub-haloes (Mateo 1998; Baumgardt and Mieske 2008). The survival to the present of the Sgr dSph within the tides of the MW depends upon its DM to keep its stars (Ibata et al. 1997; Ibata and Razoumov 1998). The old GC population by contrast have no appreciable DM component, Moore (1996) put an upper limit on the

mass to light ration of 2.5. The inner DM clumps have probably now been accreted on to the MW and only the outer sub-haloes remain.

The stream from the Sgr galaxy has been confirmed by several studies (Vivas et al. 2001; Newberg et al. 2002; Da Costa and Armandroff 1995). But the Sgr dSph is probably not the only accreted object. Many satellites are expected to have coplanar obits with the MW disk and be accreted as ring like structures in the outer disk (Helmi et al. 2003). Their location makes them hard to detect.

The Monoceros tidal stream, or the Galactic anti-centre stellar structure (GASS) was first detected in the Sloan Digital Sky Survey (SDSS) (Yanny et al. 2000). This stream of stars with metallicites distinct from the metal-poor halo population is also thought to be the remnant of a dwarf galaxy, but its progenitor has not been identified. The Sextans dwarf and the cluster Pal 5 are in the right locations to be associated with the stream. Another possible Monoceros stream candidate is the Canis Major dwarf irregular (dIrr) (Peñarrubia et al. 2005). Our location in the MW disk makes it difficult to observe circum-planar accretion structure like the Monoceros tidal stream.

The discovery of SMC stars in the bridge and LMC disk (Nidever et al. 2011; Olsen et al. 2011) show that the SMC is being accreted onto the LMC. The LMC-SMC system is a case study of accretion processes that can inform our knowledge of the MW accretion of satellites.

Understanding of the formation and evolution of the Galaxy will require the chemical tagging of individual stellar populations (Freeman and Bland-Hawthorn 2002). The tagging will allow identification of the progenitor structures that gave rise to these scattered remnants in the disk and halo. This is the grand project of Galactic archeology towards which this study contributes. This study considered the role of the GC IC 4499 in the context of accretion structures in the MW halo. Accretion processes within the Magellanic system, as well as the global interactions of the system within the MW halo are constrained by the chemical and dynamical evidence from observations.

1.3 The Magellanic System

The LMC is about one hundredth the size of the MW and is the fourth largest object in the LG after the M31, MW, and M33 galaxies. It is the largest object in the MW halo. Originally classified as an irregular galaxy, subtle spiral structure became apparent in the 1960's with two spiral arms seen most clearly in HI maps of the galaxy (McGee and Milton 1966; Hindman 1967). Irregular and patchy regions seen in HII images correspond strongly to extreme Population I star formation. The most striking example is the 30 Doradus complex of newly formed stars, supernova shells and star forming gas clouds, the Tarantula nebula. The most obvious visible feature of the galaxy is the strong stellar bar, which does not appear in H1 images.

Spiral galaxies are often classified according to the Hubble tuning fork diagram. Normal spirals are arranged as Sa, Sb, Sc...Sm in order of decreasingly tight spiral arms, (higher arm pitch angles), and smaller central bulges (Hubble

1927; van den Bergh 1998). The other tine of the tuning fork is the barred spiral galaxies SBa, SBb, SBc...SBm, ordered in the same sense as the spirals but with the addition of a bar feature. Sometimes a third, intermediate, tine is invoked for weaker bars, S(B)a, S(B)b, S(B)c...S(B)m.

The classification of the LMC by various authors has been varied with some early authors classifying it as irregular, Im. The LMC was classified by de Vaucouleurs and Freeman (1972) as an SB(s)m, spiral barred, with loose arms and weak or no bulge, with the (s) denoting the bar and spiral arms emerge from the centre of the galaxy, rather than an SB(r)m where the bar and arms emerge from an annulus around the centre. The SMC is classified similarly but is SB(s)m *peculiar*. The Magellanic cloud then represents an intermediate type galaxy between grand design spiral disks and the irregulars. Representing a natural progression of spiral types it is not necessary to invoke MW interaction to explain its morphology.

The integrated colours of galaxies reveal the stellar populations within the galaxy. There does not appear to be any colour difference between spiral and barred spiral galaxies (de Vaucouleurs 1961). This indicates the nature of the bar is dynamical; the similar stellar populations implied by colour in both spiral types mean the bar features are not based on primordial abundance nor on age.

It is less than 100 years since nearby LG galaxies were shown to lie outside the MW (Hubble 1929). The LG contains two massive $\sim 10^{12} M_{\odot}$ disk galaxies, the MW (MW) and M31, the Great Andromeda Nebula, each at the centre of a subgroup of the LG. The total LG is a collection of at least 35 galaxies of different types (Grebel 2001; Mateo 1998; van den Bergh 1999) and as many as 100 within 3 Mpc most of which are associated to some degree, (McConnachie 2012). Two thirds of the LG galaxies are found within 600 kpc of the two subgroups (Grebel 2001). These two subgroups are remarkably similar in scale and scope each with two substantial disk galaxies, and a similar number of dwarf satellites. In the MW subgroup the LMC is the most massive satellite at $\sim 10^{10} M_{\odot}$, in the Andromeda subgroup the satellite galaxy M33, Triangulum is also of the same order $\sim 10^{10} M_{\odot}$. The SMC is a dwarf irregular (dIrr), the remaining galaxies in the MW subgroup are dIrr or dwarf spheroidal/elliptical dSph/d/E.

The Magellanic system comprises the SMC and the LMC along with HI features associated with the two galaxies, the Magellanic Bridge, the leading arm and the remarkable 150° long Magellanic stream (MgS). First discovered at the Parkes radio telescope Mathewson et al. (1974) the HI features showed the unified nature of the Magellanic system. The disturbed nature of the system means we are witness to a local Galactic group scale hierarchical structure formation event. In addition the system is at such proximity that we are able to observe individual stars as detailed tracers of Galactic scale interactions.

The very first studies with the new science of radio astronomy in the 1950-60's revealed the connected nature of the Magellanic system. The LMC and SMC were clearly embedded in HI envelopes much larger than the stellar system (Kerr et al. 1954; McGee and Milton 1966). Figure 1.1 shows an early map made with the Australian 36 foot Potts Hill radio telescope of the 21cm HI emission

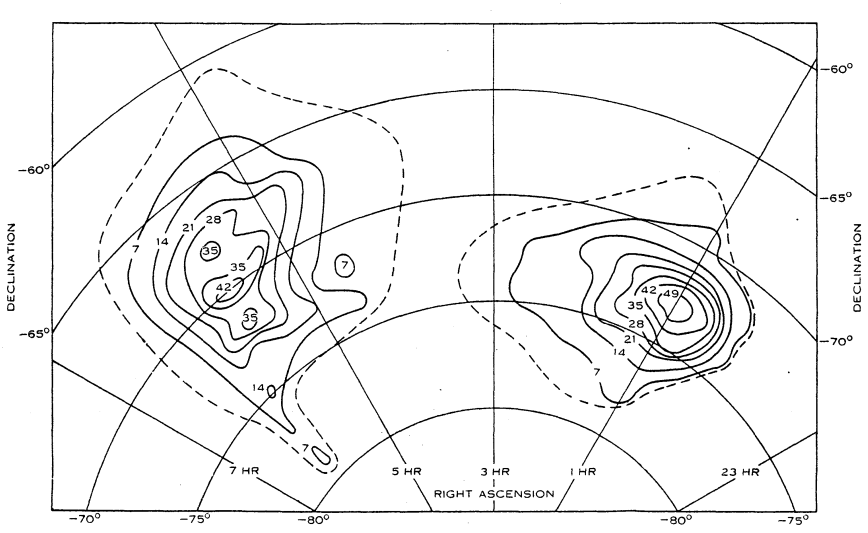

Figure 1.1: Figure 1 from Kerr et al. (1954) showing the integrated 21cm emission at low resolution of about 1°.0

line around the clouds. The narrow line emission allowed velocity information to be explored. The map is of the integrated flux from the different velocity components along the line of sight. A major finding was that the HI distribution is offset from the stellar light distribution by as much as 1°.2 (Marel and Cioni 2001), a phenomena confirmed by subsequent studies, (e.g. Kim et al. 1998; Staveley-Smith et al. 2003). The first hint of galactic rotation is also noted by the authors. However as shown by later studies, and in this thesis, they are detecting the projection of the proper motion into the radial line of sight. The transverse proper motion effect dwarfs the actual rotation signature of the LMC galaxy.

The MgS feature was first observed by Mathewson et al. (1974) and is shown in Figure 1.2. The 150° MgS feature runs from the clouds, passes through the south galactic pole and crosses the plane of the MW, over 150 kpc. Unlike the many streams associated with dwarf galaxy accretion on to the MW, the MgS feature is only seen in HI with no conclusive stellar counterpart yet discovered. Most models in the literature have emphasised the role of the MW in creating the stream (Gardiner and Noguchi 1996).

The existence of a bridge was first proposed by de Vaucouleurs (1954) from observations of star counts between the clouds. Unlike the bridge the MgS has no stellar counterpart. The peculiar negative velocity $V_{GSR} \approx$ -216 km s^{-1} at the tip of the MgS at $l = 90°$, $b = -30°$ was attributed originally to hydrodynamic pressure braking the gas (Mathewson et al. 1974). The implication was that there must exist an intergalactic medium density at least 2×10^{-4} atom cm^{-3} (Oort 1970) to cause this effect. The leading arm structure however is not

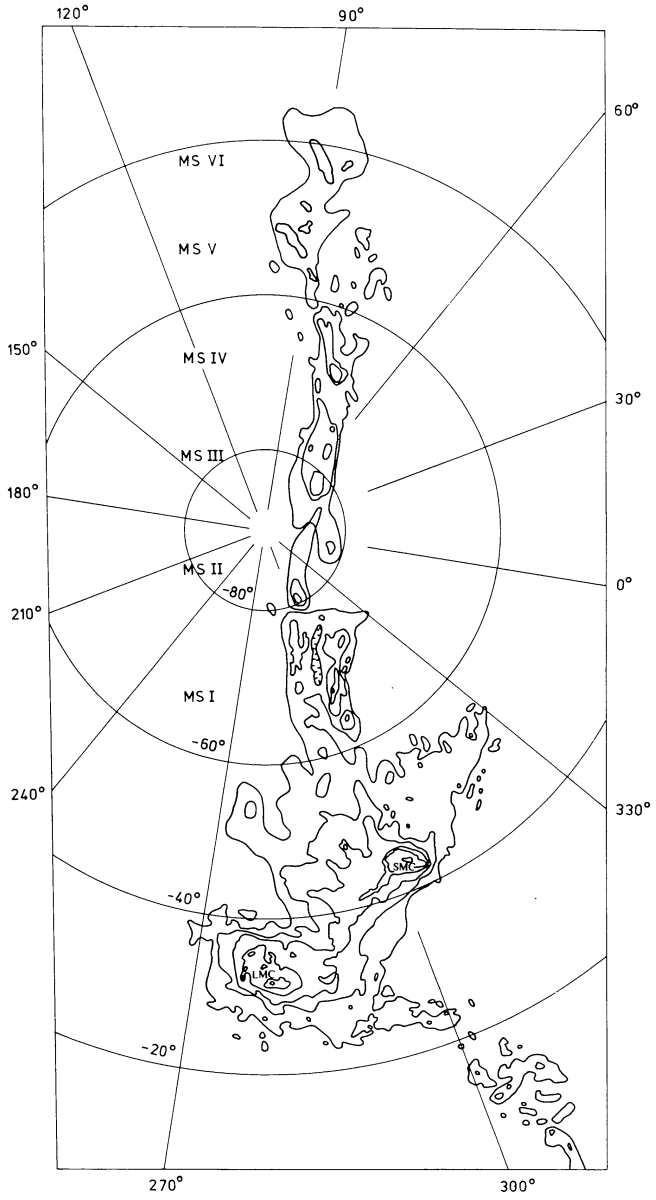

Figure 1.2: Figure 1 from Mathewson and Ford (1984) at higher resolution, 15′, meta-image of several Parkes studies of the Magellanic system. The integrated nature of the two galaxies within the HI envelope and the vast extent of the stream is illustrated.

explained by a gas braking model. Leading arm features suggest a tidal origin such as the leading feature in the Sgr tidal stream (Majewski et al. 2003).

The extent of the HI envelope was later revealed by the much larger Parkes radio telescope. Figure 1.2 shows the result of twenty years worth of studies at the Parkes radio telescope, (McGee and Milton 1966; Hindman 1967; Mathewson et al. 1979; Mathewson and Ford 1984). A similar map from the latest large scale Parkes survey with the multi-beam receiver, the HI Parkes All-Sky Survey (HIPASS) (Putman et al. 2003) is shown in Figure 1.3. With higher sensitivity, the spatial resolution is still defined by the 64 metre aperture at 21cm of $15'$ with a velocity resolution of $26\,\mathrm{km\,s^{-1}}$.

The MgS in particular illustrates most clearly the extremely disturbed nature of the common HI envelope of the Magellanic system. The stream at first appears to be indicative of ram pressure of the MW halo medium on the HI envelope, (Mathewson and Schwarz 1976). But later studies seem to indicate that the density in the halo is insufficient to create the required pressure (Murali 2000). Mastropietro et al. (2005) ran an hydrodynamic simulation of several orbits of the LMC through the halo which not only produced the observed MgS feature, but also a stellar halo, which is not observed. The interaction of the LMC-SMC system can alone create the MgS phenomenon through tidal mechanisms, (Besla et al. 2010; Diaz and Bekki 2011). If this is the case then there is no need for multiple orbits through through the MW halo to explain the morphologies.

Spatially separate but near the stream are a population of high velocity clouds detected in HIPASS. They are at a similar velocity to the nearby stream at around $-200\,\mathrm{km\,s^{-1}}$ Galactocentric radial velocity, with a very low dispersion of $45\,\mathrm{km\,s^{-1}}$ indicating a common origin (Westmeier and Koribalski 2008). It is proposed they are filamentary remnants of a once larger stream. The clouds may correspond to the kind of tail feature seen in numerical simulations of the Magellanic system Gardiner and Noguchi (1996).

Hertzsprung (1920) first noted the LMC and SMC were co-moving and the extent to which proper motion would affect the projected radial velocity component of LMC disk plane circular velocities. With only 18 planetary nebula velocities he estimates a proper motion component perpendicular to the line of sight of $560\,\mathrm{km\,s^{-1}}$ to $600\,\mathrm{km\,s^{-1}}$. This estimate is higher than contemporary HST proper motion estimates, but correctly presages the large modern value $476\,\mathrm{km\,s^{-1}}$ Piatek et al. (2008). Wilson (1944) also estimated $471\,\mathrm{km\,s^{-1}}$ to $649\,\mathrm{km\,s^{-1}}$, and both these values seemed odd at the time given the velocity dispersion of the MW sub-group. In hindsight these early studies pointed toward the modern view of the Magellanic Clouds as interlopers into the Galactic halo with velocities too large to be gravitationally bound to the MW. While subsequent studies have taken the projection effects into account, it is only recently that the magnitude of the proper motion has been appreciated (Kallivayalil et al. 2006; Piatek et al. 2008; Vieira et al. 2010).

Models that assumed many MW orbits of the Magellanic system still found that many features could be attributed to SMC-LMC interactions, such as the stream, including the bifurcated nature (Connors et al. 2006). However recent

proper motion data implies that the Magellanic system is on its first approach to the MW, (Kallivayalil et al. 2006; Vieira et al. 2010), and may even be on an unbound hyperbolic orbit (Besla et al. 2007). If the Magellanic system has made at least one orbit of the MW then the MW mass implied by its velocity is higher than most estimates. Modellers are now looking at SMC-LMC self interactions to explain the stream. These new models have implications for the other morphologies of the system.

New explanations for the morphology of the LMC-SMC are required in the absence of multiple MW orbits for the system. Nidever et al. (2008) suggest gas ejected from the supergiant shells in the HI are the source for the stream and leading arm, which drift away from the clouds at $49\,\mathrm{km\,s^{-1}}$. Subsequently a low metallicity has been found in the gas in the tip of the MgS (Fox et al. 2010) which is more suggestive of a SMC origin for the stream HI, although the metallicity is poor even for the SMC. The suggestion is the gas is from the periphery of the SMC galaxy and is less enriched as a consequence. This SMC origin is more consistent with the gas being stripped by LMC-SMC interaction, from the SMC periphery.

Sinusoidal patterns in the MgS are suggestive of periodicity and may possibly be the result of LMC disk rotation (Nidever et al. 2008). A problem with this hypothesis is the different velocities imparted to the stream would tend to scatter the stream, when what we witness is a very extended coherent structure. The stream distance is as yet uncertain. While the head is probably about the same distance as the clouds themselves between 50 kpc to 60 kpc the distance to the tail is uncertain, due in part to a lack of stellar tracers.

Simulations of LMC formation from an early accretion of DM sub-haloes predict a small halo of stars at large radii that originally formed in the sub-haloes (Brook et al. 2013). Borissova et al. (2004, 2006) detect some evidence for a halo in an old metal-poor population of RR Lyrae stars with a velocity dispersion of about $50\,\mathrm{km\,s^{-1}}$, larger than the disk value of about $25\,\mathrm{km\,s^{-1}}$ (Cole et al. 2005) in the inner LMC. 43 RR Lyrae with a large dispersion of $53\,\mathrm{km\,s^{-1}}$ were also observed by Minniti (2003). The presence of a potential halo population in the inner LMC is also noted by (Subramaniam and Subramanian 2009). Muñoz et al. (2006) also find a small number of stars with LMC-like metallicities at large radii, but a substantial MW-style halo is not observed around the LMC.

The mass of the LMC has been estimated as high as $1.5 \times 10^{10}\ M_{\odot}$ (Schommer et al. 1992) and as low as $6 \times 10^{9}\ M_{\odot}$ (Meatheringham et al. 1988). The tidal effect of the Magellanic sytem on the MW disk may be responsible for the large scale warp noted in the MW disk. The mass of the Magellanic system alone is too small to affect the spiral structure of the MW, unless the impact on the MW dark matter halo is strong enough to affect the MW disk (Weinberg 1995) .

In another indication that the LMC-SMC may have formed in isolation, it appears only moderately likely, $p = 0.1$, in a ΛCDM universe for a MW host to contain a pair of galaxies of the size of the LMC-SMC (Boylan-Kolchin et al. 2010). Massive sub-halos like the clouds are typically absorbed at later times in

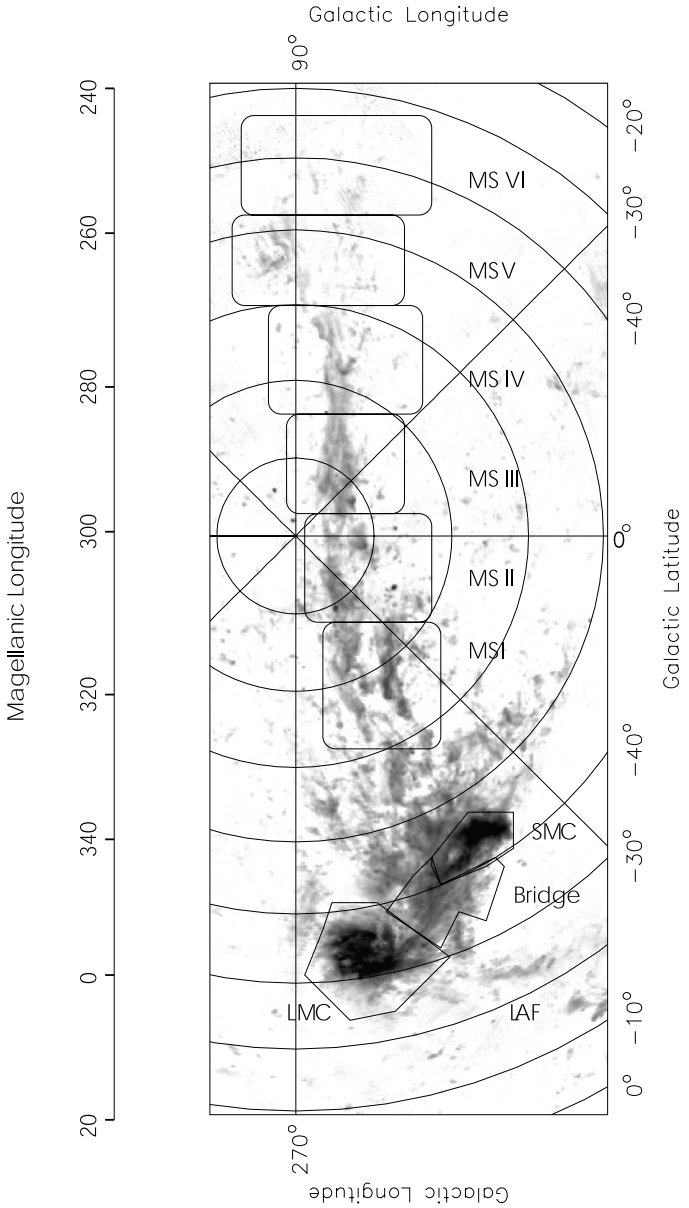

Figure 1.3: Revealing even more of the stream, the latest large scale HI survey of the Magellanic system using the Parkes multi-beam receiver from Figure 5. of Putman et al. (2003), shows HI column density on a logarithmic scale.

simulations of dark matter halos. It is likely the clouds have not arrived until recently.

The nature of the HI within the LMC is revealed in detail in the Australia Telescope Compact Array aperture synthesis mosaic image from Kim et al. (1998) (Figure 1.4). Here the spatial resolution is $1''$. The most striking features are the flocculent spiral structure and the voids in the interstellar medium. The voids are thought to be cleared by supernovae (SNe), stellar winds and UV from young clusters. Molecular cloud formation is enhanced within the walls of these voids (Dawson et al. 2013) .

Shock compression of the interstellar medium along with the turbulence of colliding flows create density conditions conducive to star formation. Understanding these feedback processes is increasingly recognised as important for star formation history and galactic evolution. Exactly how super-shells contribute to star formation rates is not yet well understood. The study of this phenomenon in the nearby LMC may illustrate the role of stellar feedback on the molecular fraction of entire galaxies.

Of the nine major H I holes in the LMC, six are associated with Hα shells ionised by young stars (Staveley-Smith et al. 2003), and at least two of these are associated with non-MW high velocity clouds (HVC). Bekki and Chiba (2007c) suggest that the HVCs could be associated with in-falling SMC material. The presence of young clusters that are strangely metal-poor (Grocholski et al. 2006), hints at accreted SMC material as raw material for LMC star formation.

The HI envelope around the Magellanic system is the main diagnostic of the large scale inter-galactic interactions between the SMC, LMC and MW. The galactic scale of the features, especially the MgS, indicate Gigayear timescales. The question which now faces researchers is whether the Magellanic system is an intact example of SMC-LMC interaction, or whether the disturbed morphology is a result of LMC-SMC interaction with the MW galaxy. Both interactions have probably left their mark on the Magellanic system in but in differing proportions.

The bar itself could be an example of such a morphology. The bar may have been induced as a result of interaction with the SMC, or perhaps induced by tidal interaction with the MW. It could also be an internal dynamic resonance within its own spiral structure. This study undertook to sample the chemical and dynamical tracers in the LMC bar to shed some light on the bar feature.

1.3.1 Bars in Disks

The phenomenon of spiral arms and bars is a manifestation of resonances within the disk structure as formulated in the classic paper by Lynden-Bell and Kalnajs (1972). Spiral features and bars are essentially a wave phenomenon, transferred through the response of the orbits of stars to the gravity of the density perturbation. These waves can grow, decay and reflect, forming standing patterns in the velocity field.

The main mechanism of propagation is via transference of angular momentum. This occurs most readily when the orbit of an object is in resonance with the wave angular momentum. The co-rotation circle is at the radius where the

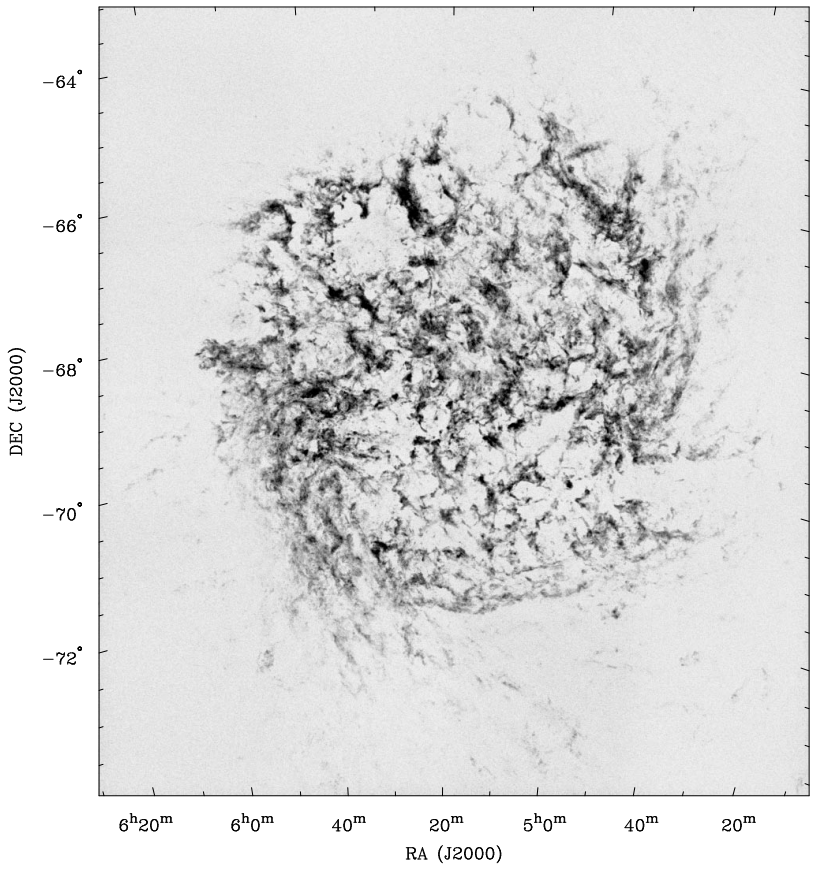

Figure 1.4: Figure 1. from Kim et al. (1998) showing the highest density HI component in the line of sight illustrates the disturbed spiral structure and voids in the interstellar medium.

wave pattern moves at the circular velocity of disk orbits. The angular momentum density is the distribution of masses with a particular angular momentum. Inside this co-rotation the angular momentum density is *negative* and outside the angular momentum density is *positive* relative to the co-rotation wave. The stars with lower angular momentum than the wave pattern are emitters of angular momentum, and stars with higher angular momentum than the wave are absorbers. The emitter stars do work against the gravitational force of the wave and lose energy, and that energy is picked up by the wave. The wave then does work on the absorbers, and transfers energy to them.

Another way of looking at the energy transfer is that the stars inside or outside co-rotation have the bar density wave pass by them more often, at a frequency greater than at co-rotation. For inner stars the bar pattern density is dragging on their orbital speed, and for outer stars the bar density gives an orbital impetus. At co-rotation the density moves with the stars. The pattern itself feeds on the energy transfer and grows. It grows especially given an anti-axisymmetric disturbance.

The kinetic energy of the galaxy is a combination of its rotational and its random, or thermal motions. To increase random motions requires the rotational energy to decrease. To decrease the angular momentum of the fraction of mass with a given GM/R^2 is accomplished by increasing R in the denominator (Lynden-Bell and Kalnajs 1972). Masses at larger radii can pick up angular momentum from the inner regions. Gravitational torques from the inner to the outer masses via the wave density transfer angular momentum outwards.

The wave resonances are energy minimisation points which form the patterns of bars and spirals. The pattern arises due to the virialization of the disk as the angular momentum is transferred outwards, increasing the random motions and the entropy of the galaxy. One pattern that minimises the energy is a trailing spiral structure. The gravitational torque from the inner to the outer is a leading torque, as the potential leads from the inner disk. The masses exterior are accelerated with respect to the inner mass. In order to lower the rotational energy the spiral minimisation pattern trails the forcing torque. A bar is another common pattern of density resonance that can transfer angular momentum.

Disks are unstable to bar resonances, which appear observationally to occur in both isolated disks and disks with companions. About 70% of disks show bar features (Eskridge et al. 2000). Disks with companions are more likely to show a bar feature (Gerin et al. 1990). In models companions speed up the formation of already present disk bar instabilities. It seems most disks are ready to form bars and that interactions speed up the process. The companions seem to accomplish this by absorbing angular momentum from the bar resonance. The transference of bar angular momentum to the outer disk and halo is also seen in models (Athanassoula and Bosma 2003). The satellite interaction is an extreme example of this angular momentum transfer process. The bar actually represents *negative* angular momentum density. Transferring angular momentum outwards to a satellite then actually strengthens the bar, by making it more angular momentum poor. The bar can grow in length as a result.

Models of a disk galaxy with a 1/4 mass small companion galaxy find that a bar can be easily created (Berentzen et al. 2004). The SMC is about 3/5 of the mass of the LMC (Bekki and Stanimirović 2009; van der Marel et al. 2002). While the last SMC interaction is estimated to have been only 200 MYr ago, these bars are expected to be long lived (Gerin et al. 1990). Previous passages of the SMC would have triggered the bar and subsequent fly-bys would serve to strengthen the bar, unless the SMC were to pass through the disk then the entire LMC could be disturbed (Berentzen et al. 2003).

Bars can tend to push gas toward the centre of the disk galaxy. The bar's gravitational torque on the gas at the leading edge of the bar robs the gas of angular momentum, slowing its orbit, and it falls inwards (Bournaud et al. 2005). The ends of the bar are regions of high gas density and low shear so star formation may be possible (Athanassoula 2000). Casetti-Dinescu et al. (2012) find two prominent clumps of young OB stars at either end of the LMC bar.

A cool disk will be susceptible to bar instabilities, whereas a warm disk with large velocity dispersion is stable to bars (Das et al. 2008). The existence of a bar in the LMC suggests there may be inflowing gas which can cool a disk, and the bar itself help to drive gas inwards. The Magellanic type SBm barred spirals have quite thick disks with the mean axial ratio being 0.35 (Odewahn 1996).

Bosma (1996) find that a sample of barred and unbarred galaxies show no statistical difference in rotation curves, in shape or maximum velocities. Just like spiral galaxies they exhibit typical rotation curves. Odewahn (1996) shows that for Magellanic type barred galaxies, the presence of a nearby companion is more probable.

Bars may become thick and box-like in profile. The vertical scale height of some inner orbits increases due to resonance with the bar speed (Combes et al. 1990). The increased velocity dispersion that might be expected in a boxy profile is not detected in this study. Subramaniam and Subramanian (2009) find some evidence for a flared LMC bar, thinner at the centre, from red clump depth estimation techniques.

Two types of bar evolution have been proposed, spontaneous bars and tidally driven bars (Miwa and Noguchi 1998). The spontaneous bar being triggered by light perturbations, and the tidal bar by strong interactions. But Berentzen et al. (2004) find this distinction is hard to unravel in simulations, and the dichotomy is more of a continuum of types.

RR Lyrae stars in the LMC show an increased scale height in the bar region (Borissova et al. 2004, 2006; Haschke et al. 2012a). The question is whether these old population tracers are part of an old halo with higher dispersion, or a bar that stands out from the disk. They may be consistent with an old bar population with extended vertical orbital components, making the bar box-like if viewed edge on.

The LMC appears to present ideal conditions for a bar. It is a thick disk, without a strong halo. It has been interacting with a nearby satellite the SMC. It has a HI gaseous envelope that can absorb energy and keep the stellar disk cool. The bar may be slightly flared at the ends (Subramanian and Subramaniam

2009), which is a typical evolutionary effect. The SMC has either made the LMC disk unstable during recent fly-bys in the last 5 billion years, or has amplified an existing instability.

Star formation may be induced by tidal and hydrodynamic shocks and gas infalls induced by galaxy-galaxy interaction. Star formation histories can provide clues to past dynamical events if they can be correlated with interactions. Large Magellanic morphological features such as the Inter Cloud Region (ICR) or bridge and the MgS are indicative of interactions. The bar of the LMC is of particular interest, as the strongest feature of the galaxy it must be one of the keys to the the history of the Magellanic Clouds. The LMC bar has been the object of much speculation as stellar data in the central regions has been sparse in comparison to the periphery of the galaxy. In this thesis observations in the crowding limited centre of the galaxy reveal the history of the LMC through chemical and dynamical properties of the stellar population of the bar.

1.3.2 Star Formation History of the Magellanic Clouds

Before recent proper motion estimates in the last ten years, interaction with the MW over several orbits was the paradigm for understanding the Magellanic Clouds' history and morphology. Models by Gardiner and Noguchi (1996) and Connors et al. (2006) were based on several Magellanic orbits of the MW in order to create some of the observed HI features.

MW tidal or ram pressure models for the Magellanic morphology rely on several orbits over 4 Gyr (Mastropietro et al. 2005). These scenarios are ruled out by higher proper motion. There does appear to be ram compression of cold HI and molecular gas on the leading eastern edge of the LMC (Marx-Zimmer et al. 2000). But invoking ram pressure and tides from the MW has failed to explain the leading arm feature in particular.

The stream, the leading arm, and bridge can all be recreated by models of SMC-LMC self interactions (Nidever et al. 2010; Diaz and Bekki 2012). The split nature of the stream is indicative of the interplay and exchanges of material between the two galaxies (Diaz and Bekki 2011). The leading arm fails to fit the notion of MW tidal or ram pressure and only SMC-LMC interactions can reproduce this feature in models.

There are new observations that support the notion of interactions between the clouds. Olsen et al. (2011) find a minor population of stars in the LMC that seem to have SMC metallicities. Stars have been found in line with the HI bridge that seem to connect a wing of material from the SMC to the periphery of the LMC (Casetti-Dinescu et al. 2012). This may be early evidence of tidal accretion of material from the SMC to the LMC during close fly-bys.

The question now is whether the clouds are on a bound or unbound orbit. The current velocity estimates, between $466\,\mathrm{km\,s^{-1}}$ to $490\,\mathrm{km\,s^{-1}}$, put the clouds on the edge of unbound energy or just marginally bound. The first passage scenario (Besla et al. 2007, 2010) itself has some criticisms. The MgS require the clouds to have been bound to the MW for at least 2 Gyr according to Diaz and Bekki (2012). First passage models also give the incorrect result that the

clouds are headed for an interaction with each other in the near future, rather than the recent past, which is what star formation evidence suggests (Harris and Zaritsky 2009; Glatt et al. 2010).

The SFH of the clouds gives us clues to the dynamical interactions that may have induced stellar birth. Spatially the star formation rate (SFR) seems largely consistent across the LMC disk with a slightly higher SFR for the bar region in the last 4 Gyr. Metallicities in RR Lyraes, a tracer of old populations, are very smooth across the LMC (Haschke et al. 2012b). Stellar metallicity in general doesn't show much variation (Cole et al. 2009; Grocholski et al. 2006), but once again there is a slight metal increase in the bar region. The SMC, which is much smaller, has seen star formation suppressed in the outer regions and move toward the centre in the last 3.5 Gyr. Similarly the very youngest objects in the the LMC are found preferentially towards the centre (Gallart et al. 2008) and the H II regions.

Weisz et al. (2013) have been able to go deeper, to fainter magnitudes, further down the LMC main sequence (MS) with the Hubble Space Telescope. They show that the clouds shared a common slow and constant SFR at > 12 Gyr. The slow SFR suggests they formed in isolation from the MW. The LMC had a faster rate from 10 Gyr to 12 Gyr, suggestive of self enrichment and enhancement of star formation, as the SMC inhabited similar environs. There are no periodic SFR peaks which might be expected if the Magellanic system had been orbiting the MW. There are peaks in the SMC at 9 Gyr and 4.5 Gyr which may indicate interaction with the LMC. From 3.5 Gyr there is a rise in the SFR across the Magellanic system which may mark the beginning of the MW interaction.

That the Magellanic binary system formed in isolation would not be surprising. A binary system lasting more than 5 Gyr is itself unusual , to have a triple galactic system SMC-LMC-MW stable over many orbits would be highly unlikely (Liu et al. 2011). In addition simulations on cosmological scales show that Magellanic type satellites are often accreted late onto host MW size galaxies (Boylan-Kolchin et al. 2011). If the Magellanic Clouds were accreted earlier they would be expected to lie on more circular orbits. It is likely too that they are marginally bound rather than unbound (Vieira et al. 2010; Kallivayalil et al. 2013), and their fast and eccentric orbit argues for late accretion.

Recent slight downward adjustments on the proper motion of the clouds suggest that they are bound to the MW (Vieira et al. 2010; Costa et al. 2009). Models based on the revised proper motions from SPM (Vieira et al. 2010) of about $466\,\mathrm{km\,s^{-1}}$ place the clouds on a highly eccentric bound orbit, not much less than the value for an unbound orbit $476\,\mathrm{km\,s^{-1}}$ (Besla et al. 2007; Piatek et al. 2008). Bound or unbound, the implication is that the SMC-LMC interactions are just as important to their history as recent MW interactions.

It appears from several studies that there are periods of star formation that are co-incidental in the SMC and LMC. Young clusters show two peaks of formation in the LMC at 125 and 800 Myr, and in the SMC at 160 and 630 Myr (Glatt et al. 2010). In addition Harris and Zaritsky (2009) find two peaks at 100 and 500 Myr in the two clouds. They also find another peak at 2 Gyr common to both clouds. A model based on the slightly lower revised proper motion

(Vieira et al. 2010; Costa et al. 2009) can reproduce a SMC-LMC interaction at about 200 Myr (Diaz and Bekki 2012). Models with a first infall scenario and SMC-LMC iteractions can also reproduce star forming close encounters at 150 Myr and 2 Gyr (Růžička et al. 2010).

Numerical simulations of recent Magellanic histories show that LMC-SMC close encounters over the last 2 Gyr, in addition to an approaching MW, can trigger patchy star formation in the LMC along the bar and regions like 30 Doradus (Bekki 2007). Another clue to the cause of the extreme Population I stars in the LMC is the existence of clusters like NGC 1718 which at intermediate age of about 2 Gyr have very low metallicity (Grocholski et al. 2006). In the case of this cluster -0.8 [Fe/H] where the other LMC clusters are spread very tightly around -0.4 [Fe/H]. SMC metal poor gas could have been accreted into the LMC during these close interactions, inducing increased star formation, including many other metal poor objects (Bekki and Chiba 2007c, , and references therein). In addition some LMC HI morphology like giant HI bubbles and holes could be the result of high velocity SMC gas flows into the disk (Staveley-Smith et al. 2003).

There is a big gap in the cluster SFH of the LMC (Smecker-Hane et al. 2002; Harris and Zaritsky 2009). Only a handful of clusters are found with ages 4-12 Gyr (Cole et al. 2000). There are many clusters with ages greater than 12 Gyr (Suntzeff et al. 1992). These old clusters have metallicities of around -1.8 dex (Da Costa 1991; Olszewski et al. 1991) and the young clusters have [Fe/H] $\approx$ -0.5 dex. There appears to have been a long period of quiescence when no clusters were formed. The cluster age gap is much more pronounced than the field star formation gap (Carrera et al. 2008). While there has been an increase in field star formation in the last 2-5 Gyr it is not as dramatic as the cluster increase (Cole et al. 2009; Baumgardt et al. 2013).

Cioni (2009) find a metallicity gradient in AGB stars decreasing from the centre to the outer disk, which they hypothesise could be the result of two major star formation events which created an old halo and thick disk, then an additional younger thin disk and bar. A reanalysis of the same data, allowing for different age populations, shows that there is little evidence for a metallicity gradient (Feast et al. 2010). The bar does demonstrate a dominant younger population from a brighter main-sequence turnoff (TO) in colour-magnitude diagram (CMD) studies(Smecker-Hane et al. 2002). The inferred age of this population depends on stellar evolution models (Skillman and Gallart 2002). The intermediate age population in the bar thus contains clues to the SFH of the LMC.

The nature of the bar feature has been discussed but a lack of evidence and even seemingly conflicting evidence has lead to varied speculation. Haschke et al. (2012a) find evidence of a bar projected above the disk by 5 kpc using RR Lyrae tracers , whereas Subramanian and Subramaniam (2010) do not using red clump stars as tracers. The RR Lyrae stars of Haschke et al. (2012a) may in fact be the long sought kinematically hot halo perhaps detected by Borissova et al. (2004, 2006). Subramanian and Subramaniam (2009) also find some evidence of an inner halo in the RR Lyrae data. In the past Connolly, L. P. (1985) also

found an handful of RR Lyrae that appear to be in the foreground of the LMC according to radial velocity estimates.

There have been proposals that the bar may be a spatially separate feature from the disk (Zhao and Evans 2000; Zaritsky 2004). The suggestion is that it lies in front of, or above the disk. It has also been hypothesised that the bar has serious warps (Subramaniam 2003), or contains a counter-rotating population (Subramaniam and Prabhu 2005). While it has been established that the bar is not a separate feature (Subramaniam and Subramanian 2009) there still remain many questions.

An aim of this thesis was to compare a large sample of LMC disk field and bar field stars to establish the nature of those two primary morphologies, disk and bar. While only a limited subset of the planned observations was obtained some of the fundamental questions regarding this closest disk galaxy have been addressed. Uncertainties in the proper motion of the LMC are now due mostly to lack of knowledge of the internal kinematics and geometry of the LMC (Kallivayalil et al. 2013). This study takes the largest sample set of spectroscopic velocities in the central LMC and puts constraints on important disk parameters. The robust statistical technique of Markov chain Monte Carlo (MCMC) is employed to take account of errors in our observations, and incorporate knowledge of disk geometry as clearly defined prior distributions with uncertainties. A new systemic velocity value is estimated giving the radial component of the critical space motion of the LMC. Metallicity estimates obtained constrain the SFH of the galaxy.

1.4 Globular Clusters in the Milky Way Halo

The MW halo contains about 160 GCs, a few of which at least may represent the core remnants of ancient dwarf galaxies. Globulars usually represent a single coeval population but multiple populations have been detected in some large globulars such as ωCentauri, M22 and NGC 1851 (Gratton et al. 2012; Joo and Lee 2013a). The conception of some globulars as dwarf galaxies with complex SFH has been proposed for M54, ωCentauri and NGC 2419 (Mackey and van den Bergh 2005, and references therein).

GCs are an excellent laboratory for stellar studies as their populations are coeval, for the most part . A common main sequence turn-off (TO) point, a distinct HB, along with other evolutionary features indicate a common age for the stars in these systems. These oldest objects in the halo are remnants of the earliest ages of the universe. We can look back in time to the most distant visible galaxies in the universe or study these fossil objects within easy reach in the MW halo.

Population synthesis is the science of modelling stellar populations, in particular the populations of GCs. Combined with the theory of stellar evolution we can probe the ages of ancient populations. The variations within GCs such as size and central density shed light on enrichment feedback mechanisms and their effect on the evolution of the population. GCs populations demonstrate

the enrichment of the primordial interstellar medium (ISM), the role of SNe and Population III nucleosynthesis.

Given a population synthesis model of the stars in a cluster or galaxy, artificial colour-magnitude diagrams can be generated. These models can be generated for different ages and metallicities. Isochrone models are fitted to observed CMDs from photometric studies to enable ages of objects to be estimated. A spectroscopic metallicity estimate allows an age and SFH to be determined with much more accuracy (Cole et al. 2009). Population modelling is easiest where a single stellar population is present, as in most globular clusters, making globulars an important test bed for understanding stellar evolution.

The research in this thesis provides insight into some of the above questions. We can estimate an age from the metallicity of the globular cluster. The equivalent width of the Ca II triplet absorption lines in the spectra of late life red giant stars is a proxy for the amount of non-hydrogen elements in the stars. This measure is well calibrated for metal poor populations. The sample of stars measured gives a statistical estimate for the metallicity of the globular cluster population.

This study provides detailed physical parameters for just one of the existing sample of 157 known MW globular clusters, (Harris 1996). Estimates of the bulk properties of the cluster provide information for researchers on the mass-luminosity function for the Galaxy and ultimately the universe. The abundance and mass of IC 4499 also has a bearing on the initial mass function (IMF) for halo objects at the low mass scale.

1.4.1 Abundances and the Origins of GCs

Observations of the numbers of stars within populations generally show agreement with theory of star formation at intermediate mass, but there is an excess of low mass objects being created in the MW at the present time, and some evidence of excess high mass numbers in some cluster environments (Kroupa 2002). There are difficulties with bias in observations that need to be taken into account when estimating the IMF. High mass, high luminosity objects are easier to detect, but very high mass stars only live $10^6 - 10^7$ years. There are biases in observing short lived stages in stellar evolution such as the HB, (Catelan 2009b). Samples in the MW are full of long lived, low mass stars. In GCs we are biased toward giant stars when it comes to spectroscopic abundances as these luminous stars are the easiest to measure. Salpeter (1955) found this relation between the number of stars as a function of mass and the the mass of the object,

$$\frac{\partial N}{\partial M} \propto M^{\Gamma} \tag{1.1}$$

Where Γ is -1.35 for a sample of MW stars with stellar mass range,

$$0.1M_{\odot} < M < 100M_{\odot} \tag{1.2}$$

and the average mass is only about $0.5M_{\odot}$. For very low mass objects the Salpeter (1955) universal relation does not hold. Kroupa (2002) Γ appears to be about -0.3 for stars less than $0.5M_{odot}$ and greater than $0.08M_{\odot}$, and 0.7 for less than $0.08M_{\odot}$. Chabrier (2005) estimate a linear drop in Γ for stars less than a $M_{\odot}$.

It appears the underlying IMF first identified by Salpeter (1955) has a large scatter caused by factors such as stellar dynamical processes, binaries, star formation feedback and environment (Kroupa 2002). More massive stars are thought to have formed in the past Chabrier (2003), when lower metallicity meant the rate of cooling of clouds was slower, so the clouds had time to get bigger before they cooled and condensed. However the MW and LMC do not show dramatically different IMFs despite the metallicity difference (Kroupa 2002) indicating the IMF has only a weak [Fe/H] dependance. Large clusters $> 10^6 M_{\odot}$would seem to favour a top heavy IMF (Murray 2009). These systems become heated and optically thick to infrared radiation driving the Jean's mass larger than one $M_{\odot}$.

Observations provide the evidence to constrain the IMF in our Galaxy and other systems. Modern multi-object fibre spectrometers now enable studies of large samples, (e.g Lane et al. 2011; Székely et al. 2007). Most stars form in systems rather than in isolation and this complicates the estimation of the IMF. The IMF estimation for systems contain assumptions such as constant birth rate over the system's history, which are unlikely to be true. The SFH links the Present Day Mass Function (PDMF) with the IMF.

As part of their bottom-up Galaxy formation hypothesis Searle and Zinn (1978) postulated that the halo globular cluster population formed in isolation from the MW proto-disk, as no radial gradient in metallicity is seen referenced to the MW centre. The gas from which they formed fell into the forming MW disk taking kinetic energy with it and leaving the globulars in isolated orbits in the MW gravitational field.

It is in the horizontal branch that the variation in metallicity appears most evident in GC studies. For a given metallicity, the position of a star along the red-blue dimension of the HB is attributable to variation in mass primarily (Faulkner 1966). Mass variation in a single stellar population in a GC is probably due to variation in mass loss on the RGB ascent. Mass loss is observed to occur near the top of the RGB while the mechanisms are not well understood (Origlia et al. 2002). The mass loss occurs before the helium flash, in which the He core and outer shell do not appear to mix.

The more metal poor clusters have a bluer HB than the more metal rich in general. This morphology is due primarily to abundances (Marino et al. 2013). While He to C fusion is the primary reaction in the core, the fusion of H in a shell surrounding the core via the CNO cycle affects the structure of an HB star. The scarcity of CNO catalysts in a metal poor star reduce the contribution of the H fusion shell to the stellar flux for a given mass He core (Faulkner 1966). Hydrostatic equilibrium makes the metal poor star more compact for its flux and so it is hotter and bluer. Additionally metal poor stellar atmospheres have less ionised metals to provide electrons and their lower H^- opacity allows more

energy to radiate out of the star, without forcing the atmosphere outward by radiation pressure, again keeping them compact. This makes them bluer at the same energy flux than a more metal rich object.

There is another effect, the second parameter effect (Lee et al. 1990), where the HB morphology seems to depend on age. Age estimates from CMD studies using the TO seem to show redder HB types with increasing age. This is also reflected in the radial distribution of halo objects (Lee 1992). While the second parameter effect remains controversial, it does appear to be a real effect. Age is perhaps not the only effect, with mass loss, environment, stellar rotation and other parameters playing some role, but age seems to be the main second parameter.

The effect of binaries is hard to model in single stellar population models. At least 60% of MS stars are in binary or multiple systems, (Duquennoy and Mayor 1991). Mass transfer in binary systems explains blue-stragglers lagging on the blue side of the MS turn-off. Most IMF models ignore such details and take a broad brush approach. While the concept of a single stellar population is a vital theoretical tool, it may not be a realistic description of globular clusters. The single stellar population remains however the foundation of our understanding of stellar evolution in groups. Multiple populations within GCs are considered in the next section.

Where there is variation in Fe abundances it is informative to compare abundances of other fusion products as a function of Fe. Comparison of [C/Fe] , [N/Fe] and [O/Fe] abundances where the sum C+N+O = *constant*, shows that the CNO stellar nucleosynthesis cycle has been at work. Similarly evidence of Mg-Al cycling in abundances implies extremely high temperatures ($> 70 \times 10^6$ K) which requires massive stars. Imbalances in CNO ratios indicate pollution from stellar feedback or primordial contamination.

Some GCs have been shown to be associated with stellar streams and linked to their host galaxies by chemical tagging. Other GCs are ancient relics of the first formation episode of the MW. Yet others are uniquely associated with extant galaxies like the LMC. This study looks at the little studied GC IC 4499 in order to understand its place in the MW halo.

1.4.2 Multiple Populations in Globular Clusters

Globular clusters have been important laboratories for stellar evolution because their single stellar populations represent a model of coeval generation with mass alone as a variable, distributed according to a single IMF. Convective mixing, nucleosynthesis and mass loss are able to be studied as a function of mass. Modern studies have shown that this is only a first approximation, and that detailed spectroscopic and photometric examination has revealed multiple generations of stars within GCs (Gratton et al. 2012, and references therein). The first clusters to reveal multiple populations were massive GCs such as 47 Tucanae (e.g. Cannon et al. 1998; Lane et al. 2010), ω Centauri (Bedin et al. 2004; Sollima et al. 2007), and M54 (Carretta et al. 2010). Many GCs have now been shown exhibit more than a single population (Milone et al. 2013).

Liight element Li, C, N abundance variations in GCs have been known for a long time (Kraft 1979; Hesser and Harris 1979; Da Costa 1997). Abundance variations have been seen seen in evolved RGB and un-evolved MS stars (Cannon et al. 1998; Gratton et al. 2001). MS stars do not have the convective mechanisms to bring advanced nucleosynthesis products from the core to the surface. This points to fundamental differences in populations that are hard to ascribe to factors such as self-enrichment, fast rotating stars, poor mixing of primordial gas or cluster merging. While there are valid hypotheses concerning the role of peculiar environmental effects and self-pollution (Bekki and Chiba 2007a), the consensus is moving toward multiple generations being the explanation for imhomogeneities (Milone et al. 2013).

While light element variations are common, heavy iron peak element variations are not seen except in massive cluster environments (Cohen 1981; Joo and Lee 2013b). Heavy element Ca and Si enhancements seen in all cluster stars, show that supernovae Type II (SNe II) have been the dominant polluters in the GC environment (Gratton et al. 2004). Massive clusters like M4 (Marino et al. 2008), M22 (Marino et al. 2013) show clear evidence of multiple populations and indicate higher star forming efficiency goes with higher mass.. MW GCs have a single [Fe/H] except for ω Centauri (Sollima et al. 2007) which leads some to think this extremely massive cluster may contain accreted populations or be the remnant core of a dwarf galaxy (Bekki and Norris 2006).

Examples of triple MS have been found within the narrow colour spread MS of NGC 2808 MS (Piotto et al. 2007) and NGC 6752 (Milone et al. 2013). Multiple populations were first noticed in massive clusters but now it appears true for most GCs (Gratton et al. 2012). Those in the Magellanic system show the some extreme multiple populations with several MS TO (Glatt et al. 2008; Milone et al. 2009), where a gas rich environment and tidal interactions may have triggered several episodes of star formation.

Gratton et al. (2012) propose three generations to explain light element abundances within a typical GC; an extreme primordial precursor generation in the very early universe which are no longer extant; a first generation of "polluters" which enriched the cluster to the present day level, of which a percentage are still visible today; and thirdly a second generation of Population II stars which now form the bulk of stars in GCs at typical low metallicity. The extreme progenitor Population III were massive and quickly pre-enriched the cluster molecular cloud with SNe II iron-peak and α elements, raising the metallicity to the present level (Bekki and Chiba 2007b). Then the first generation "polluters" gave rise to the light element abundance anomalies in the second generation. The first generation represent typically around 30% of the GC populations today (Carretta et al. 2010).

The first generation is proposed to have been more massive and burnt H at higher temperatures in order to generate observed light element abundances through proton capture processes (Denisenkov and Denisenkova 1989). The Na-O and especially the Mg-Al anti-correlation seen in many clusters require higher temperature than achieved by the present population, implying the first generation polluters were more massive, but not so massive as to create heavy

elements (Carretta et al. 2010). This means either the IMF was more top heavy for the first generation or the GCs were more massive (Prantzos and Charbonnel 2006), which would imply that GCs have been "evaporating", losing stars to the tides of the MW. Carretta et al. (2010) estimate clusters must have been twenty times larger than at present. Evaporation has removed most of the "polluter" generation, while the Population II stars reside in what was once the dense core of the cluster. Mackey and van den Bergh (2005) estimate the present GC population may represent only two-thirds of the original.

The metal-poor halo stars may be the evaporated remnant "polluters" of the once extremely massive GCs (Helmi 2008). The gas as well as the first generation stars evaporated into the halo ending star formation within GCs. The question of dark matter and the "missing satellites" is still a problem for ΛCDM models (Klypin et al. 1999; Moore 1996; Moore et al. 2006). More massive early GCs could represent at least part of the the "missing satellites". These multiple generations within GCs occurred within a short cosmological time in the early universe. Detailed archaeology of multiple star formation episodes in GCs will reveal important clues as to the role of effects like stellar feedback and mass loss in suppressing the formation of more satellite galaxies in dark matter haloes.

The Na-O anti-correlation is not seen in galactic or halo field stars (Gratton et al. 2012). Only stars in GCs exhibit the O-Na anti-correlation abundance anomaly (Gratton et al. 2001) indicating some peculiar GC environmental effect which remains unexplained. The Na-O abundance signature is proposed as a definition of GC populations by Carretta et al. (2010).

IC 4499, one subject of this thesis, does not show photometric colour spreads that would multiple generations (Sarajedini 1993; Ferraro et al. 1995; Walker and Nemec 1996; Walker et al. 2011). A high resolution spectroscopic study that might identify abundance anomalies in IC 4499 has not yet been undertaken.

1.4.3 IC 4499, A Special Globular Cluster?

IC 4499 is noteworthy in having an extremely high specific frequency of RR Lyrae variables; its value of $S_{RR} = 113.4$[1] is second only to the smaller Fornax 1 globular cluster (Mackey and Gilmore 2003) and the tiny outer halo cluster Pal 13 (Harris 1996). About 100 RR Lyrae stars have been identified and represent ≈68% of the the total HB population (Sarajedini 1993). Most of the RR Lyrae have P ≤0.6 d, making it an Oosterhoff Type I (OoI) cluster (Clement et al. 2001; Walker and Nemec 1996). Metallicity may be an important factor in determining the Oosterhoff classification of a cluster, as most OoI clusters tend to be more metal-rich than [Fe/H] = −1.8 on the ZW84 scale, while Oosterhoff Type II (OoII) clusters more metal-poor (Sandage 1993). It is thought that shorter-period RR Lyrae stars have not evolved off of the zero-age horizontal branch (ZAHB), while the longer-period variables are evolving through the RR Lyrae instability strip on the way to the asymptotic giant branch. The measurement of accurate cluster parameters in this study therefore has the po-

[1] $S_{RR} \equiv N_{RR}10^{0.4(7.5+M_v)}$ for a cluster of absolute magnitude M_V with N_{RR} variables.

tential to shed light on the evolutionary pathways of horizontal branch stars (e.g., Clement and Rowe 2000; Pritzl et al. 2000).

IC 4499 has been proposed as a "young" globular cluster with an age 2-4 Gyr younger than clusters with similar metallicity (Ferraro et al. 1995), where age is established by differential magnitude and colour comparisons with the TO. The method compares magnitude difference between the HB and TO, and the colour difference between the RGB and TO. In clusters of similar metallicity, the magnitude difference increases and the colour difference decreases with increasing age (Lee et al. 1990). Ferraro et al. (1995) adopt a value of [Fe/H] $= -1.8$ on the ZW84 scale in their work, and find that IC 4499 is essentially coeval with Arp 2 and NGC 5897. However, this matter is not settled, as the similarly-derived compilation of 55 globular cluster ages by Salaris and Weiss (2002) finds an age of 12.1 $\pm$1.4 Gyr for IC 4499, not significantly younger than the average of metal-poor clusters. While the latter study assumed the cluster was 0.3 dex more metal-rich than Ferraro et al. (1995) did, they arrived at a similar conclusion about the cluster coevality with Arp 2 and NGC 5897. Careful consideration of the cluster metallicity must be made in order to help resolve this discrepancy, which motivated this study.

Fusi Pecci et al. (1995) noted that IC 4499 lies near a great circle around the Galaxy that passes through other possibly "young" globulars, including Pal 12 and Rup 106. The suggestion that IC 4499 was part of a large remnant structure was a forerunner of the modern studies of halo substructure based on searching for tidal streams and RGB overdensities. In the past decade there has been a rapidly growing awareness of substructures in the Galactic halo (e.g., Morrison et al. 2000; Yanny 2000; Vivas et al. 2001; Newberg et al. 2002). Apart from the tidal stream of the disrupting Sgr dwarf spheroidal, one of the strongest structures detected in photometric surveys is the Galactic Anticentre Stellar Structure, which is also known as the Monoceros tidal stream or ring (e.g., Newberg et al. 2002; Ibata et al. 2003).

The Monoceros stream may be associated with the tidal disruption of a dwarf galaxy close to the plane of the MW, possibly the Canis Major dwarf irregular (e.g., Helmi et al. 2003; Martin et al. 2005); it is also possible that the Monoceros stream is a dynamical structure intrinsic to the thick disk of the MW (e.g., Piatti and Clariá 2008; Younger et al. 2008). Several MW star clusters have been suggested as members of the Monoceros stream (Martin et al. 2004; Frinchaboy et al. 2004; Peñarrubia et al. 2005; Piatti and Clariá 2008; Warren and Cole 2009, and numerous references therein), and this could have strong impacts on studies of the statistics of the MW globular cluster population if a number of clusters are found to have extragalactic origins.

Peñarrubia et al. (2005) propose several clusters as members of the Monoceros stream based on position and velocity. IC 4499 is projected in the right position, but Peñarrubia et al. (2005) do not publish a velocity for the cluster, although it appears to be plotted around $0\,\mathrm{km\,s^{-1}}$ in their Figure 11 *bottom panel*. This study was designed to take a spectroscopic sample of RGB stars in IC 4499 to place the cluster in velocity space and chemically "tag" it to constrain its possible membership in tidal streams.

Bibliography

E Athanassoula. Gas Flow in Barred Galaxies. *Stars*, 221:243, 2000.

E Athanassoula and A Bosma. Evolution and destruction of bars. *Astrophysics and Space Science*, 284(2):491–494, April 2003.

H Baumgardt and S Mieske. High mass-to-light ratios of ultra-compact dwarf galaxies - evidence for dark matter? *Monthly Notices of the Royal Astronomical Society*, 391(2):942–948, December 2008.

H Baumgardt, G Parmentier, P Anders, and E K Grebel. The star cluster formation history of the LMC. *Monthly Notices of the Royal Astronomical Society*, 430(1):676–685, March 2013.

Luigi R Bedin, Giampaolo Piotto, Jay Anderson, Santi Cassisi, Ivan R King, Yazan Momany, and Giovanni Carraro. ω Centauri: The Population Puzzle Goes Deeper. *The Astrophysical Journal*, 605(2):L125–L128, April 2004.

Kenji Bekki. Triggered star formation in the Magellanic Clouds. *Triggered Star Formation in a Turbulent ISM*, 237:373–377, 2007.

Kenji Bekki and Masashi Chiba. Massive Stars and Globular Cluster Formation. *The Astrophysical Journal*, 665(2):1164–1172, August 2007a.

Kenji Bekki and Masashi Chiba. Massive Stars and Globular Cluster Formation. *The Astrophysical Journal*, 665(2):1164–1172, August 2007b.

Kenji Bekki and Masashi Chiba. The Magellanic squall: gas replenishment from the Small to the Large Magellanic Cloud. *Monthly Notices of the Royal Astronomical Society: Letters*, 381(1):L16–L20, October 2007c.

Kenji Bekki and John E Norris. The Origin of the Double Main Sequence in ω Centauri: Helium Enrichment due to Gas Fueling from Its Ancient Host Galaxy? *The Astrophysical Journal*, 637(2):L109–L112, February 2006.

Kenji Bekki and Snežana Stanimirović. The total mass and dark halo properties of the Small Magellanic Cloud. *Monthly Notices of the Royal Astronomical Society*, 395(1):342–350, May 2009.

C L Bennett, D Larson, J L Weiland, N Jarosik, G Hinshaw, N Odegard, K M Smith, R S Hill, B Gold, M Halpern, E Komatsu, M R Nolta, L Page, D N Spergel, E Wollack, J Dunkley, A Kogut, M Limon, S S Meyer, G S Tucker, and E L Wright. Nine-year Wilkinson Microwave Anisotropy Probe (WMAP) Observations: Final Maps and Results. *The Astrophysical Journal Supplement*, 208(2):20, October 2013.

I Berentzen, E Athanassoula, C H Heller, and K J Fricke. Numerical simulations of interacting gas-rich barred galaxies: vertical impact of small companions. *Monthly Notice of the Royal Astronomical Society*, 341(1):343–360, May 2003.

I Berentzen, E Athanassoula, C H Heller, and K J Fricke. The regeneration of stellar bars by tidal interactions: numerical simulations of fly-by encounters. *Monthly Notices of the Royal Astronomical Society*, 347(1):220–236, January 2004.

G Besla, N Kallivayalil, L Hernquist, R P van der Marel, T J Cox, and D Kereš. Simulations of the Magellanic Stream in a First Infall Scenario. *The Astrophysical Journal Letters*, 721:L97, October 2010.

Gurtina Besla, Nitya Kallivayalil, Lars Hernquist, Brant Robertson, T J Cox, Roeland P. van der Marel, and Charles Alcock. Are the Magellanic Clouds on Their First Passage about the Milky Way? *The Astrophysical Journal*, 668(2):949–967, October 2007.

Gurtina Besla, N Kallivayalil, L Hernquist, R van der Marel, T Cox, and D Keres. Simulations of the Magellanic Stream in a First Infall Scenario. *American Astronomical Society*, 217:42404, 2011. (c) 2011: American Astronomical Society.

J Borissova, D Minniti, M Rejkuba, D Alves, K H Cook, and K C Freeman. Properties of RR Lyrae stars in the inner regions of the Large Magellanic Cloud. *Astronomy and Astrophysics*, 423(1):97–109, August 2004.

J Borissova, D Minniti, M Rejkuba, and D Alves. Properties of RR Lyrae stars in the inner regions of the Large Magellanic Cloud. *Astronomy and Astrophysics*, 460(2):459–466, December 2006.

A Bosma. Global Rotational Properties of Barred Galaxies. *Barred galaxies. Astronomical Society of the Pacific Conference Series*, 91:132, 1996.

F. Bournaud, F. Combes, and B. Semelin. The lifetime of galactic bars: central mass concentrations and gravity torques. *Monthly Notices of the Royal Astronomical Society: Letters*, 364(1):L18–L22, November 2005.

Michael Boylan-Kolchin, Volker Springel, Simon D M White, and Adrian Jenkins. There's no place like home? Statistics of Milky Way-mass dark matter haloes. *Monthly Notices of the Royal Astronomical Society*, 406(2):896–912, August 2010.

Michael Boylan-Kolchin, Gurtina Besla, and Lars Hernquist. Dynamics of the Magellanic Clouds in a Lambda cold dark matter universe. *Monthly Notices of the Royal Astronomical Society*, 414(2):1560–1572, June 2011.

Chris B Brook, Maider S Miranda, Brad K Gibson, Kate Pilkington, and Greg S Stinson. The Lowest Metallicity Stars in the LMC: Clues from MaGICC Simulations. *Publications of the Astronomical Society of Australia*, 30:42, July 2013.

R D Cannon, B F W Croke, R A Bell, J E Hesser, and R A Stathakis. Carbon and nitrogen abundance variations on the main sequence of 47 Tucanae. *Monthly Notices of the Royal Astronomical Society*, 298(2):601–624, August 1998.

G Carraro, R Zinn, and C Moni Bidin. Whiting 1: the youngest globular cluster associated with the Sagittarius dwarf spheroidal galaxy. *Astronomy and Astrophysics*, 466(1):181–189, April 2007.

R. Carrera, C. Gallart, Eduardo Hardy, A. Aparicio, and R Zinn. The Chemical Enrichment History of the Large Magellanic Cloud. *The Astronomical Journal*, 135(3):836–849, March 2008.

E. Carretta, A. Bragaglia, R. G. Gratton, S. Lucatello, M. Bellazzini, G. Catanzaro, F. Leone, Y. Momany, G. Piotto, and V. D'Orazi. Detailed abundances of a large sample of giant stars in M 54 and in the Sagittarius nucleus. *ArXiv e-prints*, June 2010.

E Carretta, A Bragaglia, R G Gratton, A Recio-Blanco, S Lucatello, V D'Orazi, and S Cassisi. Properties of stellar generations in globular clusters and relations with global parameters. *Astronomy and Astrophysics*, 516:55, June 2010.

D. I. Casetti-Dinescu, K. Vieira, T. M. Girard, and W. F. van Altena. Constraints on the Magellanic Clouds' Interaction from the Distribution of OB Stars and the Kinematics of Giants. *Astrophys. J.*, 753:123, July 2012. doi: 10.1088/0004-637X/753/2/123.

M Catelan. Horizontal branch stars: the interplay between observations and theory, and insights into the formation of the Galaxy. *Astrophysics and Space Science*, 320:261–309, April 2009a.

M Catelan. Horizontal branch stars: the interplay between observations and theory, and insights into the formation of the Galaxy. *Astrophysics and Space Science*, 320:261–309, April 2009b.

G. Chabrier. The Initial Mass Function: from Salpeter 1955 to 2005. In E. Corbelli, F. Palla, and H. Zinnecker, editors, *The Initial Mass Function 50 Years Later*, volume 327 of *Astrophysics and Space Science Library*, page 41, January 2005.

Gilles Chabrier. Galactic Stellar and Substellar Initial Mass Function. *The Publications of the Astronomical Society of the Pacific*, 115(8):763–795, July 2003.

Mei-Yin Chou, Katia Cunha, Steven R Majewski, Verne V Smith, Richard J Patterson, David Martinez-Delgado, and Doug Geisler. A Two Micron All Sky Survey View of the Sagittarius Dwarf Galaxy. VI. s-process and Titanium Abundance Variations Along The Sagittarius Stream. *The Astrophysical Journal*, 708(2):1290–1309, December 2009.

M R L Cioni. The metallicity gradient as a tracer of history and structure: the Magellanic Clouds and M33 galaxies. *Astronomy and Astrophysics*, 506(3): 1137–1146, November 2009.

C. M. Clement and J. Rowe. The Globular Cluster ω Centauri and the Oosterhoff Dichotomy. *Astron.J*, 120:2579–2593, November 2000. doi: 10.1086/316815.

C. M. Clement, A. Muzzin, Q. Dufton, T. Ponnampalam, J. Wang, J. Burford, A. Richardson, T. Rosebery, J. Rowe, and H. S. Hogg. Variable Stars in Galactic Globular Clusters. *Astron.J*, 122:2587–2599, November 2001. doi: 10.1086/323719.

J G Cohen. Abundances in globular cluster red giants. IV - M22 and Omega Centauri. *Astrophysical Journal*, 247:869, August 1981.

Judith G Cohen. Palomar 12 as a Part of the Sagittarius Stream: The Evidence from Abundance Ratios. *The Astronomical Journal*, 127(3):1545–1554, March 2004.

Andrew A Cole, Tammy A Smecker-Hane, and John S Gallagher. The Metallicity Distribution Function of Red Giants in the Large Magellanic Cloud. *The Astronomical Journal*, 120:1808, October 2000.

Andrew A Cole, Eline Tolstoy, John S Gallagher, and Tammy A Smecker-Hane. Spectroscopy of Red Giants in the Large Magellanic Cloud Bar: Abundances, Kinematics, and the Age-Metallicity Relation. *The Astronomical Journal*, 129:1465, March 2005.

Andrew A Cole, Aaron J Grocholski, Doug Geisler, Ata Sarajedini, Verne V Smith, and Eline Tolstoy. Breaking the age-metallicity degeneracy: The metallicity distribution and star formation history of the Large Magellanic Cloud. *The Magellanic System: Stars*, 256:263–268, March 2009.

F. Combes, F Debbasch, D Friedli, and D Pfenniger. Box and peanut shapes generated by stellar bars. *Astronomy and Astrophysics (ISSN 0004-6361)*, 233:82–95, July 1990.

Connolly, L. P. The RR Lyrae stars in the direction of the Large Magellanic Cloud. *Astrophysical Journal*, 299:728–740, December 1985.

Tim W Connors, Daisuke Kawata, and Brad K Gibson. N-body simulations of the Magellanic stream. *Monthly Notices of the Royal Astronomical Society*, 371(1):108–120, September 2006.

E. Costa, R. A. Méndez, M. H. Pedreros, M. Moyano, C. Gallart, N. Noël, G. Baume, and G. Carraro. The Proper Motion of the Magellanic Clouds. I. First Results and Description of the Program. *Astron.J*, 137:4339–4360, May 2009. doi: 10.1088/0004-6256/137/5/4339.

G S Da Costa. The Age-Abundance Relations and Age Distributions for the Star Clusters of the Magellanic Clouds. In *The Magellanic Clouds: Proceedings of the 148th Symposium of the International Astronomical Union*, page 183, 1991.

G S Da Costa. Abundance anomalies in globular clusters. *International Astronomical Union Symposium*, 189:193–202, 1997.

G. S. Da Costa and T. E. Armandroff. Abundances and Kinematics of the Globular Cluster Systems of the Galaxy and of the Sagittarius Dwarf. *Astron.J*, 109:2533–+, June 1995. doi: 10.1086/117469.

M Das, E Laurikainen, H Salo, and R Buta. Variation of bar strength with central velocity dispersion in spiral galaxies. *Astrophysics and Space Science*, 317(3-4):163–168, July 2008.

J R Dawson, N M McClure-Griffiths, T Wong, John M Dickey, A Hughes, Y Fukui, and A Kawamura. Supergiant Shells and Molecular Cloud Formation in the Large Magellanic Cloud. *The Astrophysical Journal*, 763(1):56, January 2013.

G. de Vaucouleurs. The Magellanic Clouds and the Galaxy. *The Observatory*, 74:23–31, February 1954.

G de Vaucouleurs and K C Freeman. Structure and dynamics of barred spiral galaxies, in particular of the Magellanic type. *Vistas in Astronomy*, 14(1): 163–294, July 1972.

Gerard de Vaucouleurs. Integrated Colors of Bright Galaxies in the u, b, V System. *Astrophysical Journal Supplement*, 5:233, January 1961.

P. A. Denisenkov and S. N. Denisenkova. Possible Explanation of the Correlation Between Nitrogen and Sodium Over Abundances for Red Giants in Globular Clusters. *Astronomicheskij Tsirkulyar*, 1538:11, June 1989.

Jonathan Diaz and Kenji Bekki. Constraining the orbital history of the Magellanic Clouds: a new bound scenario suggested by the tidal origin of the Magellanic Stream. *Monthly Notices of the Royal Astronomical Society*, page 257, March 2011. © 2011 The Authors Monthly Notices of the Royal Astronomical Society © 2011 RAS.

Jonathan D Diaz and Kenji Bekki. The Tidal Origin of the Magellanic Stream and the Possibility of a Stellar Counterpart. *The Astrophysical Journal*, 750 (1):36, May 2012.

A Duquennoy and M Mayor. Multiplicity among solar-type stars in the solar neighbourhood. II - Distribution of the orbital elements in an unbiased sample. *Astronomy and Astrophysics (ISSN 0004-6361)*, 248:485–524, August 1991.

O J Eggen, D Lynden-Bell, and A R Sandage. Evidence from the motions of old stars that the Galaxy collapsed. *Astrophysical Journal*, 136:748, November 1962.

Paul B Eskridge, Jay A Frogel, Richard W Pogge, Alice C Quillen, Roger L Davies, D L DePoy, Mark L Houdashelt, Leslie E Kuchinski, Solange V Ramírez, K Sellgren, Donald M Terndrup, and Glenn P Tiede. The Frequency of Barred Spiral Galaxies in the Near-Infrared. *The Astronomical Journal*, 119(2):536–544, February 2000.

John Faulkner. On the Nature of the Horizontal Branch. I. *Astrophysical Journal*, 144:978, June 1966.

Michael W Feast, Oyirwoth P Abedigamba, and Patricia A Whitelock. Is there a metallicity gradient in the Large Magellanic Cloud? *Monthly Notices of the Royal Astronomical Society: Letters*, 408(1):L76–L79, September 2010.

I. Ferraro, F. R. Ferraro, F. F. Pecci, C. E. Corsi, and R. Buonanno. Young globular clusters in the Milky Way: IC 4499. *Mon. Not. R. Astron. Soc.*, 275: 1057–1076, August 1995.

Andrew J Fox, Bart P Wakker, Jonathan V Smoker, Philipp Richter, Blair D Savage, and Kenneth R Sembach. Exploring the Origin and Fate of the Magellanic Stream with Ultraviolet and Optical Absorption. *The Astrophysical Journal*, 718(2):1046–1061, August 2010.

Ken Freeman and Joss Bland-Hawthorn. The New Galaxy: Signatures of Its Formation. *Annual Review of Astronomy and Astrophysics*, 40:487–537, 2002.

P. M. Frinchaboy, S. R. Majewski, J. D. Crane, I. N. Reid, H. J. Rocha-Pinto, R. L. Phelps, R. J. Patterson, and R. R. Muñoz. Star Clusters in the Galactic Anticenter Stellar Structure and the Origin of Outer Old Open Clusters. *Astrophys. J., Lett.*, 602:L21–L24, February 2004. doi: 10.1086/382504.

F. Fusi Pecci, M. Bellazzini, C. Cacciari, and F. R. Ferraro. The Young Globular Clusters of the Milky Way and the Local Group Galaxies: Playing with Great Circles. *Astron.J*, 110:1664–+, October 1995. doi: 10.1086/117639.

Carme Gallart, Peter B Stetson, Ingrid P Meschin, Frederic Pont, and Eduardo Hardy. Outside-In Disk Evolution in the Large Magellanic Cloud. *The Astrophysical Journal*, 682:L89, August 2008.

Lance T Gardiner and Masafumi Noguchi. N-body simulations of the Small Magellanic Cloud and the Magellanic Stream. *Monthly Notices of the Royal Astronomical Society*, 278(1):191–208, January 1996.

Doug Geisler, George Wallerstein, Verne V Smith, and Dana I Casetti-Dinescu. Chemical Abundances and Kinematics in Globular Clusters and Local Group Dwarf Galaxies and Their Implications for Formation Theories of the Galactic Halo. *The Publications of the Astronomical Society of the Pacific*, 119(8):939–961, September 2007.

M Gerin, F. Combes, and E Athanassoula. The influence of galaxy interactions on stellar bars. *Astronomy and Astrophysics (ISSN 0004-6361)*, 230:37–54, April 1990.

K Glatt, E K Grebel, and A Koch. Ages and luminosities of young SMC/LMC star clusters and the recent star formation history of the Clouds. *Astronomy and Astrophysics*, 517:50, July 2010.

Katharina Glatt, Eva K Grebel, Elena Sabbi, John S III Gallagher, Antonella Nota, Marco Sirianni, Gisella Clementini, Monica Tosi, Daniel Harbeck, Andreas Koch, Andrea Kayser, and Gary Da Costa. Age Determination of Six Intermediate-Age Small Magellanic Cloud Star Clusters with HST/ACS. *The Astronomical Journal*, 136(4):1703–1727, October 2008.

R G Gratton, P Bonifacio, A Bragaglia, E Carretta, V Castellani, M Centurion, A Chieffi, R Claudi, G Clementini, F D'Antona, S Desidera, P Francois, F Grundahl, S Lucatello, P Molaro, L. Pasquini, C Sneden, F Spite, and O Straniero. The O-Na and Mg-Al anticorrelations in turn-off and early subgiants in globular clusters. *Astronomy and Astrophysics*, 369:87–98, April 2001.

Raffaele Gratton, Christopher Sneden, and Eugenio Carretta. Abundance Variations Within Globular Clusters. *Annual Review of Astronomy &Astrophysics*, 42(1):385–440, September 2004.

Raffaele G Gratton, Eugenio Carretta, and Angela Bragaglia. Multiple populations in globular clusters. Lessons learned from the Milky Way globular clusters. *The Astronomy and Astrophysics Review*, 20:50, February 2012.

E K Grebel. The Local Group. *Microlensing 2000: A New Era of Microlensing Astrophysics*, 239:280, 2001.

A. J. Grocholski, A. A. Cole, A. Sarajedini, D. Geisler, and V. V. Smith. Ca II Triplet Spectroscopy of Large Magellanic Cloud Red Giants. I. Abundances and Velocities for a Sample of Populous Clusters. *Astron.J*, 132:1630–1644, October 2006. doi: 10.1086/507303.

Jason Harris and Dennis Zaritsky. The Star Formation History of the Large Magellanic Cloud. *The Astronomical Journal*, 138(5):1243–1260, November 2009.

W. E. Harris. A Catalog of Parameters for Globular Clusters in the Milky Way. *Astron.J*, 112:1487, October 1996. doi: 10.1086/118116.

Raoul Haschke, Eva K Grebel, and Sonia Duffau. Three-dimensional Maps of the Magellanic Clouds using RR Lyrae Stars and Cepheids. I. The Large Magellanic Cloud. *The Astronomical Journal*, 144(4):106, October 2012a.

Raoul Haschke, Eva K Grebel, Sonia Duffau, and Shoko Jin. Metallicity Distribution Functions of the Old Populations os the Magellanic Clouds from RR Lyrae Stars. *The Astronomical Journal*, 143(2):1–11, January 2012b.

A. Helmi, J. F. Navarro, A. Meza, M. Steinmetz, and V. R. Eke. On the Nature of the Ringlike Structure in the Outer Galactic Disk. *Astrophys. J., Lett.*, 592:L25–L28, July 2003. doi: 10.1086/377364.

Amina Helmi. The stellar halo of the Galaxy. *The Astronomy and Astrophysics Review*, 15(3):145–188, June 2008.

E. Hertzsprung. On the motion of the Magellanic clouds. *Mon. Not. R. Astron. Soc.*, 80:782, June 1920.

J E Hesser and G L H Harris. Further spectroscopic evidence bearing on the M22-Omega Centauri comparison. *Astrophysical Journal*, 234:513, December 1979.

J. V. Hindman. A high resolution study of the distribution and motions of neutral hydrogen in the Small Cloud of Magellan. *Australian Journal of Physics*, 20:147, 1967.

E. P. Hubble. The classification of spiral nebulae. *The Observatory*, 50:276–281, September 1927.

E. P. Hubble. A spiral nebula as a stellar system, Messier 31. *Astrophys. J.*, 69: 103–158, March 1929. doi: 10.1086/143167.

R A Ibata and A O Razoumov. Archer of the Galactic disk? The effect on the outer HI disk of the Milky Way of collisional encounters with the Sagittarius dwarf galaxy. *Astronomy and Astrophysics*, 336:130–136, August 1998.

R. A. Ibata, G. Gilmore, and M. J. Irwin. A dwarf satellite galaxy in Sagittarius. *Nature*, 370:194–196, July 1994. doi: 10.1038/370194a0.

R. A. Ibata, M. J. Irwin, G. F. Lewis, A. M. N. Ferguson, and N. Tanvir. One ring to encompass them all: a giant stellar structure that surrounds the Galaxy. *Mon. Not. R. Astron. Soc.*, 340:L21–L27, April 2003. doi: 10.1046/j.1365-8711.2003.06545.x.

Rodrigo A Ibata, Rosemary F G Wyse, Gerard Gilmore, Michael J Irwin, and Nicholas B Suntzeff. The Kinematics, Orbit, and Survival of the Sagittarius Dwarf Spheroidal Galaxy. *Astronomical Journal v.113*, 113:634–655, February 1997.

Kathryn V Johnston, Lars Hernquist, and Michael Bolte. Fossil Signatures of Ancient Accretion Events in the Halo. *Astrophysical Journal v.465*, 465:278, July 1996.

Seok-Joo Joo and Young-Wook Lee. Star Formation Histories of Globular Clusters with Multiple Populations. I. ω CEN, M22, and NGC 1851. *The Astrophysical Journal*, 762(1):36, January 2013a.

Seok-Joo Joo and Young-Wook Lee. Star Formation Histories of Globular Clusters with Multiple Populations. I. ω CEN, M22, and NGC 1851. *The Astrophysical Journal*, 762(1):36, January 2013b.

N. Kallivayalil, R. P. van der Marel, C. Alcock, T. Axelrod, K. H. Cook, A. J. Drake, and M. Geha. The Proper Motion of the Large Magellanic Cloud Using HST. *Astrophys. J.*, 638:772–785, February 2006. doi: 10.1086/498972.

N. Kallivayalil, R. P. van der Marel, G. Besla, J. Anderson, and C. Alcock. Third-epoch Magellanic Cloud Proper Motions. I. Hubble Space Telescope/WFC3 Data and Orbit Implications. *Astrophys. J.*, 764:161, February 2013. doi: 10.1088/0004-637X/764/2/161.

F J Kerr, J F Hindman, and B J Robinson. Observations of the 21 cm Line from the Magellanic Clouds. *Australian Journal of Physics*, 7:297, 1954.

S. Kim, L. Staveley-Smith, M. A. Dopita, K. C. Freeman, R. J. Sault, M. J. Kesteven, and D. McConnell. An H i Aperture Synthesis Mosaic of the Large Magellanic Cloud. *Astrophys. J.*, 503:674, August 1998. doi: 10.1086/306030.

Anatoly Klypin, Andrey V Kravtsov, Octavio Valenzuela, and Francisco Prada. Where Are the Missing Galactic Satellites? *The Astrophysical Journal*, 522 (1):82–92, September 1999.

Anatoly Klypin, HongSheng Zhao, and Rachel S Somerville. ΛCDM-based Models for the Milky Way and M31. I. Dynamical Models. *The Astrophysical Journal*, 573(2):597–613, July 2002.

R P Kraft. On the nonhomogeneity of metal abundances in stars of globular clusters and satellite subsystems of the Galaxy. *In: Annual review of astronomy and astrophysics. Volume 17. (A79-54126 24-90) Palo Alto*, 17:309–343, 1979.

P Kroupa. The Initial Mass Function and Its Variation (Review). *Modes of Star Formation and the Origin of Field Populations*, 285:86, 2002.

R. R. Lane, B. J. Brewer, L. L. Kiss, G. F. Lewis, R. A. Ibata, A. Siebert, T. R. Bedding, P. Székely, and G. M. Szabó. AAOmega Observations of 47 Tucanae: Evidence for a Past Merger? *Astrophys. J., Lett.*, 711:L122–L126, March 2010. doi: 10.1088/2041-8205/711/2/L122.

R R Lane, L L Kiss, G F Lewis, R A Ibata, A Siebert, T R Bedding, P Székely, and G M Szabó. AAOmega spectroscopy of 29 351 stars in fields centered on ten Galactic globular clusters. *Astronomy and Astrophysics*, 530:31, June 2011.

Y.-W. Lee. The chronology of the formation of the Galaxy. *Publications of the Astronomical Society of the Pacific*, 104:798–804, September 1992. doi: 10.1086/133056.

Y.-W. Lee, P. Demarque, and R. Zinn. The horizontal-branch stars in globular clusters. I - The period-shift effect, the luminosity of the horizontal branch, and the age-metallicity relation. *Astrophys. J.*, 350:155–172, February 1990. doi: 10.1086/168370.

Lulu Liu, Brian F Gerke, Risa H Wechsler, Peter S Behroozi, and Michael T Busha. HOW COMMON ARE THE MAGELLANIC CLOUDS? *The Astrophysical Journal*, 733(1):62, May 2011.

D Lynden-Bell and A J Kalnajs. On the generating mechanism of spiral structure. *Monthly Notices of the Royal Astronomical Society*, 157:1, 1972.

Andrea V Macciò, Ben Moore, Joachim Stadel, and Jürg Diemand. Radial distribution and strong lensing statistics of satellite galaxies and substructure using high-resolution ΛCDM hydrodynamical simulations. *Monthly Notices of the Royal Astronomical Society*, 366(4):1529–1538, March 2006.

A. D. Mackey and G. F. Gilmore. RR Lyrae stars in four globular clusters in the Fornax dwarf galaxy. *Mon. Not. R. Astron. Soc.*, 345:747–761, November 2003. doi: 10.1046/j.1365-8711.2003.07001.x.

A D Mackey and Sidney van den Bergh. The properties of Galactic globular cluster subsystems. *Monthly Notices of the Royal Astronomical Society*, 360 (2):631–645, June 2005.

Steven R Majewski, M F Skrutskie, Martin D Weinberg, and James C Ostheimer. A Two Micron All Sky Survey View of the Sagittarius Dwarf Galaxy. I. Morphology of the Sagittarius Core and Tidal Arms. *The Astrophysical Journal*, 599(2):1082–1115, December 2003.

Roeland P van der Marel and Maria-Rosa L Cioni. Magellanic Cloud Structure from Near-Infrared Surveys. I. The Viewing Angles of the Large Magellanic Cloud. *The Astronomical Journal*, 122:1807, October 2001.

A F Marino, S Villanova, G Piotto, A P Milone, Y Momany, L R Bedin, and A M Medling. Spectroscopic and photometric evidence of two stellar populations in the Galactic globular cluster NGC 6121 (M?4). *Astronomy and Astrophysics*, 490(2):625–640, November 2008.

A F Marino, A P Milone, and K Lind. Horizontal Branch Morphology and Multiple Stellar Populations in the Anomalous Globular Cluster M 22. *The Astrophysical Journal*, 768(1):27, May 2013.

N. F. Martin, R. A. Ibata, M. Bellazzini, M. J. Irwin, G. F. Lewis, and W. Dehnen. A dwarf galaxy remnant in Canis Major: the fossil of an in-plane accretion on to the Milky Way. *Mon. Not. R. Astron. Soc.*, 348:12–23, February 2004. doi: 10.1111/j.1365-2966.2004.07331.x.

N. F. Martin, R. A. Ibata, B. C. Conn, G. F. Lewis, M. Bellazzini, and M. J. Irwin. A radial velocity survey of low Galactic latitude structures - I. Kinematics of the Canis Major dwarf galaxy. *Mon. Not. R. Astron. Soc.*, 362: 906–914, September 2005. doi: 10.1111/j.1365-2966.2005.09339.x.

M Marx-Zimmer, U Herbstmeier, J M Dickey, F Zimmer, L Staveley-Smith, and U Mebold. A study of the cool gas in the Large Magellanic Cloud. I. Properties of the cool atomic phase - a third H i absorption survey. *Astronomy and Astrophysics*, 354:787–801, February 2000.

C Mastropietro, B Moore, L Mayer, J Wadsley, and J Stadel. The gravitational and hydrodynamical interaction between the Large Magellanic Cloud and the Galaxy. *Monthly Notices of the Royal Astronomical Society*, 363(2):509–520, October 2005.

Mario L Mateo. Dwarf Galaxies of the Local Group. *Annual Review of Astronomy and Astrophysics*, 36:435–506, 1998.

D. S. Mathewson and V. L. Ford. H I surveys of the Magellanic System. In S. van den Bergh and K. S. D. de Boer, editors, *Structure and Evolution of the Magellanic Clouds*, volume 108 of *IAU Symposium*, pages 125–136, September 1984.

D. S. Mathewson and M. P. Schwarz. The origin of the Magellanic Stream. *Mon. Not. R. Astron. Soc.*, 176:47P–51P, August 1976.

D S Mathewson, M N Cleary, and J D Murray. The Magellanic stream. *Astrophysical Journal*, 190:291–296, June 1974.

D. S. Mathewson, V. L. Ford, M. P. Schwarz, and J. D. Murray. The Magellanic Stream - Observational considerations. In W. B. Burton, editor, *The Large-Scale Characteristics of the Galaxy*, volume 84 of *IAU Symposium*, pages 547–556, 1979.

Alan W McConnachie. The Observed Properties of Dwarf Galaxies in and around the Local Group. *The Astronomical Journal*, 144(1):4, July 2012.

R X McGee and Janice A Milton. 21 cm hydrogen-line survey of the Large Magellanic Cloud. II. Distribution and motions of neutral hydrogen. *Australian Journal of Physics*, 19:343, 1966.

Stephen J Meatheringham, Michael A. Dopita, Holland C Ford, and B Louise Webster. The kinematics of the planetary nebulae in the Large Magellanic Cloud. *Astrophysical Journal*, 327:651–663, April 1988.

A P Milone, L R Bedin, G Piotto, and J Anderson. Multiple stellar populations in Magellanic Cloud clusters. I. An ordinary feature for intermediate age globulars in the LMC? *Astronomy and Astrophysics*, 497(3):755–771, April 2009.

A P Milone, A F Marino, G Piotto, L R Bedin, J Anderson, A. Aparicio, A Bellini, S Cassisi, F D'Antona, F Grundahl, M Monelli, and D Yong. A WFC3/HST View of the Three Stellar Populations in the Globular Cluster NGC 6752. *The Astrophysical Journal*, 767(2):120, April 2013.

D Minniti. Kinematic Evidence for an Old Stellar Halo in the Large Magellanic Cloud. *Science*, 301(5639):1508–1510, September 2003.

T. Miwa and M. Noguchi. Dynamical Properties of Tidally Induced Galactic Bars. *Astrophys. J.*, 499:149, May 1998. doi: 10.1086/305611.

Ben Moore. Constraints on the Global Mass-to-Light Ratios and on the Extent of Dark Matter Halos in Globular Clusters and Dwarf Spheroidals. *Astrophysical Journal Letters v.461*, 461:L13, April 1996.

Ben Moore, Sebastiano Ghigna, Fabio Governato, George Lake, Thomas Quinn, Joachim Stadel, and Paolo Tozzi. Dark Matter Substructure within Galactic Halos. *The Astrophysical Journal*, 524(1):L19–L22, October 1999.

Ben Moore, Juerg Diemand, Piero Madau, Marcel Zemp, and Joachim Stadel. Globular clusters, satellite galaxies and stellar haloes from early dark matter peaks. *Monthly Notices of the Royal Astronomical Society*, 368(2):563–570, May 2006.

H. L. Morrison, M. Mateo, E. W. Olszewski, P. Harding, R. C. Dohm-Palmer, K. C. Freeman, J. E. Norris, and M. Morita. Mapping the Galactic Halo. I. The "Spaghetti" Survey. *Astron.J*, 119:2254–2273, May 2000. doi: 10.1086/301357.

Heather L Morrison and Paul Harding. The Galactic bulge and halo. *Astronomical Society of the Pacific*, 105:977–982, September 1993.

Ricardo R Muñoz, Steven R Majewski, Simone Zaggia, William E Kunkel, Peter M Frinchaboy, David L Nidever, Denija Crnojevic, Richard J Patterson, Jeffrey D Crane, Kathryn V Johnston, Sangmo Tony Sohn, Rebecca Bernstein, and Stephen Shectman. Exploring Halo Substructure with Giant Stars. XI. The Tidal Tails of the Carina Dwarf Spheroidal Galaxy and the Discovery of Magellanic Cloud Stars in the Carina Foreground. *The Astrophysical Journal*, 649(1):201–223, September 2006.

Chigurupati Murali. The Magellanic Stream and the Density of Coronal Gas in the Galactic Halo. *The Astrophysical Journal*, 529(2):L81–L84, February 2000.

Norman Murray. The Sizes and Luminosities of Massive Star Clusters. *The Astrophysical Journal*, 691(2):946–962, February 2009.

H. J. Newberg, B. Yanny, C. Rockosi, E. K. Grebel, H.-W. Rix, J. Brinkmann, I. Csabai, G. Hennessy, R. B. Hindsley, R. Ibata, Z. Ivezić, D. Lamb, E. T. Nash, M. Odenkirchen, H. A. Rave, D. P. Schneider, J. A. Smith, A. Stolte,

and D. G. York. The Ghost of Sagittarius and Lumps in the Halo of the Milky Way. *Astrophys. J.*, 569:245–274, April 2002. doi: 10.1086/338983.

David L Nidever, Steven R Majewski, and W Butler Burton. The Origin of the Magellanic Stream and Its Leading Arm. *The Astrophysical Journal*, 679(1): 432–459, May 2008.

David L Nidever, Steven R Majewski, W Butler Burton, and Lou Nigra. The 200° Long Magellanic Stream System. *The Astrophysical Journal*, 723:1618, November 2010.

David L Nidever, Steven R Majewski, Ricardo R Muñoz, Rachael L. Beaton, Richard J Patterson, and William E Kunkel. Discovery of a Large Stellar Periphery Around the Small Magellanic Cloud. *The Astrophysical Journal Letters*, 733(1):L10, May 2011.

S. C. Odewahn. Properties of the Magellanic Type Galaxies. In R. Buta, D. A. Crocker, & B. G. Elmegreen, editor, *IAU Colloq. 157: Barred Galaxies*, volume 91 of *Astronomical Society of the Pacific Conference Series*, pages 30–+, 1996.

K. A. G. Olsen, D. Zaritsky, R. D. Blum, M. L. Boyer, and K. D. Gordon. A Population of Accreted Small Magellanic Cloud Stars in the Large Magellanic Cloud. *Astrophys. J.*, 737:29–+, August 2011. doi: 10.1088/0004-637X/737/1/29.

Edward W Olszewski, Robert A Schommer, Nicholas B Suntzeff, and Hugh C. Harris. Spectroscopy of giants in LMC clusters. I - Velocities, abundances, and the age-metallicity relation. *Astronomical Journal (ISSN 0004-6256)*, 101:515–537, February 1991.

J. H. Oort. The formation of galaxies and the origin of the high-velocity hydrogen. *Astron. Astrophys.*, 7:381–404, September 1970.

Livia Origlia, Francesco R Ferraro, Flavio Fusi Pecci, and Robert T Rood. ISOCAM Observations of Galactic Globular Clusters: Mass Loss along the Red Giant Branch. *The Astrophysical Journal*, 571(1):458–468, May 2002.

J. Peñarrubia, D. Martínez-Delgado, H. W. Rix, M. A. Gómez-Flechoso, J. Munn, H. Newberg, E. F. Bell, B. Yanny, D. Zucker, and E. K. Grebel. A Comprehensive Model for the Monoceros Tidal Stream. *Astrophys. J.*, 626: 128–144, June 2005. doi: 10.1086/429903.

S. Piatek, C. Pryor, and E. W. Olszewski. Proper Motions of the Large Magellanic Cloud and Small Magellanic Cloud: Re-Analysis of Hubble Space Telescope Data. *Astron.J*, 135:1024–1038, March 2008. doi: 10.1088/0004-6256/135/3/1024.

A. E. Piatti and J. J. Clariá. The apparent overdensity of open clusters in the Canis Major overdensity. *Mon. Not. R. Astron. Soc.*, 390:L54–L58, October 2008. doi: 10.1111/j.1745-3933.2008.00536.x.

G Piotto, L R Bedin, J Anderson, I R King, S Cassisi, A P Milone, S Villanova, A Pietrinferni, and A Renzini. A Triple Main Sequence in the Globular Cluster NGC 2808. *The Astrophysical Journal*, 661(1):L53–L56, May 2007.

N Prantzos and C Charbonnel. On the self-enrichment scenario of galactic globular clusters: constraints on the IMF. *Astronomy and Astrophysics*, 458 (1):135–149, October 2006.

B. Pritzl, H. A. Smith, M. Catelan, and A. V. Sweigart. RR Lyrae Stars in NGC 6388 and NGC 6441: A New Oosterhoff Group? *Astrophys. J., Lett.*, 530:L41–L44, February 2000. doi: 10.1086/312482.

M. E. Putman, L. Staveley-Smith, K. C. Freeman, B. K. Gibson, and D. G. Barnes. The Magellanic Stream, High-Velocity Clouds, and the Sculptor Group. *Astrophys. J.*, 586:170–194, March 2003. doi: 10.1086/344477.

A S G Robotham, I K Baldry, J Bland-Hawthorn, S P Driver, J Loveday, P Norberg, A E Bauer, K Bekki, S Brough, M Brown, A Graham, A M Hopkins, S Phillipps, C Power, A Sansom, and L Staveley-Smith. Galaxy And Mass Assembly (GAMA): in search of Milky Way Magellanic Cloud analogues. *Monthly Notices of the Royal Astronomical Society*, 424(2):1448–1453, August 2012.

Adam Růžička, Christian Theis, and Jan Palouš. Rotation of the Milky Way and the Formation of the Magellanic Stream. *The Astrophysical Journal*, 725: 369, December 2010.

M. Salaris and A. Weiss. Homogeneous age dating of 55 Galactic globular clusters. Clues to the Galaxy formation mechanisms. *Astron. Astrophys.*, 388:492–503, June 2002. doi: 10.1051/0004-6361:20020554.

E. E. Salpeter. The Luminosity Function and Stellar Evolution. *Astrophys. J.*, 121:161, January 1955. doi: 10.1086/145971.

A. Sandage. The Oosterhoff period-metallicity relation for RR Lyrae stars at the blue fundamental edge of the instability strip. *Astron.J*, 106:687–702, August 1993. doi: 10.1086/116675.

A. Sarajedini. A CCD color-magnitude diagram for the globular cluster IC 4499. *Astron.J*, 105:2172–2181, June 1993. doi: 10.1086/116595.

Robert A Schommer, Nicholas B Suntzeff, Edward W Olszewski, and Hugh C. Harris. Spectroscopy of giants in LMC clusters. II - Kinematics of the cluster sample. *Astronomical Journal (ISSN 0004-6256)*, 103:447–459, February 1992.

L Searle and R Zinn. Compositions of halo clusters and the formation of the galactic halo. *Astrophysical Journal*, 225:357–379, October 1978.

E D Skillman and C. Gallart. First Results of the Coimbra Experiment. *Observed HR Diagrams and Stellar Evolution*, 274:535, 2002.

T. A. Smecker-Hane, A. A. Cole, J. S. Gallagher, III, and P. B. Stetson. The Star Formation History of the Large Magellanic Cloud. *Astrophys. J.*, 566: 239–244, February 2002. doi: 10.1086/337985.

A Sollima, F R Ferraro, M Bellazzini, L Origlia, O Straniero, and E Pancino. Deep FORS1 Observations of the Double Main Sequence of ω Centauri. *The Astrophysical Journal*, 654(2):915–922, January 2007.

Else Starkenburg, Amina Helmi, Heather L Morrison, Paul Harding, Hugo van Woerden, Mario Mateo, Edward W Olszewski, Thirupathi Sivarani, John E Norris, Kenneth C Freeman, Stephen A Shectman, R C Dohm-Palmer, Lucy Frey, and Dan Oravetz. Mapping the Galactic Halo. VIII. Quantifying Substructure. *The Astrophysical Journal*, 698(1):567–579, June 2009.

L Staveley-Smith, S Kim, M R Calabretta, R F Haynes, and M J Kesteven. A new look at the large-scale HI structure of the Large Magellanic Cloud. *Monthly Notice of the Royal Astronomical Society*, 339:87, February 2003.

A. Subramaniam and S. Subramanian. RR Lyrae stars in the inner LMC: Where did they form? *Astron. Astrophys.*, 503:L9–L12, August 2009. doi: 10.1051/0004-6361/200912694.

Annapurni Subramaniam. Large Magellanic Cloud Bar: Evidence of a Warped Bar. *The Astrophysical Journal*, 598:L19, November 2003.

Annapurni Subramaniam and Tushar P Prabhu. Evidence of a Counterrotating Core in the Large Magellanic Cloud. *The Astrophysical Journal*, 625:L47, May 2005.

Annapurni Subramaniam and Smitha Subramanian. The Mysterious Bar of the Large Magellanic Cloud: What Is It? *The Astrophysical Journal Letters*, 703 (1):L37–L40, September 2009.

S Subramanian and A Subramaniam. Depth estimation of the Large and Small Magellanic Clouds. *Astronomy and Astrophysics*, 496(2):399–412, March 2009.

S Subramanian and A Subramaniam. An estimate of the structural parameters of the Large Magellanic Cloud using red clump stars. *Astronomy and Astrophysics*, 520:24, September 2010.

Nicholas B Suntzeff, Robert A Schommer, Edward W Olszewski, and Alistair R Walker. Spectroscopy of giants in LMC clusters. III - Velocities and abundances for NGC 1841 and Reticulum and the properties of the metal-poor

clusters. *Astronomical Journal (ISSN 0004-6256)*, 104:1743–1764, November 1992.

P Székely, LL Kiss, K Szatmáry, B Csák, GÁ Bakos, and TR Bedding. Radial velocities of five globular clusters obtained with AAOmega. *Astronomische Nachrichten*, 328(8):879–882, October 2007.

E. J. Tollerud, M. Boylan-Kolchin, E. J. Barton, J. S. Bullock, and C. Q. Trinh. Small-scale Structure in the Sloan Digital Sky Survey and ΛCDM: Isolated ˜L $_*$ Galaxies with Bright Satellites. *Astrophys. J.*, 738:102–+, September 2011. doi: 10.1088/0004-637X/738/1/102.

S. van den Bergh. *Galaxy Morphology and Classification*. Cambridge University Press, April 1998.

S. van den Bergh. The local group of galaxies. *Astron. Astrophys. Rev.*, 9: 273–318, 1999. doi: 10.1007/s001590050019.

Roeland P. van der Marel, David R Alves, Eduardo Hardy, and Nicholas B Suntzeff. New Understanding of Large Magellanic Cloud Structure, Dynamics, and Orbit from Carbon Star Kinematics. *The Astronomical Journal*, 124 (5):2639–2663, November 2002. Published in: Astron.J.124:2639-2663,2002 57 pages, LaTeX, with 11 PostScript figures. Submitted to the Astronomical Journal.

K. Vieira, T. M. Girard, W. F. van Altena, N. Zacharias, D. I. Casetti-Dinescu, V. I. Korchagin, I. Platais, D. G. Monet, C. E. López, D. Herrera, and D. J. Castillo. Proper-motion Study of the Magellanic Clouds Using SPM Material. *Astron.J*, 140:1934–1950, December 2010. doi: 10.1088/0004-6256/140/6/1934.

Katherine Vieira, Terrence M Girard, William F van Altena, Norbert Zacharias, Dana I Casetti-Dinescu, Vladimir I Korchagin, Imants Platais, David G Monet, Carlos E López, David Herrera, and Danilo J Castillo. Proper-motion Study of the Magellanic Clouds Using SPM Material. *The Astronomical Journal*, 140:1934, December 2010.

A K Vivas, R Zinn, P Andrews, C Bailyn, C Baltay, P Coppi, N Ellman, T Girard, D Rabinowitz, B Schaefer, J Shin, J Snyder, S Sofia, W van Altena, C Abad, A Bongiovanni, C Briceño, G Bruzual, F Della Prugna, D Herrera, G Magris, J Mateu, R Pacheco, Ge Sánchez, Gu Sánchez, H Schenner, J Stock, B Vicente, K Vieira, I Ferrín, J Hernandez, M Gebhard, R Honeycutt, S Mufson, J Musser, and A Rengstorf. The QUEST RR Lyrae Survey: Confirmation of the Clump at 50 Kiloparsecs and Other Overdensities in the Outer Halo. *The Astrophysical Journal*, 554(1):L33–L36, June 2001.

A. R. Walker and J. M. Nemec. CCD Photometry of Galactic Globular Clusters.III.IC 4499. *Astron.J*, 112:2026–+, November 1996. doi: 10.1086/118161.

A R Walker, A M Kunder, G Andreuzzi, A Di Cecco, P B Stetson, M Monelli, S Cassisi, G Bono, R De Propris, M Dall'Ora, J M Nemec, and M Zoccali. Constraints on the formation of the globular cluster IC 4499 from multiwavelength photometry. *Monthly Notices of the Royal Astronomical Society*, 415 (1):643–654, May 2011.

Steven R Warren and Andrew A Cole. Metallicities and radial velocities of five open clusters including a new candidate member of the Monoceros stream. *Monthly Notices of the Royal Astronomical Society*, 393(1):272–296, February 2009.

Martin D Weinberg. Production of Milky Way Structure by the Magellanic Clouds. *Astrophysical Journal Letters v.455*, 455:L31, December 1995.

Martin D Weinberg. Effect of the Milky Way on Magellanic Cloud Structure. *The Astrophysical Journal*, 532(2):922–935, April 2000.

Daniel R Weisz, Andrew E Dolphin, Evan D Skillman, Jon Holtzman, Julianne J Dalcanton, Andrew A Cole, and Kyle Neary. Comparing the ancient star formation histories of the Magellanic Clouds. *Monthly Notices of the Royal Astronomical Society*, 431(1):364–371, May 2013.

T Westmeier and B S Koribalski. The scattered debris of the Magellanic Stream. *Monthly Notices of the Royal Astronomical Society: Letters*, 388(1):L29–L33, July 2008.

Ralph E Wilson. The Motions of the Magellanic Clouds. *Publications of the Astronomical Society of the Pacific*, 56:102, June 1944.

B. et al. Yanny. Identification of A-colored Stars and Structure in the Halo of the Milky Way from Sloan Digital Sky Survey Commissioning Data. *Astrophys. J.*, 540:825–841, September 2000. doi: 10.1086/309386.

Brian Yanny, Heidi Jo Newberg, Steve Kent, Sally A Laurent-Muehleisen, Jeffrey R Pier, Gordon T Richards, Chris Stoughton, John E Jr Anderson, James Annis, J Brinkmann, Bing Chen, Istvan Csabai, Mamoru Doi, Masataka Fukugita, G S Hennessy, Zeljko Ivezić, G R Knapp, Robert Lupton, Jeffrey A Munn, Thomas Nash, Constance M Rockosi, Donald P Schneider, J Allyn Smith, and Donald G York. Identification of A-colored Stars and Structure in the Halo of the Milky Way from Sloan Digital Sky Survey Commissioning Data. *The Astrophysical Journal*, 540(2):825–841, September 2000.

J. D. Younger, G. Besla, T. J. Cox, L. Hernquist, B. Robertson, and B. Willman. On the Origin of Dynamically Cold Rings around the Milky Way. *Astrophys. J., Lett.*, 676:L21–L24, March 2008. doi: 10.1086/587099.

D. Zaritsky. The Case of the Off-Center, Levitating Bar in the Large Magellanic Cloud. *Astrophys. J., Lett.*, 614:L37–L40, October 2004. doi: 10.1086/425312.

H. Zhao and N. W. Evans. The So-called "Bar" in the Large Magellanic Cloud. *Astrophys. J., Lett.*, 545:L35–L38, December 2000. doi: 10.1086/317324.

2

Spectroscopy of Red Giant Atmospheres

This study employed the techniques of spectroscopy for extracting physical information from stellar light. Spectroscopy is one of the fundamental observational methods in astronomy, along with photometry and astrometry. In this study photometric and astrometric catalogues were used to identify and locate populations for spectroscopic observations.

Spectroscopy is the measurement of emission intensity across a range of wavelengths. The intensity over the full range of wavelengths follows a Planck blackbody emission profile which is dependent on temperature. In addition to the continuum or average emission over the observed range of wavelengths there are narrow-band features due to atomic transition processes at discreet photon energies. These lines are either an excess of intensity referenced to the continuum due to emission of light, or a deficit in intensity due to absorption. Both processes are due to the interaction of matter with the electromagnetic field. This study is primarily concerned with the infrared absorption features due to ionised calcium in stellar atmospheres. This feature is strong in late-life RGB stars and is thus easily observable even with low to moderate resolution spectra.

As long as the photosphere of the star remains at equilibrium then it behaves as a black-body emitter. In a star the emission is equal to the supplied energy from the interior over long periods of time, and energy in the photosphere is well mixed, the condition of local thermodynamic equilibrium (LTE). The Planck law gives the radiance in Watts per steradian per cubic metre as,

$$B(T,\lambda) = \frac{2hc^2}{\lambda^5}(e^{\frac{hc}{\lambda k_B T}} - 1)^{-1} \tag{2.1}$$

Where k_B is the Boltzmann constant, h is the Planck constant and c is the speed of light. To find the peak wavelength at a given temperature the derivative of the Planck law is set equal to zero, and gives $\lambda \approx \frac{2.898\times10^{-3}}{T}[m]$ which is Wien's Law. For the temperature of a K type red giant star photosphere around 4000 Kelvin the above equation gives a wavelength of 724.5 nm (7245 Å) which lies in the near-infrared. Near this peak the continuum is less steep for RGB stars and this is where the Ca II triplet is found.

Photometric and astrometric catalogues are used to select RGB stars for

observation in the field of interest. Catalogues of astrometric positions and magnitudes date back at least two millennia to Hipparchus of Rhodes (150 BC). Photometry gives the brightness of stars in different colours by employing filters that admit only a limited band of the electromagnetic spectrum. There are various systems of filters, each attuned to different astrophysical parameters. While there are 167 different scientifically recognised systems (Moro and Munari 2000) there are a few that are commonly used in large surveys and databases. The various systems began to be rigorously standardised with the advent of photo-electric measurement techniques that superseded the photographic film era.

The Johnson (and Morgan) (Johnson and Morgan 1953), filter system is the most widely employed. The wide band B U V filters cover the optical wavelengths. The system was later extended to very red R, and I. Eventually infrared J,H,K,L,M,N, (Johnson 1965) bands were added to form the complete Arizona system covering even the coolest stellar objects such as M-dwarfs and carbon stars. Many observatories have their own definitions of the infrared bands. The AAO and European Southern Observatory along with other leading observatories have specific bandwidths and centres in their own systems. Other systems are often modifications to the Johnson system and often overlap Johnson bands. The Cousins system for example has the same Johnson V band but identically named yet differently defined R and I bands (Cousins 1980). The various systems are well defined so they can be cross referenced and calibrated with other systems.

The magnitude observed, the apparent magnitude, depends on the fraction of light received here on earth from the total bolometric magnitude of the star and is a function of distance for a given luminosity star. The apparent magnitude of the star observed is the integrated flux over some chosen band in a photometric system. The Bolometric magnitude is the total energy output as electromagnetic waves of the star across all wavelengths according to Planck's radiation law. Given a distance measure to the star, a parallactic distance to a nearby star for example, one can translate the apparent magnitude into an absolute magnitude, the apparent magnitude at 10 pc (Böhm-Vitense 1989). The colour of a star, the part of the spectrum showing the peak of emission indicates a temperature. The temperature is also given by the ratio of magnitudes in photometric bands. This temperature allows us to use Planck's law to calculate a bolometric magnitude or luminosity from the absolute magnitude of the star.

Even the nearest stars are so distant that the largest telescopes show them only as points in the sky. Only Betelgeuse, a huge 1000 $R_{\odot}$ giant star which is relatively close at $\approx$ 650 ly has been directly imaged resolved to show angular size (Gilliland and Dupree 1996). Even a zero dimensional point of light can reveal much through its spectrum. Electromagnetism and quantum mechanics, combined with stellar nucleosynthesis theory and physical models of stellar interiors and atmospheres allow the interpretation of stellar processes through their spectra.

The 2MASS catalogue which has an astrometric accuracy of about $\sim$ 0.1 arcseconds was employed to select RGB stars (Skrutskie 2006). The 2MASS

infrared photometric bandpasses $J(1.25\,\mu m)$, $K_s(2.16\,\mu m)$ $(1.25\,\mu m)$ were employed to create CMD's for the IC 4499 selection. The IRSF Magellanic Clouds Point Source Catalogue uses the same bandpasses with the same astrometric accuracy and was employed to select targets and configure the AAOmega fibre positioner (Kato et al. 2007).

2.1 Stellar Nucleosynthesis, Evolution and Abundances

The older a star is, the less heavy elements it contains in general . The inverse correlation between the ages of stars and their metallicities was a key piece of evidence pointing to the creation of elements heavier than hydrogen inside stars, rather than the Big Bang.

Stellar evolution begins with condensation of the proto-star from primordial gas and dust over the order of millions of years. The enrichment of the original material by previous stellar generations affect the evolution of a star. Higher metallicity enhances cooling, and reduces the Jean's mass, creating smaller stars in general. Very low metallicity stars in the universe are thought to have been more massive for this reason. After the initial formation the star will begin to fuse hydrogen into helium at its core when the temperature reaches about 10^7 K. The star spends most of its life on here on the main sequence (MS).

A star the mass of the sun will spend about 10^{10} years on the MS, where hydrogen fusion into helium occurs primarily through various proton-proton chains (Bethe 1939). A star ten times as massive will spend about 10^7 years, where the CNO cycle is the more important fusion process (Cameron 1957). The exception is very metal poor stars that lack the C, N and O catalysts. The end of the MS stage occurs when the hydrogen abundance has been exhausted to about 5% in the core leaving a mainly helium core (Iben 1967).

The cessation of core fusion means radiation pressure drops leaving the gravitational force unbalanced. The star undergoes core contraction and compression. Hydrogen to helium fusion still occurs in the region surrounding the core driving the outer layers away from the core and resulting in expansion of the star to the red giant phase. The outer atmosphere is at very large radii, typically 100 times the original radius. The temperature at the distant surface drops to 3000 K to 5000 K. Despite a lower temperature the massive surface area of the red giant star results in higher luminosity than the MS stage.

The star spends about a tenth of its life in this phase. Core growth and contraction continue slowly and the star expands and grows more luminous, climbing the giant branch. When the core contraction drives temperatures up to about 10^8 K then fusion of helium into carbon via the triple-α fusion process can begin (Iben 1967). This is known as helium flash, which marks the peak luminosity of the RGB , the tip of the branch on a colour magnitude diagram. The star then settles into a new phase of stable fusion on the horizontal branch, which sees the star contract slightly and the temperature rise.

A star's position on the ZAHB depends on its mass primarily, with more massive stars burning hotter at the blue and of the HB. The HB morphology

also depends also on metallicity, with metal rich clusters having redder HB and metal poor bluer (Armandroff and Zinn 1988). The main effect of metallicity is increased HB luminosity with age referenced to the TO. Older stars tend to be more massive and luminous. There is a region between the red and blue sometimes referred to as a gap in the HB. The gap is not due to a lack of stars, it is that the stars at these colours are variables. The variables do not appear on snapshot CMDs as their luminosity has not been averaged and plotted, leaving an empty region. This region is also known as the instability strip as it is populated by Cepheid and RR-Lyrae variable stars.

The RR-Lyrae have two modes of periodicity (Oosterhoff 1939). This has resulted in a classification of populations based on the period, the OoI, with mean period ≈0.5 days and more metal rich with [Fe/H] ≥ -1.65 and OoII with mean period 0.64 days and metal poor with [Fe/H] ≤ -1.65. One more classification has been proposed, a third Oosterhoff Type III (OoIII) covering some metal rich clusters NGC 6388 and NGC 6411 with OoII periods (Armandroff and Zinn 1988; Pritzl et al. 2000). While the majority of of halo GCs can be categorised this way some clusters, such as IC 4499 are intermediate in the period range 0.58 - 0.62 days and are Oosterhoff intermediate (OoInt).

The Oosterhoff dichotomy may hold clues to the evolution of the galaxy. Most dSph GCs fall in the OoInt category, as do the LMC clusters (Catelan 2009). The metal poor halo GCs display a dichotomy between OoI and OoII. The Oosterhoff type may be another clue to the origin of GCs like IC 4499, which is extremely rich in RR-Lyrae. There is a second parameter effect on HB morphology that is less well understood than the age-metallicity relation, which appears to be related to the age of the cluster and its distance from the centre of the Galaxy. It appears that some extreme outer halo objects which appear very old and metal-poor have redder HB than expected (Lee 1992). This age-Galactocentric radial effect, probably contains a clue the evolution of the Galaxy.

The HB stage is relatively short-lived. Even more short-lived is the asymptotic giant phase, analogous to the red giant phase, but at larger radii and higher luminosity. The helium in the core is spent, leaving a carbon and oxygen ash core. Helium burning around the core creates an even larger radius star with higher than red giant luminosity.

The late giant stages, when there is enough carbon abundance, allows the creation of α elements by the building of nuclei whose mass numbers are multiples of four, i.e. multiples of the He nucleus. Core collapse SNe II are chiefly responsible for the generation of the abundances of α elements. The preponderance of massive stars in the early universe, meant that SNe II were more important. Massive stars only last on the order of millions of years before going supernova. The evolution of stars to white dwarfs, the progenitors of supernovae Type Ia (SNe Ia), is of the order of billions of years.

At the end of the giant phase the outer atmosphere may be blown off to form a planetary nebula; the remaining electron degenerate pressure core of carbon and oxygen becomes a white dwarf star. The star has a limit of about 1.4 solar masses, depending on rotational support for more mass. Accretion

of additional material from a binary companion, for example, could lead to the heating of the degenerate white dwarf core. The core cannot increase in pressure so the temperature runs away. The temperature is high enough to allow carbon and oxygen fusion and the output from the fusion cannot be suppressed by pressure, this leads to runaway fusion in a few seconds and a SNe Ia (Khokhlov et al. 1993). The known mass of the progenitor star gives an energy for the unbinding of the star in the explosion of about 1 J to 2×10^{44} J. This results in a consistent luminosity for the SNe Ia, an absolute magnitude of -19.3. For this reason SNe Ia are used as standard candles for distance estimates to galaxies in the local universe. SNe Ia create mainly iron peak elements.

The red giant phase can also see the slow capture of neutrons over millions of years by some nucleides to form heavier elements, the s-process. The neutrons are the by-products of other fusion reactions, principally helium fusion. The release of a gamma ray allows the heavy neutron capture isotopes to decay to stable elements. The slow process means the s-process elements stay close to proton-neutron equilibrium. At certain neutron nucleon numbers 50, 82, 126, the nucleus has an especially low neutron capture cross-section, making it hard to capture neutrons and nucleosynthesis products form an abundance peak at these atomic numbers (Reeves 1968).

In contrast the r-process is a rapid accumulation of neutrons which pushes the isotopes quickly to a neutron-rich state before gamma decay occurs. They move further from equilibrium than the s-process elements to higher neutron-rich states (Seeger et al. 1965). The neutron flux needed for the r-process means it is restricted to SNe explosions or very extreme cores of massive stars.

As with the s-process, the same special neutron numbers represent a very small capture cross section. The r-process at this point becomes like the s-process, with single neutron additions and gamma decays of a neutron to a proton. These represent a kind of phase change between allowed r-process proton-neutron abundances. If the neutron bombardment ceases, then these r-process bottlenecks result in an over abundance at these special neutron counts. Because they are proton deficient compared to the s-process abundance peaks they peak at a lower atomic number 6 -12 below the s-process peak (Reeves 1968). This results in a double abundance peak, the lower one due to the r-process.

The proton rich isotopes were originally explained by Burbidge et al. (1957) by similar proton capture mechanisms to the proposed neutron capture. It was soon realised that their charges on large nuclei meant the electro-magnetic repulsion was too great for the p-process to occur. It is still a subject of current research.

2.2 Spectral classes

This study samples red giant spectral class KII to KIII stars in IC 4499 and the LMC. Spectral classes describe the temperature and atmospheric ionisation state of the stellar corona as well as the type of star. The Harvard classes, denoted by an alphabetic letter, are linear categories based on the temperature

of the star. Originally alphabetically ordered in the nineteenth century, subsequent physical knowledge of atomic processes has resulted in today's seven classes O,B,A,F,G,K,M. The Yerkes luminosity classes, denoted by a Roman numeral, are descriptive of the size measured by luminosity and describe the type of star. The Yerkes classes differentiate stars with similar temperatures but different sizes. A red giant with the same surface temperature as a dwarf star is a very different object.

K denotes a red star with surface temperature between 3700 K to 5200 K, and II indicates a bright giant star and III a giant star. Some MII-III are sampled, many of which are seen to be carbon stars. The carbon absorption lines are numerous and prominent and at first appear to be corrupt or faulty spectra with the strong Ca II lines almost obscured by the many ions of carbon. The sample was chosen from a colour magnitude diagram, formed by plotting temperature $J - K_s$ and luminosity measure K_s. The temperature range covers K stellar types and the luminosity range covers the tip of the RGB, and some of the asymptotic branch. Dwarf stars in the LMC and IC 4499 are too faint, and lie below detection limits. Some foreground Galactic dwarf star contamination is expected, their proximity making their apparent magnitude similar to distant giants. These MW dwarfs are distinguished in this study from the globular cluster by their velocities, but some small contamination is expected.

Magnesium absorption lines unique to dwarf stars can be used to distinguish them from giants (Walker et al. 2011). Increased gravity is experienced at the surface of dwarf stars compared to giants. In the atmosphere the increased density and pressure of a dwarf results in lines that are broadened compared to a giant at the same temperature. This surface gravity $log(g)$ effect on the Ca II triplet can be used to distinguish dwarfs from giants. But in this study velocity is the primary discriminator, with metallicity from the Ca II triplet as a second parameter.

2.3 Stellar Physics and Calcium Triplet Spectroscopy

Stellar nucleosynthesis theory estimates the abundances of elements which can be created in a star of a given mass. The various fusion and capture processes which give rise to the elements present in the stellar atmosphere are well understood in theory (Burbidge et al. 1957). Less clear are the plasma physics and magnetohydrodynamic currents that transport the elements from the fusion regions to the photosphere. Once in the photosphere models of stellar atmospheres are required to account for the ionisation of elements, absorption and opacity to photons, to explain the observed spectral features.

What was clear from the earliest spectroscopic studies was a marked abundance difference between certain populations which were denoted Population I and Population II stars. The more virialised and thermal nature of the kinematics of Population II stars led early authors to propose a single collapse of a proto-cloud to form the galaxy (Eggen et al. 1962). Subsequently this paradigm has been turned inside out inside out with hierarchical formation of the Galaxy

demonstrated by spectroscopic evidence of abundance patterns. Spectroscopy remains a fundamental tool in Galactic archaeology, piecing together the history of the MW from abundances and kinematics.

Stellar abundances are measured with a scale that relates the amount of iron to the amount of primordial hydrogen fusion fuel. The solar abundance is the reference point for the metallicity scale. The ratio is taken of the ratio of metals in the star to hydrogen. This is then taken as a ratio of the solar abundance of metals to hydrogen. The base 10 logarithm of this ratio is then quoted as the metallicity in the literature as dex for decimal exponent. If it has the same metallicity as the sun the ratio of stellar to solar abundance is one, and the logarithm is zero. So the abundance is quoted as [Fe/H] = 0 . A typical Population II star in a globular cluster may have an abundance of [Fe/H] = -1.0, which means its metal abundance is one tenth of solar, while [Fe/H] = -2.0 stars have abundances one hundredth of solar.

Iron is a proxy for all fusion products heavier than hydrogen, referred to rather inaccurately in the astronomical literature as "metals". A nickel isotope, which decays to iron, is the last possible product of fusion reactions with a positive net energy budget; fusion of elements to form heavier nuclei costs energy. Elements and neutron rich isotopes of elements heavier than iron are in part created by the rapid capture of neutrons in SNe II, the r-process (Seeger et al. 1965). Slow neutron capture in AGB stars with helium burning shells, the s-process, is the other way of fusing of elements heavier than iron (Schwarzschild and Härm 1967). Both processes play an equally important role in abundances of heavy elements (Cameron 1982).

Slow neutron capture requires the presence of r-process nuclei to begin with. Thus the r-process is primary and increases with importance earlier in the universe. Late life helium burning stars have strong stellar winds that distribute the s-process elements into the interstellar medium. The r-process elements are injected through explosive SNe events as well as winds. These elements take time to mix through the medium, to then be incorporated into new stellar populations.

Important to this work is the presence of the α-elements (C, N, O, Mg, Ca, Na, Ne, S, Si, Ti) (Mendel et al. 2007). α-process elements are formed by the fusion of He α nuclei with other compound α nuclei . Silicon and calcium are pure α-process elements, they are not involved in other nucleosynthesis reactions as are oxygen and magnesium, for example. Carbon arises mainly from the triple-α process, and Na from ${}^{12}_{6}C + {}^{12}_{6}C$. Silicon is only briefly involved in the fusion of iron in the final moments of super-massive stars. α-process elements are formed by nucleosynthesis within stars and in core collapse SNe II explosions. SNe II are most important in the early universe for creating and distributing O, and Ne to Ca (Maeder 1992).

In addition r-process elements are created in the core collapse. In early populations $[\alpha/Fe]$ is greater than zero dex where enrichment is dominated by SNe II. Later, as smaller stars become electron-degenerate white dwarfs they can accrete material until they become SNe Ia and mainly produce iron peak elements (Cr, Mn, Fe, Co, Ni, Cu, Zn). The point where the SNe Ia come into

play marks a decline in the $[\alpha/Fe]$ ratio relative to [Fe/H] (Mucciarelli et al. 2013). Locally in the MW $[\alpha/Fe] \approx 0.3$ for $[\alpha/H] \leq -1.0$, then $[\alpha/Fe]$ goes from 0.3 to 0 from $[\alpha/H] \approx -1.0$ to 0.0 (Mendel et al. 2007). The point of decline in the $[\alpha/Fe]$ ratio relative to [Fe/H] is different for each galaxy and cluster and depends on the IMF and SFH.

As Ca is purely an α element it makes a good indicator of global metallicity, not being involved in other nucleosynthesis processes. The Ca II triplet is empirically calibrated by comparing the observed line widths of objects whose metallicity is known from high resolution spectroscopy. The Ca II triplet lines arise from absorption by an excited state, so corrections for interstellar extinction are not as important as for the Ca II H and K blue and green lines that absorb at the ground state like the ISM (Armandroff and Zinn 1988).

Surface gravity g is related by hydrostatic equilibrium to the gas pressure P_g and density ρ in the radial direction z,

$$\frac{dP_g}{dz} = -g\rho \tag{2.2}$$

Surface gravity depends to a lesser extent upon electron pressure P_e in hydrogen dominated atmospheres. The presence of the H^- ion is the principal opacity factor in late-life RGB stars as it is ionised by $\lambda < 1.44\,\mu m$ optical to infrared flux. P_e does affect opacity and radiative equilibrium which in turn can have an effect on stellar structure (Böhm-Vitense 1989). Turbulent pressure has only been recently quantified and may contribute as much as 25% of surface pressure in RGB stars (Ludwig and Kučinskas 2012). As surface gravity decreases, so does electron pressure, and neutral calcium is more easily ionised, which serves to increase the strength of Ca II lines. Ca II triplet line widths are related to surface gravity by these pressures and by the metallicity Z. In late type stars, Ca II triplet equivalent width is proportional to ZP_g/P_e^2 (Cohen 1978).

The Ca II triplet strength was at first thought to be unrelated to metallicity. The first attempts to calibrate the Ca II triplet were for use as a luminosity measure in stellar population synthesis studies, determining the ratio of dwarfs to giants. Most galaxies have maximum energy output near 1 µm wavelength. The Ca II triplet is the strongest feature in this region that doesn't suffer from atmospheric absorption contamination and is easily observable in fainter, distant extra-galactic objects. The first quantitative studies of the effects of temperature and luminosity on the near-infrared spectra, including the Ca II triplet were undertaken in the late sixties and early seventies.

Cohen (1978) found a positive correlation of temperature T_{eff} and Ca II triplet strength, using a colour index $V-K$ to represent T_{eff}. The Ca II triplet is much stronger in red giant stars compared to dwarfs due to the low pressure and higher ionization in giant atmospheres. Cohen (1978) first proposed the Ca II triplet as a metallicity measure, once the effective temperature effect has been taken into account. The dependence on T_{eff} is a consequence of the increase of the main opacity factor, the H^- ion with increasing temperature.

Looking at a range of stellar classes Jones et al. (1984) found a simple relationship between Width (Ca II triplet) and *log* g, where δlog g = 1 gives a 1 Å change in equivalent width of the Ca II triplet, from M5 though to F0 spectral classes. However they found only a weak dependence on metallicity, with metal poor stars having slightly weaker lines. A later reanalysis of this data in a meta study found that there was in fact an effect of metallicity on the width of the Ca II triplet feature (Alloin and Bica 1989).

The interest in the Ca II triplet increased as silicon array detectors became common and were also more efficient in the infrared. This wavelength region is dominated by older populations of stars. The Ca II triplet feature is prominent in stars of spectral type F5 and redder (Diaz et al. 1989). In the integrated light from galaxies the Ca II triplet wavelength region is dominated by giants (Alloin and Bica 1989).

Theoretical models of line formation have been difficult. The wings of the lines are formed deep in the photosphere, whereas the core of the line is formed in the lower chromosphere (Linsky et al. 1970). The chromosphere in the sun at least is less dense and cooler at lower heights and gets hotter and denser as height increases. The opposite is true of the photosphere. In the 80's reliable models that assumed LTE were only available for the photosphere.

LTE models were formulated that gave calculations of line wing profiles in good agreement with observations (Smith and Drake 1987; Smith and Drake 1990). They also suggest that calcium would be a consistent measure of [α/Fe] abundances. They found that the Ca II triplet wings are actually more sensitive to [Fe/H] than *log* g. This is because electron and gas pressure increase together with increased gravity, but their effects vary inversely. Higher gas pressure weakens the line strength (Jørgensen et al. 1992), lower electron pressure increases absorption and enhances the lines. Increased metallicity also increases the electron density, as ionized Ca, Mg, Fe, and Si provide the electrons in the photosphere. The same fractional change in surface gravity has less effect than the same change in metallicity.

In environments where [α/Fe] abundance is super-solar, the elements magnesium and silicon, along with calcium contribute most of the electrons in the photosphere along with iron, in stars less than 6000 K Smith and Drake (1987). Ca is a highly robust proxy for metallicity in stars below 6000K for this reason. Cooler stars than M3 have strong molecular lines in this near-infrared region due to TiO and CN (Kordopatis et al. 2011). Because the [α/Fe] ratio is roughly constant for low metallicity [Fe/H] $\leq$ -1.0 stars in the MW, calcium is an appropriate metallicity measure for metal poor objects. The [α/Fe] plateau occurs at a lower metallicty in the LMC and at different points in different objects, depending on the influence of SNe enrichment history. The Ca II triplet still gives robust results in the LMC (Van der Swaelmen et al. 2013).

The effect of metallicity on line wings increases with temperature and with decreasing surface gravity (Smith and Drake 1990) so RGB stars are an ideal environment for Ca II triplet as a metallicity measure. Unlike Jones et al. (1984), Smith and Drake (1990) didn't find a simple relation with *log* g, but like Cohen (1978) found that temperature plays a role and also show metallicity

needs to be taken into account.

The Ca II triplet was first applied to RGB stars in globular clusters for all the reasons outlined above. Authors in observational studies usually take the sum of the equivalent widths of the two strongest lines, 8542 and 8662 Å, in order to increase signal to noise and to reduce the effect of irrelevant lines. While high resolution spectra can give detailed abundance estimates, this is difficult for faint distant objects such as halo clusters and galaxies. Here the Ca II triplet is most effective. Armandroff and Da Costa (1991) used Gaussian fitting to the line profiles. In this study it is found that a Gaussian fit underestimates the wings, which are most sensitive to metallicity. Other authors also found that Gaussian alone underestimates the line width (Cole et al. 2004; Suntzeff et al. 1992). Cole et al. (2004) found that the sum of a Gaussian and a Lorentzian makes a better fit to the line profile.

Armandroff and Da Costa (1991) also calibrate the *log* g and T_{eff} effect out using magnitude as a proxy for both these parameters. Height on the RGB indicates increasing radius and decreasing surface gravity. By fitting a linear relation between magnitude, referenced to the horizontal branch magnitude they define a reduced equivalent width value which indicates the line strength after the effects of surface gravity and temperature are taken in to account. Ttheir sample is only over a limited range of metallicities, from about -0.5 to -2.0. They note that the relation is simple for [Fe/H] ≤ -0.12, but could be complicated at higher metallicity.

The dependence of the Ca II triplet on surface gravity for younger population stars is an effective tool for the discrimination of giants from dwarfs. This was the earliest use of the Ca II triplet near-infrared feature, but it was noticed that metallicity affected line width strongly in low metallicity objects. The effect of gravity on the line widths is dominant for young and solar metallicity stars (Bica and Alloin 1987). For low metallicity stars [Fe/H] ≤ -0.5 the gravity effect is approximately linear and the main factor in line width is metallicity. A tight correlation for below solar metallicity globular cluster stars is found by Armandroff and Zinn (1988).

The Ca II triplet as an abundance measure has been popular since the early 90's as a tool for abundances in distant halo globular clusters and the Magellanic clouds. Medium resolution spectra are adequate to measure the Ca II triplet in the brightest red giants in these distant objects. Armandroff and Da Costa (1991) found the most robust measure was a sum of (two) Ca II triplet lines corrected for magnitude, as a proxy for surface gravity, the measure proving especially accurate at metallicities, [Fe/H]≤ -1.2. Rutledge et al. (1997) define a metallicity scale based on Ca II triplet measurements of globular clusters which have been well studied with a variety of methods. Using 71 GCs they relate the previous standard system, the metallicity scale of Zinn and West (1984) with the high dispersion spectra derived scale of Carretta and Gratton (1997) to the Ca II triplet equivalent width measure. Once again the Ca II triplet triplet is only able to be compared and calibrated successfully with other scales up to [Fe/H] ≤ -0.5 dex.

The Ca II triplet method is particularly useful for large studies with multi-

object spectrometry and medium resolution spectra; many stars can be studied to give robust sample statistics for populations. Many early studies rely on a handful of high resolution spectra to draw conclusions about cluster velocities and metallicities. Cole et al. (2005) showed that it was possible to apply the method to LMC galaxy RGB field stars with a variety of abundances and ages. Warren and Cole (2009) introduced the use of K_S band magnitudes from 2MASS for calibration of Ca II triplet equivalent widths. This study confirmed the approach with a single stellar population in IC 4499 (Hankey and Cole 2011). This study of the LMC field is the first time the method has been applied to mixed populations. Additional checks were made to ensure the method was valid, see Appendix D.

There are some cautionary caveats to the Ca II triplet as an [Fe/H] abundance measure. Some stellar populations exhibit odd α element ratios. Some maybe lacking in Al, some are lacking in Mg (Mucciarelli et al. 2012; Gratton et al. 2012). These metallic elements ionize and contribute to the electron pressure in stellar atmospheres. Changing abundances can affect the electron pressure P_e and the opacity and hence the line width of the Ca II triplet spectral feature. The Ca II triplet equivalent width is expected to be anti-correlated with these metallic *alpha* abundances. Imbalances in heavy iron peak elements, and Ca seem to be quite rare. But large variances in the abundances of light α elements, O, Mg, Al, Na are more common. If an imbalance in α elements is at play, it may cancel out, with a lack of one electron provider, compensated by another electron provider. Gratton et al. (2012) found an anti-correlation of [Al/Fe] and [Mg/Fe]. However a lack of electron providers in some of the population will manifest as a spread in the range of Ca II triplet values. In an homogenous population it may result in an over-estimate of the metallicity, from the Ca II triplet width, due to a lack of an electron provider.

2.4 AAOmega Spectrograph

The Anglo-Australian Telescope primary instrument is the AAOmega multi-object spectrograph. It comprises a fibre positioning system at the prime focus of the telescope, which feeds fibres that run 38 metres downstairs to the spectrograph itself (Sharp et al. 2006). The fibres have a diameter that covers 2.0 arcseconds, and the median seeing at the AAO is 1.5 arc seconds. The preceding spectrograph, the 2dF, sat atop the telescope at the prime focus with the fibre positioner. The current arrangement is more stable as it doesn't move.

The AAOmega spectrograph has two light paths. A dichroic filter separates the red and the blue wavelengths into two light paths and two independent grating and camera arms. The grating itself is a volume-phase holographic transmission grating. The transmission of light through a clear medium reduces the light loss in comparison to a reflection grating. The grating is encased within the material and so is easier to handle for the operators of the spectrograph compared to the easily damaged ultra-fine reflective surface gratings. The material has a three dimensional structure of varying refractive index giving differential

phase shifts for each wavelength. The incoming stellar light from each optic fibre is separated by the 1700D grating into unique ray paths for every frequency to yield a resolution of 0.9 Å per pixel at the Charge Coupled Detector in the near-infrared.

The 1700D grating employed in this study has a resolution of $\sim 10,000$ in the near-infrared, which covers 845.900 nm and includes the calcium triplet absorption feature around 860 nm. The resolution of VPH gratings is wavelength dependent, at the near-infrared the highest resolution is achieved as the wavelength is largest compared the scale of the refractive structure.

The AAOmega medium resolution spectrograph is now complemented by the high resolution HERMES spectrograph, fed by the same 2dF fibre positioner. The resolution is about 30,000 in the infrared 759 , to 789 , with three other simultaneous blue, green, red beams. It doesn't cover the Ca II triplet in the near-infrared. The scientific rationale for the HERMES spectrograph is also Galactic archaeology though detailed abundances and velocities (Freeman and Bland-Hawthorn 2002).

Bibliography

D Alloin and E Bica. A comparative study of NA I and CA II infrared lines in stars, star clusters and galaxy nuclei - an alternative to the dwarf-enriched population. *Astronomy and Astrophysics (ISSN 0004-6361)*, 217:57–65, June 1989.

T. E. Armandroff and G. S. Da Costa. Metallicities for old stellar systems from Ca II triplet strengths in member giants. *Astron.J*, 101:1329–1337, April 1991. doi: 10.1086/115769.

T. E. Armandroff and R. Zinn. Integrated-light spectroscopy of globular clusters at the infrared CA II lines. *Astron.J*, 96:92–104, July 1988. doi: 10.1086/114792.

H. A. Bethe. Energy Production in Stars. *Physical Review*, 55:434–456, March 1939. doi: 10.1103/PhysRev.55.434.

E Bica and D Alloin. Near-infrared spectral properties of star clusters and galactic nuclei. *Astronomy and Astrophysics (ISSN 0004-6361)*, 186:49–63, November 1987.

E. Böhm-Vitense. *Introduction to stellar astrophysics. Vol. 2. Stellar atmospheres.* Cambridge University Press, 1989.

E. M. Burbidge, G. R. Burbidge, W. A. Fowler, and F. Hoyle. Synthesis of the Elements in Stars. *Reviews of Modern Physics*, 29:547–650, 1957. doi: 10.1103/RevModPhys.29.547.

A. G. W. Cameron. Nuclear Reactions in Stars and Nucleogenesis. *Publications of the Astronomical Society of the Pacific*, 69:201, June 1957. doi: 10.1086/127051.

A. G. W. Cameron. The heavy element yields of neutron capture nucleosynthesis. *Astrophys. and Space Sci.*, 82:123–131, February 1982. doi: 10.1007/BF00651468.

E. Carretta and R. G. Gratton. Abundances for globular cluster giants. I. Homogeneous metallicities for 24 clusters. *Astron. Astrophys. Suppl. Ser.*, 121:95–112, January 1997. doi: 10.1051/aas:1997116.

M Catelan. Horizontal branch stars: the interplay between observations and theory, and insights into the formation of the Galaxy. *Astrophysics and Space Science*, 320:261–309, April 2009.

J G Cohen. Near-infrared luminosity-sensitive features in M dwarfs and giants, and in M31 and M32. *Astrophysical Journal*, 221:788–796, May 1978.

A A Cole, T A Smecker-Hane, E Tolstoy, T L Bosler, and J S Gallagher. The effects of age on red giant metallicities derived from the near-infrared CaII triplet. *Monthly Notices of the Royal Astronomical Society*, 347:367, 2004.

Andrew A Cole, Eline Tolstoy, John S Gallagher, and Tammy A Smecker-Hane. Spectroscopy of Red Giants in the Large Magellanic Cloud Bar: Abundances, Kinematics, and the Age-Metallicity Relation. *The Astronomical Journal*, 129:1465, March 2005.

A. W. J. Cousins. VRI photometry of southern stars. *South African Astronomical Observatory Circular*, 1:234–256, 1980.

Angeles I Diaz, Elena Terlevich, and Roberto Terlevich. Near-IR features in late type stars - Their relation with stellar atmosphere parameters. *Monthly Notices of the Royal Astronomical Society (ISSN 0035-8711)*, 239:325–345, July 1989.

O J Eggen, D Lynden-Bell, and A R Sandage. Evidence from the motions of old stars that the Galaxy collapsed. *Astrophysical Journal*, 136:748, November 1962.

Ken Freeman and Joss Bland-Hawthorn. The New Galaxy: Signatures of Its Formation. *Annual Review of Astronomy and Astrophysics*, 40:487–537, 2002.

R. L. Gilliland and A. K. Dupree. First Image of the Surface of a Star with the Hubble Space Telescope. *Astrophys. J., Lett.*, 463:L29, May 1996. doi: 10.1086/310043.

Raffaele G Gratton, Eugenio Carretta, and Angela Bragaglia. Multiple populations in globular clusters. Lessons learned from the Milky Way globular clusters. *The Astronomy and Astrophysics Review*, 20:50, February 2012.

W. J. Hankey and A. A. Cole. Radial velocity and metallicity of the globular cluster IC4499 obtained with AAOmega. *Mon. Not. R. Astron. Soc.*, 411: 1536–1546, March 2011. doi: 10.1111/j.1365-2966.2010.17788.x.

I. Iben, Jr. Stellar Evolution Within and off the Main Sequence. *Ann. Rev. Astron. Astrophys.*, 5:571, 1967. doi: 10.1146/annurev.aa.05.090167.003035.

H. L. Johnson. The Absolute Calibration of the Arizona Photometry. *Communications of the Lunar and Planetary Laboratory*, 3:73–77, 1965.

H. L. Johnson and W. W. Morgan. Fundamental stellar photometry for standards of spectral type on the revised system of the Yerkes spectral atlas. *Astrophys. J.*, 117:313, May 1953. doi: 10.1086/145697.

J E Jones, D M Alloin, and B J T Jones. The infrared CA II triplet - A luminosity indicator for stellar population synthesis. *Astrophysical Journal*, 283:457–465, August 1984.

U. G. Jørgensen, M Carlsson, and H R Johnson. The Calcium Infrared Triplet Lines in Stellar Spectra. *Astronomy and Astrophysics*, 254:258, February 1992.

Daisuke Kato, Chie Nagashima, Takahiro Nagayama, Mikio Kurita, Joel F Koerwer, Toshihide Kawai, Tomoyasu Yamamuro, Takahiro Zenno, Shogo Nishiyama, Daisuke Baba, Ryota Kadowaki, Yasuaki Haba, Hirofumi Hatano, Hideyuki Shimizu, Mamiko Nishimura, Tetsuya Nagata, Shuji Sato, Yuka Murai, Takahiro Kawazu, Yasushi Nakajima, Hidehiko Nakaya, Ryo Kandori, Nobuhiko Kusakabe, Akika Ishihara, Nagisa Kaneyasu, Jun Hashimoto, Motohide Tamura, Toshihiko Tanabé, Yoshifusa Ita, Noriyuki Matsunaga, Yoshikazu Nakada, Koji Sugitani, Ken-Ichi Wakamatsu, Ian S Glass, Michael W Feast, John W Menzies, Patricia A Whitelock, Pieter Fourie, John Stoffels, Geoff P Evans, and Tetsuo Hasegawa. The IRSF Magellanic Clouds Point Source Catalog. *Publications of the Astronomical Society of Japan*, 59: 615, June 2007.

A. Khokhlov, E. Mueller, and P. Hoeflich. Light curves of Type IA supernova models with different explosion mechanisms. *Astron. Astrophys.*, 270:223–248, March 1993.

G. Kordopatis, A. Recio-Blanco, P. de Laverny, A. Bijaoui, V. Hill, G. Gilmore, R. F. G. Wyse, and C. Ordenovic. Automatic stellar spectra parameterisation in the IR Ca ii triplet region. *Astron. Astrophys.*, 535:A106, November 2011. doi: 10.1051/0004-6361/201117372.

Y.-W. Lee. The chronology of the formation of the Galaxy. *Publications of the Astronomical Society of the Pacific*, 104:798–804, September 1992. doi: 10.1086/133056.

Jeffrey L Linsky, Richard G Teske, and Carol W Wilkinson. Observations of the Infrared Triplet of Singly Ionized Calcium. *Solar Physics*, 11:374, March 1970.

H G Ludwig and A Kučinskas. Three-dimensional hydrodynamical CO5BOLD model atmospheres of red giant stars. I. Atmospheric structure of a giant located near the RGB tip. *Astronomy and Astrophysics*, 547:118, November 2012.

Andre Maeder. Stellar yields as a function of initial metallicity and mass limit for black hole formation. *Astronomy and Astrophysics (ISSN 0004-6361)*, 264:105–120, October 1992.

Jon T Mendel, Robert N Proctor, and Duncan A Forbes. The age, metallicity and α-element abundance of Galactic globular clusters from single stellar population models. *Monthly Notices of the Royal Astronomical Society*, 379 (4):1618–1636, August 2007.

D. Moro and U. Munari. The Asiago Database on Photometric Systems (ADPS). I. Census parameters for 167 photometric systems. *Astron. Astrophys. Suppl. Ser.*, 147:361–628, December 2000. doi: 10.1051/aas:2000370.

A Mucciarelli, M Bellazzini, R Ibata, T Merle, S C Chapman, E Dalessandro, and A Sollima. News from the Galactic suburbia: the chemical composition of the remote globular cluster NGC 2419. *Monthly Notices of the Royal Astronomical Society*, 426(4):2889–2900, November 2012.

A Mucciarelli, M Bellazzini, M Catelan, E Dalessandro, P Amigo, M Correnti, C Cortés, and V D'Orazi. NGC 5694: another foster son of the Galactic halo. *Monthly Notices of the Royal Astronomical Society*, 435(4):3667–3680, November 2013.

P T Oosterhoff. Some remarks on the variable stars in globular clusters. *The Observatory*, 62:104–109, April 1939.

B. Pritzl, H. A. Smith, M. Catelan, and A. V. Sweigart. RR Lyrae Stars in NGC 6388 and NGC 6441: A New Oosterhoff Group? *Astrophys. J., Lett.*, 530:L41–L44, February 2000. doi: 10.1086/312482.

H. Reeves. *Stellar evolution and nucleosynthesis*. Gordon and Breach, New York, 1968.

G. A. Rutledge, J. E. Hesser, and P. B. Stetson. Galactic Globular Cluster Metallicity Scale from the Ca II Triplet II. Rankings, Comparisons, and Puzzles. *Publications of the Astronomical Society of the Pacific*, 109:907–919, August 1997. doi: 10.1086/133959.

M. Schwarzschild and R. Härm. Hydrogen Mixing by Helium-Shell Flashes. *Astrophys. J.*, 150:961, December 1967. doi: 10.1086/149396.

P. A. Seeger, W. A. Fowler, and D. D. Clayton. Nucleosynthesis of Heavy Elements by Neutron Capture. *Astrophys. J., Suppl. Ser.*, 11:121, February 1965. doi: 10.1086/190111.

R. Sharp, W. Saunders, G. Smith, V. Churilov, D. Correll, J. Dawson, T. Farrel, G. Frost, R. Haynes, R. Heald, A. Lankshear, D. Mayfield, L. Waller, and D. Whittard. Performance of AAOmega: the AAT multi-purpose fiber-fed spectrograph. In *Society of Photo-Optical Instrumentation Engineers (SPIE) Conference Series*, volume 6269 of *Society of Photo-Optical Instrumentation Engineers (SPIE) Conference Series*, July 2006. doi: 10.1117/12.671022.

M. F. et al. Skrutskie. The Two Micron All Sky Survey (2MASS). *Astron.J*, 131:1163–1183, February 2006. doi: 10.1086/498708.

G Smith and J J Drake. The wings of the calcium infrared triplet lines in solar-type stars. *Astronomy and Astrophysics (ISSN 0004-6361)*, 181:103–111, July 1987.

G. Smith and J. J. Drake. The wings of the calcium infrared triplet lines in late-type giant stars. *Astron. Astrophys.*, 231:125–130, May 1990.

Nicholas B Suntzeff, Robert A Schommer, Edward W Olszewski, and Alistair R Walker. Spectroscopy of giants in LMC clusters. III - Velocities and abundances for NGC 1841 and Reticulum and the properties of the metal-poor clusters. *Astronomical Journal (ISSN 0004-6256)*, 104:1743–1764, November 1992.

M Van der Swaelmen, V Hill, F Primas, and A A Cole. Chemical abundances in LMC stellar populations. II. The bar sample. *arXiv.org*, page 4224, June 2013.

A R Walker, A M Kunder, G Andreuzzi, A Di Cecco, P B Stetson, M Monelli, S Cassisi, G Bono, R De Propris, M Dall'Ora, J M Nemec, and M Zoccali. Constraints on the formation of the globular cluster IC 4499 from multiwavelength photometry. *Monthly Notices of the Royal Astronomical Society*, 415 (1):643–654, May 2011.

Steven R Warren and Andrew A Cole. Metallicities and radial velocities of five open clusters including a new candidate member of the Monoceros stream. *Monthly Notices of the Royal Astronomical Society*, 393(1):272–296, February 2009.

R. Zinn and M. J. West. The globular cluster system of the galaxy. III - Measurements of radial velocity and metallicity for 60 clusters and a compilation of metallicities for 121 clusters. *Astrophys. J., Suppl. Ser.*, 55:45–66, May 1984. doi: 10.1086/190947.

3

Radial Velocity and Metallicity of the Globular Cluster IC4499 Obtained with AAOmega

3.1 Introduction

IC 4499 is a sparsely populated globular cluster in a crowded Galactic field near the south celestial pole. It was discovered in 1900 by D. Stewart (Pickering 1908) and has been comparatively understudied, probably as its extreme southern declination presents an observational challenge to mid-latitude observers. Several photometric studies of IC 4499 have been undertaken to study the HB morphology, produce CMDs and make distance and metallicity estimates, but no detailed spectroscopic metallicity or radial velocity data have been published to date.

The globular cluster catalogue of Harris (1996) gives a distance of 18.9 kpc, which puts it 15.7 kpc from the Galactic centre and 6.6 kpc below the plane of the Galaxy, making it an outer halo cluster. From the vantage point of Earth, it is seen through the outer parts of the Galactic bulge ($\ell = 307.35°$, $b = -20.47°$), resulting in a relatively high reddening. This reddening has been estimated as high as E(B−V) ≈0.35 (Fourcade et al. 1974), but more recent work suggests smaller values of 0.15–0.25 (Sarajedini 1993; Storm 2004; Walker and Nemec 1996; Ferraro et al. 1995). The uncertainty in reddening has likely propagated through into differences in conclusions about the metallicity, distance, and age of IC 4499.

Low-resolution spectroscopic radial velocities and metallicities have been obtained for three RR Lyrae stars only (Smith and Perkins 1982). They obtain a metallicity of [Fe/H] = −1.33 ±0.3 from the strength of the singly-ionised Ca II K line using the ΔS method (Smith 1984). On the scale of Zinn and West (1984, ZW84) this becomes [Fe/H] = −1.5 ±0.3. Fusi Pecci et al. (1995) noted a discrepancy between photometric metallicity estimates, which tend to be around [Fe/H] ≈ −1.75 (Ferraro et al. 1995) and the generally higher spectroscopic estimates. More recent unpublished work by R. Cannon (1992) is quoted by

Sarajedini (1993) and Walker and Nemec (1996) as yielding [Fe/H] = −1.65 on the ZW84 scale, based on the near-infrared Ca II triplet lines of four red giants. Smith and Perkins (1982) also published radial velocities for their three RR Lyrae stars, -60, +10 and -101 km/s, all with an error of ±50 km/s.

No observational study of the Monoceros stream covers the neighbourhood of IC 4499. However, a set of numerical models of the stream, developed under the hypothesis that it is the remnant of a disrupting dwarf galaxy, have been proposed by Peñarrubia et al. (2005). In one of their best models, stellar debris stripped from a progenitor dwarf at $\ell = 245°$, $b = -18°$ encircles the Milky Way within ±30° of the Galactic plane, crossing the location of IC 4499 after nearly a complete wrap. Peñarrubia et al. (2005) suggested that IC 4499, along with several other clusters, could be candidate members of the stream on the basis of their position and the predicted radial velocities in their models. The radial velocity of IC 4499 has not yet been determined accurately enough to check for consistency with this type of model.

Following the methodology of Warren and Cole (2009), we have undertaken a spectroscopic study of IC 4499's red giants in order to obtain radial velocity and metallicity measurements for a large sample of cluster members; the aim is to shed light on questions of its relative age and possible membership in a stellar stream. We employ the relationship between CaII triplet line strengths and [Fe/H] to obtain metallicity estimates for individual giants. The near-infrared CaII triplet, resulting from absorption by the 3^2D–4^2P transition, is a strong feature of late-type giant stars (Armandroff and Zinn 1988). The equivalent width of the lines increases monotonically with metallicity, regardless of age, for stars older than 1 Gyr (e.g., Garcia-Vargas et al. 1998).

Spectroscopy of the near-infrared calcium triplet in spectral type K giants has become an accepted tool for assessing the metallicity of stellar populations (Armandroff and Da Costa 1991), being calibrated against Galactic globular clusters (Rutledge et al. 1997). Originally used in studies of old, simple stellar populations, the technique has been shown to apply to non-globular cluster stars, including open clusters and composite populations (e.g. Cole et al. 2004; Grocholski et al. 2006; Battaglia et al. 2008, and references therein).

The line strength has a strong dependence on surface gravity and a milder temperature dependence (Armandroff and Zinn 1988; Garcia-Vargas et al. 1998), which is removed using the empirical relationship between gravity, temperature, and luminosity for red giant stars. Rutledge et al. (1997) showed that using the stellar apparent magnitude with respect to the cluster horizontal branch is a robust approach to this procedure. Because of the availability of JHK_S photometry and astrometry in the 2MASS catalog, we adopt the K-band as our reference magnitude, following Warren and Cole (2009). Their relationship between $K-K_{HB}$, [Fe/H], and Ca II equivalent width is confirmed by our observations of IC 4499 and three other clusters.

We discuss our approach, observations, reductions, and analysis in the next section. Because using K magnitudes to correct for surface gravity is relatively novel compared to V or I, we re-derive the relation between K_s magnitude above the horizontal branch and CaII line strength. Using three well-studied

clusters as a calibration sample, we present new abundance and radial velocity measurements for IC 4499 in §3. We examine our data for signs of cluster rotation, and rule out rotation velocities in IC 4499 of 1 km/s or more. In §4 we discuss the implications of our results, including the contention that IC 4499 is younger than the bulk of halo globulars (Ferraro et al. 1995; Fusi Pecci et al. 1995), and the possibility that IC 4499 belongs to the Monoceros stellar stream (Peñarrubia et al. 2005).

3.2 Methodology

3.2.1 Observations

Observations were carried out on 28 May 2008 at the 3.9m Anglo-Australian Telescope at Siding Spring Observatory. The seeing was 1.4″. The AAOmega fibre-fed multi-object spectrograph (MOS) allows for up to 392 simultaneous spectra to be obtained, across a two degree field of view (Sharp et al. 2006). The 1700D grating was used, which gives a spectral resolution of about 10,000 [$\lambda/\Delta\lambda$], varying slightly across the field. This grating spectrum is in the near-infrared with usable $\lambda\lambda$ 8450 to 8700 Å, which includes the ionised calcium triplet lines at 8662, 8542 and 8498 Å. This feature is among the strongest lines in K-type giants (Armandroff and Da Costa 1986), which is the dominant spectral type for red giants at low-metallicity.

Targets were chosen from the 2MASS point source catalogue (PSC), which has a positional accuracy of about 100 mas (Skrutskie 2006); this accuracy is crucial to the success of the observations because of the necessity to accurately place the 2.0″ fibres on the targets. The selection was based on 2MASS J and K photometry with K between 10.5 and 15.0. Because of the slope of the RGB, the color selection had a slope as well, although quite steep. The red limit was set by $K > 27.0 - 15(J - K)$, and the blue limit was set by $K < 22.5 - 15(J - K)$. The selection region is shown on the CMD in Figure 3.1. The highest MOS fibre allocation priority was given to stars within the cluster half-light radius and in the upper 2.25 mag of the RGB.

The half-light and tidal radii of IC 4499 are 1.5′ and 12.35′, respectively (Harris 1996). Fibres were preferentially allocated to the centre of the 2° field. Once the cluster centre was sampled as densely as possible with fibres, the spare fibres were allocated to stars outside the cluster centre in the same colour and magnitude range. This should allow for a very precise characterisation of the radial velocity distribution of the field stars, to assist with membership decisions. Because of the density of the cluster, not all stars could be observed in a single setup. We observed two different fibre configurations with the same central position in order to maximise the yield of members. In total 569 individual stars were observed with signal to noise ≥ 15 per pixel in a two degree field around IC 4499; the targets are mapped in Figure 3.2. The fields were integrated over several exposures to mitigate systematic errors and cosmic ray contamination. The total exposure time for each IC 4499 setup was 3600 sec.

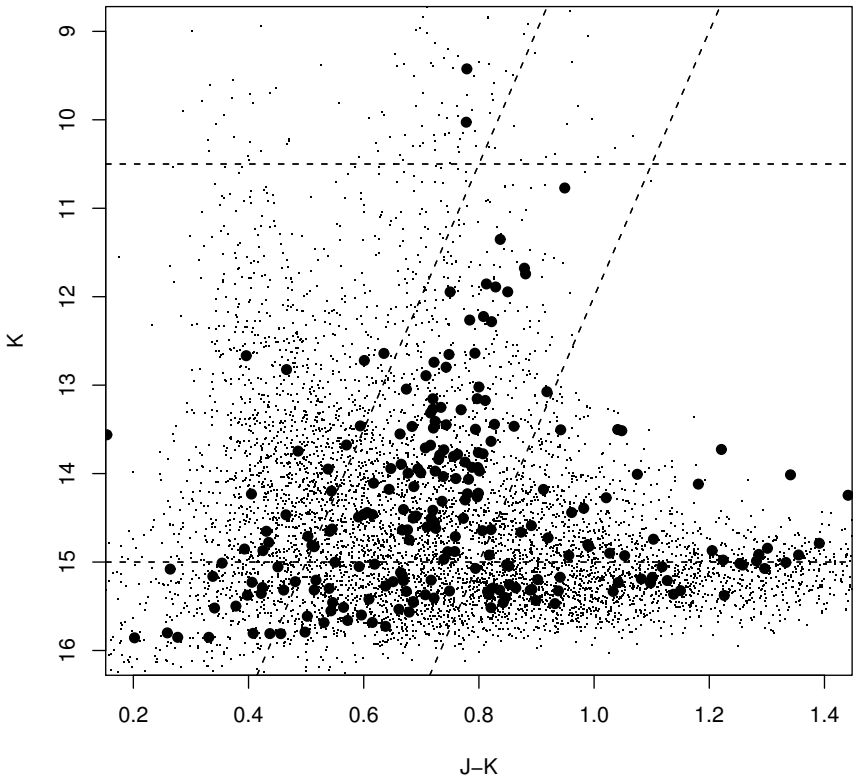

Figure 3.1: Selection of RGB stars from 2MASS PSC within 1° of the centre of IC 4499. Objects within 5′ of the cluster centre are plotted with large symbols to highlight the cluster RGB relative to the field. Our spectroscopic sample is selected from candidates within the parallelogram containing the cluster RGB.

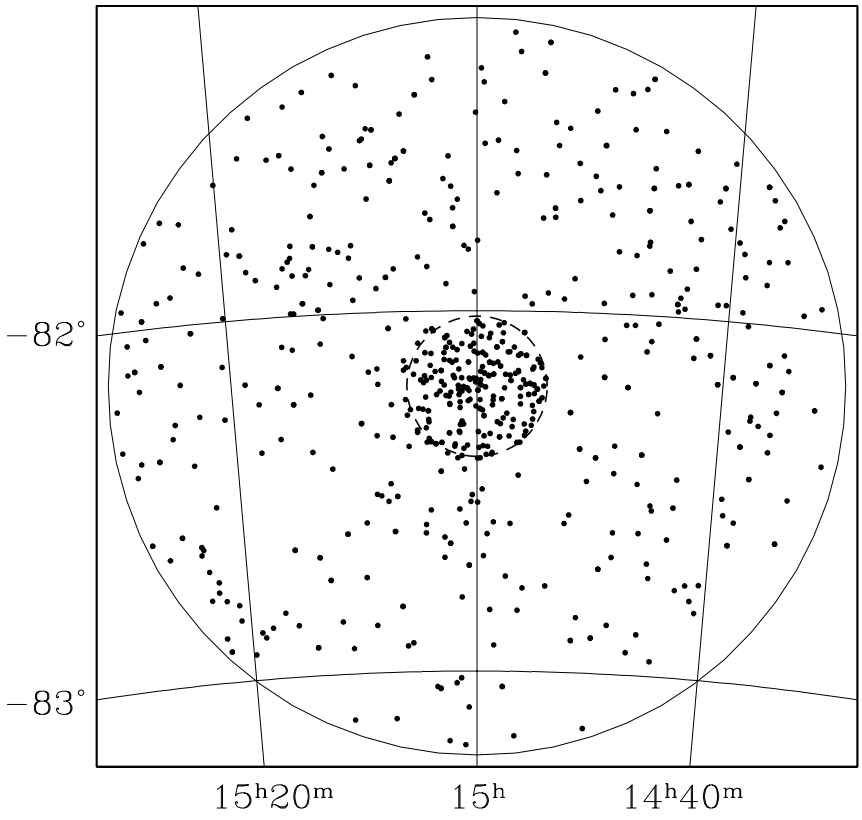

Figure 3.2: Observed targets in a 2° field around IC 4499. The tidal radius is shown by the dashed line; the fibre allocation was strongly weighted to select targets within this radius.

Three well-studied clusters were chosen as comparison objects. These were picked to yield stars of similar spectral type and metallicity to use as radial velocity templates in our cross-correlation, and to confirm that we could reproduce the relationship between K magnitude and CaT equivalent width across a range of metallicities. We used M68 (NGC 4590), M4 (NGC 6121), and M22 (NGC 6656) as our comparison objects; their positions, relevant properties, and observing details are listed in Table 3.1. For the calibration clusters, RGB stars were chosen from 2MASS J and K photometry in the regions of the selected clusters. (J−K, J) CMDs were created for square-degree areas centred on each cluster, and targets were selected from the cluster RGB locus down to and including the HB . We tried to sample as wide a range of magnitude as possible in each cluster in order to accurately model the influence of surface gravity on the CaT equivalent widths. In general, there are relatively few bright RGB stars, and the brightest, coolest stars are often contaminated by titanium oxide bands in the spectral region of interest, so sampling the bright end of the RGB while respecting the restrictions on minimum fibre spacing was a challenge. In most cases, the cluster RGB sequences are not clearly distinct from the surrounding field, and the samples were cleaned according to radial velocity and position relative to the cluster centre. The individual spectra of each target were coadded after extraction and dispersion correction.

Calibration exposures including arc lamp and screen flats were taken between each pair of science exposures in order to allow for dispersion correction and flatfielding. Sky subtraction was achieved using 20–25 dedicated sky fibres per setup, except in the case of M68, where an offset sky exposure was taken.

3.2.2 Data Reduction and Analysis

Data reduction was accomplished using the standard AAOmega reduction software *2dfdr drcontrol*. The reduction software automatically corrects for CCD bias with blank frames and an overscan bias region. Individual fibre images were traced on the CCD and then dispersion corrected, wavelength-calibrated spectra were extracted using standard procedures from arc lamp exposures and flat fields. The M68 sky subtraction was achieved by stacking and averaging the offset sky spectra. The spectra from separate exposures of the same target were combined using the IRAF *imcombine* tool. The spectra were normalised by fitting a fifth order polynomial model to the continuum with the IRAF *onedspec.continuum* task. Residual cosmic rays in the combined exposures were removed by applying simple clipping. Given the large sample size, visual inspection of each spectrum was impractical, so dead fibres, non-stellar objects, and targets with poor signal-to-noise due to fibre-centring errors were rejected automatically. Figure 3.3 shows a typical normalised spectrum. The spectral resolution achieved was 0.9 Å , with a typical signal-to-noise ratio in the continuum of 50:1 per pixel.

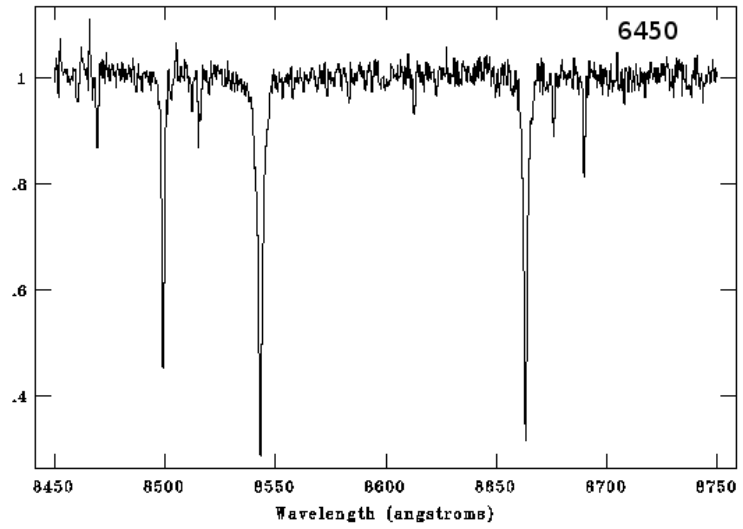

Figure 3.3: Typical spectrum of IC 4499 member RGB star showing the Ca II triplet and many weaker metal lines. Star I.D. 6450 in Table 3.3

3.2.3 Radial Velocities

After the data reduction process a total of 36 stars from the calibration clusters with velocities from the literature were chosen to be used as radial velocity templates. Published references provided online electronic data for M22 and M4 (Peterson and Cudworth 1994) (Peterson et al. 1995), which were matched with our observations using the ESO SKYCAT software tool. In the case of M68 we used the published finding charts from Harris (1975) to identify the reference stars. The chart positions were visually compared with maps made from the 2MASS catalogue to match the velocities quoted by Harris to our targets.

Of the 36 available reference stars, 19 had excellent signal to noise ratio, no cosmic rays and good sky subtraction residuals. Originally only these 19 reference spectra were employed, but it subsequently proved statistically advantageous to use all available reference spectra to reduce the standard error in the mean of the 36 cross correlations. Fifteen stars from M4, twelve from M22 and nine from M68 provided a representative sample of the reference clusters. The IRAF task *fxcor* was used to calculate the velocities of the IC 4499 stars by cross correlation with the set of reference spectra (Tonry and Davis 1979). The normalised continuum level was subtracted and a Gaussian fitted to the cross correlation to establish the velocity.

The velocity of our target stars was derived from a weighted average of cross-correlation velocities from the individual template stars. The average was constructed after automatic rejection of templates that gave large velocity er-

rors, using a Grubb test. The velocities based on each remaining template were then averaged, with weighting based on the cross-correlation errors.

Stars were defined as members of IC 4499 using three parameters. Firstly by distance from the cluster centre, stars within the tidal radius (catalogued by Harris 1996) were selected. Secondly, stars were selected around velocity over-densities. In the case of the calibration clusters these velocity distributions were located as expected according to previous studies. Stars that appeared to be normally distributed about these mean values were selected as probable members. Figure 3.4 shows the low velocity-dispersion distributions between the cluster centre and the tidal radius from which stars were selected. Some contamination of the sample from field stars with similar velocities is expected, although this is small for the calibration clusters. Stars were finally selected based on the measured equivalent widths of the three CaII triplet lines as described in the next section. Apertures were rejected in cases of low S/N, contamination by cosmic rays or other artifacts. These features resulted in odd equivalent width measurements.

The range of velocities in the disk, outer bulge, and halo towards IC 4499 is quite large, and there are several field stars projected within the tidal radius. All velocities have been translated to the heliocentric reference frame within *fxcor*, based on the time and date of the observations. The mean cluster velocities are given in Table 3.2. The velocities are in good agreement with literature references for M22 and M68, but our mean is 5.2 km/sec (4.7σ) away for M4; the origin of this difference is unknown. The mean heliocentric radial velocity of IC 4499 is 31.5 $\pm$0.4 km/sec. As seen in Figure 3.5, this is sufficiently different from the bulk of the field star velocities to allow the cluster to be defined, but there is some overlap.

3.2.4 Cluster Rotation

Lane et al. (2009) find a rotational signature in M22 and a suggestion of one in M68. They also find rotation in M4 (Lane et al. 2010). While we have a much smaller sample of stars, we can also look for such a signature. We employ Lane et al. (2009)'s method to look for signatures of rotation in M4, M22 and M68 as a check, and then in IC 4499. The position angle of the cluster rotation axis is not known a priori, so a search of parameter space is made to see if the cluster radial velocities are consistent with rotation around an arbitrary axis. For a given trial position angle we divide the cluster in half along a line 90° away and compare the mean velocity in each half of the cluster. We step around the cluster in position angle increments of 22.5°. The asymmetric sky distributions of the samples, (see Figure 3.5), alias with bin sizes and angular location adding to uncertainty. The differences in mean radial velocity between the cluster halves at each position angle are plotted in Figure 3.6.

We agree with Lane et al. (2009) on the rotation amplitude in M22: we find a line of sight rotational value of 1.8 $\pm$0.7 km/s and the axis of rotation approximately North-South, at $114° \pm 18°$, where they found 1.5 ± 0.4 km/s, approximately North-South. M4 shows amplitude 2.1 ± 0.4 km/s and axis roughly

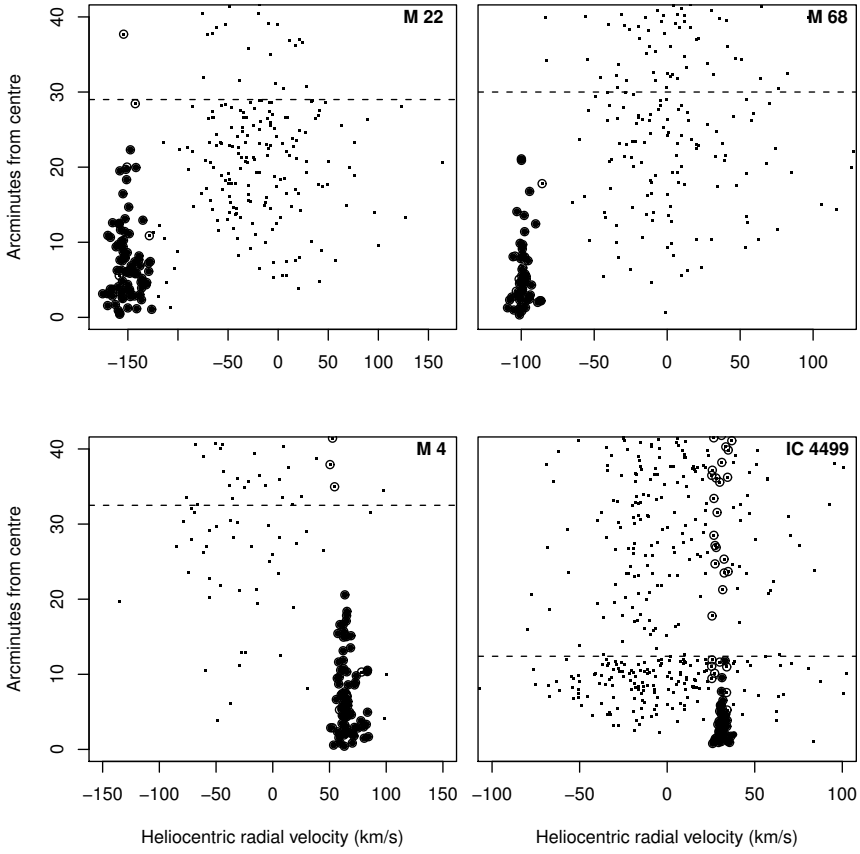

Figure 3.4: Velocities and distances from the cluster centres. The tidal radii are shown by dashed lines. Stars within the tidal radius that survived a radial velocity and metallicity clieaning are shown as solid circles . Open circles mark stars with a radial velocity that matches the cluster but fall outside the tidal radius, or have Ca II equivalent widths much different from the cluster members.

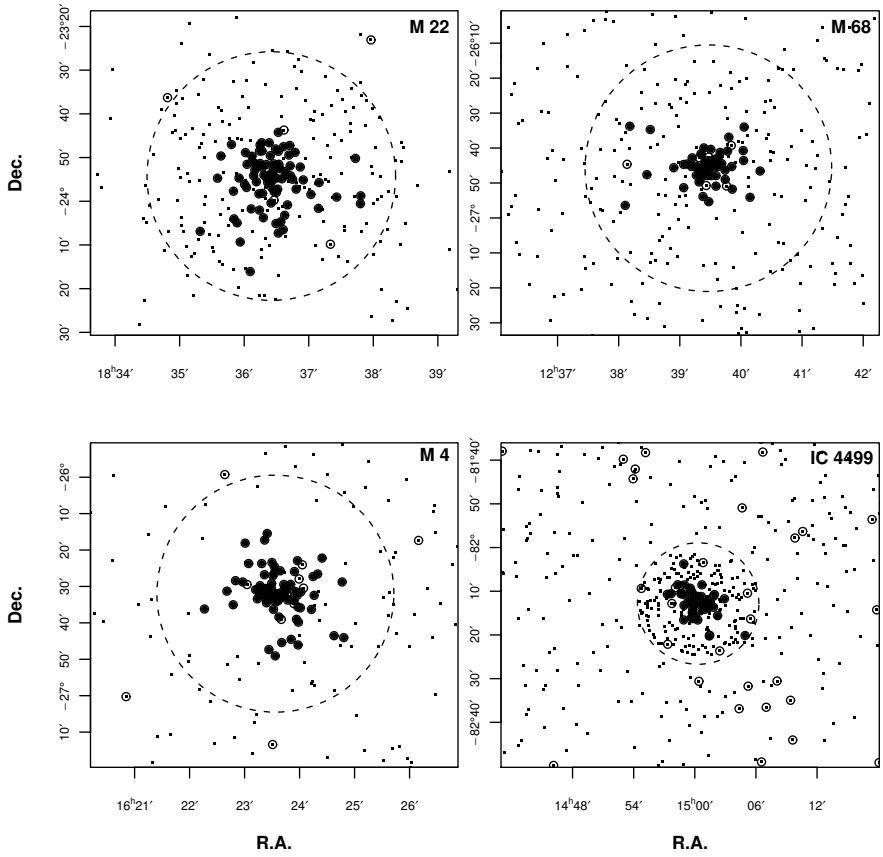

Figure 3.5: Cluster member map. Solid circles are cluster members. Open circles with similar velocities were rejected for lying outside the tidal radius, (dashed line), as metallicity outliers, or for contaminated spectra.

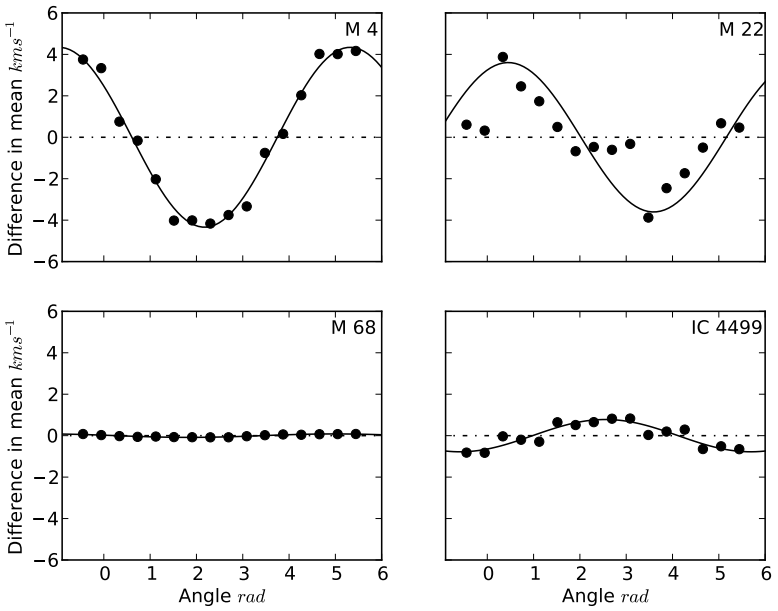

Figure 3.6: Results of cluster rotation searches shows the difference in mean radial velocity between two halves of the cluster divided by a line orthogonal with the listed position angle. Position angle is defined anticlockwise from East (PA=0) through North (PA= $\frac{\pi}{2}$) around the centre of light of the cluster. The best-fitting sine curve is shown.

North East-South West at $30^\circ \pm 12^\circ$, about double the result of Lane et al. (2010) who obtain 0.9 $\pm$0.1 km/s at an angle of 70° as do Peterson et al. (1995). There is no evidence for cluster rotation in the data for M68 and IC 4499 above the error level of 0.4 km/s. Our M22 and M4 data show that we are sensitive to rotation velocities down to at least $\approx$1 km/s, and this must therefore be a strict upper limit to the rotation of IC 4499. No correction for rotational velocity in IC 4499 is necessary when calculating velocity dispersion in the following section.

3.2.5 Virial Mass and Mass to Light Ratio

In order to estimate the cluster mass we need to assume a model for the cluster gravitational potential and use the central velocity dispersion, σ_0, and the virial theorem. Following Lane et al. (2010), a Plummer-type spherical model for the cluster mass distribution is used, (Plummer 1911). Assuming isotropic velocities

one can calculate a mass using the central velocity dispersion σ_0, where,

$$M = \frac{64\sigma_0^2 R}{3\pi\mathcal{G}}$$

where R is the half-light, or scale, radius and $\mathcal{G}$ is the gravitational constant.

To estimate σ_0, Lane et al. (2010) first bin the velocities by radius, then use a MCMC technique to estimate dispersions within the bins and subsequently fit a Plummer model. We have taken a different course, preferring not to bin the velocities, but choosing instead to fit the Plummer model to the individual data points. We assume that the individual observations are Normally distributed

$$v_i \sim \mathrm{N}\left(\mu, \sigma^2(r)\right)$$

where the line of sight velocity dispersion $\sigma(r)$ is determined by a Plummer model

$$\sigma^2(r) = \frac{\sigma_0^2}{\sqrt{1 + (r/R)^2}}.$$

Here σ_0, the central velocity dispersion, is the main parameter of interest, R the half light radius and μ the systemic mean cluster velocity. Assumptions are made about the initial distributions of parameters, an improper uniform prior for μ, and weakly informative Normal priors for R and σ_0. We then fit the model by MCMC using a Metropolis within Gibbs algorithm (Gilks et al. 1998). There were 26×10^3 samples drawn, with the first 6×10^3 discarded as 'burn-in', an initial period where the Markov Chain explores parameter space.

The median value of the distribution of σ_0 samples is 2.5 $\pm$0.5 km/s. The median is used as an estimator as the distribution is skewed toward higher values, because the model has a lower bound for central velocity dispersion at zero, but no upper bound. Velocity dispersion has not been constrained to zero at the tidal radius as in a King model (King 1966). The mean value is thus slightly higher at 2.6 km/s. The value of μ, the cluster mean systemic velocity from MCMC simulation is 31.5 km/s and agrees with the classical sample mean estimator, the sum of velocities divided by the number of samples. The value of the half light radius from simulation is $102 \pm 18''$ and agrees within error with the starting reference value of $107 \pm 19''$ (Trager et al. 1993).

The distribution of cluster mass, a function of the velocity dispersion samples from MCMC simulation, is shown in Figure 3.7. The median mass is $93 \pm 37 \times 10^3 M_\odot$ where the error is 1σ. McLaughlin and van der Marel (2005) also estimate a mass for IC 4499 using a power law model, as well as King and Wilson models, fitted to the light distribution of the cluster. They obtain mass estimates of $125 - 138 \times 10^3 M_\odot$ for IC 4499 and central velocity dispersions of 2.88 $-$ 2.96 km/s. This spectroscopic study finds a lower value but agrees with the photometry-based results within errors. For an absolute magnitude $M_V = -7.33$, we estimate a mass to light ratio of 1.3 $\pm$0.5 M/L_V in solar units. Our lower mass gives a smaller value than McLaughlin and van der Marel (2005) who estimate 1.874. This M/L_V ratio is similar to other globulars and indicates that there is not a significant dark matter component to the cluster.

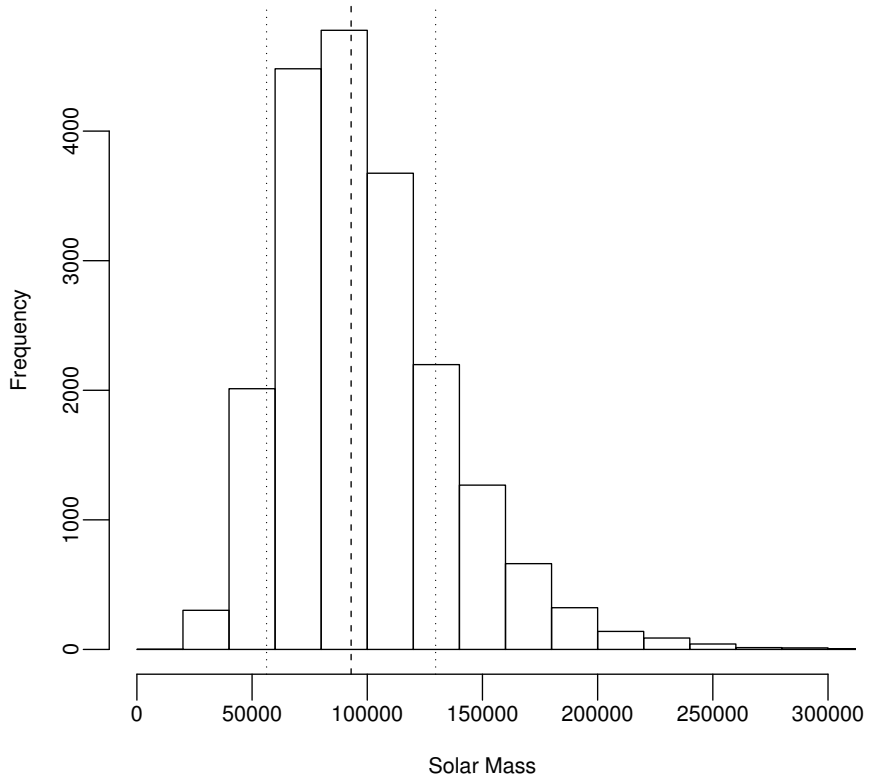

Figure 3.7: Distribution of Markov Chain Monte Carlo simulations of mass, based on a central velocity dispersion model. Standard deviation $37 \times 10^3 M_\odot$ is shown around the median value, $93 \times 10^3 M_\odot$.

3.2.6 Equivalent Widths and Metallicities

The cluster samples are each assumed to represent a single stellar population. The sample does not include any stars above the RGB tip, where lower surface gravity results in the line width being more sensitive to metallicity (Garcia-Vargas et al. 1998), or low temperature M stars where line width responds more to effective temperature resulting in lower values, and TiO bands confuse the interpretation.

Low signal-to-noise spectra in which one or more of the Ca II triplet lines were badly distorted were rejected. As a diagnostic we compared the ratios of each line with respect to the others. A line with too large or small a value with respect to the others indicates a problem with the data or the line fitting results. Spectra with odd line ratios were rejected from further analysis. In Figure 3.8 the ratios are plotted for an IC 4499 cluster sample to identify outliers.

A wavelength range is chosen in the spectrum that encompasses the line feature and a representative portion of the normalised continuum. The line and continuum bandpasses are taken as defined in Armandroff and Da Costa (1991). The sum of a Gaussian and a Lorentzian, a Penny function, is fitted to the line profiles using the same FORTRAN code as Cole et al. (2004), which is a modified version of the code of Armandroff and Da Costa (1986), to give an equivalent width for each line. The Penny function has been shown to be a better approximation for high metallicity, high resolution spectra (Warren and Cole 2009). Model atmospheres of late-type giants indicate the wings are more sensitive to metallicity than other parameters such as surface gravity and effective temperature (Smith and Drake 1990).

The equivalent widths of the three triplet lines are summed to give the CaII index. Some authors sum the two strongest lines for low signal to noise data or low resolution spectra (Rutledge et al. 1997). Here, having a high signal to noise ratio, the sum of three lines is taken to give the full equivalent width ΣW. Results for ΣW in the sample stars in IC 4499 are shown in Table 3.3.

Next a reduced equivalent width W' is derived in which the linear dependence on the magnitude height on the RGB is taken into account. This *magnitude* parameter represents the effects of the effective temperature and stellar surface gravity on the line strengths (Armandroff and Da Costa 1991). Because red giants lie along a narrow sequence in the luminosity (surface gravity) vs. temperature plane, T_{eff} and log$g$ are correlated with each other and their influence on ΣW can be calibrated out using a single observable. Colour and absolute magnitude have both been used in the past to create the index W$'$, but the most robust method in the presence of distance and reddening uncertainties is to use an expression relating the magnitude of the target star to the mean magnitude of the horizontal branch (or red clump) of its parent population (Rutledge et al. 1997).

Owing to the availability and homogeneity of 2MASS near-infrared magnitudes, we adopt the procedure of Warren and Cole (2009) and use the K-band magnitude, K$-$K$_{HB}$ to derive W'. Warren and Cole (2009) defined W$'$ = ΣW $+0.45$(K$-$K$_{HB}$); because it is uncommon to use the K band in this procedure,

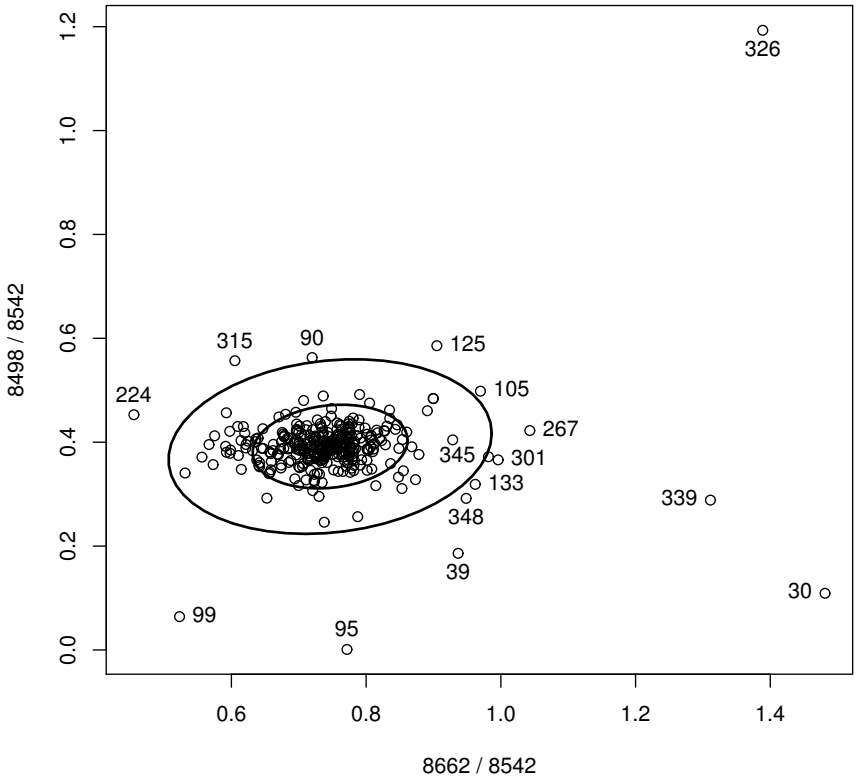

Figure 3.8: Plot of line width ratios of apertures in an IC 4499 field, with 50% and 95% confidence contour. Outlying points were considered statistically unlikely, and rejected aperture numbers are shown .

the slope is not as well-determined as that in V or I, so we rederive the relationship as a consistency check.

The mean value of the RR Lyrae variable magnitudes is used to define the horizontal branch K-magnitude, 12.21 for M22, 11.13 for M4 and 15.97 for IC 4499. K-magnitudes for RR Lyrae variables in IC4499 are found in Storm (2004) and define the magnitude of the horizontal branch. There are K-magnitudes for a few RR Lyrae stars in M22 (Kaluzny and Thompson 2001), and several for M4 (Liu and Janes 1990). Many more M4 variables are listed in Longmore et al. (1990). RR Lyrae variables in M22 and M4 were identified from those catalogued in Clement et al. (2001) and these were astrometrically correlated with 2MASS objects to obtain K magnitudes. The M68 horizontal branch K-magnitude of 14.4 is referenced from Ferraro et al. (2000) and Dall'Ora et al. (2006). For each cluster K_{HB} is taken to be constant and each star in the 2MASS PSC has a unique $K-K_{HB}$.

We plot the relative magnitude $K-K_{HB}$ against the equivalent width ΣW in Figure 3.9. The slopes of the lines β_K range from $0.29 \leq \beta_K \leq 0.65$, with a mean value of 0.47 $\pm$0.08 Å/mag. This agrees well with the value of $\beta_K = 0.48 \pm 0.01$ found by Warren and Cole (2009), who have 22 clusters, open and globular, in their sample. There is no strong reason to suspect variation in β for a globular cluster-only sample (Rutledge et al. 1997), so we adopt the better-determined value $\beta_K = 0.48 \pm 0.01$ from Warren and Cole (2009). The *reduced* equivalent width W', is the intercept of this linear model. W′ should be a constant for each cluster that only depends on metallicity. Fits to our four clusters and the literature slope are shown in Figure 3.9 and the values of W′ listed in Table 3.2.

W' is related linearly to [Fe/H] on the Carretta and Gratton (1997) scale; we follow Warren and Cole (2009) who arrived at the following relation for transforming to metallicity:

$$[Fe/H] = (-2.738 \pm 0.063) + (0.330 \pm 0.009)W'$$

The values of [Fe/H] derived from this relationship are given in Table 3.2. They agree with the literature values to better than 1σ, as expected. As emphasised by Cole et al. (2004); Warren and Cole (2009), these values are specific to the Carretta and Gratton (1997) metallicity scale. Recalibration to ZW84, the scale of Kraft and Ivans (2003), or any other metallicity scale of choice may be achieved using the W′ values, which give the correct relative metallicity ranking of the clusters no matter the specific W′-[Fe/H] conversion adopted.

3.3 The Velocity and Metallicity of IC 4499

Identifications, positions, velocities and equivalent widths for individual IC 4499 stars are given in Table 3.3. The metallicity of IC 4499 is very similar to the mean metallicity of M22, [Fe/H] = −1.52 ±0.12, and the radial velocity is v_r = 31.5 ±0.4 km/s. This is the first published spectroscopic metallicity measurement for the cluster based on more than just a few stars. Previous estimates for the radial velocity varied widely and are difficult to properly assess.

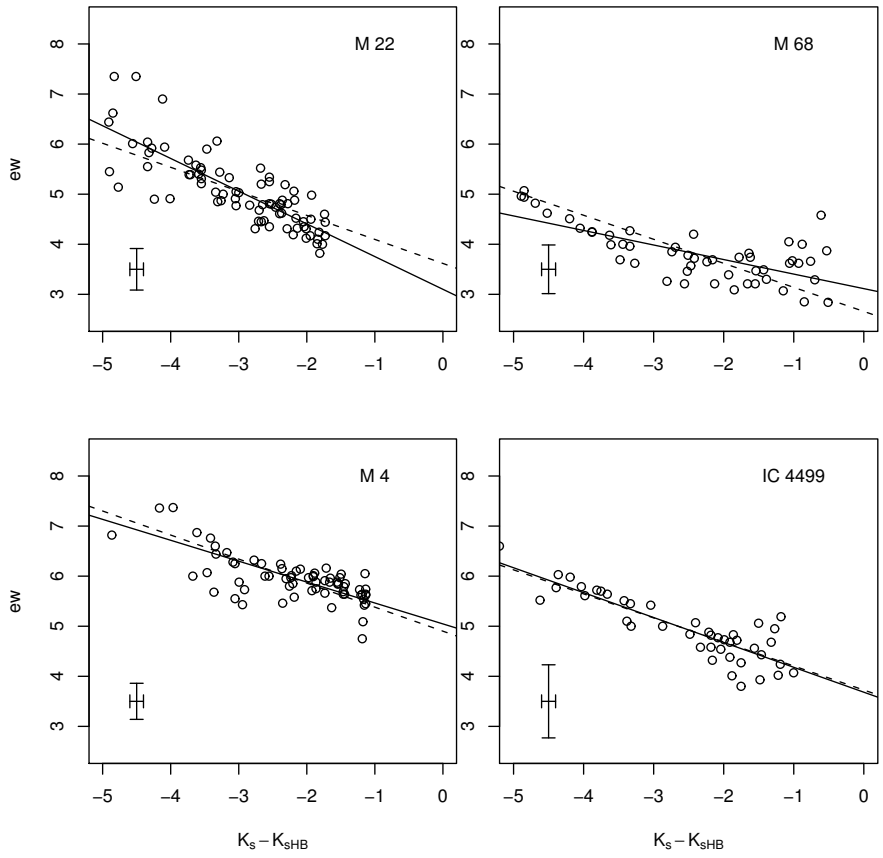

Figure 3.9: K−K_{HB} vs. ΣW for our clusters. The dashed line shows the average slope from Warren and Cole (2009), and the solid lines give the best-fit slope for each individual cluster based on our data. Typical errorbars are shown in the lower left of each panel. The intercept of the relation defines the *reduced* equivalent width W′ for each cluster.

Smith and Perkins (1982) derived a spectroscopic metallicity of [Fe/H] = −1.33 ±0.3 from three RR Lyrae variables in IC 4499. ZW84 revise this figure by recalibrating to the scale of Frogel et al. (1983) and quote [Fe/H] = −1.5 ±0.3. Ferraro et al. (1995) found this value to be too high, and adopted −1.75 based on the CMD morphology, primarily HB type and RGB colour. Later studies of the RR Lyrae population (e.g., Walker and Nemec 1996) found no inconsistencies with this value, and cite an unpublished study by R. Cannon finding [Fe/H] = −1.65 in support. Our value of [Fe/H] = −1.52 ±0.12 on the Carretta and Gratton (1997) scale translates to [Fe/H] = −1.74 ±0.10 on the ZW scale. M22, a cluster with very similar W′, has [Fe/H] = −1.75 according to Carretta and Gratton (1997), and [Fe/H] = −1.9 on the scale of Kraft and Ivans (2003), according to Da Costa et al. (2009). The latter paper also finds strong evidence for an internal spread of metallicities in M22 of up to 0.5 dex, so more detailed comparison to M22 may only serve to confuse the picture. However, we can confirm that the RR Lyrae-based result from Smith and Perkins (1982) for IC 4499 is too metal-rich, and the CMD results are robust.

The radial velocity measurement is relatively unexceptional, as a wide range of velocities are expected towards the 4th quadrant of the Galaxy. The Besançon model Galaxy (Robin et al. 2003) shows that radial velocities toward IC 4499 have a broad maximum around −15 km/s, with FWHM ≈60 km/s. If only the stars with [Fe/H] ≤ −1 are considered, the mean radial velocity is expected to be ≈25 km/s, with a very broad distribution: the FWHM of metal-weak stars in this direction is ≈110 km/s, and with tails reaching to $-150 \lesssim v_r \lesssim +350$ km/s. IC 4499 thus lies near the peak of the expected radial velocity distribution of halo stars in this direction. We are in disagreement with the average velocity of 3 RR Lyrae stars, −50 km/s, reported by Smith and Perkins (1982). Other velocity measurements are scarce; Peñarrubia et al. (2005) place IC 4499 in their Fig. 11 with $v_r = 0$, without attribution. Similarly, Fusi Pecci et al. (1995) give the cluster a Galactocentric radial velocity $v_{r,GC} \approx -130$ km/s, also without citing a source. The Fusi Pecci et al. (1995) value is not far from the measured value of v_r if we account for the solar motion; we find $v_{r,GC} = -140$ km/s.

3.3.1 Is IC 4499 Unusual?

IC 4499 has an exceptionally high frequency of RR Lyrae stars (e.g., Walker and Nemec 1996, and references therein), and has been proposed to be 2–4 Gyr younger than the average of metal-poor clusters (Ferraro et al. 1995). It is also a candidate to belong to halo substructures (Fusi Pecci et al. 1995), including the possibility of membership in the Monoceros tidal stream if that structure is due to the dissolution of a dwarf galaxy in the tidal field of the Milky Way (Peñarrubia et al. 2005). These suggestions hint towards the idea that the HB morphology can be connected to some combination of age and/or detailed elemental abundance ratios (e.g., differences in [α/Fe]). A further clue may be in the fact that the cluster is of OoI, that is, the RR Lyrae stars have periods $\lesssim$0.6 d. Catelan (2009) class IC 4499 as OoInt, as at 0.58 it is close to the edge of the OoI classification. This may place it in the range of OoInt that are

associated with the dSph populations of accreted clusters distinct from ancient halo clusters.

It is well-known that the Oosterhoff type of a cluster is related to its metallicity (e.g., Walker and Nemec 1996), but the relation is not a straightforward one. In general, the period of the variation increases with decreasing metallicity, but several clusters have been found that appear to break the rules. NGC 6388 and NGC 6441 (Pritzl et al. 2000), are metal-rich clusters displaying properties of both Oosterhoff types, metal-rich and long-period.

Sandage (1993) noted that there are very few variables in clusters with $-1.7 \leq$ [Fe/H] ≤ -1.9 on the ZW84 scale, and that the few known RR Lyrae stars present have longer than expected periods. However, he assumed [Fe/H] $= -1.5$ for IC 4499, where it should have a [Fe/H] $= -1.75$ on the ZW84 scale. Clusters of similar metallicity indeed tend to have much smaller specific frequencies of RR Lyrae stars (e.g., M22 has $S_{RR} = 7.2$, Harris 1996). This is likely because most of the HB stars at this metallicity begin their lifetimes well to the blue of the RR Lyrae instability strip (Lee et al. 1990). The extremely high specific frequency of RR Lyrae stars at the metallicity of IC 4499 suggests a larger than average stellar mass at the ZAHB . As noted by Walker and Nemec (1996), this could be indicative of a younger than average age for the cluster, or it could suggest a smaller-than-average amount of mass-loss along the cluster RGB ; Sandage (1993) already suggested that a smaller-than-average *dispersion* in mass-loss was necessary to reproduce the colour extent of IC 4499's HB . IC 4499's lower-than-average central density compared to clusters like M3 may be related to its RGB mass-loss behaviour. It is also possible that variations in the detailed elemental abundances, such as [O/Fe], play a role in determining the HB morphology.

We find M22 to have similar average metallicity to IC 4499; it has few RR Lyrae stars, a blue HB , and a higher central density, and is an OoII type cluster. This makes the 2 clusters something like a classical "second parameter" pair like M3 and M2, both with [Fe/H] ≈ -1.6 on the CG97 scale. Lee and Carney (1999) have proposed that there is an age difference between the two clusters of ≈2 Gyr, in accordance with the arguments in, e.g., Lee (1992). This is similar to the argument in Ferraro et al. (1995) that IC 4499 is ≈2–4 Gyr younger than similar-metallicity halo clusters. However the picture is complicated here because of the existence of a significant range of abundances in M22 (Da Costa et al. 2009). IC 4499 appears to have a slightly unusual Lee (1989) HB type for its metallicity, but a younger than average age cannot definitely be stated to be the cause. According to the models in Lee (1992), an age difference of $\lesssim$1 Gyr compared to M3 would be required to account for the relatively red HB morphology; the difference would be smaller if smaller-than-average mass-loss is adopted. Comparing to the HB types of other candidate "young" globulars, IC 4499 is likely to be significantly older than Rup 106, and some of the outer halo clusters like Pal 4 and Eridanus. This complicates the suggestion in Fusi Pecci et al. (1995) for a common origin shared between Rup 106 and IC 4499.

Salaris and Weiss (2002) found that IC 4499 was nearly coeval with other intermediate-metallicity clusters However, they assumed an incorrect metallic-

ity, [Fe/H] = −1.26 (CG97), and the comparison should be redone using the more accurate value [Fe/H] = −1.52 ±0.12. Salaris and Weiss (2002) conclude that all clusters with [Fe/H] ≤ −1.2 appear to be coeval within errors, at an age of ≈12 Gyr. Forbes and Bridges (2010) argue that there is a break in the age-metallicity relation for Galactic globular clusters at [Fe/H] ≈ −1.5. While there exists a class of old clusters at higher metallicity, there appears to be a group of young clusters with metallicities above the break point which they identify as accreted "young halo" clusters. Like Salaris and Weiss (2002), Forbes and Bridges (2010) find those classified as "old halo" are roughly coeval at ≈12.8 Gyr. If a reanalysis of the cluster CMD is made, using the new spectroscopic metallicity, that still suggests an age difference relative to the bulk of halo globulars, then the conclusion of Salaris and Weiss (2002) would be challenged and it would suggest that IC 4499 belongs to the "young" group of Forbes and Bridges (2010) clusters.

Carollo et al. (2007) hypothesise that halo objects are divided into two main classes, with the outer halo having lower metallicity and odd orbits suggesting accretion from low-mass dwarf galaxies, while the inner halo is higher metallicity and Galactic in origin. IC 4499 has a smaller Galactocentric distance than typical outer halo clusters, but its location where models predict an extension of the Monoceros tidal stream (Peñarrubia et al. 2005) may strengthen the idea that it has an extragalactic origin. The evidence for membership in the Monoceros stream to date has been based solely on its position within a modeled extension of the stream. At the location of IC 4499, these models predict a radial velocity that ranges between -60 km/s $\leq v_r \lesssim 100$ km/s, which has nearly complete overlap with the standard Galactic halo model for this sightline (Robin et al. 2003). An interesting feature of the Peñarrubia et al. (2005) model is that as in Fusi Pecci et al. (1995), Rup 106 and IC 4499 are suggested to be members of a single dynamically-related feature, but in the Monoceros stream model Rup 106 belongs to the trailing side of the tidal stream, while IC 4499 is a member of the leading stream. Both clusters have drifted a large distance from their progenitor: nearly 360° in the case of IC 4499, more than a complete wrap for Rup 106, and their apparent positioning as neighbours along a single great circle is coincidental.

Using the methodology of van den Bergh (1993) to classify the orbital parameters of IC 4499, the cluster is likely to be in a prograde orbit that is of a "plunging" type. However, the cluster lies near the limit for circular orbits, suggesting that there is a relatively high likelihood that it is on a mildly eccentric orbit. Placing the cluster in context, it appears quite normal for its Galactocentric distance and metallicity, and membership in a tidal stream is not needed to explain its radial velocity. Because the predicted radial velocity of the Monoceros tidal stream is consistent with the expectations for the general field, further information is necessary before IC 4499 can definitely be assigned membership in a stream, or be inferred to have been accreted into the halo from a dwarf galaxy. Two observables that could help discriminate between models are the cluster proper motion and the detailed abundance ratios of the member stars.

The Monoceros stream model that matches the position and distance of IC 4499 predicts a range of proper motions in Galactic coordinates, $(-4, -1) \lesssim (\mu_l, \mu_b) \lesssim (-2, +2)$ mas/yr. On the other hand, the Besançon model suggests that most late-type halo stars at IC 4499's location will have proper motions of $(\mu_l, \mu_b) \approx (-5\pm5, 0\pm5)$ mas/yr. From this it can be seen that a proper motion in the appropriate range for stream membership is not sufficient to ensure membership, since halo stars overlap in both components (although less so in μ_l). Proper motions could make a strong negative test in that the cluster could be excluded from stream membership via this measurement.

Detailed abundance ratios are a stronger test, because of the consistency of elemental abundance ratios among field and cluster halo stars (e.g., Fulbright 2000, 2002) and the strong anomalies seen in dwarf spheroidal galaxy field stars (e.g., Shetrone et al. 2003; McWilliam and Smecker-Hane 2005; Chou et al. 2010) and clusters (e.g., Bellazzini et al. 2008; Carretta et al. 2010, and references therein). In particular the [α/Fe] vs. [Fe/H] trend and ratios of s- and r-process elements can give strong clues to the past star-formation history, initial mass function sampling, and loss of metals from a stellar system (Tolstoy et al. 2003; Venn et al. 2004). Because IC 4499 is not a very massive cluster, it is expected to be chemically homogeneous, and high-resolution spectra of just a few stars should suffice to begin characterisation of its nucleosynthetic history.

Acknowledgments

The AAO is funded by the British and Australian governments. WJH acknowledges the support of the Grote Reber Foundation. This publication makes use of data products from the Two Micron All Sky Survey, which is a joint project of the University of Massachusetts and IPAC/Caltech, funded by NASA and the NSF. This research has made use of the WEBDA database, operated at the Institute for Astronomy of the University of Vienna. IRAF is distributed by the National Optical Astronomy Observatories. The European Organisation for Astronomical Research in the Southern Hemisphere (ESO) maintain and distribute SKYCAT. Thanks to Dr. Simon Wotherspoon of the University of Tasmania for scripting the MCMC algorithm.

Table 3.1: Log of Observations

Target	α (J2000)[a]	δ (J2000)[a]	UT start	Airmass	Seeing ($''$)	t_{exp} (s)	[Fe/H] (dex)[b]	V_r (km/s)
M68	12 39 28	−25 15 39	11:43:55	1.06	1.4	2×360	−1.99 ±0.06	−96.4 ±3.9[c]
M4	16 23 34	−26 32 01	18:16:28	1.72	1.4	2×180	−1.19 ±0.03	70.9 ±0.6[d]
M22	18 36 25	−23 54 16	19:14:59	1.32	1.4	2×180	−1.48 ±0.03[†]	−148.8 ±0.8[e]
IC 4499 1	15 00 21	−82 12 46	13:09:58	1.60	1.4	2×1800		
IC 4499 2	15 00 22	−82 12 52	15:34:27	1.67	1.4	2×1800		

[a]Centre of AAOmega/2dF field; [b]Carretta and Gratton (1997); [c]Geisler et al. (1995); [d]Peterson et al. (1995); [e]Peterson and Cudworth (1994). [†]A significant range is present (Da Costa et al. 2009).

Table 3.2: Summary of results.

Cluster	$N_\star$	W′ (Å)	K_{HB} (mag)	[Fe/H]	Δ[Fe/H]	V_r (km/s)	ΔV_r (km/s)
M68	51	2.59 ±0.35	14.4[a]	−1.88 ±0.13	0.11 ±0.14	−98.6 ±1.5	−4.2 ±4.2
M4	70	4.90 ±0.34	11.13	−1.12 ±0.14	0.07 ±0.14	65.7 ±0.9	5.2 ±1.1
M22	81	3.61 ±0.46	12.21	−1.55 ±0.17	−0.07 ±0.17	−150.5 ±1.3	−1.7 ±1.5
IC 4499	43	3.70 ±0.29	15.97	−1.52 ±0.12		31.5 ±0.4	

[a]Dall'Ora et al. (2006). Δ Difference, measured−literature value.

Table 3.3: IC 4499 Members.

ID	α(J2000)[a]	δ(J2000)[a]	V_r (km/s)	ΣW (Å)	K_S[a] (mag)
4976	14:59:33.41	-82:09:17.80	31.40±1.49	5.51±0.36	12.55
4983	15:01:05.98	-82:12:36.93	31.21±1.49	5.00±0.52	12.65
5034	14:58:38.62	-82:10:30.86	32.42±1.46	4.27±0.66	14.22
5420	15:00:42.16	-82:08:32.40	32.88±1.93	4.73±0.90	13.98
5437	15:01:49.80	-82:13:39.74	31.16±1.48	5.06±0.94	14.47
5447	14:59:01.37	-82:10:50.80	28.91±1.96	5.07±0.70	13.57
5478	14:58:54.40	-82:16:34.04	33.44±1.46	4.58±0.56	13.79
5488	15:02:14.17	-82:15:35.02	30.88±1.49	4.95±1.33	14.70
5595	14:59:46.75	-82:16:15.61	30.47±1.49	5.64±0.46	12.31
5644	14:59:40.00	-82:12:22.84	27.48±1.48	4.77±0.68	13.89
5649	14:58:19.16	-82:08:30.86	30.89±1.66	6.03±0.45	11.61
5914	14:58:56.49	-82:13:14.09	32.28±1.46	3.80±0.81	14.22
5916	14:58:54.78	-82:03:44.48	31.29±1.67	5.72±0.49	12.16
5971	15:00:38.30	-82:11:12.03	30.18±1.40	6.60±0.49	10.77
6150	14:59:50.74	-82:13:10.60	30.86±1.49	4.32±0.61	13.81
6210	14:59:18.66	-82:12:40.50	30.62±1.93	5.45±0.46	12.64
6266	15:00:05.66	-82:15:51.72	34.06±1.65	4.24±1.01	14.78
6302	15:00:10.58	-82:11:17.03	31.88±1.50	5.70±0.40	12.22
6370	14:57:18.38	-82:10:41.52	31.84±1.48	4.43±0.84	14.51
6389	15:01:25.51	-82:20:14.43	30.99±1.49	5.61±0.27	11.99
6450	15:01:55.59	-82:10:45.69	34.28±1.49	5.10±0.47	12.59
6478	14:59:45.22	-82:14:47.23	29.58±1.47	4.88±0.57	13.76
6688	15:04:56.01	-82:20:08.58	33.09±1.63	5.19±1.45	14.79
6689	15:01:21.54	-82:13:45.49	31.71±1.30	4.56±0.91	14.41
6693	15:01:31.47	-82:12:24.68	29.63±1.44	3.93±0.91	14.49
6698	15:00:17.12	-82:16:35.09	29.65±1.48	5.00±0.37	13.10
6703	15:00:34.26	-82:14:45.50	38.08±1.49	5.52±0.40	11.35
6710	14:59:47.84	-82:14:13.06	36.36±1.39	4.02±1.08	14.75
6718	15:00:06.81	-82:11:52.33	26.83±1.48	4.54±0.62	13.93
6732	15:01:05.76	-82:12:57.37	28.30±1.50	4.82±0.69	13.79
6847	15:00:51.51	-82:12:50.99	34.76±1.58	4.07±1.39	14.97
6850	15:02:54.39	-82:11:43.51	31.56±1.93	5.42±0.50	12.93
7024	14:58:40.81	-82:10:36.05	31.65±1.50	4.01±1.14	14.09
7088	14:59:55.26	-82:13:13.16	29.35±1.46	4.68±0.82	14.65
7089	15:00:58.89	-82:14:09.08	30.09±1.94	4.58±0.52	13.64
7126	14:58:59.03	-82:08:33.25	29.97±1.92	4.84±0.60	13.49
7162	15:00:47.33	-82:12:51.62	35.64±1.51	4.38±0.93	14.06
7290	15:00:39.11	-82:13:17.03	25.95±1.48	4.83±0.73	14.11
7508	14:59:42.17	-82:10:05.79	31.96±2.00	4.72±2.02	14.16
7529	15:00:17.01	-82:11:11.46	31.52±1.71	5.79±0.41	11.94
7558	14:57:40.75	-82:10:33.69	30.41±1.49	5.77±1.03	11.58
7575	14:59:40.44	-82:16:04.08	31.52±1.48	5.98±0.33	11.78
7910	14:59:47.29	-82:11:09.15	33.05±1.50	4.68±0.56	14.06

[a]From 2MASS point source catalogue.

Bibliography

T. E. Armandroff and G. S. Da Costa. The radial velocity, velocity dispersion, and mass-to-light ratio of the Sculptor dwarf galaxy. *Astron.J*, 92:777–786, October 1986. doi: 10.1086/114211.

T. E. Armandroff and G. S. Da Costa. Metallicities for old stellar systems from Ca II triplet strengths in member giants. *Astron.J*, 101:1329–1337, April 1991. doi: 10.1086/115769.

T. E. Armandroff and R. Zinn. Integrated-light spectroscopy of globular clusters at the infrared CA II lines. *Astron.J*, 96:92–104, July 1988. doi: 10.1086/114792.

G. Battaglia, M. Irwin, E. Tolstoy, V. Hill, A. Helmi, B. Letarte, and P. Jablonka. Analysis and calibration of CaII triplet spectroscopy of red giant branch stars from VLT/FLAMES observations. *Mon. Not. R. Astron. Soc.*, 383:183–199, January 2008. doi: 10.1111/j.1365-2966.2007.12532.x.

M. Bellazzini, R. A. Ibata, S. C. Chapman, A. D. Mackey, L. Monaco, M. J. Irwin, N. F. Martin, G. F. Lewis, and E. Dalessandro. The Nucleus of the Sagittarius Dsph Galaxy and M54: a Window on the Process of Galaxy Nucleation. *Astron.J*, 136:1147–1170, September 2008. doi: 10.1088/0004-6256/136/3/1147.

D. Carollo, T. C. Beers, Y. S. Lee, M. Chiba, J. E. Norris, R. Wilhelm, T. Sivarani, B. Marsteller, J. A. Munn, C. A. L. Bailer-Jones, P. R. Fiorentin, and D. G. York. Two stellar components in the halo of the Milky Way. *Nature*, 450:1020–1025, December 2007. doi: 10.1038/nature06460.

E. Carretta and R. G. Gratton. Abundances for globular cluster giants. I. Homogeneous metallicities for 24 clusters. *Astron. Astrophys. Suppl. Ser.*, 121:95–112, January 1997. doi: 10.1051/aas:1997116.

E. Carretta, A. Bragaglia, R. G. Gratton, S. Lucatello, M. Bellazzini, G. Catanzaro, F. Leone, Y. Momany, G. Piotto, and V. D'Orazi. Detailed abundances of a large sample of giant stars in M 54 and in the Sagittarius nucleus. *ArXiv e-prints*, June 2010.

M Catelan. Horizontal branch stars: the interplay between observations and theory, and insights into the formation of the Galaxy. *Astrophysics and Space Science*, 320:261–309, April 2009.

Mei-Yin Chou, Steven R Majewski, Katia Cunha, Verne V Smith, Richard J Patterson, and David Martinez-Delgado. The Chemical Evolution of the Monoceros Ring/Galactic Anticenter Stellar Structure. *The Astrophysical Journal Letters*, 720(1):L5–L10, September 2010.

C. M. Clement, A. Muzzin, Q. Dufton, T. Ponnampalam, J. Wang, J. Burford, A. Richardson, T. Rosebery, J. Rowe, and H. S. Hogg. Variable Stars in Galactic Globular Clusters. *Astron.J*, 122:2587–2599, November 2001. doi: 10.1086/323719.

A. A. Cole, T. A. Smecker-Hane, E. Tolstoy, T. L. Bosler, and J. S. Gallagher. The effects of age on red giant metallicities derived from the near-infrared CaII triplet. *Mon. Not. R. Astron. Soc.*, 347:367–379, January 2004. doi: 10.1111/j.1365-2966.2004.07223.x.

G. S. Da Costa, E. V. Held, I. Saviane, and M. Gullieuszik. M22: An [Fe/H] Abundance Range Revealed. *Astrophys. J.*, 705:1481–1491, November 2009. doi: 10.1088/0004-637X/705/2/1481.

M. Dall'Ora, G. Bono, J. Storm, F. Caputo, G. Andreuzzi, G. Marconi, M. Monelli, V. Ripepi, P. B. Stetson, and V. Testa. The RR Lyrae distance scale from near-infrared photometry: current results . *Memorie della Societa Astronomica Italiana*, 77:214–+, 2006.

F. R. Ferraro, P. Montegriffo, L. Origlia, and F. Fusi Pecci. A New Infrared Array Photometric Survey of Galactic Globular Clusters: A Detailed Study of the Red Giant Branch Sequence as a Step toward the Global Testing of Stellar Models. *Astron.J*, 119:1282–1295, March 2000. doi: 10.1086/301269.

I. Ferraro, F. R. Ferraro, F. F. Pecci, C. E. Corsi, and R. Buonanno. Young globular clusters in the Milky Way: IC 4499. *Mon. Not. R. Astron. Soc.*, 275: 1057–1076, August 1995.

D. A. Forbes and T. Bridges. Accreted versus in situ Milky Way globular clusters. *Mon. Not. R. Astron. Soc.*, 404:1203–1214, May 2010. doi: 10.1111/j.1365-2966.2010.16373.x.

C. R. Fourcade, J. R. Laborde, and J. C. Arias. The globular cluster IC 4499. *Astron. Astrophys. Suppl. Ser.*, 18:3–7, October 1974.

J. A. Frogel, J. G. Cohen, and S. E. Persson. Globular cluster giant branches and the metallicity scale. *Astrophys. J.*, 275:773–789, December 1983. doi: 10.1086/161573.

J. P. Fulbright. Abundances and Kinematics of Field Halo and Disk Stars. I. Observational Data and Abundance Analysis. *Astron.J*, 120:1841–1852, October 2000. doi: 10.1086/301548.

J. P. Fulbright. Abundances and Kinematics of Field Stars. II. Kinematics and Abundance Relationships. *Astron.J*, 123:404–412, January 2002. doi: 10.1086/324630.

F. Fusi Pecci, M. Bellazzini, C. Cacciari, and F. R. Ferraro. The Young Globular Clusters of the Milky Way and the Local Group Galaxies: Playing with Great Circles. *Astron.J*, 110:1664–+, October 1995. doi: 10.1086/117639.

M. L. Garcia-Vargas, M. Molla, and A. Bressan. Calcium triplet synthesis. *Astron. Astrophys. Suppl. Ser.*, 130:513–526, June 1998. doi: 10.1051/aas:1998237.

D. Geisler, A. E. Piatti, J. J. Claria, and D. Minniti. Lower metallicity of the Galactic globular cluster system: Calcium triplet spectroscopy of metal-poor globular cluster giants. *Astron.J*, 109:605–617, February 1995. doi: 10.1086/117305.

W. R. Gilks, S. Richardson, and D. J. Spiegelhalter. *Markov Chain Monte Carlo in Practice*. Chapman and Hall, Boca Raton, Florida, 1998.

A. J. Grocholski, A. A. Cole, A. Sarajedini, D. Geisler, and V. V. Smith. Ca II Triplet Spectroscopy of Large Magellanic Cloud Red Giants. I. Abundances and Velocities for a Sample of Populous Clusters. *Astron.J*, 132:1630–1644, October 2006. doi: 10.1086/507303.

W. E. Harris. New color-magnitude data for twelve globular clusters. *Astrophys. J., Suppl. Ser.*, 29:397–429, October 1975. doi: 10.1086/190351.

W. E. Harris. A Catalog of Parameters for Globular Clusters in the Milky Way. *Astron.J*, 112:1487, October 1996. doi: 10.1086/118116.

J. Kaluzny and I. B. Thompson. New variables in M22 globular cluster (Kaluzny+, 2001). *VizieR Online Data Catalog*, 337:30899–+, June 2001.

I. R. King. The structure of star clusters. III. Some simple dynamical models. *Astron.J*, 71:64–+, February 1966. doi: 10.1086/109857.

R. P. Kraft and I. I. Ivans. A Globular Cluster Metallicity Scale Based on the Abundance of Fe II. *Publications of the Astronomical Society of the Pacific*, 115:143–169, February 2003. doi: 10.1086/345914.

R. R. Lane, L. L. Kiss, G. F. Lewis, R. A. Ibata, A. Siebert, T. R. Bedding, and P. Székely. Testing Newtonian gravity with AAOmega: mass-to-light profiles of four globular clusters. *Mon. Not. R. Astron. Soc.*, 400:917–923, December 2009. doi: 10.1111/j.1365-2966.2009.15505.x.

R. R. Lane, L. L. Kiss, G. F. Lewis, R. A. Ibata, A. Siebert, T. R. Bedding, P. Székely, Z. Balog, and G. M. Szabó. Halo globular clusters observed with AAOmega: dark matter content, metallicity and tidal heating. *Mon. Not. R. Astron. Soc.*, pages 799–+, May 2010. doi: 10.1111/j.1365-2966.2010.16874.x.

J.-W. Lee and B. W. Carney. RR Lyrae Luminosity Differences between Oosterhoff Group I and II Cluster Systems and the Origin of the Oosterhoff Dichotomy. *Astron.J*, 118:1373–1389, September 1999. doi: 10.1086/301008.

Y.-W. Lee. *The evolution of horizontal branch stars and the calibration of globular cluster ages*. PhD thesis, Yale Univ., New Haven, CT., 1989.

Y.-W. Lee. The chronology of the formation of the Galaxy. *Publications of the Astronomical Society of the Pacific*, 104:798–804, September 1992. doi: 10.1086/133056.

Y.-W. Lee, P. Demarque, and R. Zinn. The horizontal-branch stars in globular clusters. I - The period-shift effect, the luminosity of the horizontal branch, and the age-metallicity relation. *Astrophys. J.*, 350:155–172, February 1990. doi: 10.1086/168370.

T. Liu and K. A. Janes. The luminosity scale of RR Lyrae stars with the Baade-Wesselink method. III - The absolute magnitudes of four RR Lyrae stars in the globular cluster M4. *Astrophys. J.*, 360:561–576, September 1990. doi: 10.1086/169145.

A. J. Longmore, R. Dixon, I. Skillen, R. F. Jameson, and J. A. Fernley. Globular cluster distances from the RR Lyrae log(period)-infrared magnitude relation. *Mon. Not. R. Astron. Soc.*, 247:684–695, December 1990.

D. E. McLaughlin and R. P. van der Marel. Resolved Massive Star Clusters in the Milky Way and Its Satellites: Brightness Profiles and a Catalog of Fundamental Parameters. *Astrophys. J., Suppl. Ser.*, 161:304–360, December 2005. doi: 10.1086/497429.

A. McWilliam and T. A. Smecker-Hane. The Unusual Abundance of Copper in the Sagittarius Dwarf Spheroidal Galaxy and Implications for the Origin of ω Centauri. *Astrophys. J., Lett.*, 622:L29–L32, March 2005. doi: 10.1086/429407.

J. Peñarrubia, D. Martínez-Delgado, H. W. Rix, M. A. Gómez-Flechoso, J. Munn, H. Newberg, E. F. Bell, B. Yanny, D. Zucker, and E. K. Grebel. A Comprehensive Model for the Monoceros Tidal Stream. *Astrophys. J.*, 626: 128–144, June 2005. doi: 10.1086/429903.

R. C. Peterson and K. M. Cudworth. Proper motions and radial velocities in the globular cluster M22 and the cluster distance. *Astrophys. J.*, 420:612–631, January 1994. doi: 10.1086/173590.

R. C. Peterson, R. F. Rees, and K. M. Cudworth. Radial velocities of stars in the globular cluster M4 and the cluster distance. *Astrophys. J.*, 443:124–135, April 1995. doi: 10.1086/175508.

E. C. Pickering. Nebulae discovered at the Harvard College Observatory. *Annals of Harvard College Observatory*, 60:147–194, 1908.

H. C. Plummer. On the problem of distribution in globular star clusters. *Mon. Not. R. Astron. Soc.*, 71:460–470, March 1911.

B. Pritzl, H. A. Smith, M. Catelan, and A. V. Sweigart. RR Lyrae Stars in NGC 6388 and NGC 6441: A New Oosterhoff Group? *Astrophys. J., Lett.*, 530:L41–L44, February 2000. doi: 10.1086/312482.

A. C. Robin, C. Reylé, S. Derrière, and S. Picaud. A synthetic view on structure and evolution of the Milky Way. *Astron. Astrophys.*, 409:523–540, October 2003. doi: 10.1051/0004-6361:20031117.

G A Rutledge, J E Hesser, P B Stetson, M Mateo, L Simard, M Bolte, E D Friel, and Y Copin. Galactic Globular Cluster Metallicity Scale from the Ca II Triplet I. Catalog. *Publications of the Astronomical Society of the Pacific*, 109:883, August 1997.

M. Salaris and A. Weiss. Homogeneous age dating of 55 Galactic globular clusters. Clues to the Galaxy formation mechanisms. *Astron. Astrophys.*, 388:492–503, June 2002. doi: 10.1051/0004-6361:20020554.

A. Sandage. The Oosterhoff period-metallicity relation for RR Lyrae stars at the blue fundamental edge of the instability strip. *Astron.J*, 106:687–702, August 1993. doi: 10.1086/116675.

A. Sarajedini. A CCD color-magnitude diagram for the globular cluster IC 4499. *Astron.J*, 105:2172–2181, June 1993. doi: 10.1086/116595.

R. Sharp, W. Saunders, G. Smith, V. Churilov, D. Correll, J. Dawson, T. Farrel, G. Frost, R. Haynes, R. Heald, A. Lankshear, D. Mayfield, L. Waller, and D. Whittard. Performance of AAOmega: the AAT multi-purpose fiber-fed spectrograph. In *Society of Photo-Optical Instrumentation Engineers (SPIE) Conference Series*, volume 6269 of *Society of Photo-Optical Instrumentation Engineers (SPIE) Conference Series*, July 2006. doi: 10.1117/12.671022.

M. Shetrone, K. A. Venn, E. Tolstoy, F. Primas, V. Hill, and A. Kaufer. VLT/UVES Abundances in Four Nearby Dwarf Spheroidal Galaxies. I. Nucleosynthesis and Abundance Ratios. *Astron.J*, 125:684–706, February 2003. doi: 10.1086/345966.

M. F. et al. Skrutskie. The Two Micron All Sky Survey (2MASS). *Astron.J*, 131:1163–1183, February 2006. doi: 10.1086/498708.

G. Smith and J. J. Drake. The wings of the calcium infrared triplet lines in late-type giant stars. *Astron. Astrophys.*, 231:125–130, May 1990.

H. A. Smith. Metal abundances of RR Lyrae stars - Results from Delta-S spectroscopy. *Publications of the Astronomical Society of the Pacific*, 96: 505–517, July 1984. doi: 10.1086/131370.

H. A. Smith and G. J. Perkins. Metal abundances of RR Lyrae stars in globular clusters. *Astrophys. J.*, 261:576–585, October 1982. doi: 10.1086/160368.

J. Storm. The distance to IC 4499 from K-band photometry of 32 RR Lyrae stars. *Astron. Astrophys.*, 415:987–991, March 2004. doi: 10.1051/0004-6361:20034287.

E. Tolstoy, K. A. Venn, M. Shetrone, F. Primas, V. Hill, A. Kaufer, and T. Szeifert. VLT/UVES Abundances in Four Nearby Dwarf Spheroidal Galaxies. II. Implications for Understanding Galaxy Evolution. *Astron.J*, 125:707–726, February 2003. doi: 10.1086/345967.

J. Tonry and M. Davis. A survey of galaxy redshifts. I - Data reduction techniques. *Astron.J*, 84:1511–1525, October 1979. doi: 10.1086/112569.

S. C. Trager, S. Djorgovski, and I. R. King. Structural Parameters of Galactic Globular Clusters. In S. G. Djorgovski & G. Meylan, editor, *Structure and Dynamics of Globular Clusters*, volume 50 of *Astronomical Society of the Pacific Conference Series*, pages 347–+, January 1993.

S. van den Bergh. Globular cluster orbits and second parameter effects. *Astron.J*, 105:971–975, March 1993. doi: 10.1086/116485.

K. A. Venn, M. Irwin, M. D. Shetrone, C. A. Tout, V. Hill, and E. Tolstoy. Stellar Chemical Signatures and Hierarchical Galaxy Formation. *Astron.J*, 128:1177–1195, September 2004. doi: 10.1086/422734.

A. R. Walker and J. M. Nemec. CCD Photometry of Galactic Globular Clusters.III.IC 4499. *Astron.J*, 112:2026–+, November 1996. doi: 10.1086/118161.

Steven R Warren and Andrew A Cole. Metallicities and radial velocities of five open clusters including a new candidate member of the Monoceros stream. *Monthly Notices of the Royal Astronomical Society*, 393(1):272–296, February 2009.

R. Zinn and M. J. West. The globular cluster system of the galaxy. III - Measurements of radial velocity and metallicity for 60 clusters and a compilation of metallicities for 121 clusters. *Astrophys. J., Suppl. Ser.*, 55:45–66, May 1984. doi: 10.1086/190947.

4

Large Magellanic Cloud Bar Kinematics and Metallicity with AAOmega

4.1 LMC Structure

The largest homogenous data set of late-life stars in the inner 2° of the LMC has been observed in order to address some of the fundamental questions of structure, kinematics and evolution in this nearest disk galaxy. The inner bar region has largely remained a mystery due to the difficulty of observing in this crowding-limited region. IC 4499 lay behind heavy Galactic field contamination, as described in Chapter 3. The observation and analysis of IC 4499 provided proof of the methods needed to analyse this crowded field of stars (Hankey and Cole 2011).

The LMC is the closest star forming disk galaxy to the MW. At close to 50 kpc (Gieren et al. 2005; Walker 2012) its proximity makes it possible to study individual stars, making it unique in extra-galactic astronomy as a laboratory for the study of stellar dynamics in galaxies. The AAOmega multi-object spectrograph and fibre positioner make it possible to observe objects in the crowded and high surface brightness regions at the centre of the LMC. Astrometrically accurate near infra-red catalogues are also vital, such as the Deep Near-Infrared Southern Sky Survey (Cioni et al. 2000), the Two Micron All-Sky Survey (Skrutskie et al. 2006) and the even more sensitive Infra-Red Survey Facility Magellanic Clouds Point Source Catalog (IRSF) (Kato et al. 2007).

The observations yielded an extensive sample of high-quality spectra from late-life stars in the LMC bar region, which provided measures of line of sight velocity and metallicity. MCMC statistical techniques were applied to the velocities to give robust estimates of dynamical and structural parameters for a model of the disk. Metallicity measurements provided insights into star formation history and galactic evolution.

The LMC is an easily observable naked eye disk galaxy seen almost face on. It occupies at least 20 square degrees of the southern sky, a region of $4° \times 5°$. About 21° degrees away on the sky is the visible companion SMC. The large angular extent of the LMC on the sky also means that the projection on the celestial sphere needs to be taken into account. The sky cannot be assumed to

be "flat" over such a large solid angle. The geometric projection has already been described by van der Marel et al. (2002), and subsequent authors, and this study employs their definitions and derivations.

The LMC and SMC are connected in a common HI region. The bridge of HI and stars between the galaxies is evidence of interaction between the LMC and SMC. The morphology of the LMC must also be affected to some extent by tidal interactions with the MW potential due to its proximity. There is also a possibility of DM substructure in the MW halo affecting LMC -SMC structure and motion. The internal kinematics of the LMC may hold clues to these interactions.

The LMC has been found to have two distinct components, the HI gas galaxy and the stellar disk . The HI galaxy appears more affected by environmental factors shaping the LMC (Staveley-Smith et al. 2003), tidal forces from both the MW and SMC (Olsen and Massey 2007) and possibly hydrodynamic ram stripping of gas by the MW halo. The leading South East edge of the HI disk appears to be dynamically hot, with a higher velocity dispersion, (Kim et al. 1998, Figure 8). Clumpy halo dark matter structure may also induce bar formation (Bekki 2009; Romano-Díaz et al. 2008). If the gas is preferentially affected by environment, then the stellar disk and bar retain more of the original form of the galaxy before galaxy-galaxy interactions.

The stellar disk appears quite un-disturbed in comparison to the HI. The stellar disk velocity dispersion value is at least a third of the maximum rotation velocity, (Gyuk et al. 2000) indicating that the disk is not kinematically hot, but remains rotationally supported. Unlike the MW, the old LMC stellar populations do not display a larger dispersion than the intermediate age RGB population. This indicates the lack of a pressurised halo of stars and clusters as seen around the MW.

Bessell et al. (1986) obtained one of the first spectroscopic samples of stellar velocities in the central region of the LMC. They found their small sample of very old long period variables has a systemic velocity the same as the HI gas and young objects. The velocity dispersion of $30\,\mathrm{km\,s^{-1}}$ agrees with a rotationally supported disk.

Kunkel et al. (1997) sample stars in the outer regions of the LMC. They confirm the disk nature of the galaxy and see a flattened rotation curve at large radii. Larger velocities at the very largest radii are attributed to an SMC - LMC tidal interaction. The suggestion is these stars form a polar ring, which resulted from a close SMC encounter with the outer LMC disk. Evidence for galaxy-galaxy interactions in the stellar population are not obvious. Recently, evidence of an SMC origin for kinematic outliers in the LMC have been proposed (Olsen et al. 2011). An extremely close interaction would have caused tidally stripped SMC stars to enter the LMC disk. Models have shown Magellanic self-interactions can explain the morphology of the LMC, the steam and bridge, as well as the bar feature, without invoking MW effects (Besla et al. 2012; Růžička et al. 2010). Dispensing with the need for MW interactions provides extra support for the notion that the clouds are on their first approach to the MW.

Within the gas galaxy there is evidence of two major separate kinematic components (Luks and Rohlfs 1992). In addition to the main disk 'D', which is only seen in the outer parts of the LMC, a lower velocity 'L' component may be associated with the 30 Doradus complex. This is an 'S' shaped, vaguely spiral feature. Its rotation curve follows that of the disk but is offset at a lower systemic velocity. The absence of absorption from 30 Doradus indicates it may be in front of the 'D' disk and so too is the associated L component. The 'L' component is not associated with the bar. The 'L' gas component being a prominent feature distinct from the disk has led authors to give weight to the possibility that the bar could also be separate from the disk. Separate velocity populations have not been clearly identified in the stellar population, having only been seen at marginal significance levels. Graff et al. (2000) find a sub-population at $30\,\mathrm{km\,s^{-1}}$ from the systemic velocity. This is not found in later studies.

Early studies of the disk kinematics found an S-shaped warp in the disk, especially prominent in the outer regions. A study of neutral hydrogen radio emission, Luks and Rohlfs (1992) find that what was previously thought of as a serious warp in the disk, is explained by transverse proper motion data. The magnitude of the transverse velocity has only recently been appreciated (Kallivayalil et al. 2006; Piatek et al. 2008), to the extent that the LMC may even be gravitationally unbound to the MW, (Besla et al. 2011). However the question of a disk warp still remains open. Analysis of HI velocities shows that the galaxy is well modelled by a rotating disk, with some large scale warp Kim et al. (1998). Olsen and Salyk (2002) found further evidence of a warp in the disk, using red clump magnitudes from a large photometric study of fifty fields in the outer disk regions. Their data indicates the galaxy is deformed from a flat disk in the South West region, otherwise agreeing with Marel and Cioni (2001) on the viewing angles of the main disk.

The disturbed morphology of the Magellanic system is most clearly seen in HI maps of the galaxy which also reveal a bridge of gas linking the SMC and LMC, a leading arm mainly gaseous and the Magellanic Stream of gas trailing the motion of the clouds (Staveley-Smith et al. 2003; Nidever et al. 2010). The Magellanic stream extends across half the sky and has no stellar counterpart. Prominent leading and trailing arms of gas extend well beyond the stellar disk. The centre of the stellar structure is located near the centre of the bar at the centre of the visual and infrared photometric isophotes (van der Marel et al. 2002). The dynamical centre of the gas is located about $1\overset{\circ}{.}2\pm0.6$ away from the centre of the stellar disk (Kim et al. 1998).

This study probes the inner LMC galaxy where data have been scarce. This has led to much conjecture about the nature of the bar. Using the largest homogenous set of medium resolution spectra observed to date, the nature of this most striking feature is investigated.

4.1.1 Building a Bar

The stellar bar is the most prominent feature of the LMC, easily visible by the naked eye. It is offset from the centre of the disk, which is a defining feature of the Magellanic type irregular galaxy classification proposed by de Vaucouleurs and Freeman (1972). The bar is a stellar feature not seen in the neutral H I but that is not uncommon in disk galaxies (Sellwood and Wilkinson 1993). The fields of stars observed in this study lie within the bar region of the LMC. This study investigates the nature of the bar from samples of line of sight velocities and metallicities of giant stars.

Bars in spirals are thought to arise in interacting galactic systems (Shlosman 2008). Bar formation in simulations of disk galaxies are usually a result of instabilities in the rotationally supported structure (Sellwood and Wilkinson 1993). Sources of disruption include gas inflow, accretion of minor satellites and tidal inputs from fly-bys. The bar probably drives star formation whether it is tidally induced or the result of gas accretion. LMC type irregular spiral galaxies with bars are quite common, such as NGC 4618 (Odewahn 1996). Typically the bars in these LMC type galaxies are found to have solid body rotation curves in the inner regions. In general they rotate with the disk, but are frequently sightly offset from the disk centre.

Previous studies also find no systematic variation in the stellar populations along the bar. In fact it is remarkably uniform (Nikolaev and Weinberg 2000; Cole et al. 2005). The oldest populations are the same age throughout the galaxy (Gallart et al. 2008; Smecker-Hane et al. 2002; Carrera et al. 2011), while younger and intermediate populations are preferentially found toward the inner regions. There are hints of past events triggering star formation in the LMC especially the bar, at around 4 Gyr and more recently at $\leq$1 Gyr (Harris and Zaritsky 2009; Smecker-Hane et al. 2002). The last few hundred million years have seen star formation in 30 Doradus and other regions peripheral to the bar (Harris and Zaritsky 2009).

A recent study by Haschke et al. (2012) using OGLE III RR Lyrae as standard candles conclude the bar stands out up to 5 kpc from the disk in this tracer. This vertical offset was not seen in an analysis of OGLE III red clump data by Subramaniam and Subramanian (2009). These RR Lyrae could represent a previously undiscovered halo population of the LMC rather than being tracers of the bar or disk.

Subramaniam (2003) found evidence of non-uniformity of the bar structure in the magnitudes of red clump stars from OGLE III. The suggestion is of an offset bar, possibly an accretion remnant. With a larger sample including the Magellanic Clouds Point Source Catalogue, Subramanian and Subramaniam (2010) again find a warp but in a slightly different direction. The scale of variations is about 1.5 kpc with an error of about 0.5 kpc. The warp is represented by a varying inclination angle across the face of the galaxy, with about 30° in the outer regions to as little as 16° in the central bar region. More evidence of a warped disk based on Red Clump Magnitudes as distance indicators has been found (Olsen and Salyk 2002). The location of the warp in the south-west

region of the outer disk suggests an SMC origin for the perturbation.

Suggestions of a bar structure offset from the disk (Subramaniam 2003) and a counter-rotating core (Subramaniam and Prabhu 2005) within the stellar bar have been raised. Zhao and Evans (2000) hypothesise the bar is separate from the disk and is an unvirialised structure, as does Zaritsky (2004). The spatial separation and extra depth would give the missing optical depth needed to account for microlensing event rates. They suggest that the bar and disk are misaligned in the line of sight as well as in the sky plane. The bar is proposed to be an accretion remnant core of a smaller galaxy. Following this idea up Zhao et al. (2003) find no evidence for a kinematic distinction between the disk and bar in a large spectroscopic study. However they still believe that this may be hard to see kinematically as the stars are in the same potential well, leaving open the possibility of two offset disks. This idea is pursued further in several studies (Subramaniam 2003, 2004; Subramaniam and Prabhu 2005; Subramaniam and Subramanian 2009; Subramanian and Subramaniam 2010).

Zaritsky (2004) hypothesised that the bar is in fact a bulge feature, common in disk galaxies. It appears as an off centre bar because of disk extinction of the northern hemisphere of the spheroidal bulge. They note that this novel idea would need to be proven by a large velocity dispersion finding in the central bar region. A spheroid galaxy of LMC mass would have a stellar velocity dispersion of at least $50\,\mathrm{km\,s^{-1}}$ (Gyuk et al. 2000). Later studies showed that the dispersion in the bar is not larger than in the disk, (Cole et al. 2005; Zhao et al. 2003). Bulges generally consist of old populations, and may indicate a merger history. The bulge hypothesis is not supported by the evidence.

van der Marel et al. (2002) find negative disk plane velocities in the inner 1.0 kpc, but emphasise that too much weight cannot be placed on this result as there are very small number statistics in this very inner region. If real, these negative velocities would indicate counter-rotation at the disk centre. Spectroscopic data from Zhao et al. (2003) does indeed show a local variation in the velocity gradient near the rotation centre which elsewhere trends smoothly, mainly across and slightly along the line of nodes in this region. The "V" shaped dip was noted by Subramaniam and Prabhu (2005) who correctly interpret this as further evidence for some kind of irregularity in the central bar. Their hypothesis is a counterrotating, or secondary disk feature.

The 30 Doradus complex in the North East is one of the many young clusters less than about 30 million years old associated with Shapley's constellations. Dottori et al. (1996) argue that the 30 Doradus region could be part of an offset bar that leads the stellar bar. This younger bar is a result of supersonic shocks induced by the offset stellar bar, which induced star formation as they compressed galactic HI. Clusters older than 30 million years are more closely associated with the optical stellar bar. This suggestion is of a very cosmologically recent origin for this leading bar, the cause being a slightly older but still comparatively recent stellar bar.

It may be that an off centre bar appears because of disturbances to the disk rather than the central bar region (Bekki and Chiba 2005; Bekki 2009). The bar is still at the dynamical centre of the system. The off centre bar comprises both

Table 4.1: Log of Observations

Target	α (J2000)[a]	δ (J2000)[a]	UT date	UT start	Airmass	t_{exp} (s)
LMC Bar West	05 10 00.47	−68 45 04.4	2010:01:02	16:31:32	1.58	3×1200
47 Tucanae	00 24 05.69	−72 04 53.1	2010:01:03	10:28:50	1.46	3×540
LMC Bar East	05 29 45.70	−70 05 28.3	2010:01:03	11:02:04	1.33	3×1200

[a]Centre of AAOmega-2df field

young and old LMC stellar populations. N-body simulations can produce a bar from interactions with the SMC. The suggestion is that the disk itself appears to be shifted by an interaction with some kind of MW dark halo structure. The main conclusion being that the bar already existed, as evidenced by old stellar populations in the bar.

The literature demonstrates the level of conjecture and conflicting evidence concerning the nature of the bar. The aim of this study was to obtain an homogeneous spectrographic data set that included both bar and disk stars, allowing a comparison of their properties. Only bar observations were able to be made so we supplement the study with disk data from the literature. We report on the kinematics and metallicities in two central bar fields each covering 2°, in order to shed light on the nature of the LMC bar.

4.2 Observations

4.2.1 Target Selection

The IRSF point source catalogue was used to select targets for the AAOmega observations; the catalogue goes deeper than 2MASS to a 10σ limiting K magnitude of 16.6 (Kato et al. 2007; Skrutskie et al. 2006). From the DENIS near infra-red catalogue (Cioni et al. 2000) of the Magellanic clouds a relation between I magnitude and K magnitude was found, $I_s \approx 1.01 \times Ks + 1.51$. The RGB stars are brighter at K band as expected. This relation was used to broadly compare the I magnitude used in the AAOmega signal to noise calculator and the IRSF K magnitude (Kato et al. 2007). The AAOmega sensitivity calculator indicated twenty minute exposures were needed to achieve a signal to noise ratio of 20, with seeing of 1.5" to 2.0", for I magnitudes brighter than 15.5, which translates to a K magnitude threshold of about 14. We selected Red Giant stars brighter than this limit, with magnitudes less than 13. We observed three separate exposures of fields, each for twenty minutes. See Table 4.1 for details.

CMDs were plotted for each of the ten fields covering the bar and disk, see Figure 4.1. Two populations are visible in the CMD, a Galactic RGB and a Magellanic RGB (Nikolaev and Weinberg 2000). We chose stars from the more populous Magellanic RGB with magnitudes brighter than 13, corresponding to region E in Figure 3 in Nikolaev and Weinberg (2000). We also selected from the oxygen rich asymptotic giant branch (AGB) region above the RGB tip, region

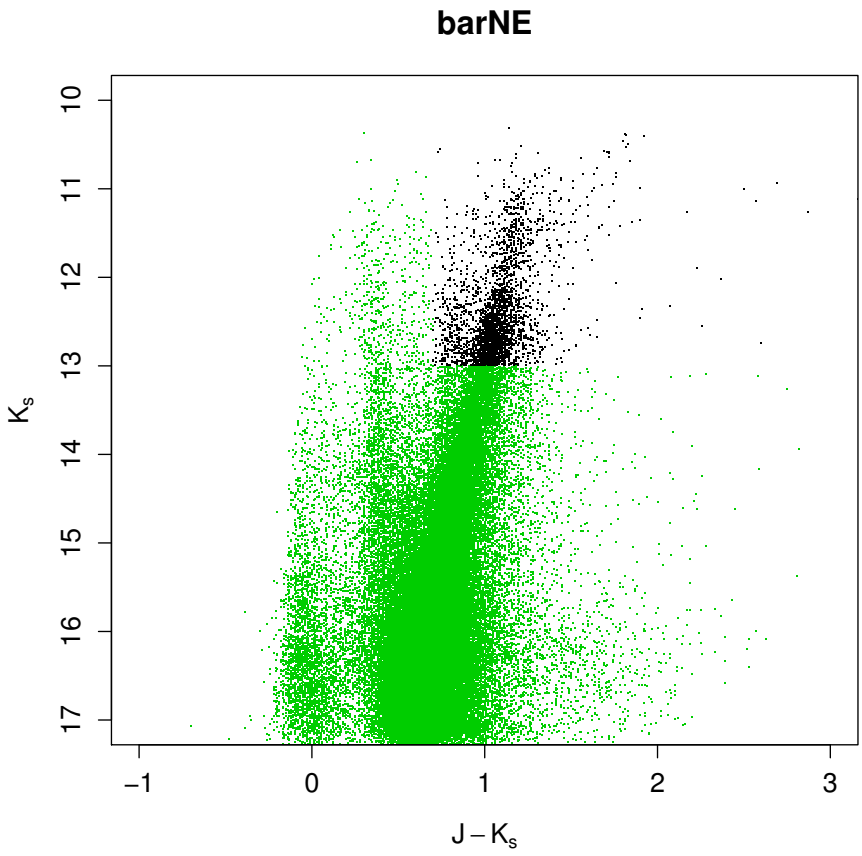

Figure 4.1: Colour magnitude target selection from the IRSF catalogue, for North East bar field.

J in Nikolaev and Weinberg (2000) which represent intermediate age stars. We also sample region I, which represents a younger population of intermediate mass giant stars. This is described as a vertical extension of the red clump defined in MACHO (Alcock et al. 2000). It is associated with the LMC and is distinguishable from the RGB below about magnitude 13 which is the region we sample (Figure: 4.1). For the purposes of the fibre configuration program we weight AGB and reddened giant stars above the RGB tip at 12.2 K magnitude by a factor of 3 so that they are as equally likely to be sampled as the much more populous RGB stars below the tip. The factor 3 is the number ratio of the two populations.

The RGB spatial density most clearly traces a bar and symmetric, undisturbed disk. The RGB stars represent an intermediate age population of about

2 Gyr and less than 6 Gyr (Cole et al. 2005), while individual stars may be up to 13 Gyr old. No dependence of stellar type or metallicity has been found in the bar region. We might expect that younger stars would be concentrated in the bar if it is a recent tidal feature that may have induced star formation. But such a population does not seem to dominate, although there are young stars in the bar. This indicates that the bar is quite an old feature. The offset nature of the bar, or conversely the disk, could be a recent phenomenon.

The potential targets are chosen if they have quality value 1 in each of J,H and K bands (Kato et al. 2007). They are sources that fit the PSF function well, are not extended or unresolved double objects, saturated, faint or "odd shaped". Additionally the IRSF adjacency criteria was used, so stars were selected only if there were no stars within the radius of the FWHM of the PSF of the object (Kato et al. 2007). The angular diameter of the AAOmega fibres is $\sim 2''$.

The dense LMC field provides a surplus of target opportunities. For each of the ten fields, the field target list was checked against every neighbouring field for duplicate targets in regions where the fields overlapped. Duplicate objects were assigned in equal numbers to one field or the other. Bright stars within a one magnitude range from 13-14 K mag were chosen from the IRSF catalogue target list as guide objects for the telescope so they had the same astrometric characteristics. Eight guide stars were chosen for the eight dedicated guide fibres and selected in a pattern that covered the field periphery evenly. Two AAOmega fibre configurations were generated for each field in case opportunities arose for extra exposures.

Critical to the success of the observations was finding good sky regions for telluric subtraction. Dark regions in the LMC were hard to find in the crowded and bright field. Digital Sky Survey red images with $1''$ resolution from the UK Schmidt telescope were plotted and emission contours added (Figure 4.3). Manual selection of sky points with the lowest emission was employed to place the sky fibre positions. Otherwise slewing away from the large LMC extent to dark sky would have been required.

Velocity reference targets in the LMC itself were Long Period Variables (LPV) chosen from Hughes and Wood (1990), whose Galactocentric velocities were converted to heliocentric for the fxcor task. This was a poor choice, as it later turned out variables don't make good reference stars. Velocity references in 47 Tucanae and Melotte 66 were originally taken from (Cole et al. 2004).

The 2MASS PSC was used for target selection and astrometry for 47 Tucanae and Melotte 66. Criteria for selection from the catalogue were AAA photometric quality, 000 confusion quality and point-like 0 extended confusion quality. The 47 Tucanae field was centred on the cluster at $00^h24'05.2'', -72°04'05''$, and Melotte 66 field at $07^h26'23'', -47°40'00''$.

Reducing the 2MASS field to 24 arcminutes the CMD of 47 Tucanae became clear (Bergbusch and Stetson 2009). The red giant branch including the red clump, the horizontal branch and associated supergiant branch extending above that were chosen. Some SMC stars may be included, mainly the brighter end supergiant, AGB, carbon and oxygen stars. The greater apparent magnitude meant we observed three exposures of nine minutes to achieve a similar signal

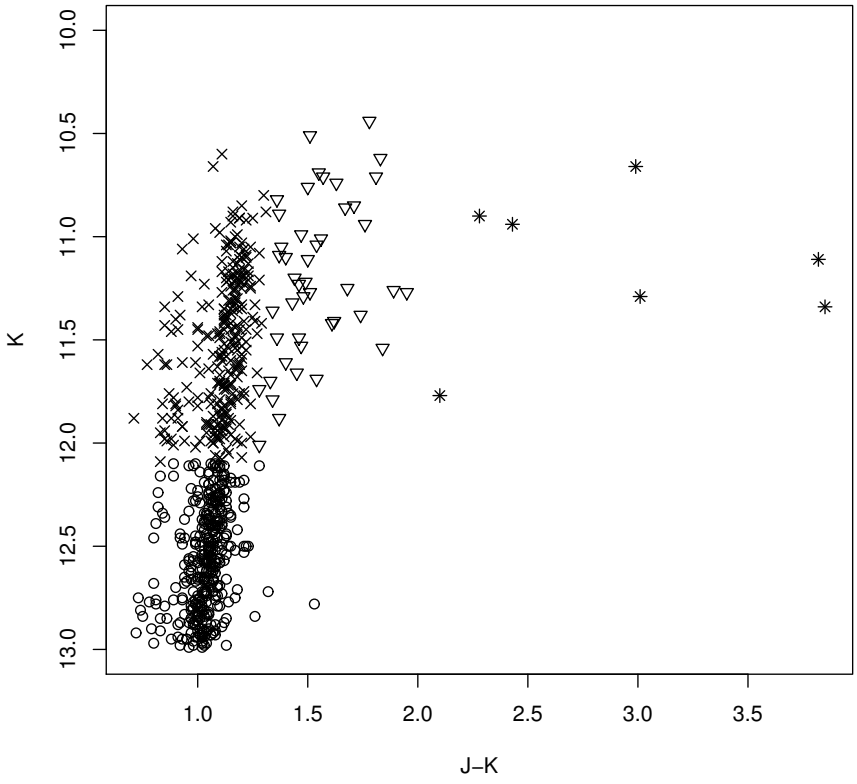

Figure 4.2: Colour magnitude diagram of the sample selected for analysis. Circles are RGB, crosses O-rich AGB, triangles C stars and asterisks C stars reddened by circumstellar dust.

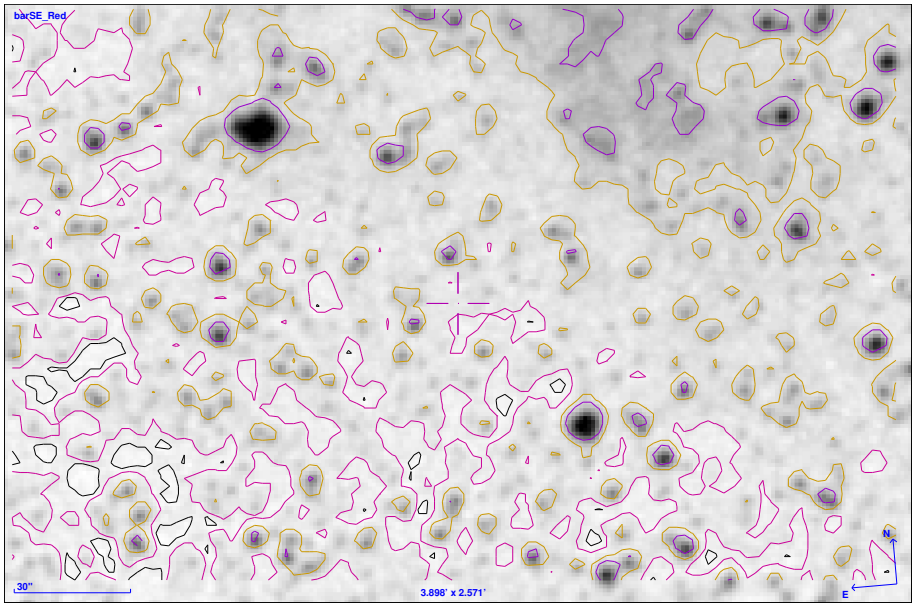

Figure 4.3: UKST DSS red image of the LMC with contours added. White regions within black contours mark low emission areas suitable for sky fibre placement.

to noise as the sixty minute LMC fields.

4.2.2 Data

Three nights were allocated but poor weather limited observations to three fields only in early January 2010. These fields are listed in Table 4.1. Two 2° fields of the central LMC bar region were observed and one field of the globular cluster 47 Tucanae, which contained many velocity template stars to be used for calibration. Three separate 20 minute exposures of each LMC bar field were made to average out cosmic ray strikes on the CCD. Flat fields and arc lamp exposures were done at the end of each observation for calibration.

A typical signal to noise ratio (SNR) for the eastern field is 35, for the western field it is a little noisier at 25 due to some light cloud near the end of the observation, Figure 4.4. There are some stars with a SNR of as little as 7, for which we get a sensible velocity, albeit with a large errors of more than $20\,\mathrm{km\,s^{-1}}$ reported by FXCOR. Later analysis suggests that even with large errors the low SNR stellar velocities are in good agreement with the high SNR stars. The Ca II triplet is such a strong feature in RGB stars that even the low SNR does not mask the information. However, we restrict our analysis to stars with a SNR of at least 15, and errors less than $20\,\mathrm{km\,s^{-1}}$. The mean error is $6\,\mathrm{km\,s^{-1}}$. There is a complete list of sources with velocities and errors in

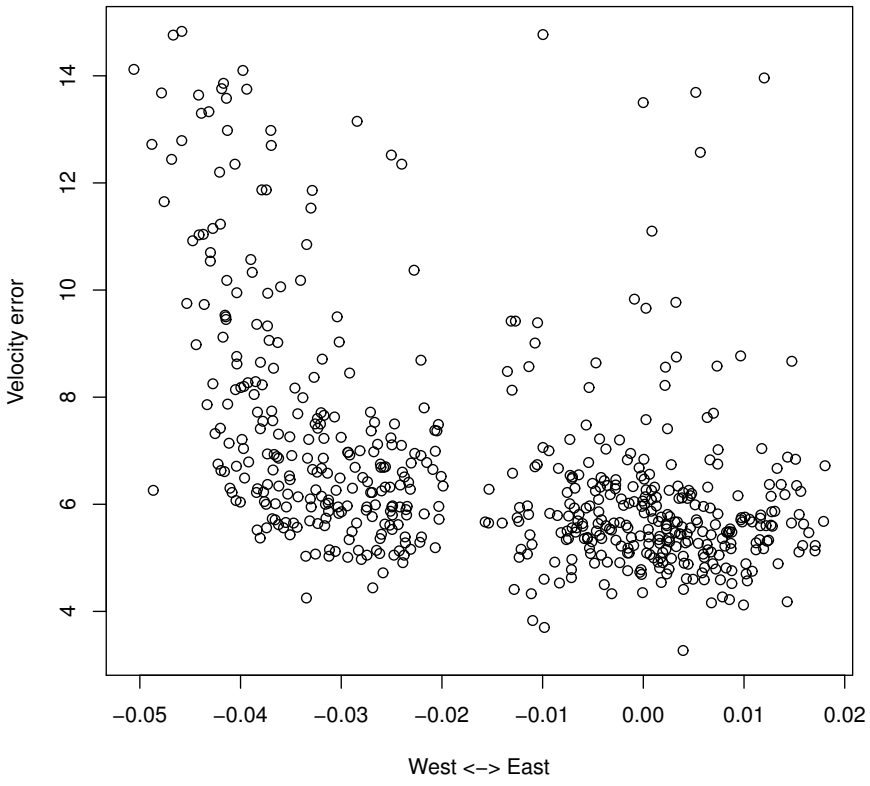

Figure 4.4: Velocity errors plotted from West to East show the western field (which had worse seeing) resulted in slightly higher errors.

Table E.1.

4.2.3 Velocity Templates

We initially used long period variables (LPV) velocity references from Hughes and Wood (1990) calibrated against three velocity templates in 47 Tucanae (Cole et al. 2004). A spread of about $30\,\mathrm{km\,s^{-1}}$ indicated the Hughes velocity references were unsatisfactory. The choice of LPV stars as velocity standards was poor as the atmospheric radii may change with luminosity resulting in varying velocities in time. While the Hughes templates have large variability, the residuals shown in Figure 4.5 show individual velocities from spectra are accurate to within about $1\,\mathrm{km\,s^{-1}}$ while the systematics show a large range. The stellar velocities given for the template spectra have errors of about $7.7\,\mathrm{km\,s^{-1}}$.

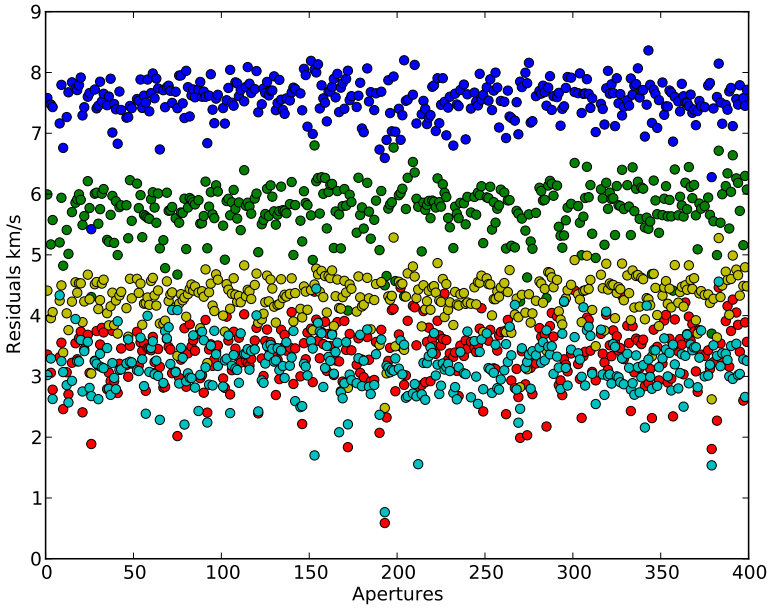

Figure 4.5: A subset of the observed 47 Tucanae velocity standards were cross-correlated with long period variables observed as standards in the LMC with velocities from Hughes and Wood (1990). The colours show individual stars showing good velocity precision within $1\,\mathrm{km\,s^{-1}}$ but poor systematic accuracy with $2\,\mathrm{km\,s^{-1}}$ to $8\,\mathrm{km\,s^{-1}}$ offset from the zero point of quoted literature velocities. These variable stars proved to be poor velocity templates.

Recent data from Lane et al. (2010) obtained with the AAOmega multi-fibre spectrograph uses a modified RAVE pipeline for velocity determination called KISS. These data are used for for comparison with our data on 47 Tucanae. There were 266 matching objects, so a high quality subset of 29 of our observed spectra were cross correlated with the velocity values published by Lane et al. (2010) which have errors estimated at less than $2\,\mathrm{km\,s^{-1}}$. Using these as templates in the IRAF FXCOR task we find agreement with our initial results within less than $5\,\mathrm{km\,s^{-1}}$.

As a check 35 velocity template spectra from Hankey and Cole (2011) also recently obtained with AAOmega were selected. Cross correlation with these spectra find agree with the correlations with the Lane et al. (2010) data within $2\,\mathrm{km\,s^{-1}}$. This indicates AAOmega multi-fibre velocity results, through fxcor, RAVE and KISS pipelines are consistent within errors across recent epochs.

There are 29 cross-correlations with template stars from 47 Tucanae and the mean of the 29 cross-correlations is quoted as the velocity measurement. We do not quote the smaller standard error in the mean as the error in the velocity, as the individual errors in each of the 29 velocity correlation estimates are not independent. The one observed science spectum is common to all 29 cross correlations. The error of $2\,\mathrm{km\,s^{-1}}$ in the template stars has not been added in quadrature with the fxcor errors. This is of no consequence given the dominance of the conservative mean value of the cross-correlation errors reported by fxcor. This is the error we quote in Table E.1.

4.3 Results

A histogram of the velocities is plotted in Figure 4.6. It is well modelled by a Gaussian distribution with mean $259\,\mathrm{km\,s^{-1}}$ shown as a solid curve. There is a slight excess at the peak of the distribution at higher velocities. The fit is not improved by modelling the velocity sample as the sum of two distributions.

There is a maximum velocity gradient in a direction NE, consistent with the disk model, Figure 4.7. Subramaniam and Prabhu (2005) also note this gradient at position angle 40° East from North.

We check for colour and velocity correlations, but find none, Figure 4.8 shows a slight effect of increasing velocity with magnitude, $6\,\mathrm{km\,s^{-1}}$ over the two magnitude data range. There is a 9% probability that this is a random effect, which suggests it is only significant at a marginal level. Whether it is a consequence of the spectroscopy or the fitting to better signal to noise spectra, or in fact a feature of the AGB and RGB populations is not known. In Figure 4.9 the best linear fit is shown.

The velocities of different populations based on colour and magnitude are shown in Figure 4.10. The difference in means is not statistically significant. The E region shows a little more variance, where there may be dwarf contamination in the RGB region. The selection criteria were based on the populations identified in Nikolaev and Weinberg (2000). We chose regions E, F, J, K from their Figure 3. There are 352 stars in our sample from region E, 270 from region

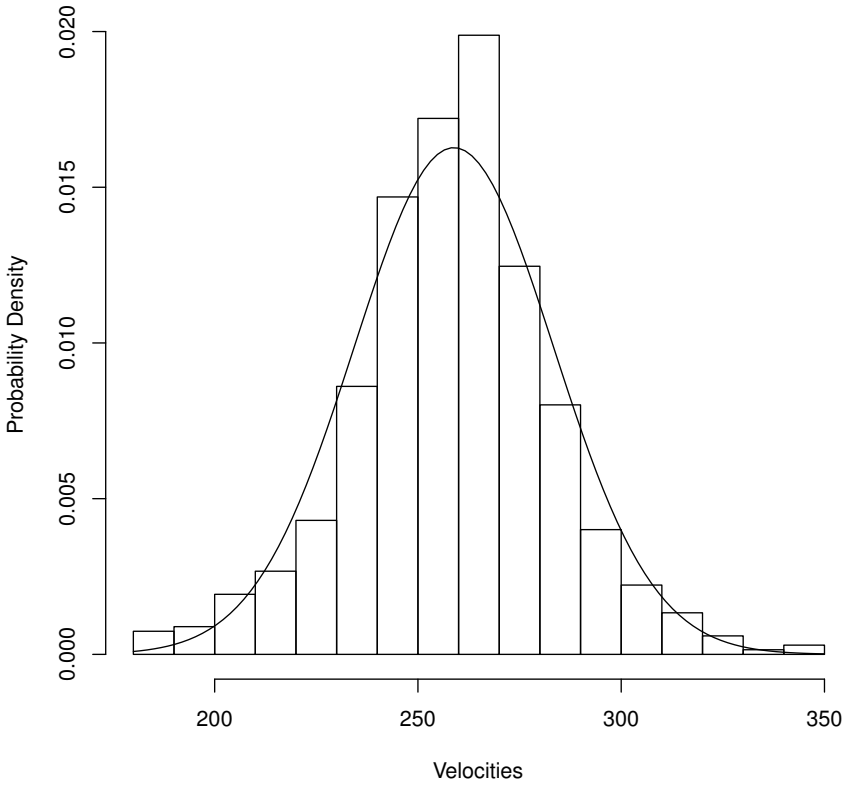

Figure 4.6: Radial velocities in our sample with theoretical Normal distribution $N(\mu = 259, \sigma = 24)$.

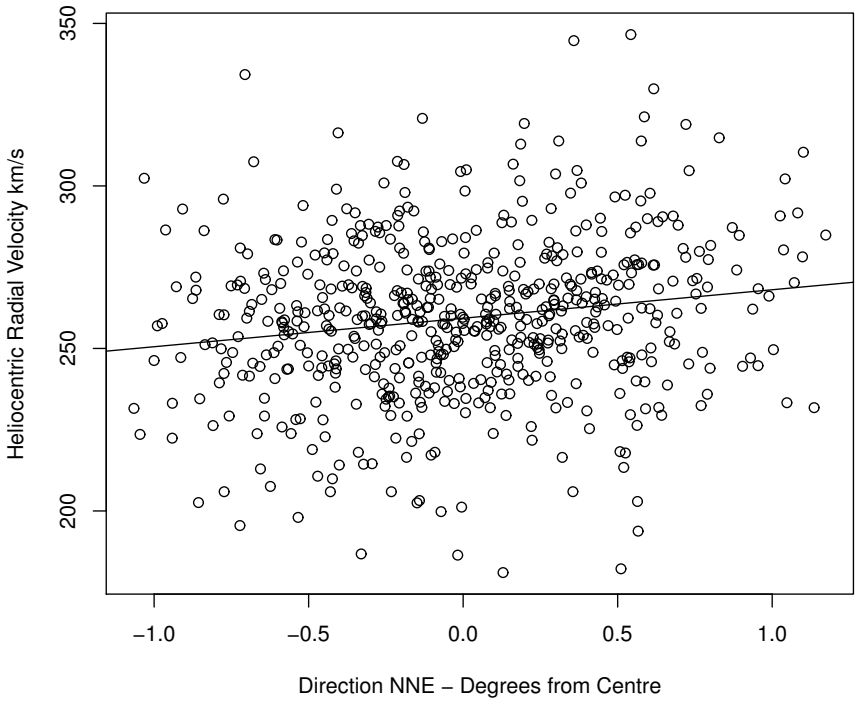

Figure 4.7: Steepest gradient of observed velocities increases in a direction NNE from the rotation centre at $9\,\mathrm{km\,s^{-1}}$ per degree, almost perpendicular to the line of nodes.

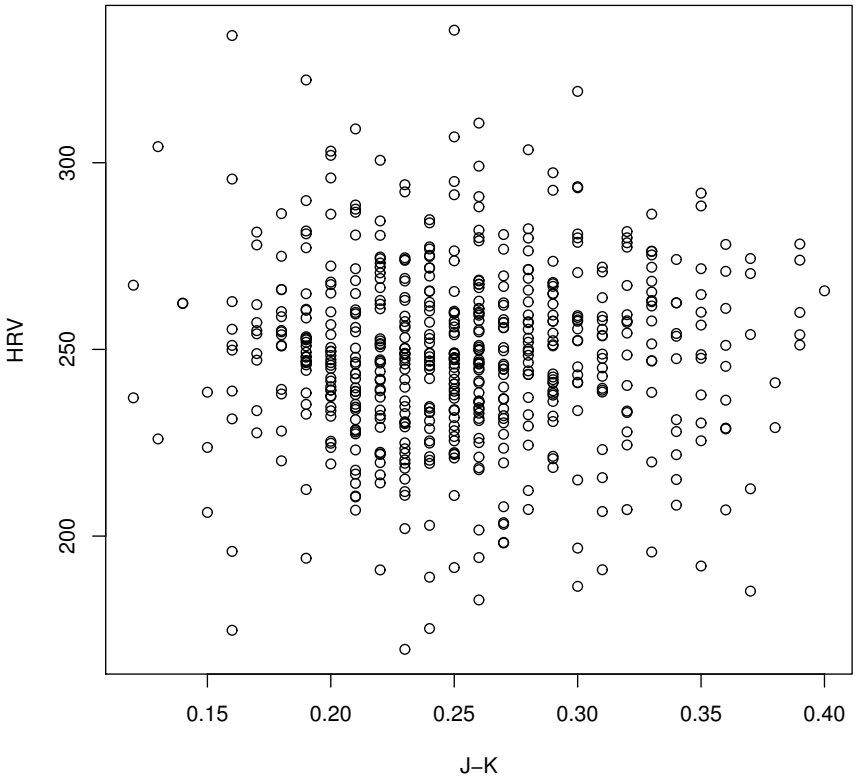

Figure 4.8: Velocity and colour show no correlation.

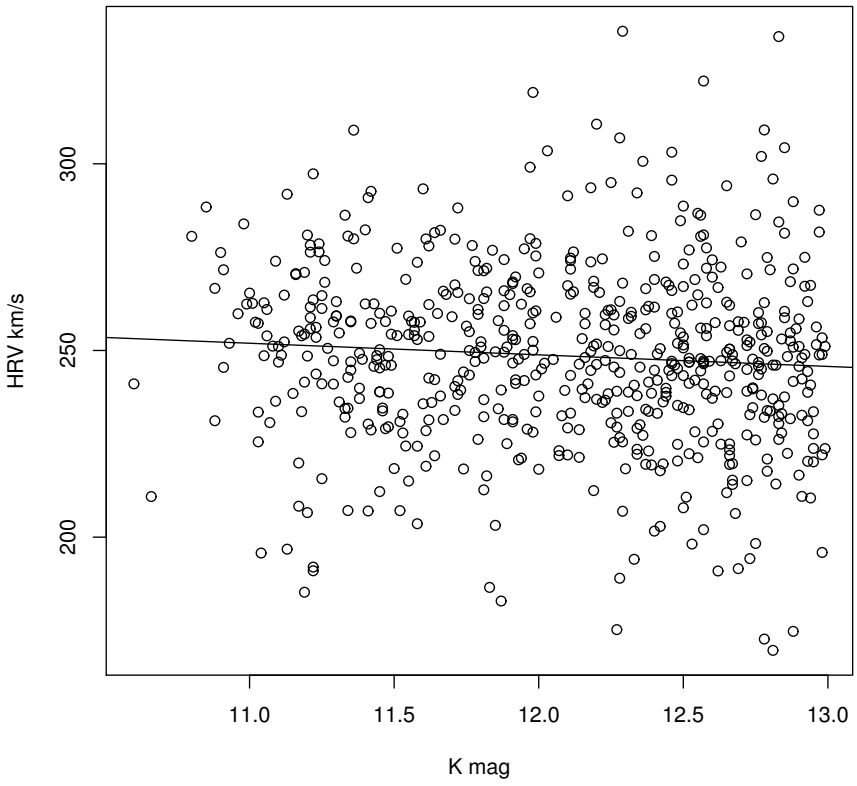

Figure 4.9: Velocity shows a very small and marginally significant dependence on magnitude in our sample.

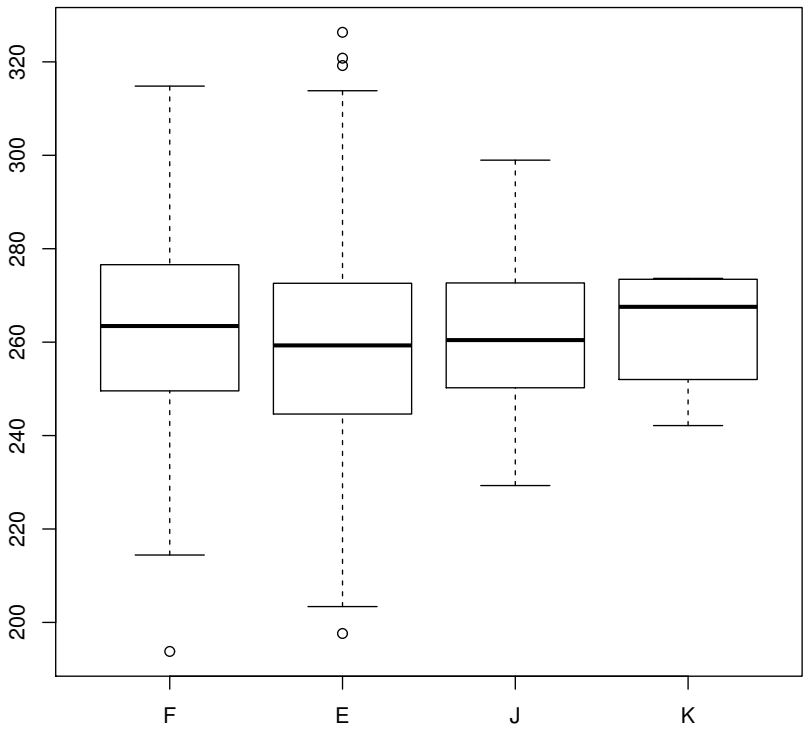

Figure 4.10: Stellar populations defined in Nikolaev and Weinberg (2000) show no systematic variation in mean and the standard deviation boxes are of similar size. Region K represents only a handful of reddened Carbon stars.

F, 45 from region J and 7 from region K. Stars redder than J-K = 1.6 are mostly carbon stars with some extremely reddened by dusty environments. The E region contains late non-helium burning RGB stars and are a dominant feature of the disk and bar. This region includes the tip of the RGB. Stars in the F region are Oxygen rich AGB mostly evolved from the RGB E region population. J region has Carbon stars and region K are the heavily reddened Carbon stars. The K region is spatially associated with the central region of the galaxy. There are only a few examples of these stars reddened by circumstellar dust. There are a very few examples of very late life AGB stars from a small sample of (Hughes and Wood 1990) which are Long Period Variables (LPV). We divided our final sample into these population types and compared their velocity distributions.

4.3.1 Comparison with Zhao

Zhao et al. (2003) (Z03) observed the largest set of velocities, 1347 stars, in the region covered by our data, Figure 4.11. Their sample has velocity errors $< 50\,\mathrm{km\,s^{-1}}$. The main features of the distribution of their data agree with ours.

Both data sets are well modelled by a Normal distribution with standard deviation of $24\,\mathrm{km\,s^{-1}}$. However there are systematic errors between the data sets. We calculate the mean velocity for a subset of their data covering the same area of sky as our fields as $273\,\mathrm{km\,s^{-1}}$. Our sample has a mean value of $259\,\mathrm{km\,s^{-1}}$, a difference of $14\,\mathrm{km\,s^{-1}}$ Figure 4.6. Van der Swaelmen et al. (2013) find a mean of $261\,\mathrm{km\,s^{-1}}$ for a sample of 103 RGB stars and Cole et al. (2005) find $257\,\mathrm{km\,s^{-1}}$ for 373 RGB stars in the bar region. We have one object in common, 2MASS i.d. 05304038-7049072. We find a velocity of $214 \pm 5\,\mathrm{km\,s^{-1}}$ whereas Z03 derive $265 \pm 16\,\mathrm{km\,s^{-1}}$, a difference of $51\,\mathrm{km\,s^{-1}}$, a large discrepancy which is investigated later in this thesis.

Figure 4.12a shows our data compared to a Normal distribution. Quantiles of the cumulative theoretical Normal distribution on the x-axis are plotted against our corresponding data on the y-axis. The deviation from Normal at the low and high ends indicates heavy tails. The deviation from a Normal distribution is only slight, a Schapiro-Wilks test of Normality gives a 98% probability of being Normally distributed. We compare Z03 from the same region with our data Figure 4.12b. The Z03 data have an identically shaped heavy tail distribution except systematically shifted to a higher median velocity of $273\,\mathrm{km\,s^{-1}}$, rather than our $259\,\mathrm{km\,s^{-1}}$.

The dip in the mean velocity near the centre of the bar that Subramaniam and Prabhu (2005) find in the Z03 data is not seen in our data, Figure 4.13. The figures are data in the same region of the sky, smoothed by a locally weighted non-linear least squares regression with the same sized kernel. We note that the dip in Z03 velocity at the centre is dependent on the amount of local weighting, or the span of the smoothing applied to the data. With larger smoothing Z03 data begin to looks like ours. The bin sizes used by Subramaniam and Prabhu (2005) are also critical in bringing this feature out in plots. The larger velocity dispersion and error in the Z03 data argues for a larger smoothing than that

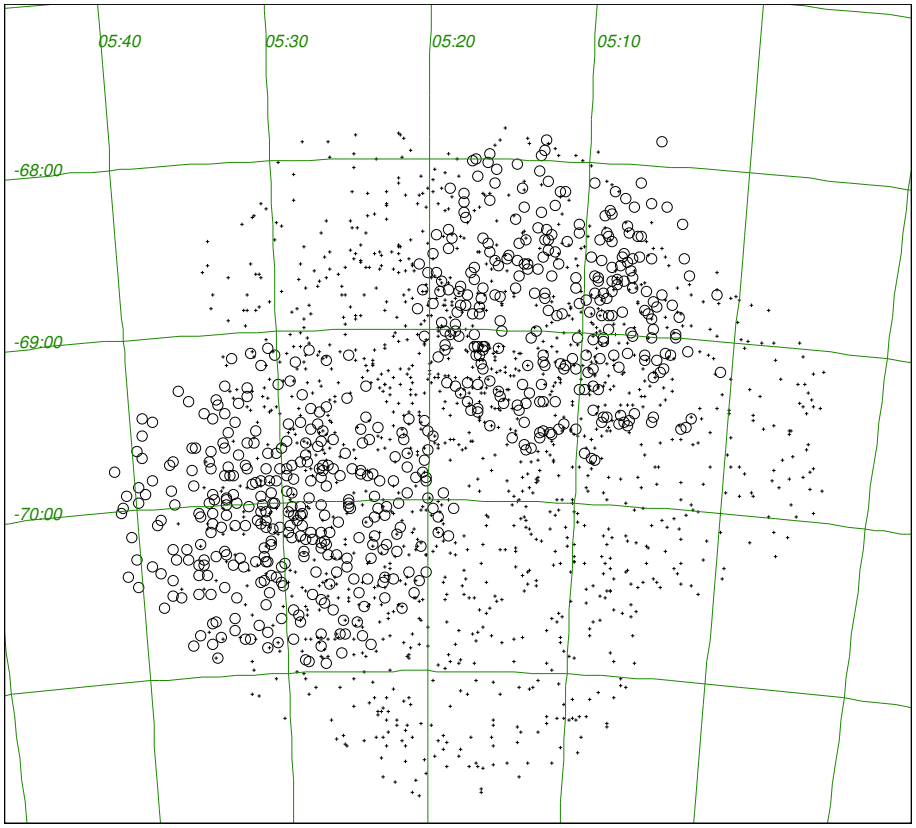

Figure 4.11: Our data, open circles, Z03 data, points.

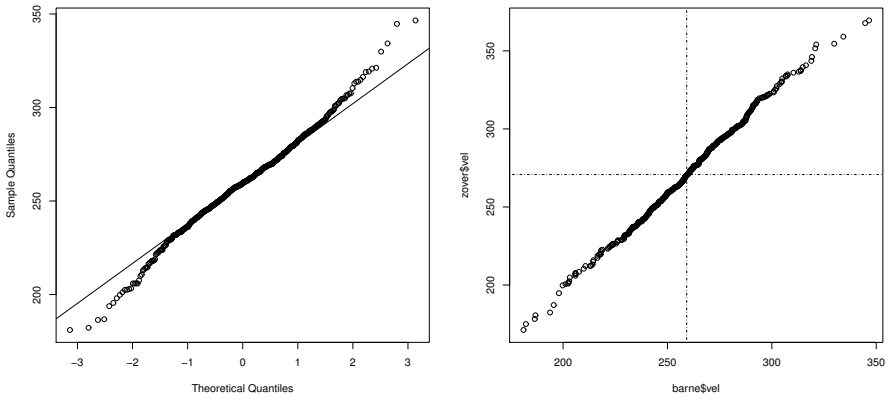

(a) Quantiles of our data compared to the (straight line) Normal distribution. Low and high tails are indicated at ends of distribution.

(b) Quantiles of our data compared to Z03 data in the same fields of LMC, median values dotted lines.

Figure 4.12

applied to our data.

Following Subramaniam and Prabhu (2005) we select a subset of our data that lies within 0°.4 either side of the line of nodes. We plot our data and Z03's data in a similar fashion to the lower left panel in Figure 3 Subramaniam and Prabhu (2005) showing the variation of LOS velocity with radial distance from the rotation centre ρ. Our data again shows very dissimilar features to the Zhao data.

Z03 data includes stars from a wider selection criteria than our data. It may be the case that the difference between our data and Z03 is due to the non- RGB population measured in their study. We select two subsets of Z03 data, one is an equivalent colour selection to our sample, and the other is everything bluer than our sample. We still see the same features in Z03 data, so selection effects are not the cause of the discrepancy. Z03 also don't find any other spatial-velocity relation. We note the effect of binning too finely in the spatial dimension along the line of nodes exaggerates the "v" shaped feature whereas greater averaging reduces the effect. The feature also appears near the boundary of three of the Zhao fields and could be due to a systematic difference between fields which were observed at different times.

Z03 has a wider colour range than our sample, so we test for parameter dependence on colour. If we subset Z03 with just the RGB colour range we still get the same shape distribution with subtle heavy tails, same mean and standard deviation, as with the whole Z03 sample.

Our large calibration set from 47 Tucanae from the same instrument, the

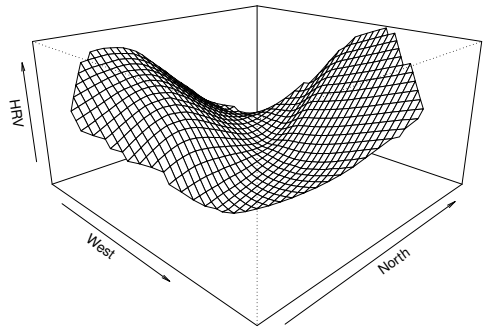

(a) Z03 Heliocentric Radial Velocity in the same region as our data showing a counter-rotation signature dip at centre.

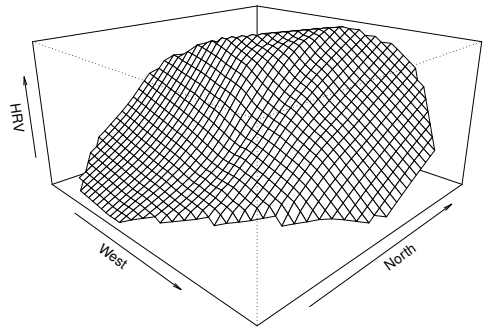

(b) Our data on the same scale show no evidence of the "velocity valley" feature seen in the Z03 data, but large scale features agree. The gradient direction and scale is shown in Figure 4.7

Figure 4.13

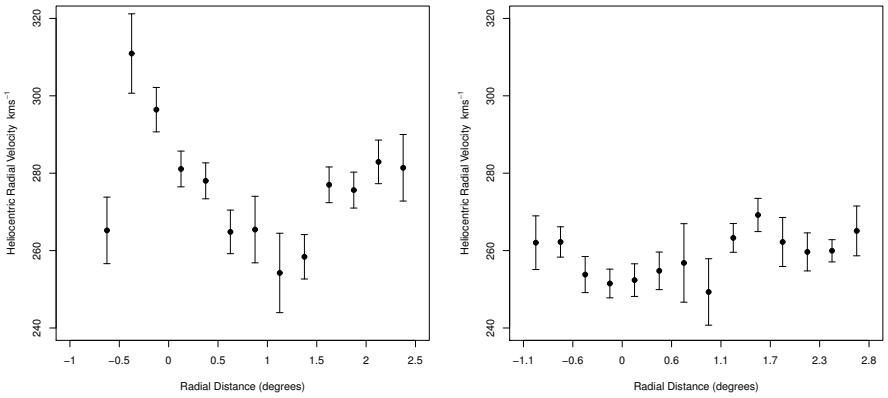

(a) Z03 data plotted in the same fashion as Figure 1 in Subramaniam and Prabhu (2005), PA=130°

(b) Our data plotted on the same scale exhibit different properties.

Figure 4.14

concurrent observations and the precision of the AAOmega spectrometer preclude any obvious systematic error in our data. The Z03 field mainly coinciding with our western field was observed over a year before the other fields. The *2df* spectrograph was located at the top of the telescope and was notorious for changing geometry at different elevations. The accuracy of the instrument was suitable for galaxy redshift surveys on cosmological scales, where rms errors estimated at $85\,\mathrm{km\,s^{-1}}$ were acceptable (Colless et al. 2001).

An attempt was made to re-reduce the raw Z03 data, which are available online at the Anglo-Australian Telescope (AAT) archive. The Z03 data were observed with the same telescope, but using the 2DF spectrograph, the antecedent of AAOmega. Z03 used a standard observing mode on the 2dF spectrograph with the 1200 V grating. Twenty dedicated sky fibres were observed in each field. We re-reduced the data using the *2dfdr* pipeine. It was hoped cross correlation with our blue spectrograph arm data might provide a way to calibrate the data sets. Sky subtraction using the dedicated fibres was largely unsuccessful. The worst cases resulted in negative flux in object spectra after sky subtraction. It is very difficult to find dark sky positions in the inner LMC fields observed. The usual process of randomly assigning sky fibres and having most of them fall on empty sky is not possible in this region.

From the remaining data with reasonable spectra, the range of spectral types that didn't match our red giant sample were discarded. This left a small sample of stellar spectra where the magnesium triplet at 5167 Å, 5173 Å and 5184 Å was clearly visible. Some velocities with errors of about $50\,\mathrm{km\,s^{-1}}$ could be obtained. The wholesale re-reduction of the Z03 data and calibration with our

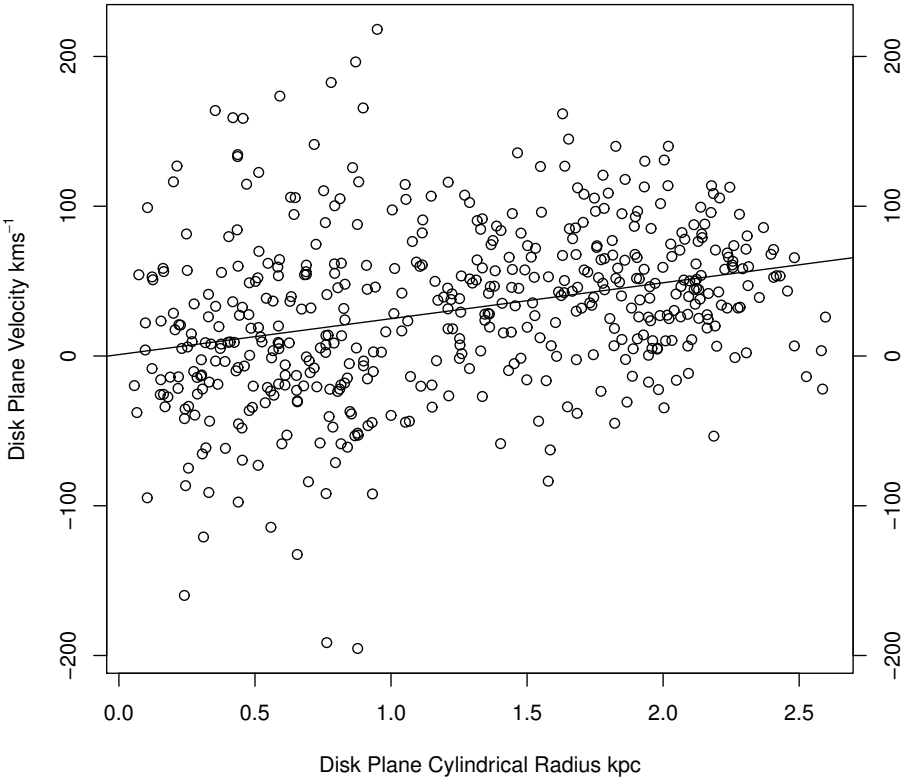

Figure 4.15: A very simple solid body rotation curve can be fitted to our stellar sample.

sample was unsuccessful.

The Z03 data are calibrated against just one velocity standard K-type giant stellar spectrum (Zhao et al. 2003). Ten good spectra from each colour range are used as templates to cross-correlate the survey stars to obtain a velocity offset from the best matching correlation. The distribution of offsets from each template is fitted to the peak of the distribution of LMC velocities, except for the K-type template which is compared to an actual velocity reference. This gives the sample internal precision, but not an absolute accuracy, and was suitable for Z03's purpose of identifying two velocity populations in the sample.

4.3.2 Disk Rotation Model

A model of the LMC disk is proposed by van der Marel et al. (2002), who took a sample of carbon stars located in the periphery of the galaxy and used these data to fit a model of line of sight velocity. The line of sight velocity of a star is a function of the angular distance on the sky from the centre of the disk structure ρ, and the position angle from North Φ. Disk plane orbits are modelled by a rotation curve $V(R')$ which is parameterised as,

$$V(R') = V_0 \frac{R^\eta}{R^\eta + R_0^\eta} \tag{4.1}$$

This is the same LMC model as employed by Alves and Nelson (2000), with geometric corrections for the large spherical angle subtended by the galaxy on the sky, and includes a term for precession of the disk inclination.

The transverse centre of mass velocity v_t can be expressed in components along the line of nodes, $v_{tc} = v_t cos(\Theta_t - \Theta)$ and perpendicular to the line of nodes $v_{ts} = v_t sin(\Theta_t - \Theta)$, where Θ_t is the angle of the transverse velocity, and Θ is the angle of line of nodes, from North. Along the line of nodes the position angle of a star Φ is the same as the line of nodes so $\Phi - \Theta = 0$. We can define a systematic motion corrected velocity, $v_{lon} \equiv v_{los} - v_{sys} \cos\rho$, which yeilds the simplified relation, given $\sin\Phi - \Theta = 0$ and $\cos\Phi - \Theta = \pm 1$,

$$\begin{aligned} v_{lon} =& v_{tc} \sin\rho - V(R') f \sin i \\ =& v_{tc} \sin\rho - V(R') \sin\rho \sin i \\ =& \sin\rho \left(v_{tc} - V(R') \sin i\right) \end{aligned}$$

showing that along the line of nodes the LOS velocity (corrected for systemic LOS motion) is simply proportional to $\sin\rho$. That is, if the LMC rotation curve $V(R')$ is linear, which it has been found to be up to 4 kpc from the centre, after which it flattens out to at least $60\,\mathrm{km\,s^{-1}}$ (Alves and Nelson 2000).

At the centre where $\rho = 0$ the line of sight velocity of the disk rotation is zero, so measurements of radial velocities here measure the systemic line of sight velocity of the galaxy directly. The only systematic source of error would be the choice of rotation centre.

The disk plane velocities were calculated from our radial velocities using the model of van der Marel et al. (2002) as follows:

$$\begin{aligned} V_{disk}(\rho,\Phi) =& [v_{sys}\cos\rho - v_t \sin\rho cos(\Phi - \Theta_t) \\ &+ D_0 (di/dt) \sin\rho \sin(\Phi - \Theta) \\ &- v_{los}] \times g^{-1} \end{aligned}$$

Where g is,

$$g = f \sin i \cos(\Phi - \Theta)$$

a function of the geometric factor,

$$f \equiv \frac{\cos i \sin \rho - \sin i \sin \rho sin(\Phi - \Theta)}{[\cos^2 i \cos^2 (\Phi - \Theta) + sin^2(\Phi - \Theta)]^{1/2}}$$

which describes the projection of the circular disk orbital velocity into the plane of the sky. Perpendicular to the line of nodes, $\cos(\Phi - \Theta)$ goes to zero at the rotation centre, making $g(f)$ small. For $g \leq 0.2$ the projection into the line of sight of disk velocity is of the order of the error in the radial velocity. We therefore exclude these data following Olsen and Massey (2007). The subset of the data employed with $|g|$ larger than 0.2 is shown in Figure 4.16.

Our data at the centre of the LMC provide weak constraints on the global orientation of the disk. We take disk geometry parameters from van der Marel et al. (2002). The centre of mass is given as $\alpha_{CM} = 5^h27^m.6$ and $\delta_{CM} = 69°.87$. We take the line of nodes of the disk as 130°, and the inclination angle of the disk to be $34°.7 \pm 6°.2$ (van der Marel et al. 2002). A recent study of Cepheid and RR Lyrae standard candles to create a 3D map of the LMC arrives at an inclination of $32° \pm 4°$ (Haschke et al. 2012). They also find line of nodes to be $115° \pm 15°$.

The values for proper motion are taken from Piatek et al. (2008) with transverse velocity of $476\,\mathrm{km\,s^{-1}}$ in a direction 78°. They find the precession and nutation terms to be consistent with zero, and we employ this result. However we note that the average of van der Marel et al. (2002) and Olsen et al. (2011) gives di/dt= -0.5162 mas /yr. For $D_0 = 50.1\,\mathrm{kpc}$ this translates to $-122.6\,\mathrm{km\,s^{-1}}$. The di/dt precession term has no effect at the very centre of the galaxy, and up to a maximum of about $6\,\mathrm{km\,s^{-1}}$ at the extrema of our observed fields.

We take an iterative approach to fitting a rotation curve to the observed velocities. For all samples we exclude velocities with errors greater than $20\,\mathrm{km\,s^{-1}}$. We estimate a systemic velocity by first assuming a model for the rotation curve. This allows us to transform the data to the plane of the LMC disk. We then use this transformed data to get a better model, then use this model to get a better systemic velocity. We show that this bootstrap method is insensitive to starting conditions.

We use the heliocentric radial velocity to estimate the systemic velocity using a very simple solid body rotation curve. This is not unreasonable in the inner 2.5 kpc of galaxy, at greater radii we expect the rotation curve to flatten out. From exploratory analysis we set the linear relation to $24\,\mathrm{km\,s^{-1}\,kpc^{-1}}$ and assume the disk velocity is zero at the centre. For each star in our sample the systemic velocity is calculated and the distribution is analysed. The distribution is close to the Normal distribution, and the mean value of systemic velocity is $250\,\mathrm{km\,s^{-1}}$ and median $251\,\mathrm{km\,s^{-1}}$.

Using this estimate of the systemic velocity we proceed to transform the heliocentric radial velocities to in disk plane velocities. The disk velocity data are grouped by radius to give equal number bins. The van der Marel et al. (2002) model was fitted to the mean values of the binned data from our sample using a

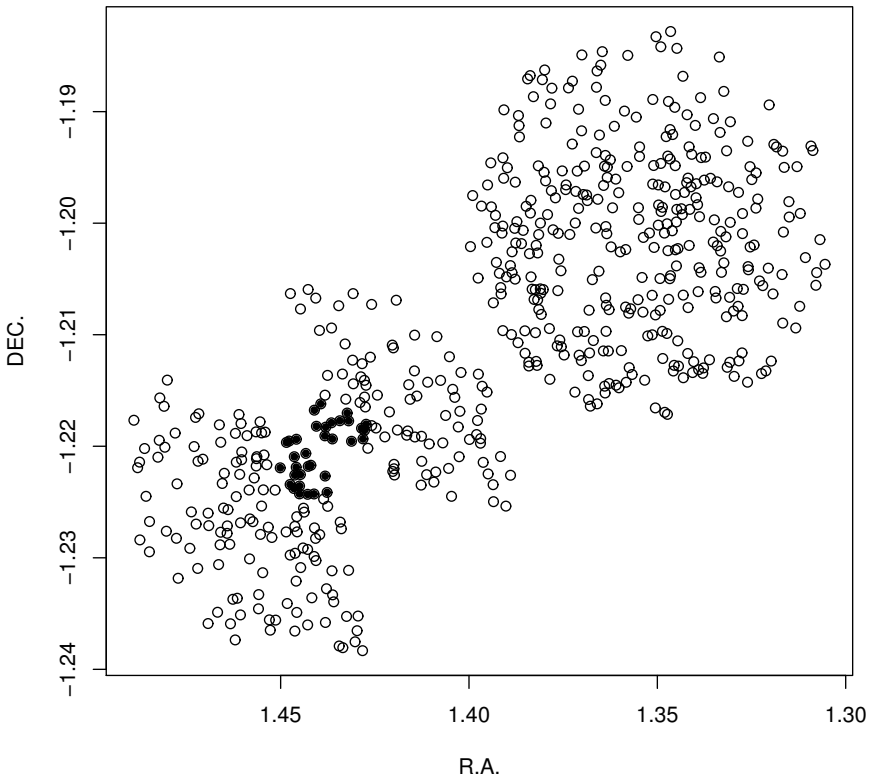

Figure 4.16: The velocity in the disk plane becomes sensitive to error perpendicular to the line of nodes at the rotation centre $\alpha_{CM} = 5^h27^m.6$ and $\delta_{CM} = 69\overset{\circ}{.}87$ (van der Marel et al. 2002). Velocities in this region have almost no component in the line of sight. The subset of data which can be transformed to disk plane velocities is shown. The solid points are a subset with heliocentric radial velocity of $248\,\mathrm{km\,s^{-1}}$, a direct measurement of the systemic velocity of the LMC without systematics.

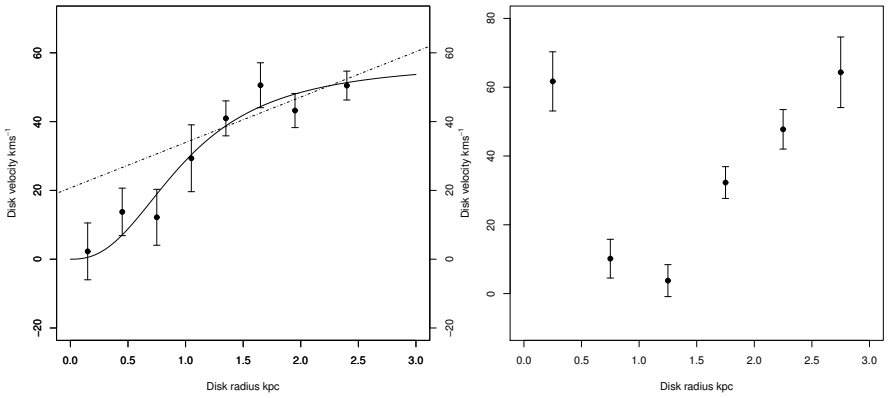

(a) Bins have even numbers of stars, the solid line is our model. The dotted line linear fit to the outer five data bins, excluding <1 kpc low velocity points, would result in a higher systemic velocity.

(b) The Z03 data transformed to disk plane velocities and binned the same as our data. The rotation curve is very different at the centre.

Figure 4.17

non-linear least squares method. We found parameters $V_0 = 57\,\mathrm{km\,s^{-1}}$, ν= 2.5 and characteristic disk radius R_0= 1.0 kpc. The fit is plotted in Figure 4.17. The error bars represent the error in the estimation of the mean value in the equal number bins, they do not represent the variability in the individual velocities.

Rather than the first simple linear model, we now use this more refined model to again estimate the systemic velocity from the measured heliocentric velocities. Such a distribution is shown in Figure 4.18a.

There is some degeneracy between the systemic velocity and the rotation curve model parameters, as we must assume model parameters to get an estimate of systemic velocity which we then plug back into our model estimation. Exploration of a range of disk model parameters show the starting systemic velocity arrived at does not depend sensitively on choice of model. For $2 < \eta < 3$, for $40\,\mathrm{km\,s^{-1}} < V_0 < 100\,\mathrm{km\,s^{-1}}$, and $0.5 < R_0 < 2.5$ the systemic velocity ranges from $249\,\mathrm{km\,s^{-1}} < V_0 < 261\,\mathrm{km\,s^{-1}}$. Yet whatever systemic velocity we choose to perform the transform, the model fitted to the transformed data by non-linear least squares is close to Equation 4.2.

$$V(R') = 57.4\frac{R^{2.5}}{R^{2.5} + 1.0^{2.5}} \tag{4.2}$$

For example, if we use a systemic velocity $260\,\mathrm{km\,s^{-1}}$ to transform the velocity data to the disk plane, we find a best fit model with $V_0 = 61\,\mathrm{km\,s^{-1}}$, $\eta = 2.4$ and $R_0 = 1.14$. When we estimate the systemic velocity using this model we again get a median of $253\,\mathrm{km\,s^{-1}}$ with a similar distribution. Re-

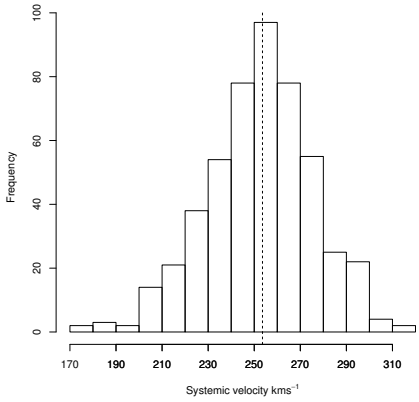

(a) The distribution of systemic velocity from each sample star. The dotted line shows the median systemic velocity $254\,\mathrm{km\,s^{-1}}$ of the LMC. The standard deviation is $23\,\mathrm{km\,s^{-1}}$, the same as the heliocentric radial velocities.

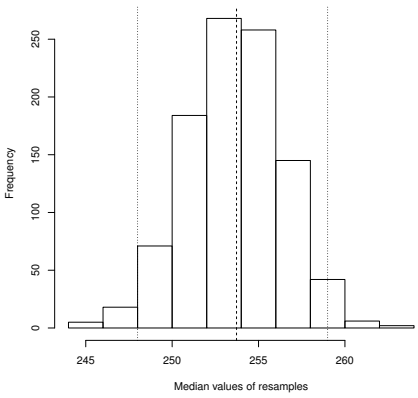

(b) Monte Carlo resampling to estimate error on systemic velocity, results in this distribution with median 254 and 95% confidence interval $248\,\mathrm{km\,s^{-1}}$ to $259\,\mathrm{km\,s^{-1}}$

Figure 4.18

iterating with systemic velocity $253\,\mathrm{km\,s^{-1}}$, and transforming the data to the disk plane, we converge on the optimal model 4.2. With this model we arrive at the distribution of systemic velocities calculated on each star in Figure 4.18a.

The distribution of systemic velocity estimates is very close to a Normal distribution, with a slight low tail. The mean value is $253\,\mathrm{km\,s^{-1}}$, however the median value, $254\,\mathrm{km\,s^{-1}}$ is a better estimator of the true value given the slight non-Normality. The standard deviation of $23\,\mathrm{km\,s^{-1}}$ reflects the standard deviation of our sample of heliocentric radial velocities. Using a bootstrap Monte Carlo resampling method to estimate the range of possible values allows for the slight non-normality of our sample, and we obtain a 95% confidence interval for the $249\,\mathrm{km\,s^{-1}}$ to $259\,\mathrm{km\,s^{-1}}$ Figure 4.18b.

The carbon stars from Kunkel et al. (1997), which were used by van der Marel et al. (2002), form a ring around the periphery of the galaxy; as well as the curious central objects, which in the VDM model appear to be counter-rotating with a disk velocity of $-30\,\mathrm{km\,s^{-1}}$. However with our model of the inner galaxy counter-rotation disappears. If the systemic line of sight velocity is forced to $263\,\mathrm{km\,s^{-1}}$ the model disk velocity at the centre is $-20\,\mathrm{km\,s^{-1}}$. The systemic velocity we estimate based our data alone is $254 \pm 5\,\mathrm{km\,s^{-1}}$

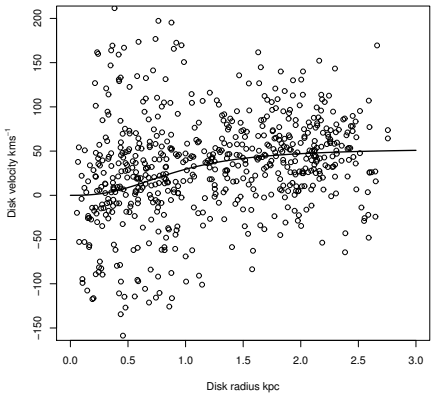

(a) Disk model fitted, plotted with the individual disk plane velocity data points.

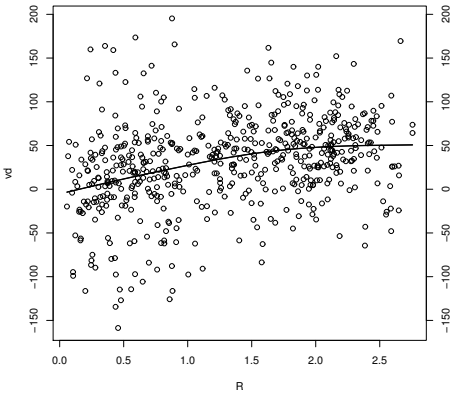

(b) Spline fit directly to the in disk plane velocity data points has a similar global shape as the disk model fit.

Figure 4.19

4.3.3 Outer field sample

A selection of data from the literature was used to refine the model and check the validity of our data. These extra velocity samples cover the region of our observations and out to several degrees beyond. Stars from outer regions in particular help constrain the model at larger radii, where our observations have not sampled. A sample of LMC stars in fields around globular clusters in the LMC from Grocholski et al. (2006) provided a sample of disk stars at larger radii, Figure 4.20d. The stars were identified as not belonging to the clusters but to the LMC disk in the background. A handful of stars identified as non-cluster with velocities less than $0\,\mathrm{km\,s^{-1}}$ were assumed not to be LMC field stars but Galactic foreground objects.

The inner LMC field stars around the cluster NGC 2019 are within a few arcminutes of the rotation centre and have a mean heliocentric velocity of $254\,\mathrm{km\,s^{-1}}$. We expect the circular galaxy rotation to go to zero near the centre, the velocity at this point should represent the systemic line of sight radial velocity of the galaxy. The LMC background stars around this cluster confirm the systemic velocity indicated by our sample.

We also included a set of red supergiant stars from Massey and Olsen (2003) which are within a few degrees of the galaxy centre, (Figure 4.20b). A large set of 377 RGB stars with velocities from Cole et al. (2005) are also sampled, (Figure 4.20a). These lie close to the rotation centre in the bar region. There is also a large set of velocities published for planetary nebulae in the bar region, Figure 4.20c, summarised by Reid and Parker (2006). We deal with this sample separately in the next section.

Figure 4.20: Locations of literature data

(a) Cole et al. (2005)

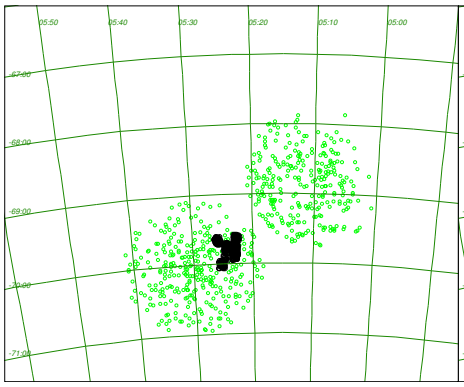

(b) Massey and Olsen (2003)

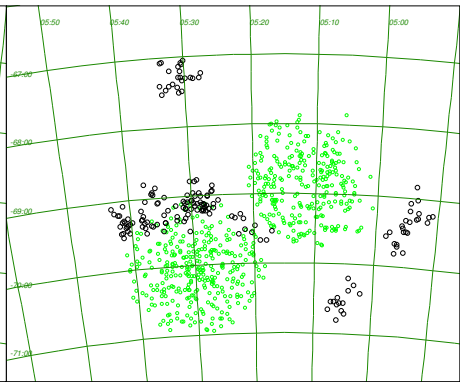

(c) Reid and Parker (2006)

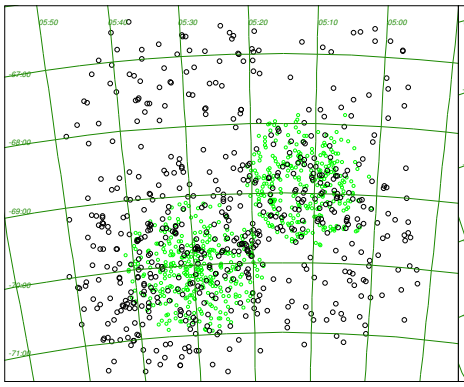

(d) Grocholski et al. (2006)

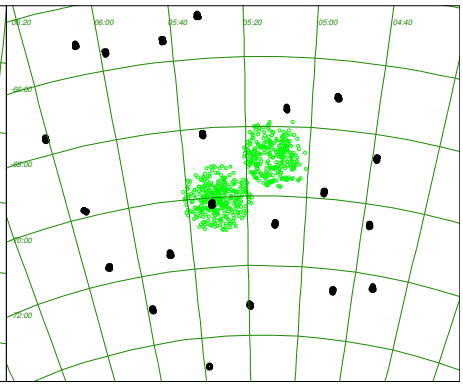

Table 4.2: Disk Models

Reference	V_0km s^{-1}	R_0kpc	V_{sys}km s^{-1}	Prop.Mot.V_{trans}km s^{-1}
Luks and Rohlfs (1992)[a]	70	1.4	274	
Kim et al. (1998) [a]	63	2.4	279	286
Alves and Nelson (2000)	72	4.0		286
van der Marel et al. (2002)	50	2.8	262	281
Olsen and Massey (2007)	74-107[b]	2.1	263-266[b]	490
Piatek et al. (2008)	120	4.0	287	475
Olsen et al. (2011)	87	2.4	263	475
This study observed	57	1.0	254	475
This study observed & literature	85	1.9	257	475
This study final MCMC estimate	79	1.9	255	475

[a]HI gas studies; [b]Various tracers, Carbon stars, red super-giant (RSG) stars and HI gas.

We find that the additional data changess the model fit slightly. The high density of the 377 stars from Cole et al. (2005) adjacent the rotation centre dominate the statistics of the central 0.5 kpc and raise the systemic velocity from 254 km s^{-1} to 257 km s^{-1}. The data in Figure 4.21 has unequal bin ranges to keep the number of stars in each radial category similar. We also explore the consequence of varying disk inclination angle in Figure 4.21. Using the model of Subramanian and Subramaniam (2010), which has a warped disk with less inclination at the centre, we see the basic rotation curve is preserved. The more face on central disk projects less disk velocity into the radial line of sight, so more disk velocity is required to account for the observed line of sight velocities. This increases the steepness of the central rotation curve slope. This demonstrates a simple rotation model is robust to variations in inclination angle.

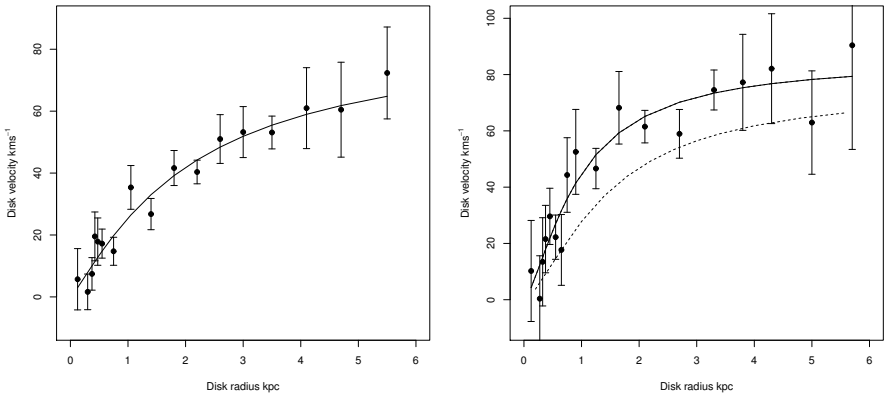

(a) The model fit to our sample plus literature data (except PNe), error bars show the standard error in the mean of the equal number bins.

(b) Warped disk model of Subramanian and Subramaniam (2010) has a more face on central region and less rotation velocity projected into line of sight. Higher rotation velocities are required to account for observations than in flat disk model (a) (dotted line).

Figure 4.21

The extra data updates the model parameters based on our sample alone. We originally fitted this model to our observations, V_0 =57 km s^{-1}, R_0= 1.0 kpc and ν= 2.5. The new model with extra data at larger radii where the rotation curve attains a steady maximum is V_0 = 85 km s^{-1}, R_0 = 1.9 kpc and ν = 1.3. The new model rises slightly less steeply to a higher maximum rotation velocity. This brings the maximum velocity closer to the HI velocity and agrees with the rotation model of Olsen et al. (2011).

Planetary Nebula

We also considered a set of PNe which were identified and measured spectroscopically by Reid and Parker (2006). While the spectroscopic velocities are not of the central object, the higher excitation lines measured are thought to come from close to the central ionising object, within $10\,\mathrm{km\,s^{-1}}$ rather than the outer regions which could be up to $50\,\mathrm{km\,s^{-1}}$ away. We find that this data set is systematically offset from our data in the same region by about $10\,\mathrm{km\,s^{-1}}$. The dispersion of the PNe velocities is $26\,\mathrm{km\,s^{-1}}$, which is exactly the same as our data plus the outer field sample dispersion which is also $26\,\mathrm{km\,s^{-1}}$. Our observations alone, which are in the inner bar region, have a standard deviation of $24\,\mathrm{km\,s^{-1}}$.

The PNe velocities, with a median heliocentric velocity $267\,\mathrm{km\,s^{-1}}$, are systematically higher than our data. The Zhao data with median $273\,\mathrm{km\,s^{-1}}$ is similarly higher. Both sets of observations were made on the *2df* spectrometer which may indicate a systematic difference with the AAOmega spectrometer. The *2df* spectrometer was located at the prime focus of the Anglo-Australian 4 metre and moved with the telescope. Mechanical stress on the spectrometer was a known problem at low elevations. We hypothesise that at the typical low elevations required when observing the LMC at declination $-71°$ the *2df* spectra have been shifted systematically. This is not a problem for the extra-galactic redshifts which the instrument was designed to observe, but a systematic difference has been noted by us in two data sets.

Apart from the offset, the PNe show an even more obvious disk rotation profile than our observations, Figure 4.22. Reid and Parker (2006) also find a rotation curve from their planetary nebula data in the centre that approximates a solid body linear profile. We transform the PNe velocity data, to the disk plane. A straight linear model of a rotation curve fit to the disk velocities gives a slope of $35\,\mathrm{km\,s^{-1}\,kpc^{-1}}$ with an intercept of $-14\,\mathrm{km\,s^{-1}}$ at the rotation centre, which represents the systematic offset of the order of $10\,\mathrm{km\,s^{-1}}$. It is once again the lack of data in the very inner regions which causes the PNe data to fail to show the steep inner rotation curve our data samples. The PNe sample has only 18 points inside 0.5 kpc which have a mean heliocentric velocity of $267\,\mathrm{km\,s^{-1}}$. Again the importance of sampling the central region of the LMC is demonstrated.

4.3.4 Simulating Model Parameters

The method of bootstrapping from model to model while updating the systemic velocity at each iteration is a little cumbersome, and convergence is not guaranteed. The circular causality is problematic, with the inter-dependence of systemic velocity and rotation model parameters potentially creating feedback. Creating a scheme to obtain samples from the distributions of the model parameters using Markov chains proved difficult. This method was used to estimate parameters for an IC 4499 Plummer density model, an appropriate approach for low sample numbers. The LMC sample plus the literature data comprises

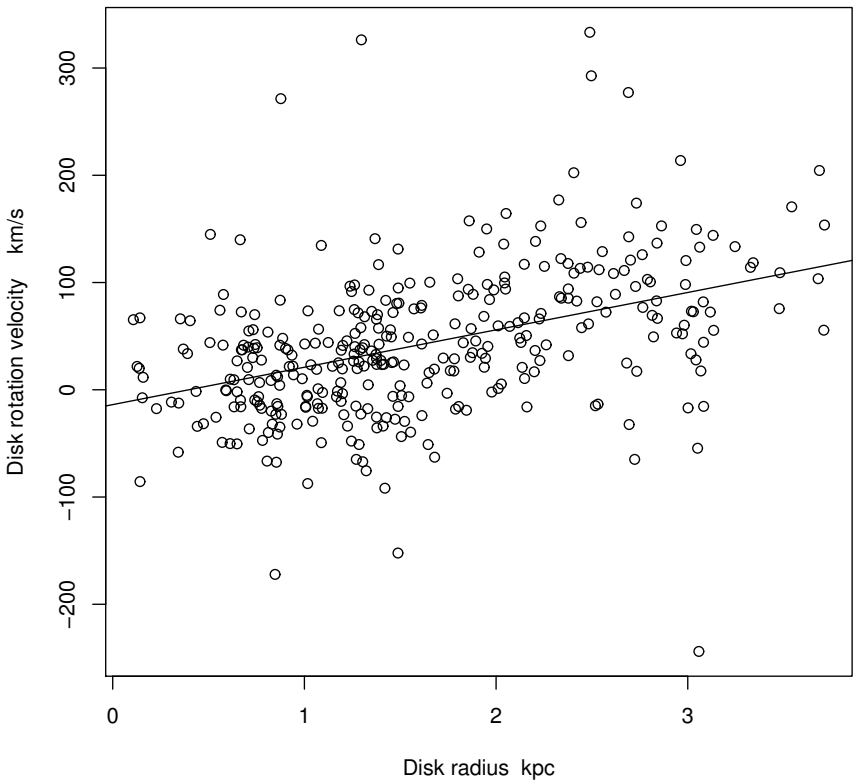

Figure 4.22: PNe radial velocity data (Reid and Parker 2006), transformed to disk plane velocities by our model, a simple linear fit to a rotation curve shown. Negative velocity at zero radius indicates higher systemic from this data.

a large sample now of 1707 stars. The MCMC method is useful in this case as it incorporates the effect of individual errors and accuracy of disk geometry assumptions on each measurement into the distribution of parameters, and gives robust error bounds.

The circular causality is illustrated in Figure 4.23. The edge between systemic velocity and model parameters nodes is where we tackle the causal loop. Using a Gibbs sampler breaks the loop by sampling for the systemic velocity, given the current state of all the other model parameters, which are held constant. Afterwards a Metropolis-Hastings algorithm is used to sample the full conditional joint distribution of rotation model parameters and disk geometry parameters within the Gibbs sampler.

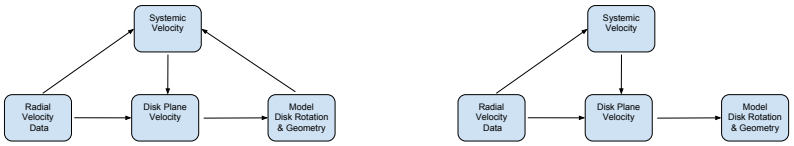

(a) A cyclic causal relation (b) Becomes an acyclic causal relation

Figure 4.23

The Metropolis method requires some tuning to control mixing and step size of the random walk through the distribution. This is accomplished by specifying priors and controlling the step size for each proposal with a scaling matrix. Allowing all parameters to vary broadly, numerical problems arose from the geometry. If the disk inclination parameter went near 90°, edge on, then problems arose from this completely unrealistic scenario. Similarly the disk inclination parameter could sometimes go towards 0°, face on, where no rotational velocities are projected into the line of sight. Yet the LMC has been shown to be inclined into the line of sight. These difficulties were overcome by adjusting the prior distributions to be more informative and hence proposals for the next step were more cautious.

It is reasonable to use informative priors where there are a range of estimates from various LMC studies into the disk geometry parameters. The priors are broad enough to cover the range of possibilities. By placing informative priors on the disk geometry parameters, like the disk rotation centre, inclination and line of nodes, we were able to keep the simulated models within reasonable bounds. The real parameters of interest, disk scale, curve shape and maximum rotation velocity were then able to be specified using only weakly informative priors. For every new sample of the parameter space the 1707 observed velocities were re-transformed to the disk plane using updated values for the parameters based on the last sample. This method then gives robust estimates of the rotation curve

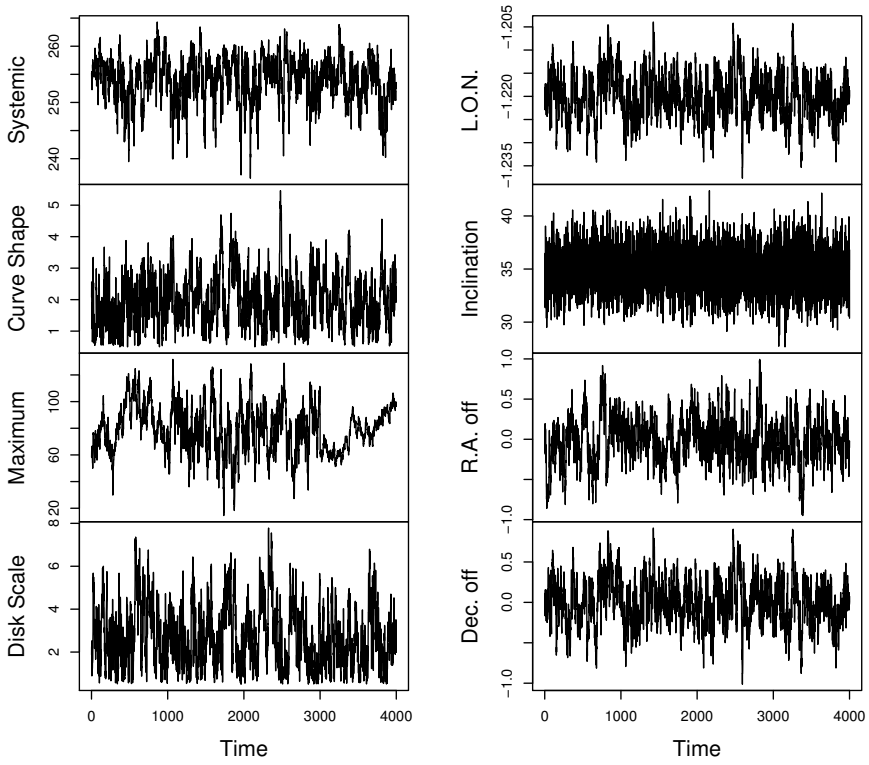

Figure 4.24: Four Markov chains of 1000 shown as time series.

parameters, and allays doubts about convergence of the bootstrap method.

Recent estimations from Hubble observations of the proper motion of the LMC by Piatek et al. (2008) were employed. Changes in disk inclination angle due to precession and nutation are taken to be zero based on Piatek et al. (2008) as opposed to the small factor used by van der Marel et al. (2002). Again the data was sub-setted to exclude data near the centre and perpendicular to the line of nodes that has a small factor g, the inverse of the projection factor. When g is less than 0.2 division results in the magnification of errors. The disk velocities were again calculated using the model of van der Marel et al. (2002).

Informative Normal priors were chosen for the rotation centre location, and line of nodes position angle. Four chains of 1000 iterations are shown as a single time series in Figure 4.24. Weakly informative Normal priors were chosen for the disk rotation model parameters. The inclination angle was originally weakly constrained and part of the full conditional distribution but caused problems as it approached an edge on disk, the disk plane velocities get extremely large, and

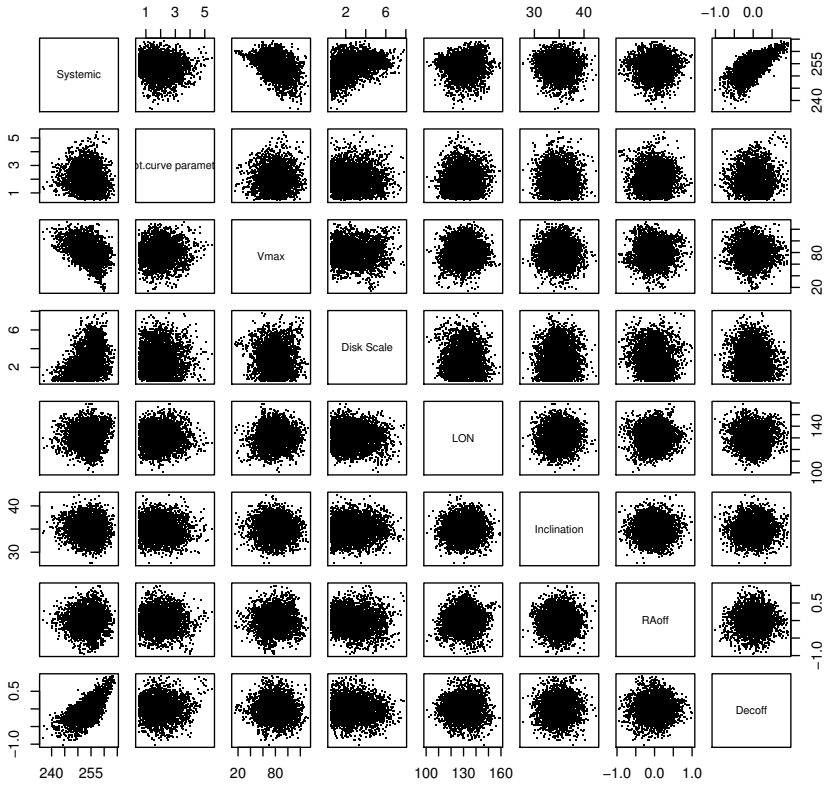

Figure 4.25: Joint distributions of pairs of disk model parameters.

for face on, zero inclination the disk plane velocities go to zero. The inclination turns out in fact to be degenerate with the maximum velocity of the rotation curve (Equation 34 van der Marel et al. 2002). The inclination angle was randomly sampled from a Normal distribution N(35°, 2°) to effectively add noise and was not part of the conditional distribution.

The systemic velocity is obtained by Gibbs sampling the full target distribution independently of the other parameters. The other parameters are then sampled with a Metropolis-Hastings algorithm which updates a six dimensional joint probability distribution. Theory guarantees that the samples obtained will be from the stationary distribution of the parameters, and the expectation value of a large sample will be representative of the population. The proposals must not have a low acceptance rate, so the sampler fails to move, or too high an acceptance rate, so the sampler moves, but too slowly in small steps. Short tuning chains are run first, and the variance of the outcomes are used in a scaling matrix, which sets the step size for proposed moves within the distribution.

The rotation centroid prior was set at the rotation centre location defined by van der Marel et al. (2002) with a standard deviation of 0.3 degree around $\alpha_{CM} = 5^h27^m.6$ and $\delta_{CM} = 69\overset{\circ}{.}87$. This results in 99% of the sampled centre locations being within one degree of the optical centre. A correlation can be seen in Figure 4.25 between the declination offset and systemic velocity. The low value tail on the systemic velocity distribution is the effect of changing declination. The perfectly Gaussian inclination angle distribution is the result of random sampling from a theoretical distribution without being conditional on the other parameters. All other parameters are fully conditional and may have odd shaped or bimodal joint distributions.

We took 5000 samples after the burn in and tuning chain period. The effective number of samples is the length L of the time series divided by the autocorrelation time. The autocorrelation of the chain time series measures the independence of the samples. For $L = 5000$ this amounts to only a couple of hundred samples for some parameters. The largest error bar was on the maximum velocity sampler, where the chain error was $2\,\mathrm{km\,s^{-1}}$. The line of nodes angle chain has a 1° error. These errors are much smaller than the standard deviation of the target distribution so the number of samples is sufficient.

We first simulated the model using our sample plus literature data (incl. Massey and Olsen 2003; Grocholski et al. 2006; Cole et al. 2005). The PNe sample of Reid and Parker (2006) is systematically higher than our other samples, but we include it in a second run, and its effect is to raise the systemic velocity by $3\,\mathrm{km\,s^{-1}}$ and lower the maximum velocity $5\,\mathrm{km\,s^{-1}}$. The subset sample of data used in the simulation is shown in Figure 4.26. The simulation results in a sample from the distribution of the model parameter values, conditioned on the observed spectroscopic velocities. Traditional measures of the moments of the distributions provide robust measures of the parameters and their errors. The distributions are shown in Figure 4.27.

The disk scale and rotation curve shape parameter have truncated Normal distributions as excursions below zero were forbidden in the algorithm. The R *MASS* library function *fitdistr* was used to fit a truncated Normal, from the *mcm* library, to the sampled distribution in these cases. The median was used as an estimate of the value of the systemic velocity, as the distribution is skewed to low values. The mean is a good estimate of the maximum velocity as the distribution is nearly normal. The parameter estimates are given in Table 4.3 with the values from the simulation including PNe data in brackets. The disk

Table 4.3: Model Parameters

Model Parameter	Estimate (with PNe)	σ (with PNe)
Systemic Velocity $\mathrm{km\,s^{-1}}$	254.6 (257.8)	3.9 (3.1)
Maximum Velocity $\mathrm{km\,s^{-1}}$	79.2 (74.2)	17.8 (10.1)
Curve Shape	1.9 (2.3)	0.9 (0.9)
Disk Scale kpc	2.5 (2.6)	1.6 (1.4)

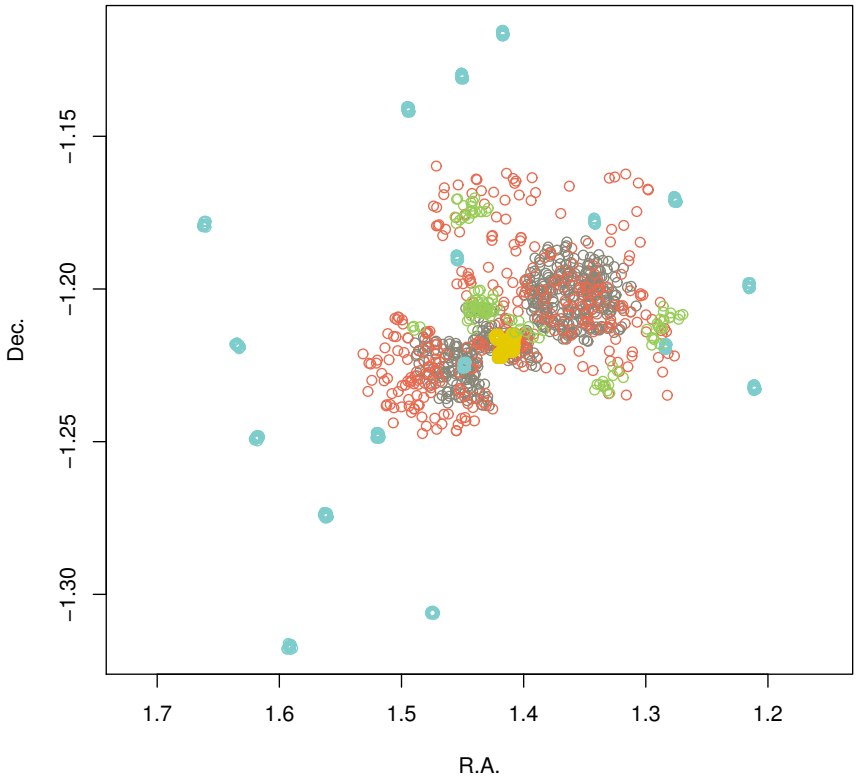

Figure 4.26: Locations of the 1707 data points in the complete MCMC sample. 494 grey stars this study; 384 blue Grocholski et al. (2006); 373 gold Cole et al. (2005); 342 red Reid and Parker (2006); 114 green Massey and Olsen (2003).

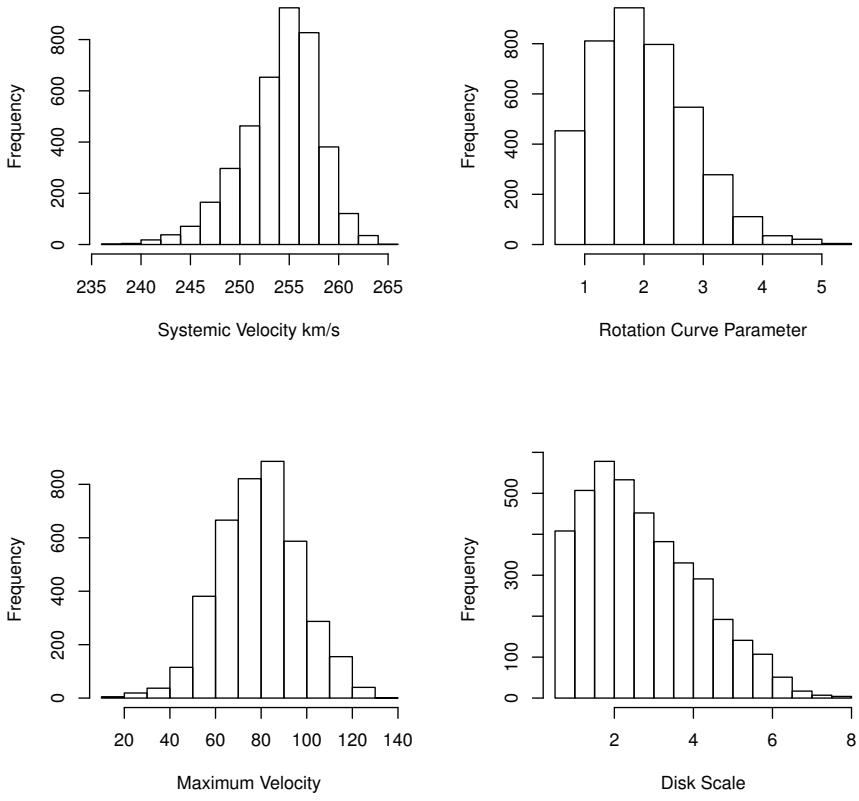

Figure 4.27: Model parameter distributions.

model parameters have informative or stricter priors. These are the range of disk structures under which the model parameter distributions are valid. The model parameters are in the stated ranges given in Table 4.3, given that the disk parameters are within the ranges in Table 4.4. Inclination is not part of the conditional distribution, but is part of the joint distribution. It is an artificially "fuzzy" fixed parameter. The model can be considered robust within the variation of this parameter.

Table 4.4: Disk Parameters

Disk Parameter	Estimate (with PNe)	σ(with PNe)
Line of Nodes	130.°7 (130.°1)	8.°7 (9.°4)
Inclination	34.°9 (35.°0)	2.°0(")
Centre R.A. offset	0.°02 (0.°009)	0.°288(")
Centre Dec. offset	0.°003 (0.°048)	0.°291(")

We also apply the MCMC model simulation to the PNe data (Reid and Parker 2006) alone to investigate the rotation curve implied by this sample. This data covers the bar and a little more of the disk than our data. The MCMC model from PNe agrees with our large sample estimate in all regards except for a systemic velocity offset of about $10\,\mathrm{km\,s^{-1}}$ and a lower maximum velocity of about $66\,\mathrm{km\,s^{-1}}$. This is the systematic offset of $10\,\mathrm{km\,s^{-1}}$ noted before. If we perform the same MCMC fit to the PNe heliocentric velocities, minus the systematic offset of $10\,\mathrm{km\,s^{-1}}$ then the model converges to our model. We find that systemic velocity goes from $266\,\mathrm{km\,s^{-1}}$ to $256\,\mathrm{km\,s^{-1}}$, the curve parameter stays close 2.1-2.2, disk scale 2.6-2.9 kpc, and maximum velocity goes up from $66\,\mathrm{km\,s^{-1}}$ to $72\,\mathrm{km\,s^{-1}}$.

Table 4.5: PNe Model Parameters

Model Parameter	Estimate	σ
Systemic Velocity $\mathrm{km\,s^{-1}}$	265.6	3.4
Maximum Velocity $\mathrm{km\,s^{-1}}$	65.7	14.0
Curve Shape	2.2	0.9
Disk Scale kpc	2.7	1.4

Correction for Asymmetric Drift

The component of circular motion of stellar tracers measured does not represent the true rotation of the disk as a whole. There are epicyclic and thermal motions, which mean the streaming velocity is always smaller than the true disk rotation. If one wants to calculate a mass or invoke the virial theorem the true circular

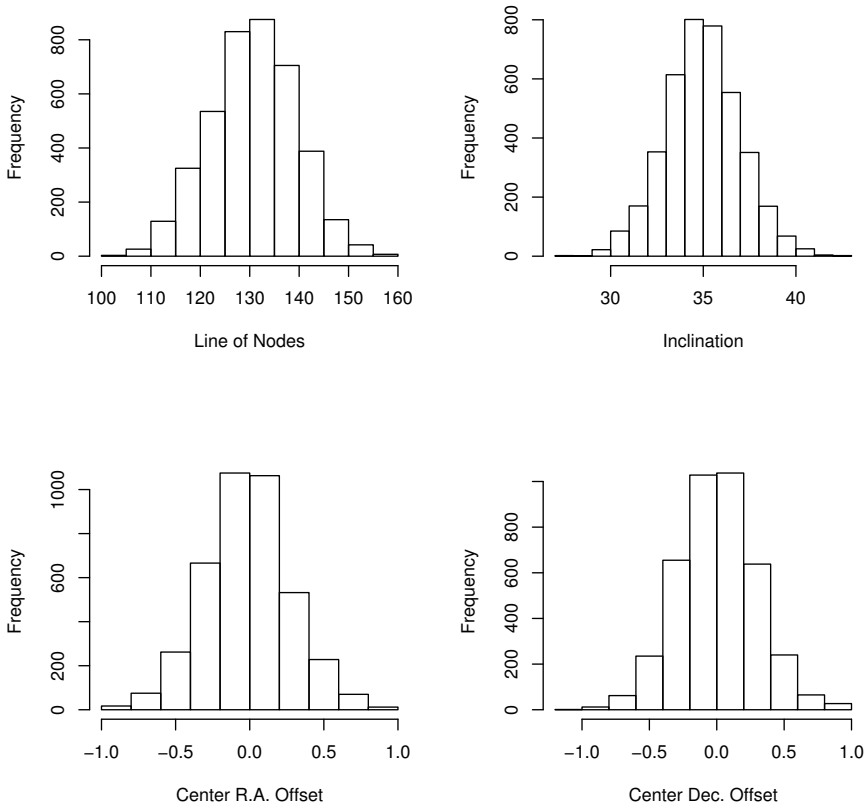

Figure 4.28: Disk geometry parameter distributions in degrees constrained by informative prior choices.

Table 4.6: PNe Disk Parameters

Disk Parameter	Estimate	σ
Line of Nodes	130.°1	9.°4
Inclination	34.°9	2.°0
Centre R.A. offset	0.°000	0.°005
Centre Dec. offset	0.°001	0.°005

velocity must be used. The asymmetric drift correction is added to the observed disk rotation velocity as $V_{circ} \approx V^2 + \kappa\sigma^2$ (van der Marel et al. 2002), where κ is a model-dependent factor that may vary with radius.

We take $\kappa \approx \partial \log \rho / \partial \log r$ which is close to 1 in the LMC modelled as a flared disk (Alves and Nelson 2000). The true maximum disk velocity is then estimated as approximately $83 \pm 17\,\mathrm{km\,s^{-1}}$ without the PNe and $78 \pm 10\,\mathrm{km\,s^{-1}}$ including the PNe data. Both estimates agree within the errors.

Counter-rotation and streaming motions

Evidence for counter-rotating or non-circular streaming motions is sought in the residuals to the model fit. Such motions would manifest as a systematic pattern in the residuals after we fit our rotation model. The model assumes circular orbits in one direction. Such motions could indicate a counter-rotating core (Subramaniam and Prabhu 2005). They may show highly elliptical orbits with their major axis along the line of nodes which appear as streaming motions along the bar (Sellwood and Wilkinson 1993). The best model of the rotation curve obtained from simulation of parameters is subtracted from the disk plane velocity.

Firstly the residual velocities from our AAOmega data in the eastern field around the rotation centre are considered. The observed disk plane velocities are subtracted from the model velocity for the radius and angle at the star's location in the galaxy. When we plot the residuals for the eastern field there is no systematic pattern in the residuals, shown in Figure 4.29. When we test the effect of North or South of the line of nodes on the residuals we find no evidence for an effect. The two groups are plotted in Figure 4.30, and while the median of the Southern group is slightly higher at $-4.4\,\mathrm{km\,s^{-1}}$ than the North at $-9.6\,\mathrm{km\,s^{-1}}$, the shared variance is so great as to completely overwhelm any difference in the samples. A one-way analysis of variance (anova) gives an F statistic of 0.239, with high probability p=0.64 that any difference could be reproduced by random sampling. This indicates that we have no evidence against the hypothesis that the two groups are the same.

Considering all the literature sample data (Cole et al. 2005; Grocholski et al. 2006; Massey and Olsen 2003) except the PNe over the full radius, we find a marginally significant difference in residuals around the line of nodes, with F = 3.7102, and p = 0.05429. Over the full radius of these data the median North of line of nodes is $7.2\,\mathrm{km\,s^{-1}}$ and South is $-4.7\,\mathrm{km\,s^{-1}}$. However, it turns out the Massey RSG data (Massey and Olsen 2003) are entirely responsible for the effect. The set of RSG show a highly significant difference in residuals North to South, F= 45.059 with p = 8.008e-10. The median residual is $30\,\mathrm{km\,s^{-1}}$ North of the line of nodes and $1\,\mathrm{km\,s^{-1}}$ South, Figure 4.32a. Subtracting the 115 Massey stars from the sample, and testing the remaining data including our sample shows a low F statistic of 0.01, and high probability that there is no difference in the residuals with p = 0.920.

If we again look only at the central 1.2 kpc with our data and Cole et al. (2005); Grocholski et al. (2006), but excluding the RSG we still find no effect.

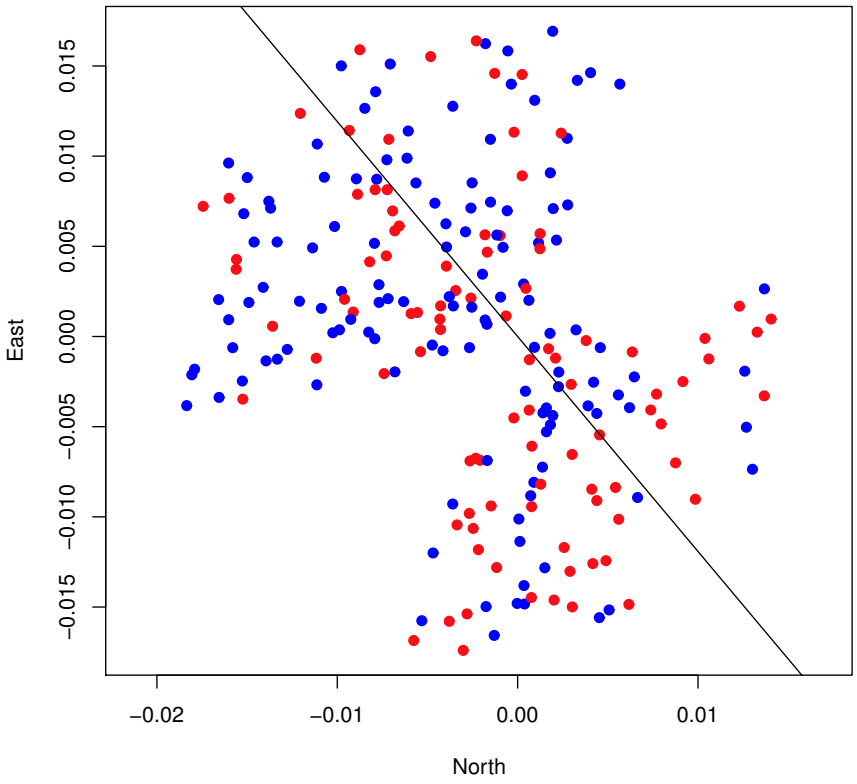

Figure 4.29: No spatial pattern in the residuals from the rotation model, North and South of the line of nodes, within 1.2 kpc of the centre.

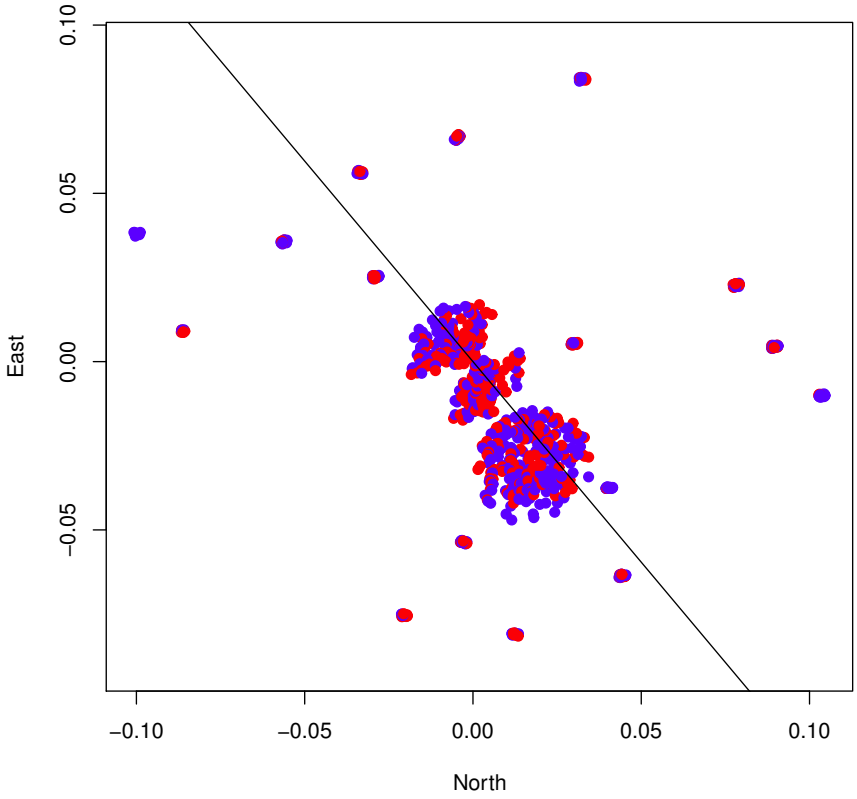

Figure 4.30: There is no significant pattern in residuals from data over all radii.

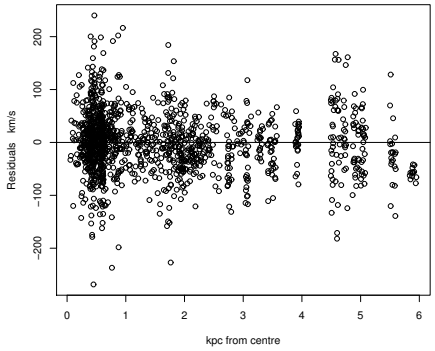

(a) Model residuals from our sample plus literature data with radius from centre in kpc

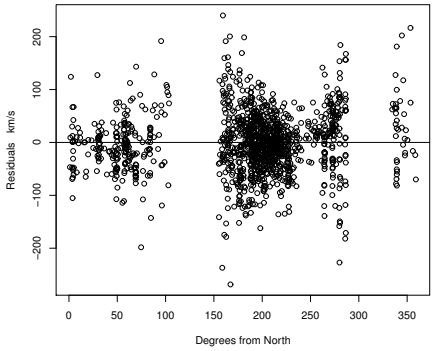

(b) Model residuals from our sample plus literature data with angle from North in degrees

Figure 4.31

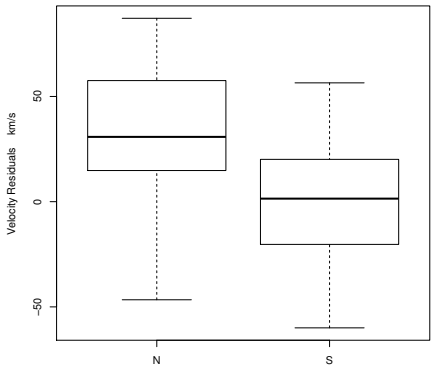

(a) Massey RSG data show a difference in residuals about the line of nodes.

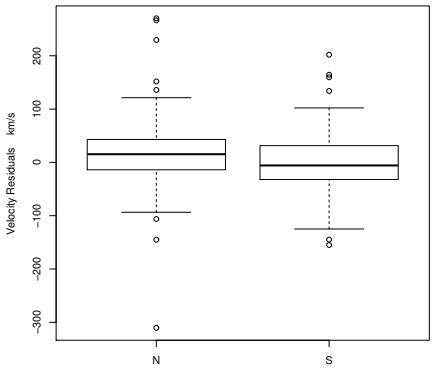

(b) The residuals from the rotation model in PNe data show a significant difference from North to South of the line of nodes in the same sense as the Massey RSG data.

Figure 4.32

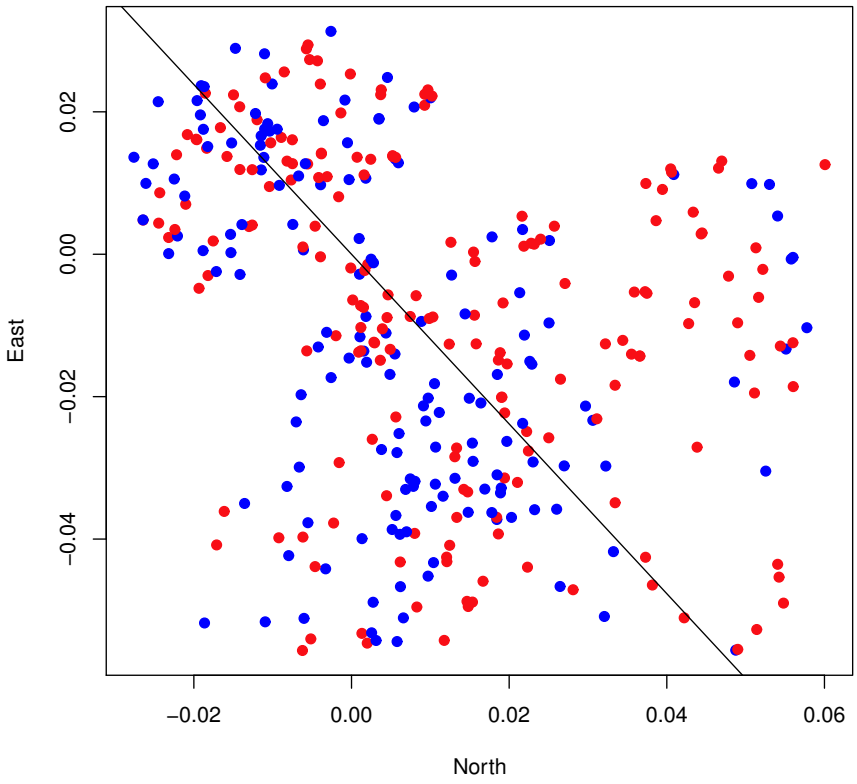

Figure 4.33: The velocity residuals from a rotation model based on the PNe data.

An anova test shows no significant difference with an F stat of 2.6545 with p = 0.1038. We have a median residual North of line of nodes at $5.0\,\mathrm{km\,s^{-1}}$ and South $-1.0\,\mathrm{km\,s^{-1}}$, which again is an effect to be expected when random sampling from the population.

Planetary nebula data over all radii also show a significant trend in the same sense as the Massey data with a mean in the North of $15.4\,\mathrm{km\,s^{-1}}$ and South $-5.7\,\mathrm{km\,s^{-1}}$, which significantly differ, F= 9.4 and p = 0.0024. Figure 4.33 and Figure 4.32b. This difference is not seen in the inner region less than 2 kpc but only over larger radii.

It is noteworthy that the RSG population and the PNe both appear to have systematically higher rotation velocities North of the line of nodes . This may indicate these populations have a slightly different rotation pattern to the more populous RGB population. It indicates that there is an excess of rotational

velocities above the line of nodes, compared to those predicted by the rotation model, and slower rotational velocities below. This pattern is difficult to interpret as a population rotating in the wrong sense, in the outer disk, and the effect is not seen in the inner 1.2 kpc. The larger than expected rotational velocities in RSG 's in the Northern part of the LMC has been noted by other authors (including, Piatek et al. 2008; Olsen and Massey 2007).

There is no statistical evidence of a difference the in the rotation velocity residuals of the sample as a whole. There is however, only a low probability that the PNe residuals are the same North and South of the line of nodes at radii greater than 1.2 kpc, and even lower probability that the Massey RSG residuals are the same. The bulk of the data, including ours, shows no residual difference at various angles or radii.

4.3.5 Metallicity

Like silicon, calcium is purely an α-element not prone to proton capture nucleosynthesis or other processes (Ivans et al. 2001). Some α elements can show variations in abundance due to proton capture or involvement in the CNO cycle. As a purely α product it is not directly related to r-process iron-peak elements, but is still a good indicator of global metallicity (Rutledge et al. 1997). The $[\alpha/Fe]$ ratio is expected to vary with SNe enrichment of the environment while the [Fe/H] ratio as measured by Ca remains constant. The effective temperature of the stellar atmosphere and the surface gravity affect the width of the lines, and these effects are calibrated out using magnitude as a single proxy for gravity and effective temperature.

The Ca II triplet width has been calibrated from earlier globular cluster studies to composite stellar populations in dwarf spheroidal galaxies in the range $-2.5 < [Fe/H] < -0.5$ dex in RGB stars (Battaglia et al. 2008). The relation is not as well calibrated for higher metallicity but our sample is in the range $-2.0 < [Fe/H] < 0.0$. The Ca II triplet as a metallicity indicator has been shown to be applicable to mixed galactic field populations of a variety of abundances and ages (Cole et al. 2004).

The velocities obtained from cross correlation with the template spectra in 47 Tucanae are used to predict where the doppler shifted line centres lie. The velocities and spectra were input into the EW Fortran program written by Da Costa and modified by A.A. Cole and described in Friel et al. (2002). The equivalent widths of the three Ca II triplet lines were estimated by fitting a Penny function to the line profile. The Penny function is a sum of a Gaussian and a Lorentzian and has been shown to better approximate the red and blue wings of the lines caused by photospheric broadening phenomena (Suntzeff et al. 1992; Cole et al. 2004).

Spectroscopic absorption lines are often modelled by fitting a Gaussian profile of the form,

$$F(\mu, \sigma) = Ae^{-\left(\frac{x-\mu}{\sigma}\right)^2} \tag{4.3}$$

The parameters of the profile function μ, σ are fitted by minimising the residuals of the data. The integral of the fitted function gives an estimate of the equivalent width of the absorption feature, in Angstroms. It has been shown by several authors Cole et al. (e.g. 2004); Suntzeff et al. (e.g. 1992) and in this study that the Gaussian fit to the line profiles underestimates the width of the lines. The Gaussian models the Maxwellian thermal velocity distribution of absorbers in the chromosphere, where the core of the Ca II triplet is created above the photosphere(Smith and Drake 1990).

The damping wings, a broadening at the edges of the lines, are created by collisions or pressure effects on absorbers. The wing features in the Ca II triplet are thought to be generated mainly at the photospheric surface of the star. The surface pressure is a function of surface gravity and temperature. Pressure induces the close range Stark and Van Der Waals effects, the effect of ions on photon energy levels absorbed. These effects create radiation damping which is a quantum mechanical phenomenon. The uncertainty principle means the wavelength spread or line width increases with increasing energy. This effect results in a Lorentzian spectral absorption profile (Böhm-Vitense 1989). The combination of the Gaussian doppler effect and Lorentzian is known as the Voigt spectral profile or Penny function. The difference in the measured equivalent widths using the two fitting functions is appreciable within the medium to high resolution observed spectra. The Gaussian was a good enough approximation in early studies with low resolution spectra.

The continuum $C(\mu)$ has been modelled by a simple low order polynomial as the flux of the red giants at these wavelengths is nearly flat. The fitted continuum is then normalised as $C(\mu) = 1$. The integrated equivalent widths of the lines are therefore measured in units of the continuum flux. The model is then the normalised continuum minus the Gaussian profile and the Lorentzian.

$$F(\mu, \sigma) = C(\mu) - A_1 e^{-1/2\left(\frac{x-\mu}{\sigma}\right)^2} - \frac{A_2 \Gamma}{(x-\mu)^2 + (\Gamma/2)^2} \tag{4.4}$$

The sample used to estimate metallicity was restricted to stars on the RGB, as the calibration of the Ca II triplet has only been established for this range. The sample was also restricted to equivalent width measurements with errors less than 1 Å. The error in equivalent width was taken as the quadrature sum of the individual line errors, which propagated through to the metallicity error. The IRAF SPLOT graphic cursor equivalent width routine was automated and applied to the spectra as a check. The IRAF method agreed with our method above to within 2%.

The ratios of the three line strengths fitted are plotted in Figure 4.34. Those spectra with unusually weak or strong lines appear as outliers away from the central distribution. Odd spectra with unusual ratios were inspected and found to exhibit either very low signal to noise, instrumental features like zero read-out at line wavelengths or cosmic ray contamination. A good subset of the sources with the most likely line width ratios was selected. Outlying spectra with unusual line width ratios were rejected as being contaminated in some way.

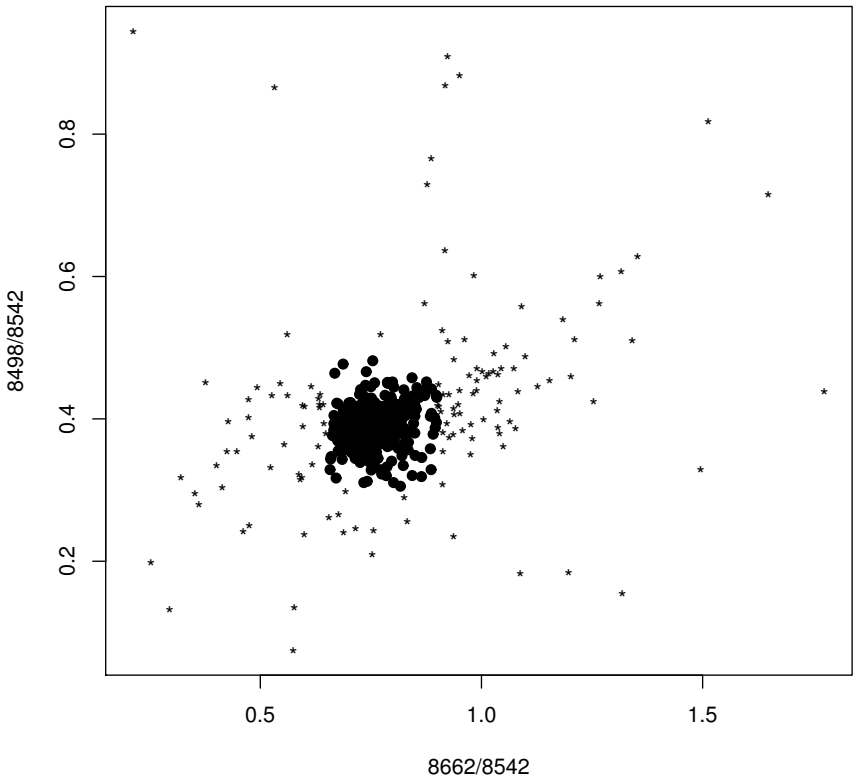

Figure 4.34: Ratios of line widths, solid points show selection for analysis, outlying starred points have one or two lines weaker, indicating contamination.

Cutting odd line ratios from the sample left 240 stars with which to estimate the metallicity distribution.

As in Chapter 3 we correct for the effect of both surface gravity and effective temperature with a single photometric measure. The dependence of the line widths on surface gravity has been studied using both open and globular clusters with single stellar populations (e.g. Rutledge et al. 1997; Warren and Cole 2009; Carrera et al. 2007). We rely on previous determinations of the magnitude of the effect from globular cluster studies (Cole et al. 2009; Hankey and Cole 2011) and obtain a reduced equivalent width using the relation,

$$W' = \Sigma W + 0.45(K - K_{HB})$$

where the difference between the star's near-infrared K_s band magnitude and the horizontal branch, $K - K_{HB}$ was used to measure the surface gravity effect on equivalent width.

The LMC has no clearly defined horizontal branch detectable in CMD studies (Nikolaev and Weinberg 2000) so the red clump location was used to define the magnitude of stars that have undergone helium core flash. This is below the magnitude limit of the 2MASS catalogue but is present in the deeper IRSF catalogue at 16.6 (Kato et al. 2007). After correcting for effective temperature and surface gravity we have a reduced equivalent width measure that now only depends on metallicity. The reduced equivalent width W' was then transformed into a metallicity using the relation,

$$[Fe/H] = (-2.738 \pm 0.063) + (0.330 \pm 0.009)W'$$

Low Metallicity Calibration at K-Band

The question of how far the Ca II triplet is a representative measure for extrame low metallicities was explored by Starkenburg et al. (2010). A linear relation exists for higher metallicities above -2.0, but below that Starkenburg et al. (2010) proposed that non-linear terms were required, based on synthetic spectra. Continuing this work but basing the calibration on observational spectra Carrera et al. (2013) undertook a study of extreme low-metallicity stars in the MW halo in order to extend the calibration of the Ca II triplet as a metallicity measure. Carrera et al. (2007) had already calibrated the Ca II for metallicities in the range $-2.2 \leq [Fe/H] \leq +0.47$ dex. Previously Battaglia et al. (2008) had found that the Ca II triplet saturates for metallicities below -2.5 dex.

Carrera et al. (2013) arrive at a calibration that allows the Ca II to be used down to [Fe/H]= -4.0. They found that some non-linear terms are required in order to fit the data, as well as cross terms. They employ absolute K_s magnitudes rather than tip of the red giant branch (TRGB) or HB reference magnitudes. The following relation is valid for up to five K_s magnitudes below the TRGB,

$$[Fe/H] = -3.33 + 0.15K_s + 0.48\Sigma Ca - 0.27\Sigma Ca^{-1.5} - 0.01\Sigma Ca \times K_s \quad (4.5)$$

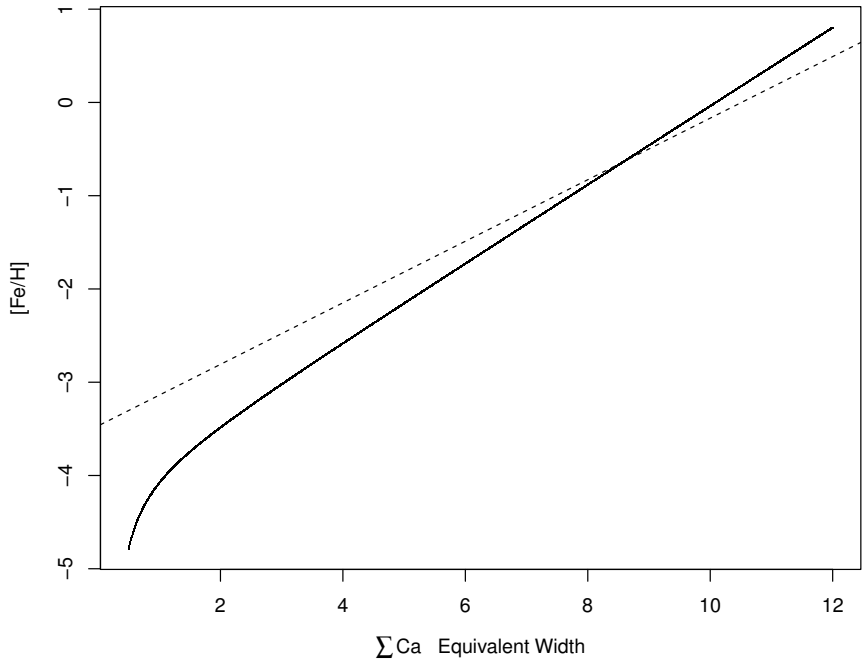

Figure 4.35: Theoretical Carrera et al. (2013) metallicity calibration for absolute magnitude K_s = -6.0 (apparent K_s = 12.4 at LMC distance) solid line, dotted line is the calibration used in this study.

We find that according to the calibration of Carrera et al. (2013) our adopted scale in this study overestimates the metallicity of stars at [Fe/H] = -1.5 by approximately 0.3 dex, and underestimates the metallicity of stars near [Fe/H] = 0.0 by about 0.1 dex. The bulk of our data is unaffected with approximately zero residual from the Carrera et al. (2013) calibration, (see Figure 4.36b), so conclusions regarding mean bar metallicity are unaffected. The main effect is a slightly extended tail of low metallicities making our results closer to that of Cole et al. (2004).

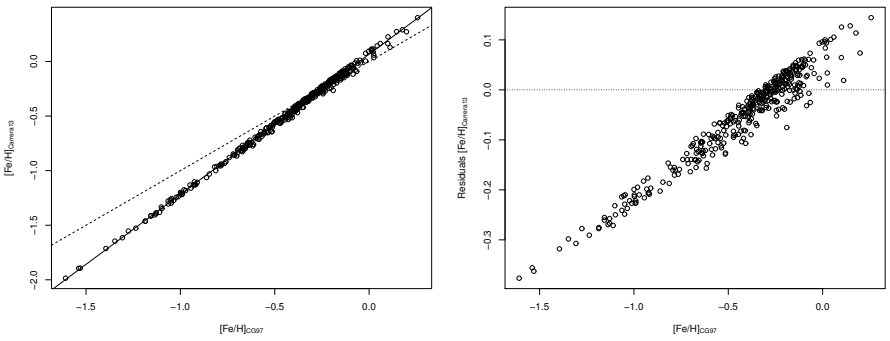

(a) Comparison of this study metallicity estimate with calibration of Carrera et al. (2013). Dotted line is this study, which overestimates low metallicity values.

(b) Residuals from comparison.

Figure 4.36

Metallicity Distribution

The metallicity distribution of the sample is plotted in Figure 4.37a. The distribution of metallicity in the sample shows the same characteristics as the Cole et al. (2005) sample. The mean of the distribution is -0.36 dex. The median, -0.31 dex, is less sensitive to the long, low tail. The long, low tailed distribution is best modelled as two Gaussians. A non-linear least squares method was used to fit a model of two Gaussians. The data were fit by a low metallicity population distributed around -0.40 dex with a standard deviation of 0.40 dex, and a metal rich population centred at -0.26 dex with a narrower standard deviation of 0.17 dex. The narrow spread, higher metallicity Gaussian contains 55% of the sample stars, and the low metal broad distribution contains 45% of the sample, see Figure 4.37b.

We can specify a model following Cole et al. (2005), with a low metallicity Gaussian distribution representing about 10% of the population centred at -1.08 with standard deviation 0.46. A non-linear least squares method fits the Gaussian narrow high metal peak at mean -0.28 with standard deviation 0.22,

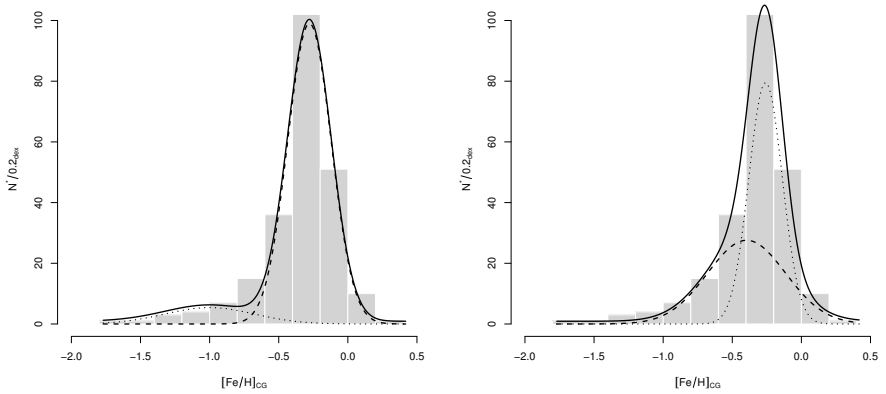

(a) Distribution of metallicity modelled with small, broad, low metallicity population centred at -1.1 dex.

(b) Distribution of metallicity modelled by two Gaussians.

Figure 4.37

see Figure 4.37a. The residual sum of squares for this model is 3.9 compared with 1.4 for the unconstrained two Gaussian fit and 6.7 for a single Gaussian fit.

The sample agrees with the findings of Cole et al. (2005) within the errors, although we note that our estimate is on the higher metallicity range of possible values. We employ K_s(star)- K_s(Red Clump) as a single proxy to remove the effects of surface gravity pressure broadening of lines and T_{eff}. The use in this study of K_s-band red clump magnitude is novel for mixed stellar populations. Previous calibrations of mixed populations have been based on V-band clump magnitudes (e.g. Cole et al. 2005). These two methods are compared in Appendix D and found to be in agreement except at the very metal-poor end of the distribution, where the K_s band method may over-estimate the metallicities slightly. Indeed we have shown above in Section 4.3.5 that our method overestimates metallicities at the metal-poor end of the scale compared to the calibration of Carrera et al. (2013). The metallicity estimate by both methods is in agreement for the bulk of the population.

Low Metallicity Population

The sample of metallicities in the LMC population was shown to be best modelled by two distributions. One with a mean [Fe/H] of -0.26 dex and σ 0.17 and one at -0.40 dex with σ 0.40. The possibility of a unique low metallicity population with characteristics that distinguish it from the bulk of the LMC was investigated. We considered the model of Cole et al. (2005), which has a low metallicity population centred at -1.08 dex σ 0.46, and was shown in the

previous section to be nearly as good a fit to our data.

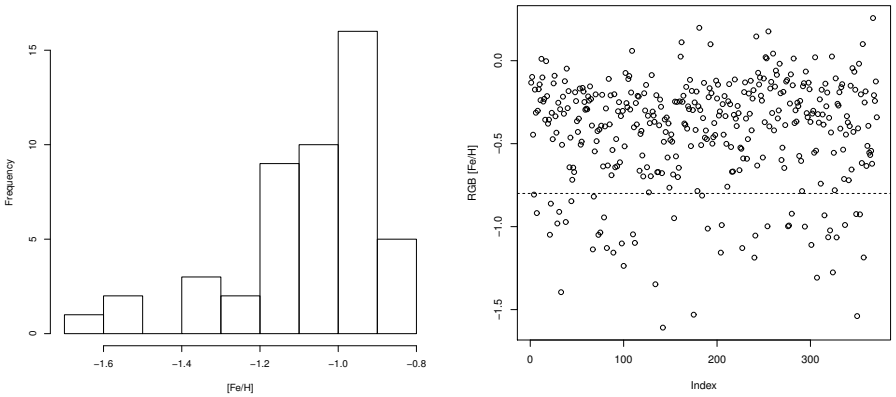

(a) Distribution of low metallcity sample.

(b) Selection of low metalicity subset cut at -0.8

Figure 4.38

The sample of RGB stars with metallicity estimates was arbitrarily cut at -0.8 dex into high and low metallicity subsets Figure 4.38b. There were 48 low metallicity stars whose distribution is shown in Figure 4.38a. The spatial distribution of these subsets was considered. A k-NN nearest neighbour statistic was employed to characterise structure in the two dimensional distribution, with k=3 as there are two categories (Hastie et al. 2009). The nearest neighbour statistic is robust to edge effects, which was appropriate for our two degree fields which have sharply defined edges. The distribution on the sky is shown in Figure 4.39a.

A Monte Carlo scheme randomly reassigned the labelling of the stars as low or high metallicity, and calculated the nearest neighbour for each star and the mean value was taken as the statistic. This was iterated 1000 times giving the distribution of statistics for the random arrangements of high and low metallicity stars shown in Figure 4.39b. The statistics for the observed distribution are shown as the vertical lines. The observed distribution has statistics that could have come from the distribution of random arrangements, showing no evidence of clustering of low metallicity stars in 2-D space.

We used the same two dimensional spatial cluster analysis in CMD 2-D space, Figure 4.40a. The high and low metallicity labels on each star were randomly re-assigned 1000 times and the distribution of statistics for each arrangement in the CMD is shown in Figure 4.40b. Also shown is the statistic for a non-random arrangement, which has zero probability of being random. The observed colour-magnitude arrangement could have come from the random distribution, albeit with a low 2% probability.

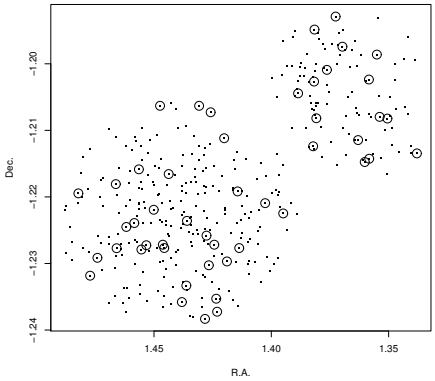

(a) Spatial pattern of all stars with metallicity estimates, those with metallicity less than -0.8 are circled.

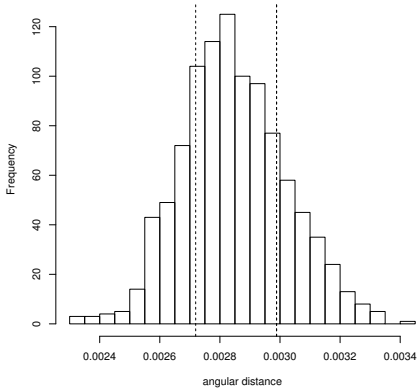

(b) Distribution of nearest neighbour statistic for 1000 random arrangements of high and low metallicity stars. The median statistic 0.0027 degrees and the mean 0.0029 shown for observed stars are consistent with being random.

Figure 4.39

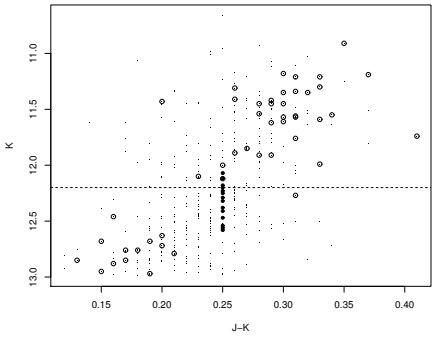

(a) Low metallicity stars are circled on the CMD. TRGB dotted line at 12.2., may be less bright for low metallicity population which is also expected to be bluer. Example of non-random solid points is shown.

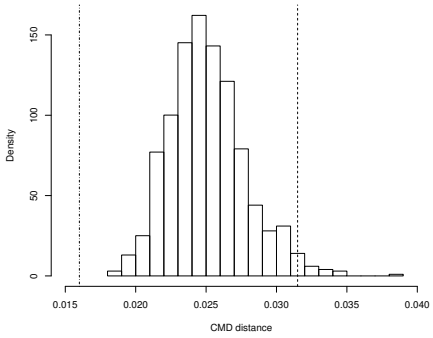

(b) Distribution of nearest neighbour statistic for 1000 random arrangements in the (J-K, K) CMD, the statistic for the observed stars is shown, with a low 0.02 probability of being drawn from the random distribution. Statistic for non-random points is 0.016 with zero probability.

Figure 4.40

The lower probability of being random gives an increased probability that the low metal population has a unique location on the CMD, it appears the TRGB is fainter and the RGB stars are bluer than the bulk population. Decreased molecular weight of the H burning shell around a given He core mass at low metallicity, results in a decrease in luminosity on the RGB (Salaris and Girardi 2005). This effect on the TRGB is more pronounced at K band magnitudes which are more sensitive to metallicity than the more common I band. In addition the low metallicity stars on the RGB in Figure 4.40a appear to be clustered towards the blue side of the RGB as expected (Girardi et al. 2002).

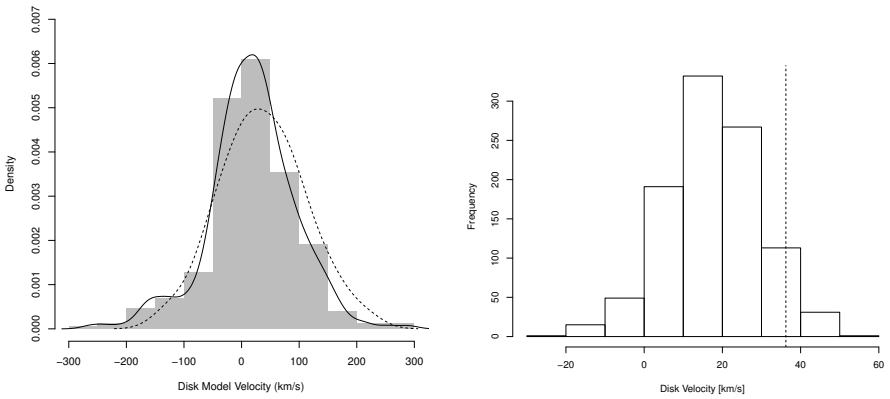

(a) Histogram of metallicity sample disk plane velocities, with solid density line. Low metallicity sample density, dotted line.

(b) Histogram of 1000 random sample draws of same size as low metallicity sample. The mean velocity of the observed low metallicity sample, dotted line, is consistent with being a randomly selected velocity sample.

Figure 4.41

The distribution of disk plane model velocities is shown in Figure 4.41a. The dotted line low metallicity velocity distribution has a slightly higher mean value than the shaded histogram of all stars with the solid line density. Taking 1000 random samples of 48 from the total population we get a distribution of the means of these samples in Figure 4.41b. The mean of the observed sample is well within the distribution of random samples, indicating the low metallicity population does not exhibit special kinematics.

4.4 Discussion

4.4.1 Rotation Curve

Our data does not extend far beyond the characteristic disk radius where the rotation curve is expected to flatten. Previous studies have tended to have larger characteristic disk radius R_0 parameters. Our lower systemic velocity means there is a steeper inner slope, which brings the turnover point of the rotation curve in closer to the centre. The addition of literature data from outside this radius helps constrain the flat outer galaxy velocity parameter, but there are more complete studies of the outer galaxy rotation curve. The extra data more importantly confirm the model fitted to our inner sample is reasonable. It has a inner rotation curve with shape parameter closer to 1 and a slightly smaller characteristic radius at 1.9 kpc (Table 4.2).

We find a solid body rotation curve in the central region which rises almost linearly at $25\,\mathrm{km\,s^{-1}\,kpc^{-1}}$. The line of nodes angle is initially fitted at 129° based on our observations alone. The addition of literature samples confirm the results based on our data alone.

The bar structure is stellar in composition, the HI gas showing no associated structure (Staveley-Smith et al. 2003). Bar kinematics might be expected to result in gas or stellar streaming motions along the line of nodes axis. Radial velocities tend to be insensitive to motions along the bar axis, which is almost perpendicular to our line of sight.

A simple model of the bar as part of an unified rotating disc fits our data, as well as a varied set of published velocity samples. A lower systemic velocity for the disk rotation model is simpler than a higher systemic velocity, which results in negative disk plane velocities in the inner 0.5 kpc, which must be explained by complex counter-rotation or non-circular streaming motions associated with the bar resonance. It is still possible that the systemic velocity of the bar may actually be different to the disk, which would suggest a small line of sight spatial offset. The bar appears transversely offset from the disk centre, and given differing HI gas components, a small line of sight offset from the disk plane would not be impossible. As expected we confirm previous studies and find that the average ratio $V_{max}/\sigma \approx 3$ is much greater than unity across our fields (van der Marel et al. 2002; Alves and Nelson 2000). This implies the LMC has a thick stellar disk that is mainly rotationally supported (Binney and Tremaine 2008).

There is no evidence of two distributions of stellar velocities. If the bar were spatially separate from the disk, evidence of a distinct velocity distribution would be expected, unless the objects are separate but co-moving. The conclusion is that the bar and disk are one and that the systemic velocity is closer to $257\,\mathrm{km\,s^{-1}}$ than $264\,\mathrm{km\,s^{-1}}$. The consequences for models of the LMC disk rotation of a lower systemic velocity for the centre of mass would be to slightly increase the rate of increase of velocity with radius in the solid body inner disk (Olsen et al. 2011).

We detect no evolutionary differences in the kinematics of the stellar pop-

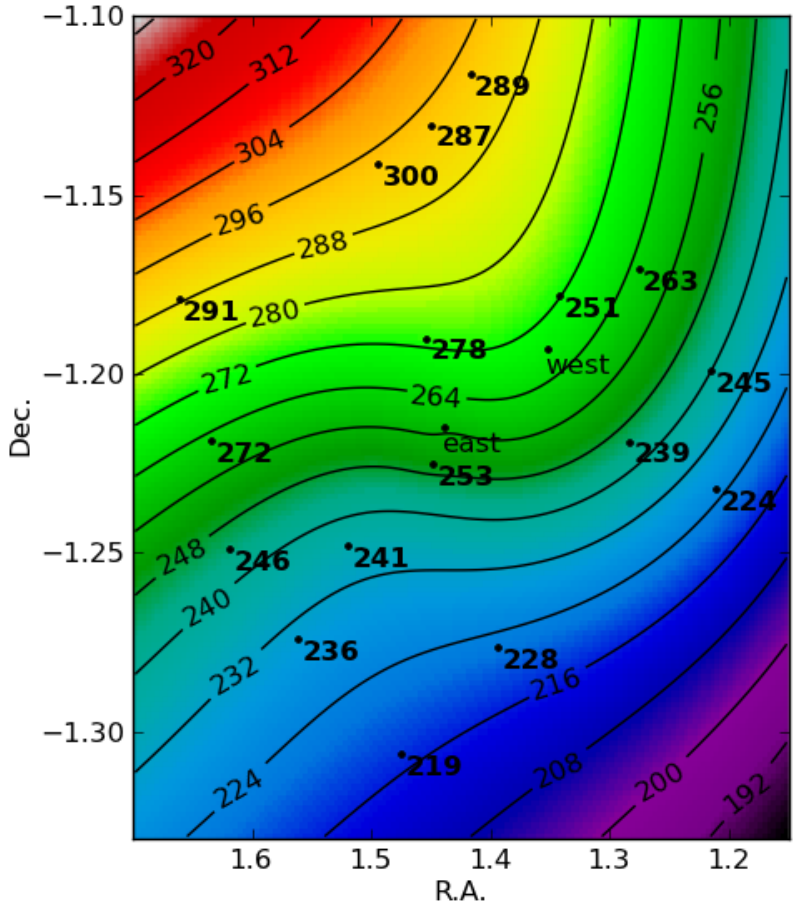

Figure 4.42: The heliocentric velocity field predicted by the model based on our data. The centres of our east and west field are shown. The mean velocities of the LMC field stars from the sample of Grocholski et al. (2006) are plotted as points. The model shows good agreement except for one field group 251 km s^{-1} near the west centre.

ulations. The various stellar populations identified in the CMD of Nikolaev and Weinberg (2000) show no variation in mean velocity or dispersion when the colour ranges of the populations are plotted against velocity and dispersion in Figure 4.10.

4.4.2 Abundances

Cole et al. (2005) find a median metallicity of -0.4 dex for a sample of 373 RGB stars in the centre of the bar region. These observations covered a small region inside our field, see Figure 4.20a. Our result of -0.36 dex agrees within the error margin. Olsen et al. (2011) find a median metallicity of -0.56 dex which is lower than our estimate and that of Cole et al. (2005). Olsen et al. (2011) find evidence of a very small population, 3%, of very low metallicity stars that correspond to SMC metallicity. Cole et al. (2005) also noticed a minor low metallicity population. We only detect a small population, 28 stars out of 240, with [Fe/H] $leq - 1.0$, which do not show a kinematic difference from the more metal rich population.

The dense stellar field in the centre of the LMC presents problems of contamination of sources by adjacent objects. For this reason care was taken to reject spectra which exhibited line width ratios inconsistent with the expected pattern observed in a single RGB stellar source, (Figure 4.34). It was assumed in these cases that one or more absorption features had light bleed in from nearby stars. Care must be taken with using the Ca II triplet in populations with mixed ages and metallicities (Rutledge et al. 1997). The effect of temperature and surface gravity on line width in single stellar populations is used to calibrate our results. The sample is restricted to well calibrated RGB stars only.

The distribution of metallicity in the sample shows the same characteristics as the Cole et al. (2005) sample, (Figure 4.37b). There is the same tail of low metallicity stars, however the distribution is shifted to lower metallicities. The distribution could be modelled as the sum of two Gaussians. There is a larger Gaussian distributed population centred at -0.3 dex while the tail of low metallicity stars could be modelled by a Gaussian centred at -1.0 , perhaps representing a less populous and older low metallicity population. The distribution reflects the LMC SFH with a long low star formation rate from 13 to 5 Gigayear and then increased rates after 5 Gigayear at higher metallicity.

The metallicity distribution found by this study is similar to that found by Carrera et al. (2008), who also find a peak for the bar region of [Fe/H] $= -0.39$ with a low metallicity tail. The disk regions outside the bar show a small decreasing gradient with galactocentric radius. The low metallicity stars were analysed for indications of unusual characteristics that may mark them as a unique population, perhaps an accretion remnant from the SMC as found by Olsen et al. (2011). No correlation was found between metallicity and any one of, spatial locattion within the bar, colour-magnitude nor velocity.

It was noted that using Gaussian fits to measure the ew results in an underestimate of the line widths. In exploratory analysis the IRAF *splot* routine was used to fit crude Gaussian models to individual spectral lines, which resulted in

a mean [Fe/H] of -0.8, demonstrating that the Gaussian model underestimates the impact pressure broadening of the wings of the spectral features. The sum of a Gaussian and Lorentzian was used in the final fit resulting in a mean [Fe/H] of -0.36.

Cioni (2009) find a small metallicity gradient across the disk and Feast et al. (2010) find a small but significant gradient in RR Lyrae stars across the LMC. Our slightly higher metallicity determination for the bar suggests enrichment of the bar compared the disk, and we are following this up (Cole & Hankey in prep.). Background disk field RGB stars from Grocholski et al. (2006) were employed to constrain the disk rotation field at large radii. We will apply our Ca II triplet equivalent width methods to disk field stars observed around the clusters of Grocholski et al. (2006) to estimate the metallicity at larger radii.

Tremonti et al. (2004) define the stellar mass-metallicity $M_\star - Z$ relation for galaxies from the Sloan Digital Sky Survey and demonstrate how enrichment increases with mass and luminosity. They propose that the origin of the relation is increased star formation efficiency with increased mass; in addition outflows of metal rich material in galactic starburst winds deplete the metals in low mass galaxies more than in massive galaxies with large gravitational potentials. Alternate possibilities are that inflows of metal poor gas deplete smaller galaxies faster or that gas is locked up in low mass, long lived stars and not quickly enriched and recycled.

Lee et al. (2006) extend the $M_\star - Z$ relation down to dwarf irregular galaxies from Spitzer near-infrared luminosities and find the correlation remains strong yet slightly different. They find little scatter in the relationship even at low mass. They therefore propose that the mass loss mechanism for dwarf galaxies must be slow and steady rather than catastrophic and that star formation efficiency is lower.

The slight enrichment of the LMC bar could indicate that the denser stellar environment is following the $M_\star - Z$ relation. Under this hypothesis two factors could be at work; firstly the bar potential is more efficient at star formation from gas; and secondly the bar entrains enriched gas outflows from the disk which fall back into the central galaxy.

The metallicity of the LMC, 8.4 on the O metallicity scale, fits the $M_\star$–Z relation, with stellar mass $10^{9.4} M_{M_\odot}$ (Tremonti et al. 2004); this yields $log(O/H) = 8.4 - 12.0 = -3.6$. Van der Swaelmen et al. (2013) find that [O/Fe]≈ 0 around [Fe/H]$= -0.5$, within the LMC. So [O/H]$\approx$[Fe/H] and agrees with our finding of a mean metallicity of -0.36 dex for the bar population.

4.4.3 The Zhao Sample

The Z03 velocity data with an error of about $30\,\mathrm{km\,s^{-1}}$ was accurate enough to look for evidence of a micro-lensing population separate from the LMC main disk. The velocity anomaly seen in the Z03 data near the centre of the disk has not appeared in the AAOmega near infra-red data. The *2df* spectrometer mounted atop the AAT was accurate enough for high velocity redshift galaxy surveys, but the varying loads on the spectrograph at different elevations were

known introduce systematic errors. The Z03 data was taken over a two year period. As both sets of velocities show the same near Normal distribution with slightly long tails we conclude that bulk properties of the samples are near identical. The variation is in the spatial distribution of velocities, which in the Z03 data coincides with the temporal separation of field observations. We have no direct evidence for this, but widely separated observations with differing elevations of the spectrograph atop the AAT could plausibly create a systematic error in the mean velocities of the fields. The larger dispersion in the Z03 distribution is a result of larger random velocity errors (up to $50\,\mathrm{km\,s^{-1}}$) compared to ours (less than $15\,\mathrm{km\,s^{-1}}$). A systematic offset of the same amount appears in the PNe data of Reid and Parker (2006) which were observed on the same *2df* spectrometer.

Both Z03 and our data sets exhibit very slight deviation from Normal, slightly heavy tails at low and high velocities. Otherwise the two data sets are nearly perfectly Gaussian, which indicates that the stellar population is virialised within the disk scale height. Our velocity dispersion, $24\,\mathrm{km\,s^{-1}}$ is that expected from disk models, smaller than that of a bulge or spheroidal structure. A measurement of RR Lyrae stars in the LMC showed a velocity dispersion of $53\,\mathrm{km\,s^{-1}}$ (Borissova et al. 2004, 2006), but we do not see such a kinematically hot population in our sample. Haschke et al. (2012) find that the RR Lyrae population appear to stand out up to 5 kpc from the disk in the centre of the galaxy, but they do not see this with the Cepheid tracers. Subramaniam and Subramanian (2009) using the same OGLE III data, looking at the red clump distance, do not see the bar standing out. This is confirmed by analysis of red clump stars from the Magellanic Clouds Point Source Catalogue, (Subramanian and Subramaniam 2013).

This study provides no evidence to the hypothesis that the bar shares a common centre and systemic velocity with the main disk galaxy structure. No evidence is found of multiple kinematic stellar populations. The bar appears to be intrinsic to the rotating thick disk structure.

4.4.4 Systemic Velocity

The most outstanding result is that the centre of mass systemic velocity, $254 \pm 5\,\mathrm{km\,s^{-1}}$, is lower than previous estimates; and indicates an even greater disconnect of the stellar disk from the HI gas disk than previously thought.

The findings of this study agree with the HI rotation curve found by Kim et al. (1998) in all respects, except for the systemic velocity, which they estimate at $279\,\mathrm{km\,s^{-1}}$. This appears to be a real offset, even though they use a much lower transverse velocity of $286\,\mathrm{km\,s^{-1}}$. Other stellar studies put the stellar systemic velocity lower than the HI, typically around $265\,\mathrm{km\,s^{-1}}$. Our study, the largest sample in the inner region of the LMC, shows the the disconnect of the stellar disk and the HI structure is even more pronounced than previously indicated. The small sample immediately around the rotation centre at $248\,\mathrm{km\,s^{-1}}$ hints at an even lower stellar systemic velocity.

A lower systemic line of sight velocity affects the LMC centre of mass 3D

space motion. Interpretations of proper motion parameters are vital for models of LMC - SMC evolution in the presence of the MW Galaxy. While Hubble based observations have constrained the centre of mass proper motion (CMPM) (Kallivayalil et al. 2006; Piatek et al. 2008). There remain uncertainties that can be large enough to make the difference between bound and unbound scenarios for the LMC - SMC system. Bekki (2011) estimate the error in any component for a barred spiral LMC of the CM velocity $\mathbf{V}_m = (V_{mx}, V_{my}, V_{mz})$ could be as large as $\Delta V = 25\,\mathrm{km\,s^{-1}}$ due to random motion in the LMC and the sample size used in determining proper motion.

If the systemic velocity is actually higher, then we have negative velocities in the inner 0.5 kpc which must be explained by counter-rotation or streaming motions associated with the bar resonance. The possibility is admitted that the systemic velocity of the bar is actually different to the disk, which could also suggest a small line of sight spatial offset. The original intent of this study was to obtain many more disk star fields to address this question comprehensively.

4.4.5 Velocity Dispersion

The velocity dispersion σ_v is $24.3\,\mathrm{km\,s^{-1}}$ in the central bar, consistent with a rotationally supported thick disk profile. The presence of a strong bar feature is also consistent with a disk-like velocity dispersion in the absence a central bulge or hot virial region (Das et al. 2008). It is inconsistent with an exponential disk profile.

We have shown there is an absence of a hot central region; instead the central galaxy has a velocity dispersion similar to the rest of the disk. This can be explained in a interacting environment like the Magellanic system as LMC gas absorbing tidal energies, leaving the stellar disk relatively undisturbed (Moster et al. 2010).

We note that a sample of 22 Carbon stars with $< R >= 0.5\,\mathrm{kpc}$ (Kunkel et al. 1997; Alves and Nelson 2000) have a velocity dispersion $\sigma = 22 \pm 1\,\mathrm{km\,s^{-1}}$ that is close to our finding. Van der Swaelmen et al. (2013) find $\sigma = 25\,\mathrm{km\,s^{-1}}$ from 103 RGB stars as do Cole et al. (2005) from 373 RGB stars and Zhao et al. (2003) find $24\,\mathrm{km\,s^{-1}}$. $\sigma = 24.1 \pm 0.2\,\mathrm{km\,s^{-1}}$ is reported by Carrera et al. (2011) in the outer disk, and $\sigma = 26.4\,\mathrm{km\,s^{-1}}$ closer to the centre (Carrera et al. 2008). Finally, Graff et al. (2000) find a velocity dispersion of $22\,\mathrm{km\,s^{-1}}$. All of these published results confirm our data and analysis.

The implications for the Magellanic system and MW halo evolution are discussed in the following, concluding chapter.

Bibliography

C Alcock, R A Allsman, D R Alves, T S Axelrod, A Basu, A C Becker, D P Bennett, K H Cook, A J Drake, K C Freeman, M Geha, K Griest, L King, M J Lehner, S L Marshall, D Minniti, C Nelson, B A Peterson, P Popowski, M R Pratt, P J Quinn, C W Stubbs, W Sutherland, A B Tomaney, T Vandehei, and D L Welch. The MACHO Project 9 Million Star Color-Magnitude Diagram of the Large Magellanic Cloud. *arXiv.org*, astro-ph, January 2000.

D. R. Alves and C. A. Nelson. The Rotation Curve of the Large Magellanic Cloud and the Implications for Microlensing. *Astrophys. J.*, 542:789–803, October 2000. doi: 10.1086/317023.

G. Battaglia, M. Irwin, E. Tolstoy, V. Hill, A. Helmi, B. Letarte, and P. Jablonka. Analysis and calibration of CaII triplet spectroscopy of red giant branch stars from VLT/FLAMES observations. *Mon. Not. R. Astron. Soc.*, 383:183–199, January 2008. doi: 10.1111/j.1365-2966.2007.12532.x.

K. Bekki and M. Chiba. Formation and evolution of the Magellanic Clouds - I. Origin of structural, kinematic and chemical properties of the Large Magellanic Cloud. *Mon. Not. R. Astron. Soc.*, 356:680–702, January 2005. doi: 10.1111/j.1365-2966.2004.08510.x.

Kenji Bekki. Formation of the off-centre bar in the Large Magellanic Cloud: a collision with a dark satellite? *Monthly Notices of the Royal Astronomical Society: Letters*, 393(1):L60–L64, February 2009.

Kenji Bekki. On the Interpretation of Recent Proper Motion Data for the Large Magellanic Cloud. *The Astrophysical Journal Letters*, 730:L2, March 2011.

P. A. Bergbusch and P. B. Stetson. A New Color-Magnitude Diagram for 47 Tucanae: A Statistical Analysis. *Astron.J*, 138:1455–1464, November 2009. doi: 10.1088/0004-6256/138/5/1455.

G. Besla, N. Kallivayalil, L. Hernquist, R. P. van der Marel, T. J. Cox, and D. Kereš. The role of dwarf galaxy interactions in shaping the Magellanic System and implications for Magellanic Irregulars. *Mon. Not. R. Astron. Soc.*, 421:2109–2138, April 2012. doi: 10.1111/j.1365-2966.2012.20466.x.

Gurtina Besla, N Kallivayalil, L Hernquist, R van der Marel, T Cox, and D Keres. Simulations of the Magellanic Stream in a First Infall Scenario. *American Astronomical Society*, 217:42404, 2011. (c) 2011: American Astronomical Society.

M. S. Bessell, K C Freeman, and P. R. Wood. The velocity dispersion of old stars in the Large Magellanic Cloud. *Astrophysical Journal*, 310:710–714, November 1986.

J. Binney and S. Tremaine. *Galactic Dynamics: Second Edition*. Princeton University Press, 2008.

E. Böhm-Vitense. *Introduction to stellar astrophysics. Vol. 2. Stellar atmospheres.* Cambridge University Press, 1989.

J Borissova, D Minniti, M Rejkuba, D Alves, K H Cook, and K C Freeman. Properties of RR Lyrae stars in the inner regions of the Large Magellanic Cloud. *Astronomy and Astrophysics*, 423(1):97–109, August 2004.

J Borissova, D Minniti, M Rejkuba, and D Alves. Properties of RR Lyrae stars in the inner regions of the Large Magellanic Cloud. *Astronomy and Astrophysics*, 460(2):459–466, December 2006.

R. Carrera, C. Gallart, E Pancino, and R Zinn. The Infrared Ca II Triplet as Metallicity Indicator. *The Astronomical Journal*, 134(3):1298, September 2007.

R. Carrera, C. Gallart, Eduardo Hardy, A. Aparicio, and R Zinn. The Chemical Enrichment History of the Large Magellanic Cloud. *The Astronomical Journal*, 135(3):836–849, March 2008.

R. Carrera, C. Gallart, A. Aparicio, and E. Hardy. Metallicities, Age-Metallicity Relationships, and Kinematics of Red Giant Branch Stars in the Outer Disk of the Large Magellanic Cloud. *The Astronomical Journal*, 142(2):61, August 2011.

R. Carrera, E Pancino, C. Gallart, and A del Pino. The near-infrared Ca II triplet as a metallicity indicator - II. Extension to extremely metal-poor metallicity regimes. *Monthly Notices of the Royal Astronomical Society*, 434 (2):1681–1691, September 2013.

M-R Cioni, C Loup, H J Habing, P Fouque, E Bertin, E Deul, D Egret, C Alard, B de Batz, J Borsenberger, M Dennefeld, N Epchtein, T Forveille, F Garzon, J Hron, S Kimeswenger, F Lacombe, T Le Bertre, G A Mamon, A Omont, G Paturel, P Persi, A Robin, D Rouan, G Simon, D Tiphene, I Vauglin, and S Wagner. DENIS Catalogue toward Magellanic Clouds (DCMC) (Cioni+ 2000). *VizieR Online Data Catalog*, 2228:0–+, 2000.

M R L Cioni. The metallicity gradient as a tracer of history and structure: the Magellanic Clouds and M33 galaxies. *Astronomy and Astrophysics*, 506(3): 1137–1146, November 2009.

A A Cole, T A Smecker-Hane, E Tolstoy, T L Bosler, and J S Gallagher. The effects of age on red giant metallicities derived from the near-infrared CaII triplet. *Monthly Notices of the Royal Astronomical Society*, 347:367, 2004.

Andrew A Cole, Eline Tolstoy, John S Gallagher, and Tammy A Smecker-Hane. Spectroscopy of Red Giants in the Large Magellanic Cloud Bar: Abundances, Kinematics, and the Age-Metallicity Relation. *The Astronomical Journal*, 129:1465, March 2005.

Andrew A Cole, Aaron J Grocholski, Doug Geisler, Ata Sarajedini, Verne V Smith, and Eline Tolstoy. Breaking the age-metallicity degeneracy: The metallicity distribution and star formation history of the Large Magellanic Cloud. *The Magellanic System: Stars*, 256:263–268, March 2009.

Matthew Colless, Gavin Dalton, Steve Maddox, Will Sutherland, Peder Norberg, Shaun Cole, Joss Bland-Hawthorn, Terry Bridges, Russell Cannon, Chris Collins, Warrick Couch, Nicholas Cross, Kathryn Deeley, Roberto de Propris, Simon P Driver, George Efstathiou, Richard S Ellis, Carlos S Frenk, Karl Glazebrook, Carole Jackson, Ofer Lahav, Ian Lewis, Stuart Lumsden, Darren Madgwick, John A Peacock, Bruce A Peterson, Ian Price, Mark Seaborne, and Keith Taylor. The 2dF Galaxy Redshift Survey: spectra and redshifts. *Monthly Notices of the Royal Astronomical Society*, 328(4):1039–1063, December 2001.

M Das, E Laurikainen, H Salo, and R Buta. Variation of bar strength with central velocity dispersion in spiral galaxies. *Astrophysics and Space Science*, 317(3-4):163–168, July 2008.

G. de Vaucouleurs and K. C. Freeman. Structure and dynamics of barred spiral galaxies, in particular of the Magellanic type. *Vistas in Astronomy*, 14:163–294, 1972. doi: 10.1016/0083-6656(72)90026-8.

H Dottori, E Bica, J J Claria, and I Puerari. Spatial Distributions of Young Large Magellanic Cloud Clusters as Tracers of a Bar Perturbation. *Astrophysical Journal v.461*, 461:742, April 1996.

Michael W Feast, Oyirwoth P Abedigamba, and Patricia A Whitelock. Is there a metallicity gradient in the Large Magellanic Cloud? *Monthly Notices of the Royal Astronomical Society: Letters*, 408(1):L76–L79, September 2010.

Eileen D Friel, Kenneth A Janes, Maritza Tavarez, Jennifer Scott, Rocio Katsanis, Jennifer Lotz, Linh Hong, and Nathan Miller. Metallicities of Old Open Clusters. *The Astronomical Journal*, 124:2693, November 2002.

Carme Gallart, Peter B Stetson, Ingrid P Meschin, Frederic Pont, and Eduardo Hardy. Outside-In Disk Evolution in the Large Magellanic Cloud. *The Astrophysical Journal*, 682:L89, August 2008.

Wolfgang Gieren, Jesper Storm, Thomas G III Barnes, Pascal Fouqué, Grzegorz Pietrzyński, and Francesco Kienzle. Direct Distances to Cepheids in the Large Magellanic Cloud: Evidence for a Universal Slope of the Period-Luminosity Relation up to Solar Abundance. *The Astrophysical Journal*, 627(1):224–237, July 2005.

L Girardi, G Bertelli, A Bressan, C Chiosi, M A T Groenewegen, P Marigo, B Salasnich, and A Weiss. Theoretical isochrones in several photometric systems. I. Johnson-Cousins-Glass, HST/WFPC2, HST/NICMOS, Washington, and ESO Imaging Survey filter sets. *Astronomy and Astrophysics*, 391:195–212, August 2002.

David S Graff, Andrew P Gould, Nicholas B Suntzeff, Robert A Schommer, and Eduardo Hardy. The Velocity Structure of Large Magellanic Cloud Carbon Stars: Young Disk, Old Disk, and Perhaps a Separate Population. *The Astrophysical Journal*, 540(1):211–216, September 2000.

A. J. Grocholski, A. A. Cole, A. Sarajedini, D. Geisler, and V. V. Smith. Ca II Triplet Spectroscopy of Large Magellanic Cloud Red Giants. I. Abundances and Velocities for a Sample of Populous Clusters. *Astron.J*, 132:1630–1644, October 2006. doi: 10.1086/507303.

G. Gyuk, N. Dalal, and K Griest. Self-lensing Models of the Large Magellanic Cloud. *The Astrophysical Journal*, 535(1):90–103, May 2000.

W. J. Hankey and A. A. Cole. Radial velocity and metallicity of the globular cluster IC4499 obtained with AAOmega. *Mon. Not. R. Astron. Soc.*, 411: 1536–1546, March 2011. doi: 10.1111/j.1365-2966.2010.17788.x.

Jason Harris and Dennis Zaritsky. The Star Formation History of the Large Magellanic Cloud. *The Astronomical Journal*, 138(5):1243–1260, November 2009.

Raoul Haschke, Eva K Grebel, and Sonia Duffau. Three-dimensional Maps of the Magellanic Clouds using RR Lyrae Stars and Cepheids. I. The Large Magellanic Cloud. *The Astronomical Journal*, 144(4):106, October 2012.

Trevor Hastie, Jerome Friedman, and Robert Tibshirani. *The elements of statistical learning : data mining, inference and prediction.* Springer series in statistics. New York, N.Y. : Springer, 2009., 2009. ISBN 9780387848570.

Shaun M G Hughes and Peter R Wood. Long-period variables in the Large Magellanic Cloud. II - Infrared photometry, spectral classification, AGB evolution, and spatial distribution. *Astronomical Journal (ISSN 0004-6256)*, 99: 784, March 1990.

Inese I Ivans, Robert P Kraft, Christopher Sneden, Graeme H Smith, R Michael Rich, and Matthew Shetrone. New Analyses of Star-to-Star Abundance Variations among Bright Giants in the Mildly Metal-poor Globular Cluster M5. *The Astronomical Journal*, 122(3):1438–1463, September 2001.

N. Kallivayalil, R. P. van der Marel, C. Alcock, T. Axelrod, K. H. Cook, A. J. Drake, and M. Geha. The Proper Motion of the Large Magellanic Cloud Using HST. *Astrophys. J.*, 638:772–785, February 2006. doi: 10.1086/498972.

Daisuke Kato, Chie Nagashima, Takahiro Nagayama, Mikio Kurita, Joel F Koerwer, Toshihide Kawai, Tomoyasu Yamamuro, Takahiro Zenno, Shogo Nishiyama, Daisuke Baba, Ryota Kadowaki, Yasuaki Haba, Hirofumi Hatano, Hideyuki Shimizu, Mamiko Nishimura, Tetsuya Nagata, Shuji Sato, Yuka Murai, Takahiro Kawazu, Yasushi Nakajima, Hidehiko Nakaya, Ryo Kandori, Nobuhiko Kusakabe, Akika Ishihara, Nagisa Kaneyasu, Jun Hashimoto,

Motohide Tamura, Toshihiko Tanabé, Yoshifusa Ita, Noriyuki Matsunaga, Yoshikazu Nakada, Koji Sugitani, Ken-Ichi Wakamatsu, Ian S Glass, Michael W Feast, John W Menzies, Patricia A Whitelock, Pieter Fourie, John Stoffels, Geoff P Evans, and Tetsuo Hasegawa. The IRSF Magellanic Clouds Point Source Catalog. *Publications of the Astronomical Society of Japan*, 59: 615, June 2007.

S. Kim, L. Staveley-Smith, M. A. Dopita, K. C. Freeman, R. J. Sault, M. J. Kesteven, and D. McConnell. An H i Aperture Synthesis Mosaic of the Large Magellanic Cloud. *Astrophys. J.*, 503:674, August 1998. doi: 10.1086/306030.

William E Kunkel, Serge Demers, M J Irwin, and Loic Albert. The Dynamics of the Large Magellanic Cloud Periphery: Mass Limit and Polar Ring. *Astrophysical Journal Letters v.488*, 488:L129, October 1997.

Richard R Lane, László L. Kiss, Geraint F Lewis, Rodrigo A Ibata, Arnaud Siebert, Timothy R Bedding, and Péter Székely. Testing Newtonian gravity with AAOmega: mass-to-light profiles and metallicity calibrations from 47 Tuc and M55. *Monthly Notices of the Royal Astronomical Society*, 401(4): 2521–2530, February 2010.

Henry Lee, Evan D Skillman, John M Cannon, Dale C Jackson, Robert D Gehrz, Elisha F Polomski, and Charles E Woodward. On Extending the Mass-Metallicity Relation of Galaxies by 2.5 Decades in Stellar Mass. *The Astrophysical Journal*, 647(2):970–983, August 2006.

T. Luks and K. Rohlfs. Structure and kinematics of neutral hydrogen gas in the Large Magellanic Cloud. *Astron. Astrophys.*, 263:41–53, September 1992.

Roeland P van der Marel and Maria-Rosa L Cioni. Magellanic Cloud Structure from Near-Infrared Surveys. I. The Viewing Angles of the Large Magellanic Cloud. *The Astronomical Journal*, 122:1807, October 2001.

Philip Massey and K A G Olsen. The Evolution of Massive Stars. I. Red Supergiants in the Magellanic Clouds. *arXiv.org*, astro-ph, September 2003. Version with eps figures embedded can be obtained from ftp://ftp.lowell.edu/pub/massey/rsgs.ps.gz Accepted by the Astronomical Journal.

Benjamin P Moster, Andrea V Maccio, Rachel S Somerville, Peter H Johansson, and Thorsten Naab. Can gas prevent the destruction of thin stellar discs by minor mergers? *Monthly Notices of the Royal Astronomical Society*, 403(2): 1009–1019, February 2010.

David L Nidever, Steven R Majewski, W Butler Burton, and Lou Nigra. The 200° Long Magellanic Stream System. *The Astrophysical Journal*, 723:1618, November 2010.

Sergei Nikolaev and Martin D Weinberg. Stellar Populations in the Large Magellanic Cloud from 2MASS. *The Astrophysical Journal*, 542:804, October 2000.

S. C. Odewahn. Properties of the Magellanic Type Galaxies. In R. Buta, D. A. Crocker, & B. G. Elmegreen, editor, *IAU Colloq. 157: Barred Galaxies*, volume 91 of *Astronomical Society of the Pacific Conference Series*, pages 30–+, 1996.

K. A. G. Olsen and P. Massey. Evidence for Tidal Effects in the Stellar Dynamics of the Large Magellanic Cloud. *Astrophys. J., Lett.*, 656:L61–L64, February 2007. doi: 10.1086/512484.

K. A. G. Olsen and C. Salyk. A Warp in the Large Magellanic Cloud Disk? *Astron.J*, 124:2045–2053, October 2002. doi: 10.1086/342739.

K. A. G. Olsen, D. Zaritsky, R. D. Blum, M. L. Boyer, and K. D. Gordon. A Population of Accreted Small Magellanic Cloud Stars in the Large Magellanic Cloud. *Astrophys. J.*, 737:29–+, August 2011. doi: 10.1088/0004-637X/737/1/29.

S. Piatek, C. Pryor, and E. W. Olszewski. Proper Motions of the Large Magellanic Cloud and Small Magellanic Cloud: Re-Analysis of Hubble Space Telescope Data. *Astron.J*, 135:1024–1038, March 2008. doi: 10.1088/0004-6256/135/3/1024.

Warren A Reid and Quentin A Parker. A new population of planetary nebulae discovered in the Large Magellanic Cloud - II. Complete PN catalogue. *Monthly Notices of the Royal Astronomical Society*, 373(2):521–550, December 2006.

E. Romano-Díaz, I. Shlosman, C. Heller, and Y. Hoffman. Disk Evolution and Bar Triggering Driven by Interactions with Dark Matter Substructure. *Astrophys. J., Lett.*, 687:L13–L16, November 2008. doi: 10.1086/593168.

G A Rutledge, J E Hesser, P B Stetson, M Mateo, L Simard, M Bolte, E D Friel, and Y Copin. Galactic Globular Cluster Metallicity Scale from the Ca II Triplet I. Catalog. *Publications of the Astronomical Society of the Pacific*, 109:883, August 1997.

Adam Růžička, Christian Theis, and Jan Palouš. Rotation of the Milky Way and the Formation of the Magellanic Stream. *The Astrophysical Journal*, 725: 369, December 2010.

M. Salaris and L. Girardi. Tip of the Red Giant Branch distances to galaxies with composite stellar populations. *Mon. Not. R. Astron. Soc.*, 357:669–678, February 2005. doi: 10.1111/j.1365-2966.2005.08689.x.

J A Sellwood and A Wilkinson. Dynamics of barred galaxies. *Reports on Progress in Physics*, 56(2):173–256, February 1993.

Isaac Shlosman. Galactic Bars in Cosmological Context. *arXiv.org*, astro-ph, December 2008.

M. F. Skrutskie, R. M. Cutri, R. Stiening, M. D. Weinberg, S. Schneider, J. M. Carpenter, C. Beichman, R. Capps, T. Chester, J. Elias, J. Huchra, J. Liebert, C. Lonsdale, D. G. Monet, S. Price, P. Seitzer, T. Jarrett, J. D. Kirkpatrick, J. E. Gizis, E. Howard, T. Evans, J. Fowler, L. Fullmer, R. Hurt, R. Light, E. L. Kopan, K. A. Marsh, H. L. McCallon, R. Tam, S. Van Dyk, and S. Wheelock. The Two Micron All Sky Survey (2MASS). *Astron.J*, 131:1163–1183, February 2006. doi: 10.1086/498708.

T. A. Smecker-Hane, A. A. Cole, J. S. Gallagher, III, and P. B. Stetson. The Star Formation History of the Large Magellanic Cloud. *Astrophys. J.*, 566: 239–244, February 2002. doi: 10.1086/337985.

G. Smith and J. J. Drake. The wings of the calcium infrared triplet lines in late-type giant stars. *Astron. Astrophys.*, 231:125–130, May 1990.

E Starkenburg, V Hill, E Tolstoy, J I González Hernández, M Irwin, A Helmi, G Battaglia, P Jablonka, M Tafelmeyer, M Shetrone, K Venn, and T de Boer. The NIR Ca ii triplet at low metallicity. Searching for extremely low-metallicity stars in classical dwarf galaxies. *Astronomy and Astrophysics*, 513:34, April 2010.

L Staveley-Smith, S Kim, M R Calabretta, R F Haynes, and M J Kesteven. A new look at the large-scale HI structure of the Large Magellanic Cloud. *Monthly Notice of the Royal Astronomical Society*, 339:87, February 2003.

Annapurni Subramaniam. Large Magellanic Cloud Bar: Evidence of a Warped Bar. *The Astrophysical Journal*, 598:L19, November 2003.

Annapurni Subramaniam. Evidence of a Misaligned Secondary Bar in the Large Magellanic Cloud. *The Astrophysical Journal*, 604:L41, March 2004.

Annapurni Subramaniam and Tushar P Prabhu. Evidence of a Counterrotating Core in the Large Magellanic Cloud. *The Astrophysical Journal*, 625:L47, May 2005.

Annapurni Subramaniam and Smitha Subramanian. The Mysterious Bar of the Large Magellanic Cloud: What Is It? *The Astrophysical Journal Letters*, 703 (1):L37–L40, September 2009.

S Subramanian and A Subramaniam. An estimate of the structural parameters of the Large Magellanic Cloud using red clump stars. *Astronomy and Astrophysics*, 520:24, September 2010.

S Subramanian and A Subramaniam. Structure of the Large Magellanic Cloud from near infrared magnitudes of red clump stars. *Astronomy and Astrophysics*, 552:144, April 2013.

Nicholas B Suntzeff, Robert A Schommer, Edward W Olszewski, and Alistair R Walker. Spectroscopy of giants in LMC clusters. III - Velocities and abundances for NGC 1841 and Reticulum and the properties of the metal-poor clusters. *Astronomical Journal (ISSN 0004-6256)*, 104:1743–1764, November 1992.

Christy A Tremonti, Timothy M Heckman, Guinevere Kauffmann, Jarle Brinchmann, Stéphane Charlot, Simon D M White, Mark Seibert, Eric W Peng, David J Schlegel, Alan Uomoto, Masataka Fukugita, and Jon Brinkmann. The Origin of the Mass-Metallicity Relation: Insights from 53,000 Star-forming Galaxies in the Sloan Digital Sky Survey. *The Astrophysical Journal*, 613(2): 898–913, October 2004.

Roeland P. van der Marel, David R Alves, Eduardo Hardy, and Nicholas B Suntzeff. New Understanding of Large Magellanic Cloud Structure, Dynamics, and Orbit from Carbon Star Kinematics. *The Astronomical Journal*, 124 (5):2639–2663, November 2002. Published in: Astron.J.124:2639-2663,2002 57 pages, LaTeX, with 11 PostScript figures. Submitted to the Astronomical Journal.

M. Van der Swaelmen, V. Hill, F. Primas, and A. A. Cole. Chemical abundances in LMC stellar populations. II. The bar sample. *Astron. Astrophys.*, 560:A44, December 2013. doi: 10.1051/0004-6361/201321109.

M Van der Swaelmen, V Hill, F Primas, and A A Cole. Chemical abundances in LMC stellar populations. II. The bar sample. *arXiv.org*, page 4224, June 2013.

Alistair R Walker. The Large Magellanic Cloud and the distance scale. *Astrophysics and Space Science*, 341(1):43–49, September 2012.

Steven R Warren and Andrew A Cole. Metallicities and radial velocities of five open clusters including a new candidate member of the Monoceros stream. *Monthly Notices of the Royal Astronomical Society*, 393(1):272–296, February 2009.

D. Zaritsky. The Case of the Off-Center, Levitating Bar in the Large Magellanic Cloud. *Astrophys. J., Lett.*, 614:L37–L40, October 2004. doi: 10.1086/425312.

H. Zhao and N. W. Evans. The So-called "Bar" in the Large Magellanic Cloud. *Astrophys. J., Lett.*, 545:L35–L38, December 2000. doi: 10.1086/317324.

HongSheng Zhao, Rodrigo A Ibata, Geraint F Lewis, and Michael J Irwin. Kinematic outliers in the Large Magellanic Cloud: constraints on star-star microlensing. *Monthly Notice of the Royal Astronomical Society*, 339:701, March 2003.

5
Building Blocks

5.1 IC 4499

The techniques of multi-object fibre spectroscopy were employed to study two objects in the MW extended halo. The GC IC 4499 was a comparatively understudied object with suggestions of an unusual horizontal branch morphology. Several photometric studies had concentrated on the abundance of RR-Lyrae variable stars. This work has been the first to establish both an accurate radial velocity and metallicity estimate from Ca II triplet spectroscopy and allow it to be placed in proper context within the pantheon of 157 known Galactic globular clusters, (Harris 1996). Globular clusters in the halo date back 10-13 billion years to the beginning of the universe, making them fundamental building blocks of the Galactic halo.

The role of halo objects in accretion and tidal interactions within the MW sub-group depend on our knowledge of their kinematics and chemistry. Clues to the enrichment by Population III objects of the primordial GC material depend on our knowledge of the abundances. Understanding of self-enrichment of Population II, environment and feedback mechanisms within single population GCs is a first step to understanding multiple population galaxy evolution. Given the large-scale homogeneity of the universe we can extrapolate what we learn of Local Group evolution to similar galaxies across the universe.

The equivalent width of the Ca II triplet has been shown to be an excellent tool for estimating metallicity in distant older metal-poor populations (Rutledge et al. 1997; Cole et al. 2004; Battaglia et al. 2008). We restrict our metallicity sample to only RGB stars for which consistent scales have been established. The equivalent widths were adjusted for surface gravity and temperature effects on line width. The results presented in Chapter 3 represent the first accurate spectroscopic velocities and metallicities for this cluster.

The near-infrared spectra of 636 red giants were obtained in and around the RR Lyrae-rich, extreme-southern globular cluster IC 4499. From spectra including the calcium triplet, radial velocities were measured by cross-correlation with template stars in well-studied globular clusters M68, M22, and M4. By combining the CaT equivalent widths with 2MASS K_s magnitudes metallicities on the Carretta and Gratton (1997) scale were derived following the method-

ology of Warren and Cole (2009). The relationship between CaT equivalent widths, K_s, and [Fe/H] is in good agreement with the work of Warren and Cole (2009). The velocity and metallicity results for the comparison clusters agree well with literature values. 43 stars were found to be probable cluster members of IC 4499 based on radial velocity association, culled by metallicity to alleviate the strong foreground contamination.

The heliocentric radial velocity of IC 4499 is estimated as $v_r = 31.5 \pm 0.4$ km/s. The velocity is typical of halo objects along this sightline, but also does not rule out membership in a tidal stream as proposed by Peñarrubia et al. (2005). The most powerful tests of stream membership, proper motion and detailed elemental abundance ratios, are not yet available for this cluster. Like many proposed associations (e.g., Piatti and Clariá 2008) the status of IC 4499 is undecided.

The metallicity of IC 4499 is [Fe/H] $= -1.52 \pm 0.12$ on the scale of Carretta and Gratton (1997), which translates to -1.74 ± 0.10 on the Zinn and West (1984) scale. This agrees with photometric estimates from the cluster CMD and unpublished work by R. Cannon (1992), but disagrees with the earlier studies of RR Lyrae stars (Smith and Perkins 1982). This value is closer to the [Fe/H] $= -1.80$ ZW84 adopted by Ferraro et al. (1995), than the [Fe/H] $= -1.50$ ZW84 assumed by Salaris and Weiss (2002). To the extent that studies of the relative ages of globular clusters (e.g., Salaris and Weiss 2002) and of the Oosterhoof RR Lyrae period-metallicity relation (e.g., Sandage 1993) incorrectly relied on overestimates of the cluster metallicity, the role of IC 4499 in these studies should be reassessed. If age is the dominant contributor to the second-parameter effect (Lee 1992), then the evidence for a young age (Ferraro et al. 1995) for IC 4499 is weak, based on its intermediate HB type. Using our metallicity value Walker et al. (2011) confirm that the cluster age is 12 ± 1 Gyr from multi-wavelength photometry, about 3 Gyr older than the Ferraro et al. (1995) age.

The cluster is slightly metal-poor compared to most OoI clusters. This tends to add weight to its classification as OoInt by Catelan (2009) as it is already on the edge of OoI periodicity. As an OoInt it is more likely associated with a dSph galaxy that has been accreted on the MW. As such the metallicity adds weight to the notion that the cluster may be part of an accretion stream.

The approach of Lane et al. (2009, 2010) is followed to search for evidence of rotation in IC 4499. This study confirms their results for M22 and M4, although the signal is noisy because less than half the number of stars were measured. There was no detection of rotation in IC 4499, which puts an upper limit of $\approx$1 km/s on the net cluster rotation.

The velocity dispersion of the cluster is estimated using a Plummer potential model. The best-fit cluster parameters are found using MCMC simulation. The most likely central velocity dispersion is $\sigma_0 = 2.5 \pm 0.5$ km/s. Using the Plummer model this translates to a cluster dynamical mass of $93 \pm 37 \times 10^3$ $M_\odot$.

This is in agreement with fits to the light profile by McLaughlin and van der Marel (2005), and using their photometry implies a mass-to-light ratio $M/L_V = 1.3$ in solar units; this result is quite normal for a globular cluster (e.g., Trager et al. 1993; Lane et al. 2010) and indicates that no DM component is

needed to explain the cluster dynamics. Baumgardt et al. (2009) also fail to find evidence of DM in globular cluster NGC 2419. No evidence has been found for a substantial DM component in globular clusters. This is in contrast to dwarf galaxies in the halo which exhibit dynamical indications of DM halos.

Andrea Kunder requested tables of our results which were plotted in Figure 11 of Walker et al. (2011) and reproduced here in Figure 5.1. DDO51-V photometry was used to distinguish foreground red dwarf stars from IC 4499 cluster red giant stars. These two populations appear at a similar apparent magnitude due to the less luminous red dwarfs being closer than the brighter red giants, and have similar colours. Our spectrographic results confirm their photometry, and assist in identifying IC 4499 red giant cluster members. The figure they present shows the spatial crowding and confusion between foreground and background also exists in this colour-colour space. Our spectroscopy confirms the Walker et al. (2011) colour-colour selection, and the consistency between the two studies is excellent.

Some observed stars in the IC 4499 field had the correct velocity and metallicity for cluster membership, but were outside the tidal radius of the cluster. These stars were not included in the cluster member sample. The tidal radius had been previously been determined from the photometric light profile. These stars outside the tidal radius may have been tidally stripped, or collisionally ejected from the cluster. A DDO51 study of possible cluster members with the correct velocity could identify cluster red giants outside the tidal radius. If they could have been identified as IC 4499 members then this may have shed some light on tidal influences on cluster evolution and MW interaction. IC 4499 may be an extended object with its own stellar stream being a part of the proposed Monoceros stream object, (Fusi Pecci et al. 1995).

Possible follow up observations were discussed with DDO51 and V filters at Cerro Tololo Inter-American Observatory (CTIO), Chile, in a region surrounding IC 4499 with the MOSAIC-II CCD imager. The observations didn't come to fruition, and this instrument has since been superseded by the Dark Energy Camera (DECam). The observation fields tentatively proposed by us to search for extra-tidal IC 4499 members are shown in Figure 5.2. The points plotted show stars selected with the correct metallicity and velocity inside and outside the tidal radius.

The mass estimate for IC 4499 from the measured velocity dispersion indicates that the mass to light ration of 1.3 is normal. The cluster is not DM dominated. This agrees with what is known about GC DM content, which have an upper mass to light ratio of 2.5 (Moore 1996). Bradford et al. (2011) note that our kinematic study of IC 4499 shows no evidence of a significant DM component to the globular cluster. Neither does their study of globular cluster Palomar 13. This is interesting as ΛCDM hierarchical models of the formation of structure in the universe can reproduce the correct amount of large structures like the MW galaxy, but there is a problem with the prediction too many small structures like dwarf galaxies and clusters (Weinberg et al. 2013).

Haschke et al. (2012) use our metallicity determination for IC 4499 to calibrate their metallicity estimates for old field stars in the LMC galaxy. They

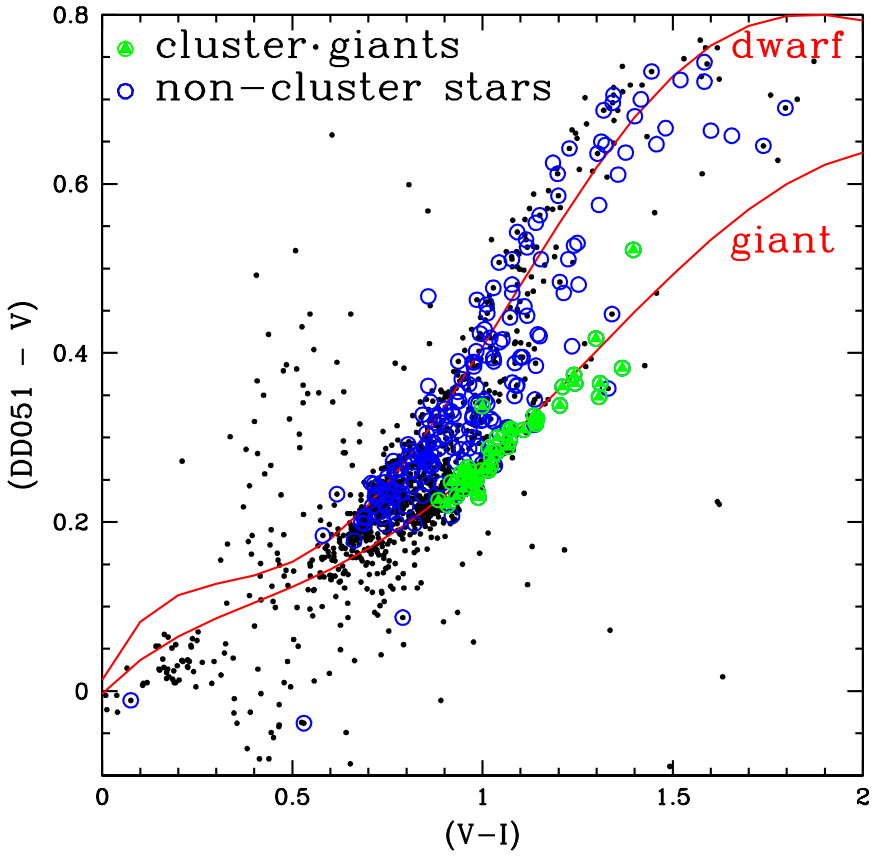

Figure 5.1: Figure 11 from Walker et al. (2011) showing our IC 4499 red giants distinct from the foreground dwarf stars. The spectroscopically confirmed cluster members from our study confirm the utility of the colour selection process. Copyright MNRAS.

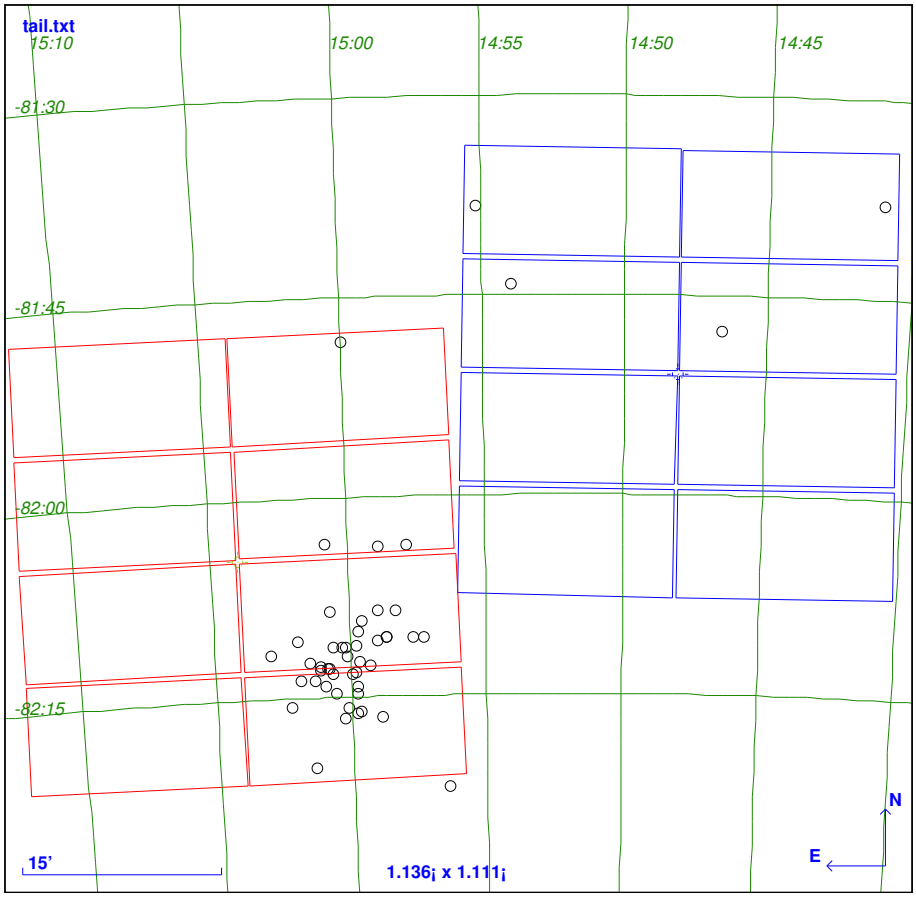

Figure 5.2: Proposed follow up fields to identify tidal tail stars near IC 4499 on the Mosaic II Imager at the CTIO 4m Blanco telescope .

estimate metallicity from parameters derived from the Fourier decomposition of RR-Lyrae light curves. IC 4499 is rich in RR Lyrae stars and so is a useful subject for comparison.

Leaman (2012) conducted a meta-analysis of published metallicities for LG dwarf galaxies, globular and open clusters. They use a sample of 49 of the 157 known globular clusters associated with the MW galaxy, (Harris 1996). They find a correlation between metallicity Z and spread in metallicity $\sigma(Z)$. Our results for IC 4499 are in agreement with the correlation, and also the bimodal nature of the correlation, where clusters have a stronger correlation, and dwarf galaxies a weaker one. This bimodal difference is explained by several generations of star formation in dwarf galaxies, as opposed to a single star formation event in a cluster. The Leaman (2012) findings allow the identification of some globular clusters as the remnant cores of dwarf galaxies.

The globular cluster IC 4499 was not found to be particularly unusual. It displayed a typical metallicity for a halo object. Its radial velocity places it in the range of allowed velocities for the Monoceros tidal stream, but again the velocity is not unusual for a halo object at this location. Its Oosterhoff type may hold clues to a potential dwarf galaxy origin.

5.2 Large Magellanic Cloud

The ancient SFH suggests the Magellanic system formed in isolation as a binary pair of galaxies. The lack of periodic SFH events events $> 4\,\mathrm{Gyr}$ suggests a lack of orbital encounters with the MW. This fits with recent proper motion studies that indicate a first passage for the Magellanic system. The similar early SFH indicates the clouds shared a primordial chemical environment. The LMC shows more signs of enrichment than the SMC, indicating gas feedback mechanisms at work; perhaps related to the bar, which we find to have a slightly higher metallicity than the disk.

The LMC is the dominant disk galaxy in the early binary system, with its spiral and bar structure induced by the dwarf spheroidal satellite SMC. The present tri-galaxy SMC-LMC-MW is rare and unstable, again indicating a recent encounter for the system. The increased SFH in the last 3.5 Gyr probably marks the beginning of the interaction with the MW. The length of the MS also indicates a similar interaction time.

The LMC contains globular clusters at least as old as the MW population. It appears in some ways to be a smaller barred disk galaxy analogue of the MW. The analogy is stretched by the sparse stellar halo around the LMC. The LMC halo may have been tidally or ram pressure stripped, like the MS on its approach to the MW.

The mean of the radial velocity sample mean of $\mu = 259\,\mathrm{km\,s^{-1}}$ with standard deviation $\sigma = 25\,\mathrm{km\,s^{-1}}$ agrees with other velocity samples in this region (Kunkel et al. 1997; Alves and Nelson 2000; Cole et al. 2005; Van der Swaelmen et al. 2013), but disagrees with the mean value of $\mu = 271\,\mathrm{km\,s^{-1}}$ of Zhao et al. (2003) who also had $\sigma = 25\,\mathrm{km\,s^{-1}}$ indicating a systematic offset in that study.

Our estimate of $255\,\mathrm{km\,s^{-1}}$ systemic velocity is conservative, with the statistical influence of literature data taken into account. A small sample of stars surrounding the rotation centre indicate the systemic velocity could be as low as $248\,\mathrm{km\,s^{-1}}$ Chapter 4, Figure 4.16.

Our finding of a disk like velocity dispersion at the centre, along with only a weak metallicity or age gradient across the LMC, rules out the bar being an ancient bulge-like structure as seen in the MW and other large disks. The LMC is metal enriched compared to the SMC. If they formed in an isolated environment the explanation is self-enrichment of the LMC. The bar feature would tend to stream gas toward the centre of the galaxy, and we have observed a slight enrichment in the bar region.

This investigation of the understudied LMC central bar region represents a crucial piece of the picture of our nearest disk galaxy. The central region should contain stars at the systemic velocity of the galaxy, where the disk rotation goes towards zero. The effect of the transverse space motion on line of sight velocities scales with $sin\rho$, so at the very centre where disk radius $\rho \to 0$, we directly measure the systemic velocity of the galaxy from the radial line of sight velocities. Systematic effects of assumed disk rotation models, geometry and a proper motion estimate are circumvented; if one can identify the centre of rotation and measure there. This study's direct measurement of a systemic velocity without systematics should constrain radially extended datasets.

We find no kinematic evidence for large scale disturbances in the stellar LMC galaxy. We may have expected to find a double-peaked velocity distribution if the bar was a separate entity. We may have expected to find a velocity dispersion larger than the rest of the disk if we had a bulge feature. Harris and Zaritsky (2006) found that a large SMC stellar sample appeared to show no signs of major tidal disturbances. The SMC appears to be a regular spheroidal flattened slightly by rotation. The SMC's irregular appearance is due to recent star formation events. We also find the LMC to be surprisingly well organised disk, with near constant velocity dispersion over its radius and what appears to be a quite well defined rotation curve. Once again the irregular appearance is due mainly to regions like 30 Doradus that are undergoing star formation events.

The constant velocity dispersion across the disk indicates that the mass distribution is not exponential, otherwise a higher velocity dispersion would be seen at the centre. Alternatively the LMC disk may be flared as proposed by Subramaniam and Subramanian (2009) and the dispersion is increased at larger radii by tidal heating.

This thesis shows stellar kinematics in the inner bar region do not indicate anything other than a rotating disk model of the LMC. However this does not preclude the sort of non circular streaming orbits along the long axis of the bar. They may exist, but the component along the bar is perpendicular to the line of sight and does not leave a strong signature in our radial velocity data, such that what we measure is dominated by the rotation of the disk as a whole. The simple circular disk rotation we have detected emphasises the intact nature of the LMC stellar disk in contrast to the highly disturbed HI galaxy. HI studies

also show a large scale simple disk rotation that agrees well with the stellar data, in spite of the discrepancy between the rotation centres.

The bar does not appear on the evidence of our stellar sample to be a separate feature. It is not the accreted remnant of a dwarf galaxy, an old bulge, nor a counter-rotating core. We postulate that it is a typical resonance in the kinematic star field induced by the SMC. Bars are typical in disk galaxies hosting a satellite. There is evidence of very close tidal encounters as SMC stars seem to have found their way into the disk of the LMC, (Olsen et al. 2011; Kunkel et al. 1997). Also low metallicity objects may be built from SMC gas accreted onto the LMC during encounters.

The slightly higher bar region metallicity detected is consistent with a small but significant gradient detected in other studies (Cioni 2009; Feast et al. 2010; Wagner-Kaiser and Sarajedini 2013). A subtly larger α abundance variance in the bar compared to the disk is detected by Van der Swaelmen et al. (2013), which may be attributable to massive young stars enriching the central galaxy. They also find that LMC $[\alpha/Fe]$ is in general sub-MW in agreement with Pompéia et al. (2008). This indicates that SNe Ia played a more significant role relative to massive star SNe II in the LMC than in the MW, and probably reflects the long slow star formation history of the LMC until recently.

A check on the metallicity calibration shows the results of slightly higher metallicity in the bar is real, see Appendix D. A small calibration difference was discovered between this near infra-red study and V band studies of matching stars. Calibration of the effect of surface gravity on metallicity was made by reference to red clump magnitude, taken as a constant 16.6 K_s. It appears that Red clump magnitude actually gets fainter with decreasing metallicity at K-band, the opposite of the effect seen at V band. This K-band study has thus tended to overestimate metallicity by 0.1 dex at [Fe/H] = -1.0 and by 0.2 dex at [Fe/H] = -1.5. Otherwise there is excellent agreement with other metallicity scales. The estimate of slightly higher bar metallicity compared to the disk remains valid.

The metallicity gradient found in this study and others reflects a star formation history where the bar plays a role in driving star formation. The higher bar metallicity may be due to gravitational torque from the bar density driving pre-enriched gas in-falls along the bar. Gas gathered at the ends of the bar appears to have triggered the birth of young stars. The bar itself is likely a result of the several interactions with the SMC over the last five billion years.

The bar transfers angular momentum from the disk stars. While the LMC has no substantial halo, it does have the SMC satellite, which is the absorber for the LMC disk angular momentum emitters. The SMC drives the bar strength and triggers periodic star formation in the LMC. The bar has probably been regenerated with the recent passage of the SMC 200 Myr to 500 Myr ago with extremely young populations associated with bar morphology (Gallart et al. 2008).

With a bar we might expect to see more non-circular motions. The results of this study don't find a substantial streaming motion along the bar, which may indicate the bar hasn't had time to drag the disk stars into elongated elliptical

orbits and dissipate their angular momentum. However due to the orientation of the LMC much of the streaming component is perpendicular to our line of sight, and may not be detected. The response of the stars to the bar may instead be represented in the thickness of the disk, or a "warming", with vertical motions representing the change from ordered angular momentum to z-motions in $a = 1$ resonance with orbits as described by Binney (1981).

The SMC itself would serve to absorb angular momentum by speeding up as it flew by the LMC. The LMC stars pile up in the bar wave in response to the tidal acceleration, dissipating angular momentum but still mostly maintaining their circular orbits. Studies of other barred galaxies have also shown simple global rotation curves (Bosma 1996; Odewahn 1996).

By showing the systemic velocity of the galaxy is about $10\,\mathrm{km\,s^{-1}}$ lower than previous estimates we resolve some mysteries. Other studies have estimated the systemic or central velocity using stars peripheral to the centre. van der Marel et al. (2002) find a slightly negative result for a handful of stars in the central region, although they do not attribute much significance to this finding due to low sample numbers. They find for stars in the inner 0.5 kpc bin a disk rotation velocity of $-27.9\,\mathrm{km\,s^{-1}}$, which is incompatible with the disk model. They suggest noncircular streaming motions at the very centre are not well modelled by a simple rotating disk. A lower systemic velocity is a simpler explanation, giving simple solid body rotation at the LMC centre. We agree with Marel (2001) who find the bar velocity profile smoothly varying.

Other studies have suggested counter-rotation at the LMC centre (Subramaniam and Prabhu 2005) or even a bar totally disconnected from the disk structure (Zaritsky 2004; Zhao and Evans 2000). This implies some serious disturbance to the disk due to accretion onto the MW over several orbits, or radical interaction with the SMC. This study show the bar retains a velocity signature of an original circular rotating disk, and probably rules out major accretion events. Subramaniam and Subramanian (2009) using red clump magnitudes do not find any evidence that the bar is spatially distinct from the disk, and this study agrees.

While our model suggests a lower systematic velocity at the centre, we agree within our errors with previous authors on disk geometry, and on the rotation curve at large radii (van der Marel et al. 2002; Olsen and Massey 2007; Olsen et al. 2011; Piatek et al. 2008). We have shown with MCMC simulations that a model of a simple rotating disk is valid within a range of adopted values for the disk rotation centre, inclination and line of nodes angle. Streaming motions along the axis of the bar may be present but are perpendicular to the radial line of sight.

The residuals from a rotation model show no significant evidence of a pattern that may indicate a structure other than a thin disk. If the bar and disk were separate structures, we would expect our sample to contain a mixture of the two populations within the inner regions. If this was the case then the residuals from a rotating disk model might be expected to trace a unique bar population. The residuals do not show evidence that there is any separate, coherent structure. The bar itself appears only as a stellar density enhancement in the disk. However

we do detect some significant differences in the residuals from the Massey RSG and Reid PNe samples. The RSG sample is a young population and may be associated with super-shell kinematics. Young populations in the LMC are associated with the scattered Shapley constellations. The young population probably has a higher asymmetric drift factor than the old and intermediate populations of the rotating disk.

A subset of 28 stars with metallicity lower than -1.0 dex do not show any statistical kinematic difference from the rest of the sample. Unlike Olsen et al. (2011) this sample doesn't exhibit any candidate accreted SMC low metallicity stars with unique kinematics. Their potential SMC stars with odd kinematics represented only 3% of their total sample. Some of the stars in this sample may be accreted SMC stars with odd kinematics but they cannot be statistically distinguished. The distribution does show a long tail of low metallicities, which could represent the LMC SFH or an accreted low metallicity population.

The lower systemic velocity is a consequence of more detailed information about the central velocity in this dataset than was previously available. Other determinations of the systemic velocity have been inferred from data surrounding the inner region. Rotation models based on velocities in the outer regions have been used to interpolate to the centre of mass velocity. The systemic velocity has been over estimated slightly in the absence of the central velocity data. This study remedies that omission and shows that a rotating disk model with lower systemic velocity explains the radial velocity observations.

Of the original three nights proposed observations of the LMC only four hours were observed due to weather. This study represents the partial fulfilment of the original goal of observing the entire central galaxy, bar and disk. From just two fields we have confirmed the existence of a rotation curve, even down to the extreme centre of the galaxy. This sample has demonstrated that counter-rotation at the core is unlikely. The mean metallicity of the bar has been shown to be higher than the that of the disk.

The proposal was on the service observing waiting list in case telescope time became available during maintenance periods or cancelled observations. While the proposal has now lapsed, spectroscopic large scale observations of the entire disk and bar are overdue. This has been achieved for the SMC with new AAOmega spectroscopic observations of the entire galaxy now completed and currently under analysis. An homogenous data set covering the entire LMC disk and bar would help resolve questions of kinematic contrasts, the metallicity gradient across the galaxy, the star formation history, and provide clues to the formation and interaction of the Magellanic system.

5.3 Making a Milky Way

The study of IC 4499 established a never before determined line of sight velocity for this ancient stellar structure. The velocity estimate places restrictions on the possible membership of IC 4499 in halo streams and contributes to understanding of accretion processes in the formation of the MW. This study also placed an

upper limit on the rotational velocity of the cluster, indicating it is pressure supported. An accurate measure of the metallicity was also obtained which allowed a more precise age-dating of the cluster. The foreground to IC 4499 was heavily crowded with stars from the MW Galaxy. The use of the AAOmega multi-fibre spectrometer on the four metre Siding Springs Anglo-Australian telescope made it possible to pick out the individual stars in the cluster from the crowded stellar field toward the bulge region of the MW.

The same instrument was again used to observe an even more crowded field at the very heart of the LMC. A rotation curve was established for the extreme inner regions where none had been able to be determined. The rotation curve also indicates a characteristic disk scale for the galaxy. The velocity dispersion observed showed that even the inner regions display a thick disk profile, so like previous studies no evidence was found of a hot pressure supported bulge or halo population. Statistically no evidence was found for a counter-rotating population or other systematic departure from the modelled circular orbits. The bar feature is consistent with a density wave feature in a rotationally supported disk.

A detection of slightly higher metallicity in the bar region relative to the outer disk confirmed previous findings of a metallicity gradient. Such a gradient indicates a bottom-up hierarchical sense of formation of the galaxy in line with the ΛCDM paradigm. We argue that since an initial rapid homogenous top-down formation and prolonged quiet evolution for half its lifetime, recent accretion and interaction have driven bottom up growth from the centre of the LMC outwards.

The velocity determined in this study for IC 4499 helps place it in the context of dynamical accretion processes that built the MW. The velocity is consistent with a typical MW halo orbit, but also within the range of simulated velocities for the Monocereos tidal stream, making its role ambiguous. Additionally the lower metallicity estimate places it further towards the OoInt classification, from its borderline OoI categorisation. This also hints at a dwarf galaxy origin for the cluster, such as Canis Major, as these satellite objects tend to be OoInt. The role of dwarf galaxies in the assembly of the MW is hidden in the tidal debris streams within the halo. The metal poor nature of IC 4499 probably rules out speculation of a young age for the cluster, placing it within the pantheon of classic ancient MW clusters, with its Oosterhoff type hinting at a metal poor dwarf galaxy origin.

The physical parameters measured do not mark out IC 4499 as particularly unusual for a MW globular. It had been postulated that the cluster is unusual for being younger than other globulars, (Ferraro et al. 1995). A similar study found IC 4499 to be coeval with other metal poor clusters, (Salaris and Weiss 2002). Using our precise estimate of metallicity, Walker et al. (2011) conclusively find that IC 4499 is coeval with other metal poor clusters at 12 ± 1 Gyr.

The velocity is not unusual for the location in the halo, (Robin et al. 2003). The velocity may place IC 4499 in the Monoceros stream, but may just as well be Galactic as the large range of stream velocities overlaps most of the Galactic model velocities at this location, (Peñarrubia et al. 2005; Robin et al. 2003). At

[Fe/H]= -1.5 dex it is not an unusual metallicity for a single stellar population halo globular cluster.

Walker et al. (2011) find an homogeneous single stellar population, so a detailed abundance analysis should reveal if the cluster can be associated with a dwarf spheroidal galaxy or is a typical halo object. The mass estimate from our velocity dispersion estimate is consistent with estimates from the light profile. There does not appear to be any need to invoke a substantial DM component to explain the kinematics. In conclusion we have helped establish that IC 4499 is an archetypical ancient metal-poor MW globular. Its exact evolution as an in situ, or accreted cluster remains an open question.

Either the MW Galaxy, the SMC or both may responsible for the disturbed LMC disk, including the bar feature. If the MW gravitational potential is responsible in the form of a clumpy DM MW halo, then the short cosmological lifetime of induced bar features adds weight to the hypothesis that the LMC and MW are undergoing a first interaction. If the bar is due to LMC-SMC interaction then again, the event is cosmologically recent, in the last few gigayears.

The finding of $24\,\mathrm{km\,s^{-1}}$ line of sight velocity dispersion is consistent with the stars in the sample being rotationally supported in a disk-like structure. Like previous studies of the central region of the LMC we do not find a velocity dispersion consistent with the bar being a spheroidal or triaxial bulge. This probably rules out major mergers in the formation history of the LMC.

The very existence of a strong bar in the LMC suggests that heating of the stellar disk is not excessive. Velocity dispersion may be negatively correlated with bar strength in disk galaxies (Das et al. 2008). Rotational velocities are compatible with a bar, whereas random thermal motions tend not to be. Our analysis shows a dominant ordered rotational distribution of energy, and a thick disk velocity dispersion, which provides a suitable environment for the bar resonance. The bar is not an unexpected feature in a disk galaxy like the LMC which has such conducive conditions. A bar serves to move angular momentum outwards from the centre of the galaxy, especially in a close encounter with the satellite SMC.

The systemic velocity is one important component of the space motion of the galaxy. Changes in the value for space velocity of the LMC have implications for the entire history of the galaxy. A lower systemic velocity may just make the Magellanic system bound to the MW. Origins of stellar features like the bar, gas features including the stream and the leading and trailing arms depend on the LMC trajectory within the MW halo.

If the LMC is on a first orbit of the MW, then we see evidence of the H1 gas galaxy absorbing the shock of the initial interaction leaving the stellar disk comparatively intact, especially for population II objects. The effect on the stellar population is recent star formation in regions like 30 Doradus, which preferentially appear toward the bow shock of the LMC as it meets the MW halo (Figure 8 Kim et al. 1998). There is also evidence for compression of cold HI gas and molecular gas on the eastern leading edge (Marx-Zimmer et al. 2000). The disk outer regions are the first to feel the tidal or ram pressure effects of MW interaction (Bekki and Chiba 2005).

The H1 gas disk is at a higher systemic velocity than the stellar disk and this study emphasises the disconnect . The 'L' component of the H1 galaxy may be more closely associated with the stellar disk, being closer in velocity space. The 'L' component two arm morphology is also vaguely spiral. The bar feature appears intrinsic to the velocity field of the stellar disk. Streaming motions along the bar are perpendicular to our line of sight and are not detected in radial velocity observations. Despite such a strong bar it is remarkable that non circular streaming motions do not smear out the circular rotation. This may indicate the bar is a recent feature associated with the recent 200-500 Myr encounter with the SMC.

The LMC morphology is a record of the various factors which have shaped the galaxy over the last few billion years. The SMC is primarily responsible for shaping the LMC over most of this time with the MW beginning to grow in importance as the clouds make their first approach. SMC encounters over a longer time may have induced the bar, and some H1 leading and trailing debris. More recent disturbances such as sporadic star formation and further disconnection of the H1 gas from the stellar disk may be due MW halo interaction. The bar structure is stellar in composition probably due to the SMC interaction, with the H1 gas showing no associated structure.

The hierarchical accretion process of building the MW Galaxy is being played out in front of us. The LMC-SMC interaction is a microcosm of the larger LG dramas, which will ultimately culminate in the amalgamation of the two major disks, M31 and the MW into a new super galaxy. Understanding the construction of galaxies is vital to comprehension of a universe founded on DM.

Disks in simulations can survive encounters with a substantial satellite of 10% the mass of the disk (Walker and Nemec 1996). The HI gas may tend to preferentially absorb kinetic energy from minor mergers and flybys compared to the stellar disk. Moster et al. (2010) model a merging environment for LG type galaxies and show that gas can reduce disk heating by absorbing kinetic energy. The HI gas appears to be bearing the brunt of the disturbances to the galaxy. The HI disk seems to show even stronger spiral features than the stellar disk (Kim et al. 1998; Staveley-Smith et al. 2003). Whatever causes the bar resonance, resonates even more strongly in the gas galaxy. The HI also shows multiple components and velocity profiles, indicating that it is more disturbed than the stellar disk. In addition the rotation centres of the HI and stellar galaxies appear to be offset.

The fact that we see the older stellar populations regularly distributed in stable and largely undisturbed orbits in the SMC ellipsoid (Zaritsky et al. 2000), and the LMC disk [this thesis], argues for a recent origin for the disturbed morphologies of the Magellanic system. Recent proper motion estimations support this hypothesis (Kallivayalil et al. 2006; Piatek et al. 2008; Vieira et al. 2010), indicating the Magellanic system is on its first orbit or first passage past the MW Galaxy.

The recent disturbances have resulted in disproportionate ram or tidal stripping of the HI component of the galaxy compared to the stellar. The effect on the HI has possibly created density conditions for recent star formation activity

at shock fronts and in turbulent wakes. The bar feature in the LMC disk, along with the spiral pattern, is probably the result of the presence of the SMC near the LMC disk, as bars are often found in galaxies with substantial companions Steinmetz and Navarro (2002). The MW grand design spiral and bar may even be a response in part at least to the presence of the Magellanic system's influence on the MW DM halo, along with the other dwarf galaxies.

The metallicity gradient is evidence that the LMC galaxy formation has been bottom up, or inside out, and the galaxy has evolved in some part due to accretion of enriched gas, in addition to self-enrichment. Brook et al. (2011) proposed removing angular momentum from the disk via outflows into the halo which then feedback to the central galaxy. The slightly higher metallicity found in the bar compared to the disk may be a clue that pre-enriched gas has recirculated back into the central region, perhaps with the aid of the bar. This creates conditions in the bar region where CMD studies suggest young metal-rich RGB stars dominate samples (Cole et al. 2009).

We do not see the SFH of the Magellanic clouds mirrored in the MW. There is little evidence for LMC effects on the MW, which indicates the Magellanic system has self-interacted independently of the MW until very recently. The SFH is reflected in the SMC at 500 Myr and at 2 Gyr (Harris and Zaritsky 2009). Interactions with the SMC and momentum exchanges would account for the LMC bar feature. Barred Magellanic type galaxies nearly always have a close companion (Odewahn 1994).

If DM played a role in the formation of Galactic GC then where is the evidence for it now? The DM is unlikely to have been tidally stripped by interaction with the Milky way (Baumgardt and Mieske 2008). Nor is DM ejected in numerical simulations. The lack of DM in globular clusters has cosmic implications for the formation of stellar groups in primordial times and may have implications for modified theories of gravity (e.g. modified Newtonian dynamics (Milgrom 1983)). The existence of DM halos in dwarf galaxies suggests some scale break for the role of DM in forming structure. This may go some way to explaining the deficit of small structure .

Steinmetz and Navarro (2002) show that in ΛCDM cosmology simulations satellite galaxies stimulate bars within disks. In fact all galaxy morphologies seem attributable to mergers and interactions disrupting the "pure" disk structure. Hierarchical structure formation is too "lumpy" in the ΛCDM paradigm, resulting in not enough disk galaxies in simulations. Disks require smooth gas flows, and ΛCDM predicts too much small structure which can disrupt disks.

Perhaps the lack of DM in GCs points to less small scale lumpiness in the DM universe. There may be some threshold of DM potential below which baryonic condensation cannot occur, possibly due to ionisation from the host galaxy in a MW type halo. DM's role in structure formation may break at a particular scale length somewhere between dwarf galaxies, which have a substantial DM components, and globular clusters which do not.

Together the GC IC 4499 and the dIrr LMC provide contrasting and complementary views of the MW Galaxy. Both objects are at vastly different scales but both are iinteracting with the MW and each other. The LMC is a substan-

tial disk that appears to have arrived late in the evolution of the MW, perhaps on its first fly-by. If IC 4499 is a tidal remnant of a dwarf satellite that has been accreted, then it points to the past merger history of the MW. If IC 4499 is a classical GC that formed in the outer regions of the halo at the same time as the proto-galactic disk, then it has a slightly unusual HB morphology, which may indicate population subtleties. These populations may hold clues to the origin of the formation of the Galactic halo at ancient times. Either way IC 4499 points to the past, and the LMC to the future of the MW.

Future observations of the planned but unobserved fields with AAOmega will allow the extension of the scope of this thesis to a comparison of the LMC disk with the bar kinematics and metallicities. Understanding the internal dynamics of the Magellanic Clouds is crucial to improvement of the systematics of the space motions of the galaxies. Objects in the MW Galaxy and halo environment provide a laboratory for the study of hierarchical galaxy formation. Multi-object spectroscopy, chemical tagging and velocity determinations of MW and halo objects will continue to shed light on the evolution of the Galaxy.

Bibliography

D. R. Alves and C. A. Nelson. The Rotation Curve of the Large Magellanic Cloud and the Implications for Microlensing. *Astrophys. J.*, 542:789–803, October 2000. doi: 10.1086/317023.

G. Battaglia, M. Irwin, E. Tolstoy, V. Hill, A. Helmi, B. Letarte, and P. Jablonka. Analysis and calibration of CaII triplet spectroscopy of red giant branch stars from VLT/FLAMES observations. *Mon. Not. R. Astron. Soc.*, 383:183–199, January 2008. doi: 10.1111/j.1365-2966.2007.12532.x.

H Baumgardt and S Mieske. High mass-to-light ratios of ultra-compact dwarf galaxies - evidence for dark matter? *Monthly Notices of the Royal Astronomical Society*, 391(2):942–948, December 2008.

H Baumgardt, P Côté, M Hilker, M Rejkuba, S Mieske, S G Djorgovski, and Peter Stetson. The velocity dispersion and mass-to-light ratio of the remote halo globular cluster NGC2419. *Monthly Notices of the Royal Astronomical Society*, 396(4):2051–2060, July 2009.

K. Bekki and M. Chiba. Formation and evolution of the Magellanic Clouds - I. Origin of structural, kinematic and chemical properties of the Large Magellanic Cloud. *Mon. Not. R. Astron. Soc.*, 356:680–702, January 2005. doi: 10.1111/j.1365-2966.2004.08510.x.

J Binney. Resonant excitation of motion perpendicular to galactic planes. *Monthly Notices of the Royal Astronomical Society*, 196:455–467, August 1981.

A Bosma. Global Rotational Properties of Barred Galaxies. *Barred galaxies. Astronomical Society of the Pacific Conference Series*, 91:132, 1996.

J D Bradford, M Geha, R R Muñoz, F A Santana, J D Simon, P Côté, P B Stetson, E Kirby, and S G Djorgovski. Structure and Dynamics of the Globular Cluster Palomar 13. *The Astrophysical Journal*, 743(2):167, December 2011.

C B Brook, G Stinson, B K Gibson, R Roškar, J Wadsley, and T Quinn. Hierarchical formation of bulgeless galaxies - II. Redistribution of angular momentum via galactic fountains. *Monthly Notices of the Royal Astronomical Society*, 419(1):771–779, October 2011.

E. Carretta and R. G. Gratton. Abundances for globular cluster giants. I. Homogeneous metallicities for 24 clusters. *Astron. Astrophys. Suppl. Ser.*, 121:95–112, January 1997. doi: 10.1051/aas:1997116.

M Catelan. Horizontal branch stars: the interplay between observations and theory, and insights into the formation of the Galaxy. *Astrophysics and Space Science*, 320:261–309, April 2009.

M R L Cioni. The metallicity gradient as a tracer of history and structure: the Magellanic Clouds and M33 galaxies. *Astronomy and Astrophysics*, 506(3): 1137–1146, November 2009.

A. A. Cole, T. A. Smecker-Hane, E. Tolstoy, T. L. Bosler, and J. S. Gallagher. The effects of age on red giant metallicities derived from the near-infrared CaII triplet. *Mon. Not. R. Astron. Soc.*, 347:367–379, January 2004. doi: 10.1111/j.1365-2966.2004.07223.x.

Andrew A Cole, Eline Tolstoy, John S Gallagher, and Tammy A Smecker-Hane. Spectroscopy of Red Giants in the Large Magellanic Cloud Bar: Abundances, Kinematics, and the Age-Metallicity Relation. *The Astronomical Journal*, 129:1465, March 2005.

Andrew A Cole, Aaron J Grocholski, Doug Geisler, Ata Sarajedini, Verne V Smith, and Eline Tolstoy. Breaking the age-metallicity degeneracy: The metallicity distribution and star formation history of the Large Magellanic Cloud. *The Magellanic System: Stars*, 256:263–268, March 2009.

M Das, E Laurikainen, H Salo, and R Buta. Variation of bar strength with central velocity dispersion in spiral galaxies. *Astrophysics and Space Science*, 317(3-4):163–168, July 2008.

Michael W Feast, Oyirwoth P Abedigamba, and Patricia A Whitelock. Is there a metallicity gradient in the Large Magellanic Cloud? *Monthly Notices of the Royal Astronomical Society: Letters*, 408(1):L76–L79, September 2010.

I. Ferraro, F. R. Ferraro, F. F. Pecci, C. E. Corsi, and R. Buonanno. Young globular clusters in the Milky Way: IC 4499. *Mon. Not. R. Astron. Soc.*, 275: 1057–1076, August 1995.

F. Fusi Pecci, M. Bellazzini, C. Cacciari, and F. R. Ferraro. The Young Globular Clusters of the Milky Way and the Local Group Galaxies: Playing with Great Circles. *Astron.J*, 110:1664–+, October 1995. doi: 10.1086/117639.

Carme Gallart, Peter B Stetson, Ingrid P Meschin, Frederic Pont, and Eduardo Hardy. Outside-In Disk Evolution in the Large Magellanic Cloud. *The Astrophysical Journal*, 682:L89, August 2008.

Jason Harris and Dennis Zaritsky. Spectroscopic Survey of Red Giants in the Small Magellanic Cloud. I. Kinematics. *The Astronomical Journal*, 131:2514, May 2006.

Jason Harris and Dennis Zaritsky. The Star Formation History of the Large Magellanic Cloud. *The Astronomical Journal*, 138(5):1243–1260, November 2009.

W. E. Harris. A Catalog of Parameters for Globular Clusters in the Milky Way. *Astron.J*, 112:1487, October 1996. doi: 10.1086/118116.

Raoul Haschke, Eva K Grebel, and Sonia Duffau. Three-dimensional Maps of the Magellanic Clouds using RR Lyrae Stars and Cepheids. I. The Large Magellanic Cloud. *The Astronomical Journal*, 144(4):106, October 2012.

N. Kallivayalil, R. P. van der Marel, C. Alcock, T. Axelrod, K. H. Cook, A. J. Drake, and M. Geha. The Proper Motion of the Large Magellanic Cloud Using HST. *Astrophys. J.*, 638:772–785, February 2006. doi: 10.1086/498972.

S. Kim, L. Staveley-Smith, M. A. Dopita, K. C. Freeman, R. J. Sault, M. J. Kesteven, and D. McConnell. An H i Aperture Synthesis Mosaic of the Large Magellanic Cloud. *Astrophys. J.*, 503:674, August 1998. doi: 10.1086/306030.

William E Kunkel, Serge Demers, M J Irwin, and Loic Albert. The Dynamics of the Large Magellanic Cloud Periphery: Mass Limit and Polar Ring. *Astrophysical Journal Letters v.488*, 488:L129, October 1997.

R. R. Lane, L. L. Kiss, G. F. Lewis, R. A. Ibata, A. Siebert, T. R. Bedding, and P. Székely. Testing Newtonian gravity with AAOmega: mass-to-light profiles of four globular clusters. *Mon. Not. R. Astron. Soc.*, 400:917–923, December 2009. doi: 10.1111/j.1365-2966.2009.15505.x.

R. R. Lane, L. L. Kiss, G. F. Lewis, R. A. Ibata, A. Siebert, T. R. Bedding, P. Székely, Z. Balog, and G. M. Szabó. Halo globular clusters observed with AAOmega: dark matter content, metallicity and tidal heating. *Mon. Not. R. Astron. Soc.*, pages 799–+, May 2010. doi: 10.1111/j.1365-2966.2010.16874.x.

Ryan Leaman. Insights Into Pre-enrichment of Star Clusters and Self-enrichment of Dwarf Galaxies from their Intrinsic Metallicity Dispersions. *The Astronomical Journal*, 144(6):183, November 2012.

Henry Lee, Evan D Skillman, John M Cannon, Dale C Jackson, Robert D Gehrz, Elisha F Polomski, and Charles E Woodward. On Extending the Mass-Metallicity Relation of Galaxies by 2.5 Decades in Stellar Mass. *The Astrophysical Journal*, 647(2):970–983, August 2006.

Y.-W. Lee. The chronology of the formation of the Galaxy. *Publications of the Astronomical Society of the Pacific*, 104:798–804, September 1992. doi: 10.1086/133056.

Roeland P van der Marel. Magellanic Cloud Structure from Near-IR Surveys II: Star Count Maps and the Intrinsic Elongation of the LMC. *arXiv*, astro-ph, May 2001. Astronomical Journal, in press. 34 pages, LaTeX, with 7 PostScript figures. Contains minor revisions with respect to previously posted version. Check out http://www.stsci.edu/ marel/lmc.html for a large scale (23x21 degree) stellar number-density image of the LMC constructed from RGB and AGB stars in the 2MASS and DENIS surveys. The paper is available with higher resolution color figures from http://www.stsci.edu/ marel/abstracts/abs_R32.html.

M Marx-Zimmer, U Herbstmeier, J M Dickey, F Zimmer, L Staveley-Smith, and U Mebold. A study of the cool gas in the Large Magellanic Cloud. I. Properties of the cool atomic phase - a third H i absorption survey. *Astronomy and Astrophysics*, 354:787–801, February 2000.

D. E. McLaughlin and R. P. van der Marel. Resolved Massive Star Clusters in the Milky Way and Its Satellites: Brightness Profiles and a Catalog of Fundamental Parameters. *Astrophys. J., Suppl. Ser.*, 161:304–360, December 2005. doi: 10.1086/497429.

M Milgrom. A modification of the Newtonian dynamics as a possible alternative to the hidden mass hypothesis. *Astrophysical Journal*, 270:365–370, July 1983.

Ben Moore. Constraints on the Global Mass-to-Light Ratios and on the Extent of Dark Matter Halos in Globular Clusters and Dwarf Spheroidals. *Astrophysical Journal Letters v.461*, 461:L13, April 1996.

Benjamin P Moster, Andrea V Maccio, Rachel S Somerville, Peter H Johansson, and Thorsten Naab. Can gas prevent the destruction of thin stellar discs by minor mergers? *Monthly Notices of the Royal Astronomical Society*, 403(2): 1009–1019, February 2010.

S. C. Odewahn. Properties of the Magellanic type spirals. 2: The frequency of companion galaxies. *The Astronomical Journal*, 107:1320–1327, April 1994.

S. C. Odewahn. Properties of the Magellanic Type Galaxies. In R. Buta, D. A. Crocker, & B. G. Elmegreen, editor, *IAU Colloq. 157: Barred Galaxies*, volume 91 of *Astronomical Society of the Pacific Conference Series*, pages 30–+, 1996.

K. A. G. Olsen and P. Massey. Evidence for Tidal Effects in the Stellar Dynamics of the Large Magellanic Cloud. *Astrophys. J., Lett.*, 656:L61–L64, February 2007. doi: 10.1086/512484.

K. A. G. Olsen, D. Zaritsky, R. D. Blum, M. L. Boyer, and K. D. Gordon. A Population of Accreted Small Magellanic Cloud Stars in the Large Magellanic Cloud. *Astrophys. J.*, 737:29–+, August 2011. doi: 10.1088/0004-637X/737/1/29.

J. Peñarrubia, D. Martínez-Delgado, H. W. Rix, M. A. Gómez-Flechoso, J. Munn, H. Newberg, E. F. Bell, B. Yanny, D. Zucker, and E. K. Grebel. A Comprehensive Model for the Monoceros Tidal Stream. *Astrophys. J.*, 626: 128–144, June 2005. doi: 10.1086/429903.

S. Piatek, C. Pryor, and E. W. Olszewski. Proper Motions of the Large Magellanic Cloud and Small Magellanic Cloud: Re-Analysis of Hubble Space Telescope Data. *Astron.J*, 135:1024–1038, March 2008. doi: 10.1088/0004-6256/135/3/1024.

A. E. Piatti and J. J. Clariá. The apparent overdensity of open clusters in the Canis Major overdensity. *Mon. Not. R. Astron. Soc.*, 390:L54–L58, October 2008. doi: 10.1111/j.1745-3933.2008.00536.x.

L. Pompéia, V Hill, M. Spite, A. Cole, F Primas, M. Romaniello, L. Pasquini, M-R Cioni, and T. Smecker Hane. Chemical abundances in LMC stellar populations. I. The inner disk sample. *Astronomy and Astrophysics*, 480(2): 379–395, March 2008.

A. C. Robin, C. Reylé, S. Derrière, and S. Picaud. A synthetic view on structure and evolution of the Milky Way. *Astron. Astrophys.*, 409:523–540, October 2003. doi: 10.1051/0004-6361:20031117.

G. A. Rutledge, J. E. Hesser, and P. B. Stetson. Galactic Globular Cluster Metallicity Scale from the Ca II Triplet II. Rankings, Comparisons, and Puzzles. *Publications of the Astronomical Society of the Pacific*, 109:907–919, August 1997. doi: 10.1086/133959.

M. Salaris and A. Weiss. Homogeneous age dating of 55 Galactic globular clusters. Clues to the Galaxy formation mechanisms. *Astron. Astrophys.*, 388:492–503, June 2002. doi: 10.1051/0004-6361:20020554.

A. Sandage. The Oosterhoff period-metallicity relation for RR Lyrae stars at the blue fundamental edge of the instability strip. *Astron.J*, 106:687–702, August 1993. doi: 10.1086/116675.

H. A. Smith and G. J. Perkins. Metal abundances of RR Lyrae stars in globular clusters. *Astrophys. J.*, 261:576–585, October 1982. doi: 10.1086/160368.

L Staveley-Smith, S Kim, M R Calabretta, R F Haynes, and M J Kesteven. A new look at the large-scale HI structure of the Large Magellanic Cloud. *Monthly Notice of the Royal Astronomical Society*, 339:87, February 2003.

Matthias Steinmetz and Julio F Navarro. The hierarchical origin of galaxy morphologies. *New Astronomy*, 7(4):155–160, June 2002.

Annapurni Subramaniam and Tushar P Prabhu. Evidence of a Counterrotating Core in the Large Magellanic Cloud. *The Astrophysical Journal*, 625:L47, May 2005.

Annapurni Subramaniam and Smitha Subramanian. The Mysterious Bar of the Large Magellanic Cloud: What Is It? *The Astrophysical Journal Letters*, 703 (1):L37–L40, September 2009.

S. C. Trager, S. Djorgovski, and I. R. King. Structural Parameters of Galactic Globular Clusters. In S. G. Djorgovski & G. Meylan, editor, *Structure and Dynamics of Globular Clusters*, volume 50 of *Astronomical Society of the Pacific Conference Series*, pages 347–+, January 1993.

Christy A Tremonti, Timothy M Heckman, Guinevere Kauffmann, Jarle Brinchmann, Stéphane Charlot, Simon D M White, Mark Seibert, Eric W Peng, David J Schlegel, Alan Uomoto, Masataka Fukugita, and Jon Brinkmann. The Origin of the Mass-Metallicity Relation: Insights from 53,000 Star-forming Galaxies in the Sloan Digital Sky Survey. *The Astrophysical Journal*, 613(2): 898–913, October 2004.

Roeland P. van der Marel, David R Alves, Eduardo Hardy, and Nicholas B Suntzeff. New Understanding of Large Magellanic Cloud Structure, Dynamics, and Orbit from Carbon Star Kinematics. *The Astronomical Journal*, 124 (5):2639–2663, November 2002. Published in: Astron.J.124:2639-2663,2002 57 pages, LaTeX, with 11 PostScript figures. Submitted to the Astronomical Journal.

M Van der Swaelmen, V Hill, F Primas, and A A Cole. Chemical abundances in LMC stellar populations. II. The bar sample. *arXiv.org*, page 4224, June 2013.

K. Vieira, T. M. Girard, W. F. van Altena, N. Zacharias, D. I. Casetti-Dinescu, V. I. Korchagin, I. Platais, D. G. Monet, C. E. López, D. Herrera, and D. J. Castillo. Proper-motion Study of the Magellanic Clouds Using SPM Material. *Astron.J*, 140:1934–1950, December 2010. doi: 10.1088/0004-6256/140/6/1934.

R Wagner-Kaiser and Ata Sarajedini. The properties of the Large Magellanic Cloud based on OGLE-III photometry of RR Lyrae stars. *Monthly Notices of the Royal Astronomical Society*, 431(2):1565–1572, May 2013.

A. R. Walker and J. M. Nemec. CCD Photometry of Galactic Globular Clusters.III.IC 4499. *Astron.J*, 112:2026–+, November 1996. doi: 10.1086/118161.

A R Walker, A M Kunder, G Andreuzzi, A Di Cecco, P B Stetson, M Monelli, S Cassisi, G Bono, R De Propris, M Dall'Ora, J M Nemec, and M Zoccali. Constraints on the formation of the globular cluster IC 4499 from multiwavelength photometry. *Monthly Notices of the Royal Astronomical Society*, 415 (1):643–654, May 2011.

Steven R Warren and Andrew A Cole. Metallicities and radial velocities of five open clusters including a new candidate member of the Monoceros stream. *Monthly Notices of the Royal Astronomical Society*, 393(1):272–296, February 2009.

David H Weinberg, James S Bullock, Fabio Governato, Rachel Kuzio de Naray, and Annika H G Peter. Cold dark matter: controversies on small scales. *arXiv.org*, June 2013.

D. Zaritsky. The Case of the Off-Center, Levitating Bar in the Large Magellanic Cloud. *Astrophys. J., Lett.*, 614:L37–L40, October 2004. doi: 10.1086/425312.

Dennis Zaritsky, Jason Harris, Eva K Grebel, and Ian B Thompson. The Morphologies of the Small Magellanic Cloud. *The Astrophysical Journal*, 534(1): L53–L56, May 2000.

H. Zhao and N. W. Evans. The So-called "Bar" in the Large Magellanic Cloud. *Astrophys. J., Lett.*, 545:L35–L38, December 2000. doi: 10.1086/317324.

HongSheng Zhao, Rodrigo A Ibata, Geraint F Lewis, and Michael J Irwin. Kinematic outliers in the Large Magellanic Cloud: constraints on star-star microlensing. *Monthly Notice of the Royal Astronomical Society*, 339:701, March 2003.

R. Zinn and M. J. West. The globular cluster system of the galaxy. III - Measurements of radial velocity and metallicity for 60 clusters and a compilation of metallicities for 121 clusters. *Astrophys. J., Suppl. Ser.*, 55:45–66, May 1984. doi: 10.1086/190947.

Appendices

A

Stellar Dynamics in Potentials

A.1 Potentials

To find the gravitational force on a point particle at $\mathbf{x}$ we have to look at all the infinitesimal elements of mass at a distance $\mathbf{x\prime}$ where the force acts as the inverse of the square of the distance, following Newton,

$$d\mathbf{F}(\mathbf{x}) = \frac{G\,m(\mathbf{x})}{|\mathbf{x}' - \mathbf{x}|^2}\, dm(\mathbf{x}') = \frac{G\,m(\mathbf{x})}{|\mathbf{x}' - \mathbf{x}|^2}\, \rho(\mathbf{x}')\, d^3\mathbf{x}' \tag{A.1}$$

Where $G = 6.673\,84 \pm 0.000\,80 \times 10^{-11}\,\mathrm{m^3 kg^{-1} s^{-2}}$ (Gillies 1997) is the universal gravitational constant. All the contributions are summed to give the force on $m(\mathbf{x})$,

$$\mathbf{F}(\mathbf{x}) = G\,m(\mathbf{x}) \int \frac{\rho(\mathbf{x}')}{|\mathbf{x}' - \mathbf{x}|^2}\, d^3\mathbf{x}' \tag{A.2}$$

The potential is defined (Binney and Tremaine 2008) as,

$$\Phi(\mathbf{x}) \equiv -G \int \frac{\rho(\mathbf{x}')}{|\mathbf{x}' - \mathbf{x}|}\, d^3\mathbf{x}' \tag{A.3}$$

so that that the acceleration is the gradient of the potential,

$$\mathbf{F}(\mathbf{x}) = m(\mathbf{x})\mathbf{a}(\mathbf{x}) = -\nabla\Phi m(\mathbf{x}) \tag{A.4}$$

To to ascertain the source or sink of the gravitational field, we take the divergence of the acceleration (Binney and Tremaine 2008),

$$\nabla \cdot \mathbf{a}(\mathbf{x}) = G \int \nabla \cdot \frac{\rho(\mathbf{x}')}{|\mathbf{x}' - \mathbf{x}|^2}\, d^3\mathbf{x}' \tag{A.5}$$

When we consider the divergence of,

$$\nabla \cdot \frac{1}{|\mathbf{x}' - \mathbf{x}|^2} = \frac{-2}{|\mathbf{x}' - \mathbf{x}|^2} + \frac{2|\mathbf{x}' - \mathbf{x}|}{|\mathbf{x}' - \mathbf{x}|^3} = 0 \text{ for } \mathbf{x}' \neq \mathbf{x} \tag{A.6}$$

the divergence is zero for all $\mathbf{x}'$, except for an infinitesimal sphere around $\mathbf{x}$, say radius h, within which region we consider the density to be constant, so the density term comes out of the integral,

$$\begin{aligned}
\nabla \cdot \mathbf{a}(\mathbf{x}) = & \quad G\rho(\mathbf{x}) \int_{|\mathbf{x}'-\mathbf{x}|\leq h} \nabla_x \cdot \frac{1}{|\mathbf{x}' - \mathbf{x}|^2}\, d^3\mathbf{x}' \\
= & \quad -G\rho(\mathbf{x}) \int_{|\mathbf{x}'-\mathbf{x}|\leq h} \nabla_{x'} \cdot \frac{1}{|\mathbf{x}' - \mathbf{x}|^2}\, d^3\mathbf{x}' \\
= & \quad -G\rho(\mathbf{x}) \int_{|\mathbf{x}'-\mathbf{x}|=h} d^2\mathbf{S}' \cdot \frac{1}{|\mathbf{x}' - \mathbf{x}|^2}
\end{aligned}$$

On the second line above, the divergence variable is changed to $\mathbf{x}'$, reversing the direction, and on the third line the integration is now over the surface elements $d^2\mathbf{S}' = |\mathbf{x}' - \mathbf{x}|h d^2\Omega$ where $d^2\Omega$ is an increment of solid angle. As on the surface $|\mathbf{x}' - \mathbf{x}| = h$ we now have,

$$\nabla \cdot \mathbf{a}(\mathbf{x}) = -G\rho(\mathbf{x}) \int d^2\Omega = -4\pi G\rho(\mathbf{x}) \tag{A.7}$$

Now we can relate the potential field Φ to the source of the gravitational force, the density in space,

$$\nabla \cdot \mathbf{a}(\mathbf{x}) = \nabla \cdot (-\nabla\Phi) = -\nabla^2\Phi = -4\pi G\rho(\mathbf{x}) \tag{A.8}$$

This gives us Poisson's second order differential equation for a gravitational field,

$$\nabla^2\Phi = 4\pi G\rho(\mathbf{x}) \tag{A.9}$$

The potential equation A.3 gives us the necessary Dirichlet boundary condition to solve the Poisson equation; $\Phi \to 0$ as $|\mathbf{x}| \to \infty$ for an isolated system. For $\rho(\mathbf{x}) = 0$ we have the Laplace equation $\nabla^2\Phi = 0$, and these elliptic partial differential equations form the basis of potential theory.

Integrating equation A.9 over any volume containing the system mass M,

$$\nabla^2\Phi = 4\pi G \int \rho(\mathbf{x})\, d^3\mathbf{x} = \int \nabla^2\Phi = \int d^2\mathbf{S} \cdot \nabla\Phi = 4\pi GM \tag{A.10}$$

This shows the potential gradient normal to any surface enclosing the mass is equal to the mass enclosed, times a constant.

Our interest lies in the velocities of stars in gravitational potentials. The simplest case is that of a circular orbit at fixed radius around a spherical potential $\Phi = \frac{-GM}{r}$. The force on the star mass m due to the potential gives us the centripetal acceleration, in spherical coordinates,

$$F(r) = ma(r) = m(-\nabla\Phi) = \frac{GmM}{r^2} = m\frac{v^2}{r} \tag{A.11}$$

Which gives the circular velocity in the simplest case,

$$v = \sqrt{\frac{GM}{r}} \tag{A.12}$$

and in terms of angular frequency,

$$\Omega = \frac{v}{r} = \sqrt{\frac{GM}{r^3}} \tag{A.13}$$

A.2 Plummer Globular Model

We can consider a globular cluster as a simple type of gravitational potential, the spherical potential.

Newton's two theorems will be required,

1. A body within a spherical shell of matter experiences no net gravitational force from the shell, we only need consider matter interior to the body as per the following theorem,

2. A body outside a spherical shell of matter experiences the same gravitational force as if all the matter were located at the centre of the sphere.

With these principles in mind we can look at the velocity of a star within a globular cluster modelled as a spherical mass distribution, a collisionless and non-rotating system. A model must replicate the observed properties of a globular cluster, a central density within a characteristic radius falling off rapidly to zero at some outer tidal radius. The the simplest model is that of a power law over the radius $\rho \propto r^{-\alpha}$. The Plummer model of a globular cluster (Plummer 1911) is an example of this type of model. This model was arrived at by

comparing the star counts at various radii in globular clusters with models of a spherical mass of gas in an isothermal state.

The potential of the Plummer model is, in spherical coordinates,

$$\Phi(r) = -\frac{GM}{r^2 + R_o} \tag{A.14}$$

Where R_o is the Plummer scale length, within which the potential is approximately constant where $r << R_o$. Outside the scale length then the potential will asymptote to zero as $r \to \infty$. Any number of power law models exist and may be a better approximation, but the Plummer potential model is analytical and we can evaluate quantities (Dejonghe 1987). It is often used in n-body simulations and a large body of literature exists on the subject. It is often used to model a spherical DM galaxy potential in simulations.

The purpose is to arrive at a mass estimate for the cluster. From velocity measurements of cluster members a velocity dispersion can be estimated at the centre of the cluster. The virial theorem relates the kinetic energy represented by the velocity dispersion with the potential energy. The Plummer model allows an analytic evaluation of a quantity for the potential energy. The first step towards a mass is to obtain the density distribution of the globular cluster by evaluating the Poisson equation A.9 for gravity in the Plummer potential. Spherical symmetry is assumed so only changes in radius are considered,

$$\nabla^2\Phi = \frac{1}{r^2}\frac{d}{dr}\left(r^2\frac{d\Phi}{dr}\right) = \frac{3GMR_o^2}{(r^2 + R_o^2)^{5/2}} = 4\pi G\rho \tag{A.15}$$

Which gives the density profile,

$$\rho(r) = \frac{3M}{4\pi R_o^3}\left(1 + \frac{r^2}{R_o^2}\right)^{-5/2} \tag{A.16}$$

Shells of cluster material thickness dr taken at some radius r will have mass,

$dm(r) = \rho(r) 4\pi r^2 dr$. That element of mass $dm(r)$ is considered in the potential of all the remaining mass interior to the shell.

$$E\ dr = \Phi(r)\rho(r)4\pi r^2 dr \tag{A.17}$$

Recalling Newton's theorems, the mass of the shells outside the shell under consideration can be ignored, and all mass interior to the shell can be considered as being point-like at the centre. We need to consider the sum of the energy between all the pairs of small elements of mass and the rest of the cluster across all radii. Mass elements are counted twice, as a member of either side of the pair, so the sum is divided by two,

$$E = \frac{1}{2}\int_0^\infty \Phi(r)\rho(r)4\pi r^2 dr \tag{A.18}$$

Taking the expressions for a Plummer potential $\Phi(r)$ (A.14) and density $\rho(r)$ (A.16) from above, we can express the potential energy as,

$$E = -\frac{1}{2}\int_0^\infty \frac{GM}{R_o}\left(1+\frac{r^2}{R_o^2}\right)^{-1/2} \frac{3M}{4\pi R_o^3}\left(1+\frac{r^2}{R_o^2}\right)^{-5/2} 4\pi r^2 dr \tag{A.19}$$

$$= -\frac{3}{2}\frac{GM^2}{R_o^4}\int_0^\infty \left(1+\frac{r^2}{R_o^2}\right)^{-3} r^2 dr \tag{A.20}$$

Integration by parts is required to simplify this integral into a standard form,

$$E = -\frac{3}{2}\frac{GM^2}{R_o^4}\int_0^\infty \left(1+\frac{r^2}{R_o^2}\right)^{-3} r^2 dr \tag{A.21}$$

$$= -\frac{3}{2}\frac{GM^2}{R_o^4}\left[-\frac{R_o^2}{4}\left(1+\frac{r^2}{R_o^2}\right)^{-2} r\,\Bigg|_0^\infty + \int_0^\infty \frac{R_o^2}{4}\left(1+\frac{r^2}{R_o^2}\right)^{-2} dr\right] \tag{A.22}$$

$$= -\frac{3}{8}\frac{GM^2}{R_o^2}\int_0^\infty \left(1+\frac{r^2}{R_o^2}\right)^{-2} dr \tag{A.23}$$

$$= -\frac{3}{8}GM^2R_o^2\int_0^\infty \left(R_o^2+r^2\right)^{-2} dr \tag{A.24}$$

The integrand is in a form now that the solution can be found in tables of common integrals (Kreyszig 1999),

$$E = -\frac{3}{8}GM^2R_o^2\int_0^\infty \left(R_o^2+r^2\right)^{-2} dr \tag{A.25}$$

$$= -\frac{3}{8}GM^2R_o^2\left[\frac{1}{2R_o^3}arctan\left(\frac{r}{R_o}\right)+\frac{r}{2R_o^2(r^2+R_o^2)}\right]\Bigg|_0^\infty \tag{A.26}$$

$$= -\frac{3}{8}GM^2R_o^2\left[\frac{1}{2R_o^3}\frac{\pi}{2}\right] \tag{A.27}$$

$$= -\frac{3\pi}{32}\frac{GM^2}{R_o} \tag{A.28}$$

Having evaluated the potential energy of a Plummer globular cluster, the virial theorem relates the velocities and enables an estimate for the mass of the cluster.

We used a Monte Carlo Markov Chain method to estimate a central velocity dispersion for the cluster, based on our observed velocities. The central velocity dispersion indicates the maximum kinetic energy due to the potential. In an isothermal sphere we can relate the measured velocity dispersion σ to the circular velocity of a test particle around the cluster mass, (Eqn 2.61 Binney and Tremaine 2008),

$$v_c = \sqrt{2}\sigma \tag{A.29}$$

The virial theorem tells us that the potential energy is twice the kinetic energy. Assuming the cluster approaches energy equilibrium.

$$\frac{1}{2}P.E. = \frac{3\pi}{64}\frac{GM^2}{r_0} = K.E. = \frac{1}{2}Mv_c^2 = \frac{1}{2}(\sqrt{2}\sigma)^2 \tag{A.30}$$

giving the mass as a function of the velocity dispersion,

$$M(\sigma) = \frac{64}{3\pi}\frac{\sigma^2 r_0}{G} \tag{A.31}$$

This formula is used to calculate the IC 4499 cluster mass from the measured velocity dispersion in Chapter 3.

Bibliography

J. Binney and S. Tremaine. *Galactic Dynamics: Second Edition*. Princeton University Press, 2008.

H. Dejonghe. A completely analytical family of anisotropic Plummer models. *Mon. Not. R. Astron. Soc.*, 224:13–39, January 1987.

G. T. Gillies. The Newtonian gravitational constant: recent measurements and related studies. *Reports on Progress in Physics*, 60:151–225, February 1997. doi: 10.1088/0034-4885/60/2/001.

Erwin Kreyszig. *Advanced Engineering Mathematics*. John Wiley & Sons, Inc., New York, NY, USA, 8th edition, 1999. ISBN 0471154962.

H. C. Plummer. On the problem of distribution in globular star clusters. *Mon. Not. R. Astron. Soc.*, 71:460–470, March 1911.

B

Statistical Tools

Our IC 4499 data was used to make some estimates of parameters for a physical model of the cluster. The 43 stars we selected as cluster members represented quite a small sample. We also had error estimates on the physical quantities measured which could also be incorporated into the model.

Classical estimation treats probabilities as a measure of the frequency of outcomes in a long run of events. These probabilities are considered to exist in a realm outside of human control as a true reality that could be perceived if only one could observe a very long series of data. The Bayesian view is that probability represents a degree of belief in the possible outcome of the event under consideration given what is known and what has been observed.

The randomness of estimates in classical statistics is a result of noise in the world, including systematics in the observer's world, while the true values of the parameters being estimated are fixed. Randomness in the Bayesian world lies in our knowledge of the model parameters. In Bayesian estimation one must postulate a prior distribution for a parameter, which represents a state of knowledge

or belief in its value. In our estimation of LMC disk rotation model parameters we incorporate prior knowledge of disk geometry from previous studies.

Our statistical needs included simple characterisation of the data observed with estimators like the mean and the median. Often the data distribution is approximately normal $N(\bar{\mu}, \sigma)$ and uncertainty is usually quoted in the literature as one standard deviation σ. The more complicated problem of fitting model parameters conditional on the data observed arose in relation to the velocity dispersion profile in IC 4499, and estimating a rotation model of the LMC.

Many authors use Maximum Likelihood Estimation to estimate velocity dispersion model parameters. But there are problems with this method, such as determining the binning scheme to be used on the data (Gunn and Griffin 1979), and the question of bias when errors in velocity measurement are of the same order as the cluster velocity dispersion and sample numbers are low (Pryor and Meylan 1993). To remove the bias in our case, given 43 stars and measurement errors comparable to the central cluster velocity dispersion, we needed to conduct Monte Carlo simulations based on the data.

B.1 Maximum Likelihood Estimation

A common approach is to use maximum likelihood estimation (MLE) as proposed by Pryor and Meylan (1993) to estimate the velocity dispersion model parameters for a globular cluster based on a sample of velocities. The accuracy of the estimator is dependant on the sample size. The sampled data $Y = (y_1.....y_n)$ come from a probability distribution $P(Y|\Theta)$ conditional on a set of unknown parameters $\Theta = (\theta_1....\theta n)$. Having measured Y we want to estimate Θ. The MLE gives the values of $\theta_1.....\theta_n$ which maximise the Likelihood function,

$$L(\Theta|Y) = \prod_{i=1}^{n} P(y_i|\Theta) \tag{B.1}$$

The problem is simplified by taking the log of the above equation to turn the product into a sum,

$$\ln(L(\Theta|Y)) = \sum_{i=1}^{n} \ln(P(y_i|\Theta)) \tag{B.2}$$

The log function preserves order, so the maxima occur in the same place as the Likelihood function. To find these maxima we differentiate and solve for the the roots of,

$$S(\Theta) = \frac{\partial}{\partial\Theta} \ln(L(\Theta|Y)) = 0 \tag{B.3}$$

$S(\Theta)$ is called the Score function and the set $\bar{\Theta}$ that satisfies $S(\Theta) = 0$ is the MLE. The second derivative of the Likelihood function is the Information function and measures the curvature at the maximum,

$$I(\bar{\Theta}) = -\frac{\partial^2}{\partial^2\Theta} \ln(L(\bar{\Theta}|Y)) \tag{B.4}$$

$I(\bar{\Theta})$ is greatest when the variance is smallest, when the peak in the Likelihood function is sharpest. The Information function is the inverse of the standard error (Aldrich 1997). The assumption being that the Likelihood is Normally distributed as the number of samples gets large. The criticism is that for many multivariate models, the assumption of normality is questionable, when the sample size is small, or parameters θ are correlated, or the parameters exist in bounded domains. Crucially the uncertainty in the MLE is especially susceptible. Taking a Taylor series around the Likelihood maximum to investigate the distribution at this point,

$$\ln(L(\Theta)) \approx \ln(L(\bar{\Theta})) + \frac{\partial}{\partial\Theta}\ln(L(\bar{\Theta}))(\Theta - \bar{\Theta}) + \frac{1}{2}\frac{\partial^2}{\partial^2\Theta}\ln(L(\bar{\Theta}))(\Theta - \bar{\Theta})^2 + ... \quad \text{B.5}$$

The first term is some constant, the second term is zero at the maximum, and the third term contains the Information function, B.4, so ignoring higher order terms,

$$\ln(L(\Theta)) \approx a - \frac{1}{2}I(\Theta - \bar{\Theta})(\Theta - \bar{\Theta})^2 \quad \text{B.6}$$

so that,

$$L(\Theta) \approx A\exp - \frac{(\Theta - \bar{\Theta})^2}{2(I(\Theta - \bar{\Theta})^{-1/2})^2} \quad \text{B.7}$$

which shows that the Likelihood is approximately Normally distributed $L(\Theta) \sim N(\bar{\Theta}, I(\Theta - \bar{\Theta})^{-\frac{1}{2}})$ with mean $\bar{\Theta}$ and covariance $1/\sqrt{I}$. When the Likelihood deviates from Normal, then the theory of uncertainty in the MLE becomes invalid. For small finite sample sizes Normality is not a given, especially when one starts binning the sample and assuming Normality within the bin. Bounded domains for parameters θ_i also cause the Taylor series argument to fail.

B.2 Bayesian Estimation

Bayesian estimation does not necessarily assume a Normal probability distribution. When employing MLE methods the assumption of a Normal (or Gaussian) distribution must be made (e.g. Mucciarelli et al. 2012). The Bayesian parameters themselves as well as the observed data are treated as random variables. This is in contrast to MLE where the data alone are random variables. In the case of the velocity dispersion profile for IC 4499 we have only 43 stars in

our sample, and several parameters. It was therefore decided to use a Markov Chain Monte Carlo technique to estimate the distribution of the parameters in the velocity dispersion model.

A starting point in Bayesian estimation is the adoption of a prior distribution. This represents our knowledge of the problem. This can be very general, such as: the parameter of interest is greater than zero. The prior only becomes problematic if it is too narrow, or too informative, restricting the exploration of the parameter space to too small a region Figure B.2a. A too general prior is less damaging, but can result in slow convergence to the distribution of the parameter. The non-informative prior means we encode no knowledge of the distribution of the parameter, the weakly-informative prior means we include some idea of the domain of the parameter.

Thomas Bayes' concept of inverse probability is argued for by equating the two forms for stating the conditional probability of A and B both occurring,

$$P(AB) = P(A)P(B|A) \tag{B.8}$$

$$P(AB) = P(B)P(A|B) \tag{B.9}$$

In words, the probability of observing both A and B, is the probability of A multiplied by the probability of B given A has already occurred. This is the same as the probability of B occurring multiplied by the probability of A given we already have seen B. Equation (B.9) rearranged gives,

$$P(A|B) = \frac{P(AB)}{P(B)} \tag{B.10}$$

Substitution of (B.8) for $P(AB)$ results in the statement of Bayes' Theorem,

$$P(A|B) = \frac{P(A)P(B|A)}{P(B)} \tag{B.11}$$

Bayes' Theorem was originally formulated to estimate the conditional probability of observing an event A given that another event B has already been observed, when one knows the probability of the events on the RHS of B.11 from observation and from prior knowledge. In our case we wish to estimate some parameters based on observed data. We wish to estimate the probability distribution of parameters Θ given the set of observation Y, which is called the posterior distribution,

$$P(\Theta|Y) = \frac{P(\Theta)P(Y|\Theta)}{P(Y)} \tag{B.12}$$

Where the $P(Y)$ in the denominator is a normalising factor, the sum probability of the observed data given all possible sets of parameters. This integral is hard in practice to calculate.

$$P(\Theta|Y) = \frac{P(\Theta)P(Y|\Theta)}{\int_\Theta P(Y|\Theta)P(\Theta)d\Theta} \tag{B.13}$$

The usual approach is to simulate the posterior without calculating the normalisation factor, to just find a distribution that is proportional to the posterior. The posterior parameter space is explored using a Markov Chain which steps around the distribution. The Markov property is that the probability of the next step is only conditional on the present state, and has no memory of past states. The chain can explore all the space, because any chain can communicate with any other chain. This is assured by the property that the probability of arriving at any given point, given any starting point, is greater than zero, known as the irreducibility property (Gilks et al. 1998). For exploring a stationary distribution we also require aperiodicity which for the continuous target distribution under consideration is true. It is assured the chain will converge to the target distribution π (Tierney 1996). For arbitrarily large n the the distribution of the

chain $(X_0.....X_n)$ will become closer and closer to π.

Each X is a vector of the j parameters to be estimated, $X_i = (x_0, x_1, ...x_j)$

The heart of the Markov Chain is the transition kernel which represents the probability of stepping from a point X to another point in the set of points in the target distribution, or the state space. The target distribution is the posterior distribution in our problem (B.13). The kernel should ideally be reversible, or symmetric in the sense that it has equal probability of stepping from X_n to X_{n+1} as from X_{n+1} to X_n within the target distribution. The direction of time is immaterial, the chain could equally probably have been created with the steps taken in reverse. This property guarantees the target distribution π is stationary. After many iterations the chain should explore an unbiased, large representative sample of the posterior, target distribution.

We can start an an arbitrary X_0 and the irreducibility, connected, property assures us that the chain will approach the target distribution. In practice X_0 is chosen to be close to the target distribution to avoid a prolonged time for the chain to reach the target distribution. This can be done by some exploratory short chain runs to see where the chain converges. As soon as the chain attains an X_t within the target distribution then theory guarantees that all following points in the chain will be from the target distribution (Tierney 1996).

The Metropolis Hastings method takes a proposal point from distribution $q(.|X_t)$. This distribution is chosen to roughly approximate the target distribution $\pi(X)$ so that convergence is quicker. In Bayesian inference the proposal distribution is the prior chosen based on previous knowledge. A new point is generated from the proposal distribution. The Metropolis-Hastings algorithm also introduces an acceptance algorithm to ensure reversibility.

$$\alpha(X_n, X_{n+1}) = min\left(1, \frac{\pi(X_{n+1})q(X_n|X_{n+1})}{\pi(X_n)q(X_{n+1}|X_n)}\right) \qquad \text{(B.14)}$$

If the probability of the proposed X_{n+1} conditional on the prior distribution is greater than the current X_n then X_{n+1} is accepted with probability α =1. Otherwise the probability of acceptance is low, and chain is likely to stay at X_n while a new proposal is computed. Our method employs symmetric gaussian proposals so that $q(X_n|X_{n+1}) = q(X_{n+1}|X_n)$ and we can employ the simpler Metropolis algorithm,

$$\alpha(X_n, X_{n+1}) = min\left(1, \frac{\pi(X_{n+1})}{\pi(X_n)}\right) \tag{B.15}$$

For our Metropolis algorithm we also take the log of the $\pi(X_i)$ so the ratio becomes a difference, and numerical problems with near zero probabilities are avoided. Taking the ratio of the two proposals eliminates the need to normalise.

The Gibbs sampler looks at each parameter $x_i \in X$ whilst holding all other parameters $x_{-i} \in X$ constant. The Gibbs sampler accepts all proposals with probability $\alpha = 1$. The Gibbs sampler then samples from the complete conditional distribution.

Theory assures us that given infinitely many iterations the sampler will converge to the target distribution. In practice a finite set of samples is taken, for modern computers this can be a large number. There still remain a number of practical considerations given the finiteness of the sample. The burn in period is the number of steps taken for the sampler to converge to the stationary distribution. After the burn in period the chain will be independent of the starting point chosen. The burn in points are taken out of the sample. From here the sampler is left to mix and provide a sample of the posterior. The length of the burn in period is dependent on the complexity of the problem, specifically the number of parameters. It also depends on the distance between the target distribution and the starting point, a large distance may require some number of iterations for the sampler to find the stationary distribution. The chain

can be autocorrelated and a significant lag time will reveal any patterns. The length of the chain divided by the lag time will give the number of completely independent samples.

Slow mixing means nearby points are correlated to some degree. If successive samples are not moving easily then their current location depends strongly on recent locations in the sample space. Thinning is a technique to reduce this dependence. Only a subset of the sample is selected with every m^{th} point being chosen, the gap $(m-1)$between points in the chain being sufficient to ensure the points are independent.

Multiple chains, with different starting points can be run and the samples combined to ensure a better representation of the target distribution. This eliminates any dependence on the starting position. This can be desirable by averaging out chains that get "stuck" somewhere in an odd corner of the target distribution space, or which fail to find modes of multi-modal distributions.

The Metropolis-Hastings sampler requires a proposal distribution be chosen. The proposal can have two extreme effects. If the proposal is too limiting the proposed steps are small, most steps are accepted and the mixing is slow, and the chain fails to converge rapidly to the target distribution Figure B.2a. If the proposal is too broad then large steps are taken into low probability regions and the proposed step will not be accepted. Non-acceptance results in slow mixing as the chain fails to move often. A good prior indicates the location of the target distribution, and most proposals are in the vicinity of the target Figure B.1a. The Metropolis-Hastings algorithm can have problems with target distributions that are curved (Gilks et al. 1998).

The Gibbs sampler is good at sampling odd shaped distributions as all proposals are accepted , but fails to explore multi-modal distributions completely. These problems occur in a minority of posterior distributions. The Normal dis-

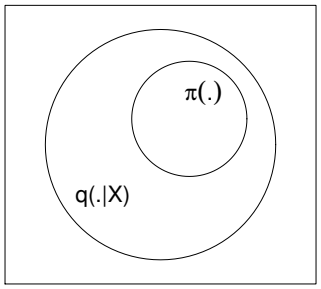

(a)

Figure B.1: Prior $q(.|X)$ is general enough to include target distribution $\pi(.)$ and helps define location. Prior not too broad so proposals have high probability of acceptance.

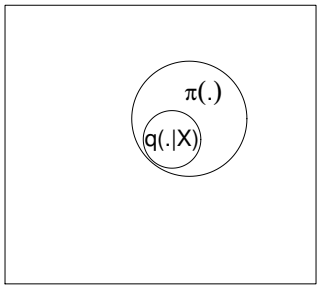

(a)

Figure B.2: Prior too narrow and restrictive, proposals are nearly always accepted, but fails to propose moves to some regions of $\pi(.)$ and chain will not converge to target distribution.

tribution density on a logarithmic scale (log-normal) is concave for example. However exploratory exploration of the posterior and tuning of the proposal are common practice to avoid problems associated with odd shaped and multi-modal posterior distributions.

We choose the Bayesian estimation technique in the problem of estimating the velocity dispersion profile in the globular cluster IC 4499. We have a small sample size of 43 from which to estimate a multidimensional model, where the different parameters may have unique probability densities. Some of the parameters are on bounded domains. The radius from the cluster centre is always positive for example.

Within the sample scheme we adopt a weakly informative prior that assumes the measured velocities are distributed as Normal. The Gibbs sampler is used to find the mean while the other parameters are held constant. At each iteration we then employ the Metropolis algorithm to sample the full conditional distribution of the other parameters. The other parameters may display correlations and have unusual distributions. The use of the Cholesky decomposition of the correlation matrix of the parameters to control the step size, tends to remove the effects of correlations between parameters (Gilks et al. 1998). This sophisticated Metropolis within Gibbs scheme is the work of Dr. Simon Wotherspoon. Most computer packages use the Gibbs sampler alone. Once we have a sample from the target distribution, we use classical statistics to describe the resulting parameter distributions, using measures like median, mean, and quantiles.

B.3 MCMC Algorithm

The following script in the R programming language is used to generate a representative sample from the posterior distribution of model parameters. The techniques outlined above are employed here and we describe the implementa-

tion with reference to the following code.

The first ten lines define the Plummer velocity dispersion model and parameters, $R.mu$ the mean characteristic radius of the Plummer model, $R.sd$ the dispersion of R. The central velocity dispersion is K in the code. The model is conditional on measured astrophysical quantities, r the radius from the cluster centre, v the measured velocity and se the estimated error in measurement. The sampler parameters are also defined, the number of iterations, $n.iters$ and the thinning gap to reduce correlation $n.thins$.

The Gibbs sampler samples for mu the mean velocity from the full conditional distribution given the data and errors observed. The Metropolis sampler used adds a random size step to the current $p = [K, R]$ vector to generate a proposal, then compares the ratio of the probabilities of the proposed and current p to another random number and accepts or rejects the proposed move.

R code IC 4499 velocity dispersion, Metropolis within Gibbs sampler

```
mcmc.glob <- function(r,v,se,
                      R.mu,R.sd,
                      start,V,
                      n.iters,n.thin) {
  ## Log posterior (up to additive const)
  log.posterior <- function(mu,p) {
    ## p = (K,R)
    s <- sqrt(p[1]^2/sqrt(1+(r/p[2])^2)+se^2)
    sum(dnorm(v,mu,s,log=T))+dnorm(p[2],R.mu,R.sd,log=T)
  }
  ## Initialize
  p <- start
  L <- chol(V)
  ch <- matrix(0,n.iters,3)
  colnames(ch) <- c("mu","K","R")
  for(k1 in 1:n.iters) {
    for(k2 in 1:n.thin) {
      ## Gibbs sample for mu
      tau <- 1/(p[1]^2/sqrt(1+(r/p[2])^2)+se^2)
      S1 <- sum(tau)
      S2 <- sum(tau*v)
      mu <- rnorm(1,S2/S1,1/sqrt(S1))
      ## Metropolis sample for p=(K,R)
      p1 <- p+rnorm(2)%*%L
      if(all(p1>0)) {
        logp <- log.posterior(mu,p)
        logp1 <- log.posterior(mu,p1)
        if(logp1 - logp > log(runif(1))) {
          p <- p1
        }
      }
    }
    ch[k1,] <- c(mu,p)
  }
  ch
}
d <- read.table("velocity.data",header=T)
## Fit initial model
V <- diag(c(0.1,0.0001)^2)
fit <- mcmc.glob(d$radius,d$velocity,d$error,
                 R.mu=0.030,R.sd=0.005,
                 start=c(3,0.025),V=V,
                 n.iters=1000,n.thin=10)
## Tune proposal
for(i in 1:3) {
  V <- var(fit[,2:3])/3
  fit <- mcmc.glob(d$radius,d$velocity,d$error,
                   R.mu=0.030,R.sd=0.005,
                   start=c(3,0.025),V=V,
                   n.iters=5000,n.thin=10)
  w <- i+1
  f <- paste("plot",w,sep="")
  ff <- paste(f,".png")
  png(file=ff)
  plot(as.ts(fit))
  dev.off()
}
## Final sample
V <- var(fit[,2:3])/3
fit <- mcmc.glob(d$radius,d$velocity,d$error,
                 R.mu=0.030,R.sd=0.005,
                 start=c(3,0.025),V=V,
                 n.iters=20000,n.thin=10)
```

The MCMC algorithm is adapted to the higher dimensional problem of a rotation curve and disk geometry parameters for the LMC. Once again we use Metropolis within Gibbs, this time to circumvent causal circularity, incorporate errors and return robust error estimates. The systemic velocity depends on having a model, and the model is conditioned on disk velocities, which are calculated using the systemic velocity. The details of the transformation are in Chapter 4 and based on the work of van der Marel et al. (2002).

Gibbs sampling for the systemic velocity conditional on the data and errors while holding other all parameters constant we can then take this value as constant in the next sampler. We then Metropolis sample a six dimensional full joint conditional distribution of disk model parameters conditional on the transformed velocities. The inclination angle is just randomly selected at each iteration from a normal distribution to make it a " fuzzy" fixed parameter. The scheme is numerically cumbersome and slow requiring a re-transformation of every sample member velocity with the updated parameters at each iteration. This reflects the circular nature of the causal dependencies. While not elegant, it does work.

Adapted R code LMC disk rotation model, Metropolis within Gibbs sampler

```
mcmc.glob <- function(vel, se, vra, vdec,
                      Vo.mu, Vo.sd, mu.mu, mu.sd, Ro.mu, Ro.sd,
                      lon.mu, lon.sd, ra.mu, ra.sd, dec.mu, dec.sd,
                       start,V,
                       n.iters, n.thin) {
  log.posterior <- function(vsys,p) {
    ## p = ( mu, Ro, Vo, lon , ra, dec)
      vlos <- vel-vsys*cos(r)-tranv*sin(r)*cos(phi-trana)
      g <- abs(F*sin(incl)*cos(adiff))
  ###  disk velocity
      vd <- vlos/g
      sum(dnorm(vd,VR,se,log=T))+dnorm(p[1],mu.mu,mu.sd,log=T)+dnorm(p[2],Vo.
          mu,Vo.sd,log=T)+dnorm(p[3],Ro.mu,Ro.sd,log=T)+dnorm(p[4],lon.mu,
          lon.sd,log=T)+dnorm(p[5],ra.mu,ra.sd,log=T)+dnorm(p[6],dec.mu,dec.
          sd,log=T)
  }
  ## Initialize constants
   ## piatek'08
  radians <- 2*pi/360.0
  tranv <- 490.0  ### km/s
  trana <- 77.5*radians
  i.mu=35*radians
  i.sd=2*radians
  d0 <- 50.1
  Ddidt <- 0
  ###  start proposal
   p <- start
    L <- chol(V)
  ch <- matrix(0,n.iters,8)
  colnames(ch) <- c("Systemic velocity", "Rot.curve parameter", "Vmax", "Disk
       Scale", "LON", "RA","Dec","Inclination")
    for(k1 in 1:n.iters) {
    #### random sample for inclination on third iteration
    if (k1 %% 3 != 0){
      incl <- rnorm(1,i.mu,i.sd)
    }
    for(k2 in 1:n.thin) {
        ## Gibbs sample for vsys
        y <- cos(abs(-pi/2-p[6]))*cos(abs(-pi/2-vdec))+sin(abs(-pi/2-p[6]))*
            sin(abs(-pi/2-vdec))*(cos(p[5]-vra))
```

```
36          r <- acos(y)
37        cosphi<-seq(length(vdec))
38        phi<-seq(length(vdec))
39            for ( i in 1:length(vdec)) {
40          cosphi[i] <- -cos(vdec[i])*sin(vra[i]-p[5])/sin(r[i])
41
42          gamma2 <- cos(abs(-pi/2-(-pi/2-p[6])))*cos(abs(-pi/2-vdec[i]))+sin(
                abs(-pi/2-(-pi/2-p[6])))*sin(abs(-pi/2-vdec[i]))*cos((pi+p[5])-
                vra[i])
43        poldist2 <- acos(gamma2)
44
45        if ((poldist2-pi/2) < 0.0){
46          phi[i] <- -acos(cosphi[i])-pi/2
47          } else
48          {phi[i] <- acos(cosphi[i])-pi/2
49        }
50      }
51            adiff <- phi-p[4]
52          fnum <- cos(incl)*cos(r)-sin(incl)*sin(r)*sin(adiff)
53        fdenom <- sqrt(cos(incl)**2*cos(adiff)**2+sin(adiff)**2)
54        F <- fnum/fdenom
55        R <- d0*sin(r)/F
56    VR <- p[2]*(R**p[1])/(R**p[1]+p[3])
57         vsys <- (1/cos(r))*(vel-tranv*sin(r)*cos(phi-trana)-Ddidt*sin(r)*sin(
                adiff)+F*VR*sin(incl)*cos(adiff) )
58             tau <- 1/se
59          S1 <- sum(tau)
60          S2 <- sum(tau*vsys)
61    vsys <- rnorm(1,S2/S1,1/sqrt(S1))
62            ## Metropolis sample for p = ( mu, Ro, Vo, lon , ra, dec)
63            p1 <- p+(1*rnorm(6))%*%L
64      if(all(p1[1:4]>0.5)) {
65          logp <- log.posterior(vsys,p)
66          logp1 <- log.posterior(vsys,p1)
67          if(logp1 - logp > log(runif(1))) {
68                     p <- p1
69          }
70        }
71      }
72      ch[k1,] <- c(vsys,p,incl)
73    }
74    ch
75  }
76  d <- read.table("data.txt",header=T)
77  ## Initial sample for tuning
78  V <- diag(c(0.2, 1.0, 1.0,0.2,0.01,0.01)^2)
79  fit <- mcmc.glob(d$vel,d$verr,d$ra,d$dec,
80                   Vo.mu=80,Vo.sd=10, mu.mu=2.0, mu.sd=1.0, Ro.mu=2.0,Ro.sd
                        =2.0,
81       lon.mu=2.269,lon.sd=0.175,ra.mu=1.44, ra.sd=0.005, dec.mu=-1.22, dec.sd
             =0.005,
82                   start=c(2.0, 60.0, 2.0,2.27,1.44,-1.22),V=V,
83                   n.iters=1000,n.thin=2)
84  ## Final sample
85  V <- var(fit[,2:7])/5
86  fit <- mcmc.glob(d$vel,d$verr,d$ra,d$dec,
87                   Vo.mu=80,Vo.sd=10, mu.mu=2.0, mu.sd=1.0, Ro.mu=2.0,Ro.sd
                        =2.0,
88      lon.mu=2.269,lon.sd=0.175, ra.mu=1.44, ra.sd=0.005, dec.mu=-1.22, dec.sd
             =0.005,
89                   start=c(2.0, 60.0, 2.0,2.27,1.44,-1.22),V=V,
90                   n.iters=10000,n.thin=2)
```

Bibliography

John Aldrich. R. A. Fisher and the Making of Maximum Likelihood 1912-1922. *Statistical Science*, 12(3):162–176, November 1997.

W. R. Gilks, S. Richardson, and D. J. Spiegelhalter. *Markov Chain Monte Carlo in Practice*. Chapman and Hall, Boca Raton, Florida, 1998.

J E Gunn and R F Griffin. Dynamical studies of globular clusters based on photoelectric radial velocities of individual stars. I - M3. *Astronomical Journal*, 84:752–773, June 1979.

A Mucciarelli, M Bellazzini, R Ibata, T Merle, S C Chapman, E Dalessandro, and A Sollima. News from the Galactic suburbia: the chemical composition of the remote globular cluster NGC 2419. *Monthly Notices of the Royal Astronomical Society*, 426(4):2889–2900, November 2012.

C Pryor and G Meylan. Velocity Dispersions for Galactic Globular Clusters. In *Structure and Dynamics of Globular Clusters. Proceedings of a Workshop held in Berkeley*, page 357, January 1993.

Luke Tierney. Introduction to general state-space markov chain theory. *Markov chain Monte Carlo in practice*, pages 59–74, 1996.

Roeland P. van der Marel, David R Alves, Eduardo Hardy, and Nicholas B Suntzeff. New Understanding of Large Magellanic Cloud Structure, Dynamics, and Orbit from Carbon Star Kinematics. *The Astronomical Journal*, 124 (5):2639–2663, November 2002. Published in: Astron.J.124:2639-2663,2002 57 pages, LaTeX, with 11 PostScript figures. Submitted to the Astronomical Journal.

C

Programming

C.1 Programming tasks and tools

Data reduction was carried out using the AAOmega *2dfdr* reduction pipeline. This software is largely automatic, once the observer has set the correct parameters for the sky subtraction scheme. Setting up of the observation fields for the *2df* fibre positioner was accomplished using the AAT *configure* software . The observer supplies a list of candidate stars to *configure* which uses simulated annealing algorithms to arrange the fibres in a way the robot can place them from the inside out without fouling (Miszalski et al. 2006). It importantly samples from the list of candidate stars without bias. A list of tracking stars was also required, preferably in the periphery of the field and within a fixed magnitude range to keep the field position while tracking. These lists were generated by filtering the 2MASS catalogue based on position and magnitude, using *R* statistical software to select, (Venables and Smith 2004). Python scripts were used to output the lists in the correct syntax for the fibre positioner *configure* software.

Spectra were plotted and analysed using the PyRAF application protocol interface to IRAF tasks. The IRAF scripting language was initially used for batch tasks, but is less user friendly than the Python language. Python scripting of batch IRAF tasks was used for such tasks as editing AAOmega FITS headers, and creating new headers for tasks, including coordinate conversion from sexagesimal hours, minutes and degrees to decimal radian measures of angular distances on the sky. This was required to calculate angles and distances from the centre of the galaxy or cluster to transform to IC 4499 spherical or LMC disk coordinates. A Python script was written to calculate an LMC disk rotation model by reading in the Line of Sight (LOS) velocity data, transforming positions to an LMC disk frame, fitting a circular rotation velocity model to the disk velocities and then translating the model into a map of the projected LOS velocities on the sky. Python scripts were used to read in online catalogues and data from other studies, then cross match them with our data as required.

The Aladin sky atlas was also used to positionally cross match online catalogues and images with local data (Bonnarel et al. 2000). The Aladin atlas has access to online astronomical resources at Simbad and VizieR which include all-sky surveys such as GLIMPSE, IRAS, 2MASS and DSS. The Aladin sky

atlas allows catalogue objects to be plotted over archival images. We used this feature to plot UK Schmidt DSS red images, then add contours and 2MASS catalogue objects, to find low brightness regions to place sky subtraction fibres within the crowded LMC inner bar fields.

Some small sections of the spectra were missing due to dead areas on the CCD, these appeared as zero counts and looked like square absorption lines, see Figure: C.1. The bias frames must have had the same fault and didn't correct this in the reduction process. The artificial lines would have affected velocity cross correlations with template spectra, and may have exaggerated equivalent width measurements. These zero regions appeared at different wavelengths for different apertures due to the dispersion solution, so setting a fixed wavelength region mask was not feasible. A Python script was written to find the zero values, then estimate an average value of the spectral continuum for a small range of pixels either side of the zero region and interpolate the continuum across the spurious line feature. No real absorption features had zero flux, so the algorithm didn't apply to real features, see Figure: C.2. Where the zero region appeared inside a strong Ca II line profile of interest, the algorithm successfully recovered the shape of the profile, Figures: C.3 C.4. The script was written to offer interactive user input to check that the algorithm was performing as expected, then once the parameters were tuned the script was allowed to run as an automated task.

R statistical programming language was used for exploratory data analysis, to perform statistical tasks on the data, as well as to generate most plots. The Python MATLAB-like matplotlib library was used to generate the colour plot of the LMC line of sight velocity field, Figure 4.42 in Chapter 4. Monte Carlo Markov Chain simulation algorithm for the velocity dispersion model of IC 4499 were coded in *R*, with much assistance from Dr. Simon Wotherspoon B.3. The simulations of model parameters fro the LMC disk rotation model was an adaption of Dr. Wotherspoon's scheme to a larger and higher dimensional problem B.3.

Acknowledgements

PyRAF is a product of the Space Telescope Science Institute, which is operated by AURA for NASA. IRAF is written and supported by the National Optical Astronomy Observatories (NOAO).

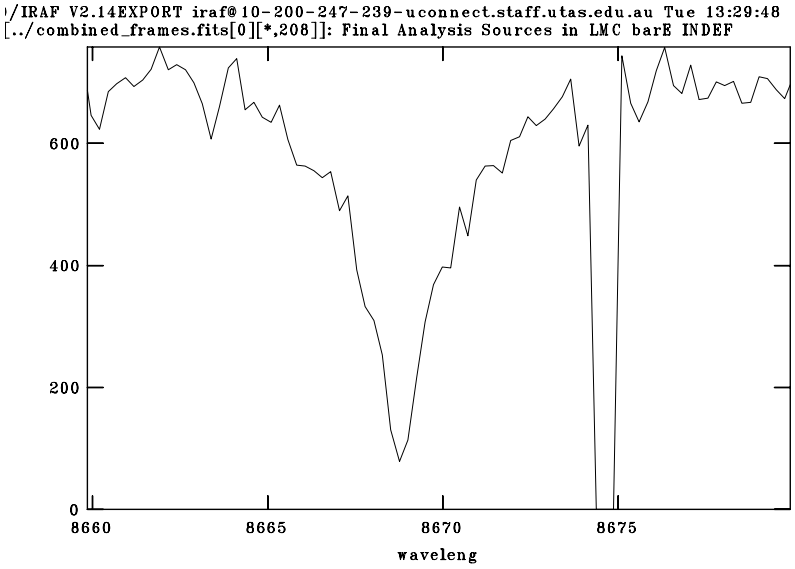

Figure C.1: Spectrum from LMC East field showing CCD zero readout looks like a strong line near wing of 8662$\mathring{A}$ Ca II line.

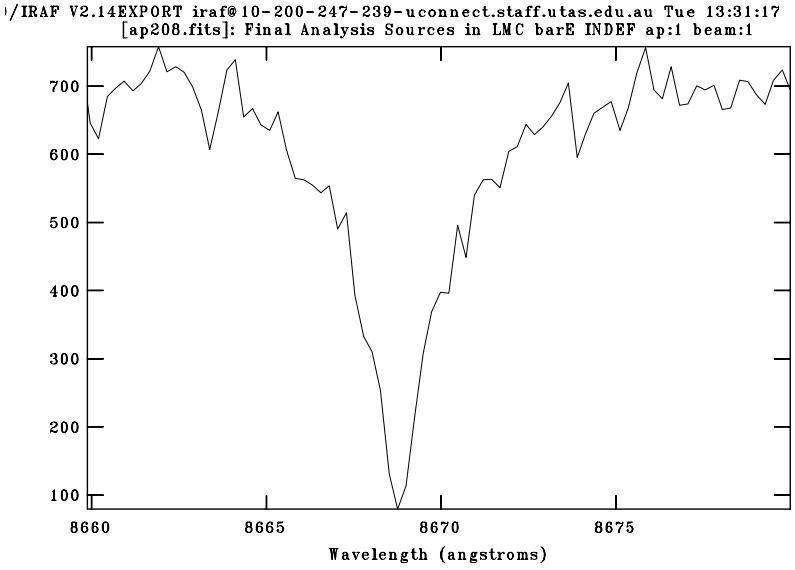

Figure C.2: Spectrum after interpolation algorithm applied

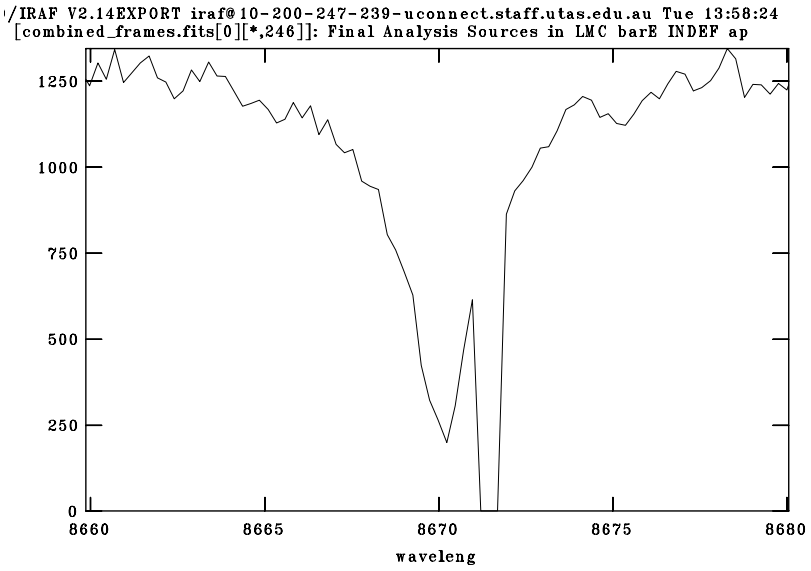

Figure C.3: Spectrum from LMC East field showing CCD zero readout within (redshifted) 8662$\mathring{A}$ Ca II line.

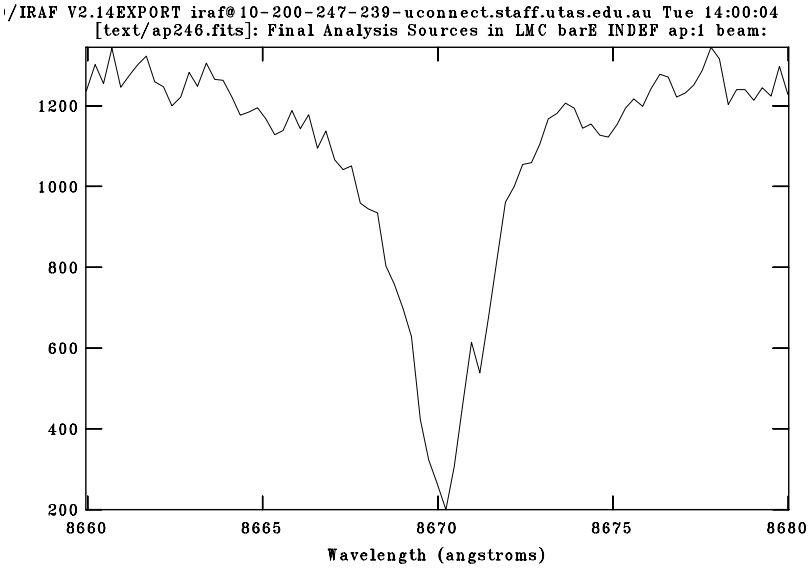

Figure C.4: Spectrum of 8662$\mathring{A}$ Ca II line after interpolation algorithm applied.

Bibliography

F. Bonnarel, P. Fernique, O. Bienaymé, D. Egret, F. Genova, M. Louys, F. Ochsenbein, M. Wenger, and J. G. Bartlett. The ALADIN interactive sky atlas. A reference tool for identification of astronomical sources. *Astron. Astrophys. Suppl. Ser.*, 143:33–40, April 2000. doi: 10.1051/aas:2000331.

B. Miszalski, K. Shortridge, W. Saunders, Q. A. Parker, and S. M. Croom. Multi-object spectroscopy field configuration by simulated annealing. *Mon. Not. R. Astron. Soc.*, 371:1537–1549, October 2006. doi: 10.1111/j.1365-2966.2006.10777.x.

W. N. Venables and D. M. Smith. *An Introduction to R*, 2004.

D
Calibration

D.1 Ca II Triplet Metallicities From NIR Magnitudes (Andrew A. Cole)

Warren was concerned that his metallicity values for the 240 RGB stars in his bar sample of 585 were coming out slightly higher than previous values. To me it looked more or less within the systematics of the calibration but I decided it would be worth checking on one possible systematic while Warren worked on finalising the kinematics chapter.

Dueling Wavelengths

The Ca II triplet equivalent width is not a pure metallicity indicator since the lines are very sensitive to pressure broadening and slightly sensitive to temperature (Jørgensen et al. 1992; Cenarro et al. 2001; Diaz et al. 1989). Because the RGB at a given [Fe/H] makes a single locus in the HR diagram, a single photometric measurement is enough to almost completely remove the temperature and surface gravity dependences. Multiple approaches are in the literature.

Previous work on the LMC bar (Cole et al. 2005) followed a customary approach in using $(V-V_{RC})$ to remove the $\log g$ and $T_{\rm eff}$ effects. Da Costa and Hatzidimitriou (1998) showed how this could be applicable to star clusters of a range of ages and Cole et al. (2004) showed that it was possible to apply the method even for field populations (i.e., a mixture of age and metallicity).

Warren and Cole (2009) pioneered using the K_S band magnitudes for cluster studies based on the wide availability of 2MASS data, and Hankey and Cole (2011) confirmed this approach. However it had not yet been verified for a mixture of populations.

Aims

To see if the metallicity results depend on the bandpass of the photometric calibrator, and account for any discrepancies.

Method

I matched each star to a star in the Magellanic Clouds Photometric Survey catalog (Zaritsky et al. 2004). This gives UBVI magnitudes for all our stars that have JHK magnitudes. Note that 24 out of 669 stars had no match within $1''$; 2 out of 669 stars had double matches, but in both cases the second match was 2–3 mag fainter and obviously not the spectroscopic target.

The median position offset between MCPS and 2MASS positions was $0''.28$. Many stars didn't have any U magnitudes, which is unfortunate from an SED modeling perspective. The BVIJHK mags are in a file called *mcpsmatch_clean.pos*.

Now I can assume the V_{RC} of the bar = 19.22 $\pm$0.12, following Cole et al. (2005), and use the calibration from Cole et al. (2004): [Fe/H] = -2.966 +0.362 (ΣW +0.73ΔV). Only stars for which Warren derived a metallicity, bounded by the region from $0.9 \leq$ V$-$I ≤ 2 and I >14.5, were used. The metallicities derived using the Cole et al. (2004) calibration and the Warren and Cole (2009) calibration were compared.

Results

Converting to a V-band corrector for the equivalent widths does not change the results for the mean metallicity or peak of the distribution:

$$[M/H]^{K}_{WC9} = -0.32 \pm 0.33$$

$$[M/H]^{V}_{C04} = -0.33 \pm 0.28$$

This shows that for the dominant population it makes little difference what photometric corrector is used in deriving the metallicity.

However, a significant trend with metallicity is observed. A linear least-squares fit to the data gives:

$$[M/H]_{C04} = 1.199[M/H]_{WC9} + 0.075 \quad \text{(D.1)}$$

with a reduced $\chi^2 = 1.5$, with $\sigma = 0.06$ for 204 stars. This relation shows that at the metal rich end the two are nearly equal, but for metallicities below [Fe/H] ≈ -0.4 the near infrared based metallicities are systematically lower than the metallicities derived using V magnitudes. The equivalence point between the two methods is found to lie at [Fe/H] = -0.377. The fit is shown in Figure D.1.

This shows every sign of being related to a calibration effect. Because the K-band and V-band magnitudes give identical results in star clusters, we can remain confident that the AAOmega equivalent widths are compatible with the results from other telescopes. Therefore the offset may be due to differences in the way that simple stellar populations combine in a complex system like the LMC.

The solution is related to the discussion in §5 of Cole et al. (2004), in which variations in $V-V_{HB}$ are shown to account for $\lesssim$0.1 mag of difference in the derived metallicity of composite populations. The situation is exaggerated in the K-band because clump/HB stars get *fainter* with decreasing metallicity, the opposite of the behaviour in the V-band. In the V-band, age and metallicity effects nearly cancel out, while in K-band they reinforce each other (provided the metallicity increases with time).

The effect is demonstrated clearly in Grocholski and Sarajedini (2002) where it is shown that the K-band magnitude of the clump decreases by $\gtrsim$0.8 mag over the range $-0.5 \geq$ [Fe/H] ≥ -1.3. This is additional to an 0.3 mag decrease over the range 4–12 Gyr (at constant metallicity).

The red clump population of the LMC bar is dominated by the intermediate-age, metal-rich component. Therefore any population-related calibration offsets due to population admixtures will be negligible for the dominant population. This is observed (V and K band samples agree). If we then follow Salaris and Girardi (2002) and Grocholski and Sarajedini (2002) in estimating the change in K-band magnitude of the red clump between a dominant population at [M/H] $= -0.4$ and a minority old population at [M/H] $= -1.3$, we estimate $\approx$1 mag of K band shift. The metallicity calibration of Warren and Cole (2009) then leads us to the result that the K-band gravity estimator has led us to overestimate the RGB metallicities by 0.1 dex at -1, and by 0.2 dex at -1.5. This shift is of the magnitude and sense observed.

Conclusions

The K-band stellar parameter corrector for Ca II triplet metallicity estimates can be more sensitive to age and metallicity mixtures than using the V-band corrector. The size and sense of the resulting systematic errors depends on the mixture of populations, but for the LMC bar results in the overestimate of metallicities in the metal-poor end.

The characteristic metallicity of the dominant population is not affected by this systematic, and we do not find a significant offset between the V-corrected metallicities and the K-corrected metallicities for the LMC RGB stars in our sample. The bar really is just a bit more metal-rich than the disk.

This issue must be re-examined when dealing with the large sample of SMC stars in a forthcoming paper.

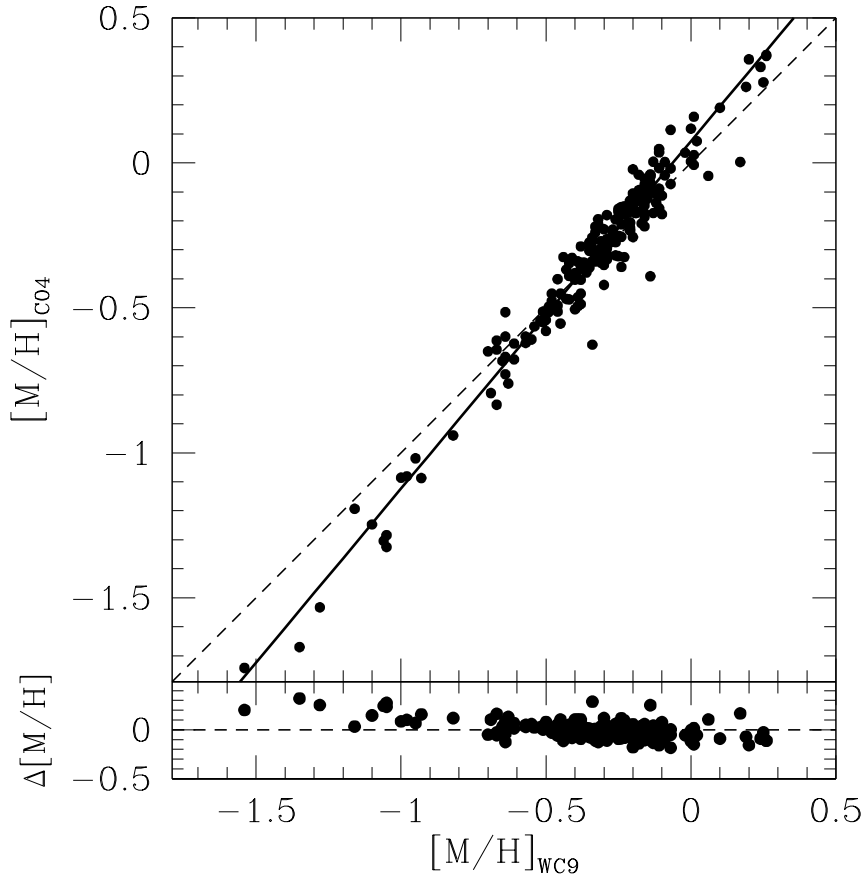

Figure D.1: Comparison of the metallicities derived using two different bandpasses for the photometric stellar parameter corrector. WC9 = 2MASS K_S band Warren and Cole (2009); C04 = MCPS I band Cole et al. (2004). The dashed line shows the line of equality; the solid line in the upper figure shows the linear relation described by Eq. D.1.

Bibliography

A J Cenarro, J Gorgas, N Cardiel, S Pedraz, R F Peletier, and A Vazdekis. Empirical calibration of the near-infrared Ca ii triplet - II. The stellar atmospheric parameters. *Monthly Notices of the Royal Astronomical Society*, 326 (3):981–994, September 2001.

A A Cole, T A Smecker-Hane, E Tolstoy, T L Bosler, and J S Gallagher. The effects of age on red giant metallicities derived from the near-infrared CaII triplet. *Monthly Notices of the Royal Astronomical Society*, 347:367, 2004.

Andrew A Cole, Eline Tolstoy, John S Gallagher, and Tammy A Smecker-Hane. Spectroscopy of Red Giants in the Large Magellanic Cloud Bar: Abundances, Kinematics, and the Age-Metallicity Relation. *The Astronomical Journal*, 129:1465, March 2005.

G S Da Costa and D Hatzidimitriou. Ca II Triplet Spectroscopy of Giants in Small Magellanic Cloud Star Clusters: Abundances, Velocities, and the Age-Metallicity Relation. *The Astronomical Journal*, 115(5):1934–1945, May 1998.

Angeles I Diaz, Elena Terlevich, and Roberto Terlevich. Near-IR features in late type stars - Their relation with stellar atmosphere parameters. *Monthly Notices of the Royal Astronomical Society (ISSN 0035-8711)*, 239:325–345, July 1989.

Aaron J Grocholski and Ata Sarajedini. WIYN Open Cluster Study. X. The K-Band Magnitude of the Red Clump as a Distance Indicator. *The Astronomical Journal*, 123(3):1603–1612, March 2002.

W. J. Hankey and A. A. Cole. Radial velocity and metallicity of the globular cluster IC4499 obtained with AAOmega. *Mon. Not. R. Astron. Soc.*, 411: 1536–1546, March 2011. doi: 10.1111/j.1365-2966.2010.17788.x.

U. G. Jørgensen, M Carlsson, and H R Johnson. The Calcium Infrared Triplet Lines in Stellar Spectra. *Astronomy and Astrophysics*, 254:258, February 1992.

Maurizio Salaris and Léo Girardi. Population effects on the red giant clump absolute magnitude: the K band. *Monthly Notice of the Royal Astronomical Society*, 337:332, November 2002.

Steven R Warren and Andrew A Cole. Metallicities and radial velocities of five open clusters including a new candidate member of the Monoceros stream. *Monthly Notices of the Royal Astronomical Society*, 393(1):272–296, February 2009.

Dennis Zaritsky, Jason Harris, Ian B Thompson, and Eva K Grebel. The Magellanic Clouds Photometric Survey: The Large Magellanic Cloud Stellar Catalog and Extinction Map. *The Astronomical Journal*, 128(4):1606–1614, October 2004.

E

LMC data tables

Table E.1: Full sample of LMC stars.

ID[a]	α(J2000)[a]	δ(J2000)[a]	HRV	error	K_s^a	H[a]	J[a]	ΣEW (Å)	error	W' (Å)	[Fe/H](dex)[b]
05130841-6846473	05:13:08.410	-68:46:47.30	263.1	6.27	12.2	13.25	12.44	10.234	0.686546	8.122	-0.05974
05184812-6846112	05:18:48.120	-68:46:11.20	295.38	6.7	10.98	12.08	11.22	10.743	0.543308	8.0454	-0.085018
05191689-6846401	05:19:16.890	-68:46:40.10	239.73	5.8	12.54	13.67	12.79	9.198	0.949537	7.2492	-0.347764
05173364-6847312	05:17:33.640	-68:47:31.20	269.47	5.77	11.86	12.97	12.13	9.67	0.725276	7.3948	-0.299716
05163709-6848478	05:16:37.090	-68:48:47.80	290.08	6.5	11.62	12.48	11.79	10.638	0.575338	8.2476	-0.018292
05154448-6847195	05:15:44.480	-68:47:19.50	267.24	5.34	12.89	14	13.16	9.489	0.827307	7.7082	-0.196294
05194618-6851123	05:19:46.180	-68:51:12.30	229.62	5.8	12	13.07	12.23	8.698	0.590096	6.49	-0.5983
05204604-6852314	05:20:46.040	-68:52:31.40	226.33	5.39	11.55	12.73	11.85	9.139	0.652877	6.715	-0.52405
05180062-6851244	05:18:00.620	-68:51:24.40	271.03	5.63	11.55	12.67	11.83	10.158	0.555688	7.734	-0.18778
05173989-6851357	05:17:39.890	-68:51:35.70	279.58	6.69	12.44	13.48	12.67	8.341	0.881019	6.3442	-0.646414
05171071-6854420	05:17:10.710	-68:54:42.00	271.34	6.75	11.79	12.94	12.05	9.436	0.937297	7.1272	-0.388024
05164608-6852073	05:16:46.080	-68:52:07.30	253.08	6.22	11.95	12.99	12.18	10.155	0.794191	7.923	-0.12541
05181430-6854070	05:18:14.300	-68:54:07.00	273.83	5.97	11.88	12.72	12.05	10.216	0.615767	7.9504	-0.116368
05122856-6848328	05:12:28.560	-68:48:32.80	262.83	11.53	11.23	12.44	11.57				
05152564-6848257	05:15:25.640	-68:48:25.70	288	5.97	12.12	13.2	12.37	7.43	0.72269	5.2796	-0.997732
05191143-6857233	05:19:11.430	-68:57:23.30	265.17	6.28	12.15	13.2	12.38	9.409	1.196808	7.273	-0.33991
05164080-6854282	05:16:40.800	-68:54:28.20	255.48	6.98	11.45	12.67	11.75	7.765	0.902262	5.293	-0.99331
05182028-6858224	05:18:20.280	-68:58:22.40	253.5	7.1	11.92	12.85	12.13	9.767	0.607456	7.5206	-0.258202
05201809-6902132	05:20:18.090	-69:02:13.20	258	6.65	12.02	13.01	12.23	10.252	0.961832	8.0536	-0.082312
05190058-6900441	05:19:00.580	-69:00:44.10	304.75	10.37	12.65	13.67	12.88	9.575	1.358728	7.679	-0.20593

[0] [a]From 2MASS point source catalogue; [b] (Caretta & Gratton, 1997)

Table E.1: Full sample of LMC stars, continued

ID[a]	α(J2000)[a]	δ(J2000)[a]	HRV	error	K_s^a	H[a]	J[a]	ΣEW (Å)	error	W' (Å)	[Fe/H](dex)[b]
05181441-6900338	05:18:14.410	-69:00:33.80	265.47	5.05	11.55	12.77	11.89	7.933	0.757077	5.509	-0.92203
05183469-6901508	05:18:34.690	-69:01:50.80	271.7	5.16	11.98	12.86	12.18	10.072	0.678013	7.8544	-0.148048
05152355-6856240	05:15:23.550	-68:56:24.00	260.63	4.97	12.92	13.99	13.17	10.109	0.890328	8.3426	0.013058
05185566-6905085	05:18:55.660	-69:05:08.50	231.71	6.91	12.95	13.9	13.13	9.574	1.25497	7.822	-0.15874
05170509-6901505	05:17:05.090	-69:01:50.50	246.01	5.53	12.74	13.82	12.97	9.017	0.948507	7.1642	-0.375814
05185419-6907060	05:18:54.190	-69:07:06.00	279.03	7.8	12.87	13.91	13.08	8.712	1.566765	6.9216	-0.455872
05192260-6909501	05:19:22.600	-69:09:50.10	253.01	7.38	12.91	13.94	13.11				
05151586-6859580	05:15:15.860	-68:59:58.00	289.42	5.89	11.95	12.78	12.14	9.629	0.485413	7.397	-0.29899
05170095-6905378	05:17:00.950	-69:05:37.80	251.89	5.62	12.74	13.74	12.94	9.045	0.861028	7.1922	-0.366574
05163108-6905326	05:16:31.080	-69:05:32.60	242.03	5.95	11.91	12.96	12.15	9.788	0.70871	7.5368	-0.252856
05162041-6905451	05:16:20.410	-69:05:45.10	301.6	6.32	12.88	13.87	13.07	9.259	0.818101	7.4734	-0.273778
05162939-6906535	05:16:29.390	-69:06:53.50	262.66	5.05	12.99	13.95	13.17	8.296	0.844567	6.5632	-0.574144
05165384-6908477	05:16:53.840	-69:08:47.70	306.7	6.6	12.25	13.34	12.5	9.657	0.638822	7.569	-0.24223
05164083-6908554	05:16:40.830	-69:08:55.40	264.47	5.95	12.58	13.68	12.83	8.402	0.881232	6.4724	-0.604108
05184797-6918245	05:18:47.970	-69:18:24.50	258.34	6.34	12.05	13.19	12.36	8.106	0.715287	5.922	-0.78574
05152710-6906055	05:15:27.100	-69:06:05.50	242.1	5.08	12.83	13.88	13.06	9.646	0.801048	7.8364	-0.153988
05163658-6911537	05:16:36.580	-69:11:53.70	266.18	6.51	11.76	12.63	11.93	10.215	0.603447	7.8918	-0.135706
05181649-6919375	05:18:16.490	-69:19:37.50	265.22	5.96	11.19	12.39	11.51				
05162759-6913252	05:16:27.590	-69:13:25.20	258.17	5.28	12.68	13.62	12.87	7.155	0.651418	5.2734	-0.999778
05172745-6918285	05:17:27.450	-69:18:28.50	274.26	6.78	11.01	11.99	11.25	10.788	0.522788	8.1048	-0.065416
05125726-6900062	05:12:57.260	-69:00:06.20	245.05	5.95	12.38	13.47	12.63	9.371	0.861456	7.3454	-0.316018

Table E.1: Full sample of LMC stars, continued

ID[a]	α(J2000)[a]	δ(J2000)[a]	HRV	error	K_s^a	H[a]	J[a]	ΣEW (Å)	error	W' (Å)	[Fe/H](dex)[b]
05175248-6922077	05:17:52.480	-69:22:07.70	298.43	7.49	10.85	12.05	11.2				
05164886-6919030	05:16:48.860	-69:19:03.00	230.22	5.29	12.66	13.73	12.9	9.723	1.027219	7.8318	-0.155506
05132117-6902418	05:13:21.170	-69:02:41.80	279.34	5.01	12.94	13.96	13.2	9.027	0.771534	7.2702	-0.340834
05172680-6925236	05:17:26.800	-69:25:23.60	233.71	5.72	12.34	13.37	12.57	9.869	1.075638	7.8242	-0.158014
05155789-6917465	05:15:57.890	-69:17:46.50	260.51	5.96	11.44	12.44	11.67	10.378	0.576262	7.9012	-0.132604
05113930-6854082	05:11:39.300	-68:54:08.20	236.04	5.95	12.63	13.69	12.87	9.687	0.876111	7.7814	-0.172138
05171302-6928087	05:17:13.020	-69:28:08.70	280.44	6.52	12.4	13.47	12.63	9.201	0.732092	7.185	-0.36895
05164612-6927537	05:16:46.120	-69:27:53.70	282.83	6.99	10.91	12.1	11.26	7.67	0.650721	4.9388	-1.110196
05164288-6929076	05:16:42.880	-69:29:07.60	271.36	7.37	12.32	13.39	12.57	9.392	0.841029	7.3376	-0.318592
05152010-6921179	05:15:20.100	-69:21:17.90	245.52	5.9	12.37	13.42	12.61	8.612	1.102797	6.5816	-0.568072
05151444-6923228	05:15:14.440	-69:23:22.80	238.37	6.41	11.42	12.71	11.78				
05133320-6912076	05:13:33.200	-69:12:07.60	233.05	6.42	12.86	13.86	13.08	9.184	0.851526	7.3888	-0.301696
05150415-6925558	05:15:04.150	-69:25:55.80	253.92	6.77	11.76	12.92	12.05	8.946	0.793192	6.6228	-0.554476
05155625-6933249	05:15:56.250	-69:33:24.90	237.79	5.19	12.75	13.48	12.88	10.213	0.745045	8.365	0.02045
05135032-6918407	05:13:50.320	-69:18:40.70	262.67	4.72	11.89	13.04	12.18	8.921	0.679743	6.6602	-0.542134
05111929-6853255	05:11:19.290	-68:53:25.50	269.11	5.03	11.35	12.5	11.67	6.861	0.637848	4.341	-1.30747
05123001-6910363	05:12:30.010	-69:10:36.30	256.4	5.49	12.18	13.28	12.45	9.449	0.695539	7.3274	-0.321958
05123267-6908197	05:12:32.670	-69:08:19.70	252.11	6.97	12.52	13.69	12.82	9.131	0.847359	7.1726	-0.373042
05140940-6925589	05:14:09.400	-69:25:58.90	280.88	6.36	11.19	12.42	11.55				
05140149-6927394	05:14:01.490	-69:27:39.40	283.63	12.35	11.26	12.42	11.6				
05131745-6921279	05:13:17.450	-69:21:27.90	245.56	6.25	11.46	12.34	11.66	10.064	0.791278	7.5968	-0.233056

Table E.1: Full sample of LMC stars, continued

ID[a]	α(J2000)[a]	δ(J2000)[a]	HRV	error	K_s^a	H[a]	J[a]	ΣEW (Å)	error	W' (Å)	[Fe/H](dex)[b]
05133124-6925175	05:13:31.240	-69:25:17.50	266.26	12.52	11.75	12.96	12.1				
05142479-6937220	05:14:24.790	-69:37:22.00	285.35	5.82	12.18	13.25	12.43	8.179	0.778576	6.0574	-0.741058
05122007-6911577	05:12:20.070	-69:11:57.70	265.13	6.3	11.91	12.97	12.15	10.024	0.737161	7.7728	-0.174976
05133601-6932169	05:13:36.010	-69:32:16.90	250.82	5.39	11.87	12.94	12.12	9.591	0.750291	7.3206	-0.324202
05124072-6924403	05:12:40.720	-69:24:40.30	234.39	5.36	12.07	13.27	12.38	9.31	0.635917	7.1356	-0.385252
05132847-6941413	05:13:28.470	-69:41:41.30	269.57	8.69	12.9	13.92	13.09	8.236	1.380473	6.46	-0.6082
05122283-6924416	05:12:22.830	-69:24:41.60	235.95	5.14	11.89	13	12.15	7.74	0.822268	5.4792	-0.931864
05130355-6940587	05:13:03.550	-69:40:58.70	210.7	6.95	12.75	13.92	13.02				
05123608-6935319	05:12:36.080	-69:35:31.90	243.73	5.13	12.87	13.99	13.12	8.5	1.267509	6.7096	-0.525832
05123453-6937385	05:12:34.530	-69:37:38.50	257.01	4.91	12.01	13.29	12.32				
05122010-6934425	05:12:20.100	-69:34:42.50	299	7.5	12.97	14.01	13.18	9.122	1.019775	7.3796	-0.304732
05111981-6911084	05:11:19.810	-69:11:08.40	236.27	5.83	12.57	13.65	12.81	9.818	0.763451	7.8836	-0.138412
05113527-6924343	05:11:35.270	-69:24:34.30	214.53	5.95	12.42	13.49	12.66	9.477	0.660747	7.4706	-0.274702
05115450-6935137	05:11:54.500	-69:35:13.70	244.61	5.87	12.27	13.32	12.51	9.8	0.712256	7.7216	-0.191872
05114391-6936022	05:11:43.910	-69:36:02.20	265.66	5.61	11.57	12.77	11.88	7.493	0.806803	5.0786	-1.064062
05110824-6913018	05:11:08.240	-69:13:01.80	258.44	6.49	12.57	13.62	12.79	9.194	0.801517	7.2596	-0.344332
05111757-6934201	05:11:17.570	-69:34:20.10	279.39	5.44	11.91	13.1	12.2	7.455	0.87826	5.2038	-1.022746
05105596-6931560	05:10:55.960	-69:31:56.00	205.91	4.44	12.33	13.29	12.52	9.042	0.55984	6.9924	-0.432508
05101974-6902019	05:10:19.740	-69:02:01.90	255.02	5.69	11.23	12.26	11.48	10.957	0.727646	8.3794	0.025202
05101654-6912423	05:10:16.540	-69:12:42.30	293.46	5.03	12.85	13.71	13.02	6.237	0.661463	4.437	-1.27579
05103441-6908526	05:10:34.410	-69:08:52.60	280.89	6	11.16	12.37	11.46				

Table E.1: Full sample of LMC stars, continued

ID[a]	α(J2000)[a]	δ(J2000)[a]	HRV	error	K_s^a	H[a]	J[a]	ΣEW (Å)	error	W' (Å)	[Fe/H](dex)[b]
05110123-6911408	05:11:01.230	-69:11:40.80	320.79	6.26	12.78	13.78	12.99	8.614	1.187742	6.7804	-0.502468
05101010-6933418	05:10:10.100	-69:33:41.80	218.9	5.05	12.29	13.35	12.5	8.69	0.934343	6.6212	-0.555004
05095886-6920027	05:09:58.860	-69:20:02.70	257.63	9.03	11.05	12.29	11.4				
05094248-6919421	05:09:42.480	-69:19:42.10	288.22	5.12	11.84	12.95	12.11	8.223	0.650723	5.9382	-0.780394
05093112-6942144	05:09:31.120	-69:42:14.40	271.2	5.99	12.48	13.53	12.72	9.958	0.941281	7.9804	-0.106468
05093079-6913345	05:09:30.790	-69:13:34.50	235.12	6.15	12.95	13.83	13.1	6.828	0.921231	5.076	-1.06492
05094288-6907308	05:09:42.880	-69:07:30.80	285.86	6.65	12.6	13.68	12.82	9.251	1.017415	7.331	-0.32077
05085689-6943355	05:08:56.890	-69:43:35.50	263.54	7.37	12.73	13.76	12.95	9.741	1.111834	7.8834	-0.138478
05084699-6944133	05:08:46.990	-69:44:13.30	259.31	7.72	12.52	13.55	12.73	9.036	1.27716	7.0776	-0.404392
05090430-6927002	05:09:04.300	-69:27:00.20	283.51	5.86	12.8	13.78	13.01	9.34	0.915046	7.516	-0.25972
05090541-6918379	05:09:05.410	-69:18:37.90	260.05	5.74	11.95	13.03	12.19	9.716	0.883921	7.484	-0.27028
05084917-6919170	05:08:49.170	-69:19:17.00	282.4	7.66	12.72	13.74	12.94	10.175	1.311871	8.3126	0.003158
05091374-6912111	05:09:13.740	-69:12:11.10	222.4	5.07	10.66	11.73	10.91	10.578	0.590503	7.7268	-0.190156
05082542-6930518	05:08:25.420	-69:30:51.80	282.74	7.25	12.11	13.21	12.35	9.218	0.97585	7.0628	-0.409276
05082242-6929064	05:08:22.420	-69:29:06.40	244.6	9.5	12.52	13.58	12.79	7.304	1.23905	5.3456	-0.975952
05080663-6929210	05:08:06.630	-69:29:21.00	256.67	7.63	12.72	13.75	12.92				
05084267-6908459	05:08:42.670	-69:08:45.90	306.59	7.99	12.81	13.78	13.01	9.639	0.978817	7.8198	-0.159466
05091420-6902216	05:09:14.200	-69:02:21.60	275.99	5.57	11.81	12.71	12.04	10.173	0.505063	7.8738	-0.141646
05071517-6931202	05:07:15.170	-69:31:20.20	273.88	6.02	11.4	12.52	11.67	9.175	0.813337	6.679	-0.53593
05071111-6927588	05:07:11.110	-69:27:58.80	276.58	7.71	11.72	12.87	11.97	8.485	0.983966	6.1426	-0.712942
05065307-6930278	05:06:53.070	-69:30:27.80	257.86	8.71	12.82	13.84	13.03	9.654	1.457836	7.8396	-0.152932

Table E.1: Full sample of LMC stars, continued

ID[a]	α(J2000)[a]	δ(J2000)[a]	HRV	error	K_s^a	H[a]	J[a]	ΣEW (Å)	error	W' (Å)	[Fe/H](dex)[b]
05063821-6931349	05:06:38.210	-69:31:34.90	248.71	6.67	11.45	12.6	11.74	7.775	0.717514	5.303	-0.99001
05063533-6929549	05:06:35.330	-69:29:54.90	269.98	7.42	12.16	13.27	12.42	8.501	1.181547	6.3698	-0.637966
05081418-6858276	05:08:14.180	-68:58:27.60	248.15	9.02	12.93	13.99	13.18	9.038	1.426529	7.2764	-0.338788
05093582-6852464	05:09:35.820	-68:52:46.40	262.71	5.56	12.9	13.69	13.06				
05083851-6902242	05:08:38.510	-69:02:24.20	268.24	5.43	12.71	13.89	13	9.961	1.420372	8.0938	-0.069046
05061360-6927236	05:06:13.600	-69:27:23.60	243.6	7.21	12.8	13.8	13.02				
05083584-6901286	05:08:35.840	-69:01:28.60	218.05	6.19	11.41	12.67	11.77				
05085797-6848212	05:08:57.970	-68:48:21.20	255.92	6.37	12.48	13.5	12.73				
05074940-6907279	05:07:49.400	-69:07:27.90	260.17	7.26	11.88	13.02	12.16	9.22	0.928445	6.9544	-0.445048
05073172-6911192	05:07:31.720	-69:11:19.20	259.08	5.65	11.93	13.01	12.18	9.532	0.849629	7.2904	-0.334168
05050889-6929429	05:05:08.890	-69:29:42.90	265.08	10.18	12.87	13.83	13.06	8.723	1.154848	6.9326	-0.452242
05045937-6928096	05:04:59.370	-69:28:09.60	248.02	16.28	12.77	13.75	12.95				
05035462-6934188	05:03:54.620	-69:34:18.80	205.92	18.05	12.82	13.87	13.05				
05084514-6853463	05:08:45.140	-68:53:46.30	271.75	5.71	11.99	13.05	12.2	9.389	0.779275	7.1762	-0.371854
05030363-6931392	05:03:03.630	-69:31:39.20	260.34	15.64	12.88	13.86	13.06				
05024783-6930493	05:02:47.830	-69:30:49.30	242.31	6.01	11.91	13	12.17				
05051174-6914078	05:05:11.740	-69:14:07.80	255.31	12.7	12.95	13.88	13.12				
05054990-6908211	05:05:49.900	-69:08:21.10	267.21	9.94	11.88	12.59	12.04	9.553	1.044173	7.2874	-0.335158
05065500-6906239	05:06:55.000	-69:06:23.90	235.35	6.89	12.34	13.48	12.61				
05022821-6927479	05:02:28.210	-69:27:47.90	248.74	16.48	12.61	13.63	12.81				
05081789-6853299	05:08:17.890	-68:53:29.90	304.97	9.06	12.18	13.39	12.48				

Table E.1: Full sample of LMC stars, continued

ID[a]	α(J2000)[a]	δ(J2000)[a]	HRV	error	K_s^a	H[a]	J[a]	ΣEW (Å)	error	W' (Å)	[Fe/H](dex)[b]
05044595-6912229	05:04:45.950	-69:12:22.90	279.17	7.55	11.96	13.03	12.18				
05055267-6906203	05:05:52.670	-69:06:20.30	245.05	6.05	11.46	12.56	11.71				
05064492-6900261	05:06:44.920	-69:00:26.10	292.3	6.23	11.4	12.53	11.68	7.775	1.34973	5.279	-0.99793
05042925-6910555	05:04:29.250	-69:10:55.50	242.4	9.36	11.33	12.53	11.62				
05045998-6908090	05:04:59.980	-69:08:09.00	253.06	7.72	11.64	12.69	11.88				
05065156-6859017	05:06:51.560	-68:59:01.70	247.29	8.23	12.6	13.67	12.82	9.713	1.233271	7.793	-0.16831
05080878-6853074	05:08:08.780	-68:53:07.40	234.61	5.56	12.99	14.01	13.19				
05091023-6841416	05:09:10.230	-68:41:41.60	225.97	6.29	12.67	13.72	12.9	9.696	1.386317	7.8096	-0.162832
05043198-6905264	05:04:31.980	-69:05:26.40	287.8	13.75	12.39	13.5	12.66				
05040985-6905416	05:04:09.850	-69:05:41.60	283.1	14.1	11.37	12.52	11.68				
05052973-6900268	05:05:29.730	-69:00:26.80	249.57	6.79	11.38	12.5	11.65				
05082958-6847382	05:08:29.580	-68:47:38.20	247.84	8.65	12.24	13.37	12.5	8.142	1.366179	6.0492	-0.743764
05072760-6852097	05:07:27.600	-68:52:09.70	304.43	6.22	11.6	12.75	11.9	7.675	1.005921	5.275	-0.99925
05022178-6907060	05:02:21.780	-69:07:06.00	247.74	18.91	12.24	13.29	12.46				
05004421-6910552	05:00:44.210	-69:10:55.20	258.21	11.15	11.29	12.2	11.49				
05025918-6904328	05:02:59.180	-69:04:32.80	269.17	10.18	11.47	12.56	11.73				
05052114-6857314	05:05:21.140	-68:57:31.40	274.14	15.91	12.93	13.94	13.15				
05035160-6859394	05:03:51.600	-68:59:39.40	261.28	7.87	11.8	12.76	11.99				
05035273-6858409	05:03:52.730	-68:58:40.90	260.58	9.45	11.78	12.67	11.98				
05053290-6853528	05:05:32.900	-68:53:52.80	273.76	8.76	11.94	12.79	12.08	10.394	1.35292	8.1572	-0.048124
04594519-6904261	04:59:45.190	-69:04:26.10	228.12	18.96	11.49	12.69	11.8				

Table E.1: Full sample of LMC stars, continued

ID[a]	α(J2000)[a]	δ(J2000)[a]	HRV	error	K_s^a	H[a]	J[a]	ΣEW (Å)	error	W' (Å)	[Fe/H](dex)[b]
05054504-6852142	05:05:45.040	-68:52:14.20	252.44	6.07	11.19	12.16	11.39	10.531	1.017016	7.9342	-0.121714
05055962-6851070	05:05:59.620	-68:51:07.00	259.87	9.95	12.67	13.62	12.84				
05084826-6845291	05:08:48.260	-68:45:29.10	249.63	5.37	12.39	13.2	12.54	8.141	0.623675	6.1202	-0.720334
05033086-6852015	05:03:30.860	-68:52:01.50	261.35	13.33	12.58	13.64	12.83				
05053230-6847494	05:05:32.300	-68:47:49.40	283.7	9.53	11.78	12.83	12.01				
05051353-6849304	05:05:13.530	-68:49:30.40	242.56	6.61	11.62	12.47	11.78	10.534	1.139056	8.1436	-0.052612
05034508-6852382	05:03:45.080	-68:52:38.20	260.84	8.25	11.38	12.3	11.57				
05041302-6848304	05:04:13.020	-68:48:30.40	247.99	10.7	11.81	12.9	12.08				
05081440-6844553	05:08:14.400	-68:44:55.30	291	10.33	11.99	13	12.29				
05045786-6845032	05:04:57.860	-68:45:03.20	268.84	15.21	12.26	13.33	12.47				
05012252-6843238	05:01:22.520	-68:43:23.80	221.4	16.31	11.17	12.31	11.51				
05004204-6842182	05:00:42.040	-68:42:18.20	216.5	19.23	12.91	13.91	13.12				
05055588-6844161	05:05:55.880	-68:44:16.10	255.41	9.12	11.35	12.47	11.62	9.194	1.495308	6.674	-0.53758
05095268-6848195	05:09:52.680	-68:48:19.50	288.9	6.86	11.21	12.49	11.6				
05064987-6843175	05:06:49.870	-68:43:17.50	239.58	6.22	11.98	12.83	12.16	9.326	0.995306	7.1084	-0.394228
05031746-6837510	05:03:17.460	-68:37:51.00	258.95	17.43	11.78	12.78	11.97				
05072538-6841026	05:07:25.380	-68:41:02.60	262.27	12.35	12.66	13.69	12.87				
05065699-6839356	05:06:56.990	-68:39:35.60	267.83	13.58	11.02	12.17	11.31				
05075271-6842382	05:07:52.710	-68:42:38.20	240.28	7.04	11.48	12.53	11.73	10.304	0.775564	7.8464	-0.150688
05092039-6845541	05:09:20.390	-68:45:54.10	272.28	9.33	11.43	12.61	11.77				
05033921-6831516	05:03:39.210	-68:31:51.60	260.51	12.44	12.16	12.99	12.35				

Table E.1: Full sample of LMC stars, continued

ID[a]	α(J2000)[a]	δ(J2000)[a]	HRV	error	K_s^a	H[a]	J[a]	ΣEW (Å)	error	W' (Å)	[Fe/H](dex)[b]
05075621-6840506	05:07:56.210	-68:40:50.60	251.55	8.18	11.92	13.04	12.21	8.908	1.278972	6.6616	-0.541672
05020885-6821478	05:02:08.850	-68:21:47.80	244.48	14.12	12.92	13.94	13.16				
05054591-6832330	05:05:45.910	-68:32:33.00	268.16	13.64	11.45	12.64	11.8				
05063254-6832017	05:06:32.540	-68:32:01.70	257.65	7.86	12.63	13.71	12.88				
05081280-6841027	05:08:12.800	-68:41:02.70	312.87	6.49	12.36	13.21	12.58				
05070146-6833080	05:07:01.460	-68:33:08.00	249.57	7.32	11.72	12.84	12.01				
05060984-6831277	05:06:09.840	-68:31:27.70	251.29	19.85	12.87	13.85	13.07				
05035397-6820034	05:03:53.970	-68:20:03.40	235.57	12.72	11.03	12.23	11.38				
05070262-6837275	05:07:02.620	-68:37:27.50	276.49	13.86	12.21	13.31	12.45				
05051102-6822597	05:05:11.020	-68:22:59.70	280.99	14.76	12.56	13.52	12.78				
05073683-6832484	05:07:36.830	-68:32:48.40	260.07	13.76	11.08	12.36	11.47				
05064376-6825049	05:06:43.760	-68:25:04.90	297.78	8.98	11.72	12.84	11.98				
05062821-6824558	05:06:28.210	-68:24:55.80	233.38	10.92	12.29	13.37	12.54				
05045744-6814025	05:04:57.440	-68:14:02.50	257.55	6.26	11.91	12.95	12.17	9.108	1.140215	6.8568	-0.477256
05072133-6834057	05:07:21.330	-68:34:05.70	248.49	6.63	12.16	13.05	12.36				
05091928-6839413	05:09:19.280	-68:39:41.30	261.96	8.29	12.42	13.6	12.69				
05090546-6840245	05:09:05.460	-68:40:24.50	241.45	8.05	12.93	13.99	13.14				
05071841-6824050	05:07:18.410	-68:24:05.00	254.04	13.3	12.18	13.3	12.44				
05081752-6836269	05:08:17.520	-68:36:26.90	258.38	8.62	12.57	13.53	12.77				
05073183-6831243	05:07:31.830	-68:31:24.30	264.93	6.75	11.51	12.73	11.88	8.759	0.805668	6.3158	-0.655786
05070537-6815099	05:07:05.370	-68:15:09.90	236.15	14.83	11.41	12.62	11.76				

Table E.1: Full sample of LMC stars, continued

ID[a]	α(J2000)[a]	δ(J2000)[a]	HRV	error	K_s^a	H[a]	J[a]	ΣEW (Å)	error	W' (Å)	[Fe/H](dex)[b]
05064605-6806361	05:06:46.050	-68:06:36.10	275.63	13.68	11.05	12.24	11.38				
05055929-6813039	05:05:59.290	-68:13:03.90	272.6	11.65	12.24	13.06	12.43				
05085590-6834063	05:08:55.900	-68:34:06.30	249.93	6.04	12.34	13.18	12.55				
05081857-6827340	05:08:18.570	-68:27:34.00	263.93	7.42	11.92	12.85	12.11				
05102894-6824448	05:10:28.940	-68:24:44.80	217.83	7.21	12.5	13.64	12.77				
05083741-6816263	05:08:37.410	-68:16:26.30	240.01	11.04	11.47	12.74	11.85				
05073522-6811526	05:07:35.220	-68:11:52.60	276.28	12.79	11.88	12.76	12.06				
05084575-6824370	05:08:45.750	-68:24:37.00	285.99	15.49	12.5	13.59	12.72				
05083745-6825316	05:08:37.450	-68:25:31.60	261.21	11.23	12.98	14.01	13.21				
05082794-6817590	05:08:27.940	-68:17:59.00	276.49	9.73	11.71	12.86	12				
05082029-6809352	05:08:20.290	-68:09:35.20	290.51	9.75	11.34	12.19	11.55				
05074484-6835495	05:07:44.840	-68:35:49.50	250.28	7.14	12.09	12.92	12.27				
05091121-6750559	05:09:11.210	-67:50:55.90	268.38	18.86	12.66	13.69	12.9	10.946	2.251802	9.0548	0.248084
05120735-6840334	05:12:07.350	-68:40:33.40	279.71	6.91	11.91	13	12.17	10.418	0.563722	8.1668	-0.044956
05114488-6835541	05:11:44.880	-68:35:54.10	248.81	7.31	12.15	13.27	12.46				
05094055-6807105	05:09:40.550	-68:07:10.50	270.83	11.03	12.35	13.4	12.6				
05111427-6827492	05:11:14.270	-68:27:49.20	246.24	5.52	11.63	12.72	11.92				
05102869-6821467	05:10:28.690	-68:21:46.70	275.81	6.71	11.12	12.23	11.41	9.634	0.925005	7.0036	-0.428812
05085163-6818371	05:08:51.630	-68:18:37.10	247.08	10.54	12.31	13.44	12.56				
05091131-6826535	05:09:11.310	-68:26:53.50	262.78	6.3	12.79	13.64	12.95				
05094079-6833146	05:09:40.790	-68:33:14.60	239.16	8.27	11.96	13.11	12.32	6.948	1.304623	4.7208	-1.182136

Table E.1: Full sample of LMC stars, continued

ID[a]	α(J2000)[a]	δ(J2000)[a]	HRV	error	K_s^a	H[a]	J[a]	ΣEW (Å)	error	W' (Å)	[Fe/H](dex)[b]
05112388-6810449	05:11:23.880	-68:10:44.90	232.42	12.98	11.93	13.06	12.22				
05124491-6752258	05:12:44.910	-67:52:25.80	278.18	15.89	11.9	12.94	12.11				
05125047-6756352	05:12:50.470	-67:56:35.20	302.16	12.2	12.1	13.16	12.35				
05130388-6758226	05:13:03.880	-67:58:22.60	290.78	9.5	11.2	12.33	11.5				
05123415-6807278	05:12:34.150	-68:07:27.80	287.2	15.55	10.9	12.06	11.23				
05130613-6803243	05:13:06.130	-68:03:24.30	244.7	8.14	12.08	13.19	12.36				
05120087-6815256	05:12:00.870	-68:15:25.60	245.23	8.2	12.41	13.43	12.65				
05124005-6833398	05:12:40.050	-68:33:39.80	264.54	5.66	12.84	13.84	13.03	9.906	0.861893	8.1012	-0.066604
05143395-6801313	05:14:33.950	-68:01:31.30	233.3	10.57	12.1	13.18	12.32	9.867	1.356772	7.707	-0.19669
05130690-6823327	05:13:06.900	-68:23:32.70	238.74	7.56	12.83	13.88	13.09	9.743	1.055438	7.9334	-0.121978
05092034-6833309	05:09:20.340	-68:33:30.90	269.76	18.81	10.89	12.26	11.39				
05134988-6827420	05:13:49.880	-68:27:42.00	268.33	6.53	12.16	13.28	12.43	9.904	0.812068	7.7728	-0.174976
05125519-6818080	05:12:55.190	-68:18:08.00	304.7	7.41	12.34	13.42	12.57	10.419	1.221799	8.3742	0.023486
05121562-6825467	05:12:15.620	-68:25:46.70	231.44	6	12.39	13.42	12.59				
05141150-6810109	05:14:11.500	-68:10:10.90	244.51	11.87	11.03	12.18	11.35				
05123354-6824250	05:12:33.540	-68:24:25.00	257.89	6.94	12.67	13.74	12.93	10.79	1.504712	8.9036	0.198188
05161512-6758043	05:16:15.120	-67:58:04.30	284.89	11.87	11.88	13.25	12.25				
05154889-6803412	05:15:48.890	-68:03:41.20	270.25	12.98	12.31	13.52	12.61				
05155364-6808315	05:15:53.640	-68:08:31.50	249.62	10.06	12.44	13.57	12.73				
05162372-6801040	05:16:23.720	-68:01:04.00	231.78	8.54	12.67	13.72	12.89				
05140043-6816492	05:14:00.430	-68:16:49.20	243.91	7.74	12.11	13.2	12.35	10.413	1.131682	8.2578	-0.014926

Table E.1: Full sample of LMC stars, continued

ID[a]	α(J2000)[a]	δ(J2000)[a]	HRV	error	K_s^a	H[a]	J[a]	ΣEW (Å)	error	W' (Å)	[Fe/H](dex)[b]
05103188-6844083	05:10:31.880	-68:44:08.30	269.83	6.34	11.7	12.8	12				
05165632-6806185	05:16:56.320	-68:06:18.50	291.7	6.46	11.71	12.83	11.99	9.056	1.200759	6.7088	-0.526096
05143461-6820542	05:14:34.610	-68:20:54.20	279.85	5.95	11.54	12.68	11.82	7.931	0.708132	5.5022	-0.924274
05135456-6836274	05:13:54.560	-68:36:27.40	218.25	4.25	12.68	13.48	12.83	5.521	0.760785	3.6394	-1.538998
05123674-6827430	05:12:36.740	-68:27:43.00	262.42	6.93	12.72	13.76	12.94	10.945	1.178907	9.0826	0.257258
05161049-6814255	05:16:10.490	-68:14:25.50	247.07	8.17	12.48	13.54	12.69	11.016	1.45583	9.0384	0.242672
05122679-6831121	05:12:26.790	-68:31:12.10	213.39	5.62	12.57	13.62	12.8	8.383	1.10404	6.4486	-0.611962
05175092-6812069	05:17:50.920	-68:12:06.90	280.32	11.86	11.92	13.03	12.19	8.146	1.416622	5.8996	-0.793132
05115574-6831431	05:11:55.740	-68:31:43.10	244.95	6.64	12.91	13.74	13.1	10.577	1.102177	8.8058	0.165914
05184401-6810219	05:18:44.010	-68:10:21.90	310.37	7.5	11.97	13.06	12.23	10.983	1.118414	8.7606	0.150998
05145696-6833306	05:14:56.960	-68:33:30.60	289.93	8.37	11.36	12.52	11.68				
05130118-6837560	05:13:01.180	-68:37:56.00	271.41	6.14	10.96	12.04	11.21	9.775	0.585223	7.0678	-0.407626
05174884-6815134	05:17:48.840	-68:15:13.40	266.1	7.6	12.49	13.48	12.7	9.328	1.320202	7.3552	-0.312784
05174720-6818426	05:17:47.200	-68:18:42.60	262.1	6.86	11.98	13.15	12.28				
05141630-6829147	05:14:16.300	-68:29:14.70	260.24	7.69	12.97	13.99	13.22	9.99	0.852466	8.2476	-0.018292
05163838-6827370	05:16:38.380	-68:27:37.00	271.54	5.6	12.76	13.69	12.94	7.34	0.83992	5.4968	-0.926056
05123193-6846199	05:12:31.930	-68:46:19.90	276.97	6.86	12.11	13.09	12.31	9.844	0.713127	7.6888	-0.202696
05141141-6840440	05:14:11.410	-68:40:44.00	263.38	5.64	10.93	12.08	11.21	9.156	0.597573	6.4344	-0.616648
05161179-6832151	05:16:11.790	-68:32:15.10	255.14	6.58	12.93	13.95	13.12	10.368	0.992077	8.6064	0.100112
05103287-6840321	05:10:32.870	-68:40:32.10	303.68	5.73	11.42	12.57	11.71	7.196	0.596436	4.7096	-1.185832
05161743-6829366	05:16:17.430	-68:29:36.60	280.76	7.23	12.6	13.66	12.84	9.46	0.961292	7.54	-0.2518

Table E.1: Full sample of LMC stars, continued

ID[a]	α(J2000)[a]	δ(J2000)[a]	HRV	error	K_s^a	H[a]	J[a]	ΣEW (Å)	error	W' (Å)	[Fe/H](dex)[b]
05142162-6835299	05:14:21.620	-68:35:29.90	285.55	6.1	12.11	13.07	12.34	9.898	0.633301	7.7428	-0.184876
05155077-6835164	05:15:50.770	-68:35:16.40	245.92	6.08	11.86	12.99	12.12	8.656	0.585951	6.3808	-0.634336
05184760-6825086	05:18:47.600	-68:25:08.60	274.13	6.97	12.65	13.68	12.91	10.787	1.224746	8.891	0.19403
05153593-6837293	05:15:35.930	-68:37:29.30	193.79	5.15	11.87	12.97	12.13	9.018	0.526562	6.7476	-0.513292
05142358-6845149	05:14:23.580	-68:45:14.90	230.8	5.87	12.37	13.46	12.6	9.144	0.713051	7.1136	-0.392512
05183143-6828123	05:18:31.430	-68:28:12.30	314.81	6.92	12.03	13.16	12.31	8.817	0.653958	6.6234	-0.554278
05193190-6826427	05:19:31.900	-68:26:42.70	284.79	7	11.82	12.94	12.15				
05121289-6852357	05:12:12.890	-68:52:35.70	319.21	7.5	12.28	13.36	12.53	9.898	1.016723	7.8244	-0.157948
05184484-6831271	05:18:44.840	-68:31:27.10	235.91	5.14	11.54	12.71	11.86	9.01	0.766356	6.5812	-0.568204
05145858-6834574	05:14:58.580	-68:34:57.40	313.82	6.6	12.77	13.78	12.97	8.495	0.85375	6.6566	-0.543322
05194361-6833311	05:19:43.610	-68:33:31.10	281.7	7.53	11.79	12.97	12.07	8.73	0.841062	6.4212	-0.621004
05170738-6842110	05:17:07.380	-68:42:11.00	275.79	13.15	10.88	12.19	11.3				
05133927-6838197	05:13:39.270	-68:38:19.70	257.02	10.85	12.46	13.51	12.69	11.069	0.842147	9.0818	0.256994
05170539-6838148	05:17:05.390	-68:38:14.80	275.68	8.45	12.12	13.22	12.58				
05172271-6840057	05:17:22.710	-68:40:05.70	262.22	5.65	12.66	13.66	12.89	9.564	0.715221	7.6728	-0.207976
05203803-6836469	05:20:38.030	-68:36:46.90	268.9	7.11	12.77	13.91	13.05				
05192974-6840158	05:19:29.740	-68:40:15.80	260.82	6.69	11.1	12.3	11.46				
05163079-6845164	05:16:30.790	-68:45:16.40	296.61	6.69	12.49	13.56	12.73	9.541	0.752506	7.5682	-0.242494
05200581-6840015	05:20:05.810	-68:40:01.50	278.05	7.24	12.37	13.47	12.63	10.381	1.013788	8.3506	0.015698
05180461-6846533	05:18:04.610	-68:46:53.30	259.32	7.12	11.81	12.65	12	10.223	0.6571	7.9238	-0.125146
05191475-6842523	05:19:14.750	-68:42:52.30	229.43	6.32	12.42	13.45	12.68	9.969	1.044002	7.9626	-0.112342

Table E.1: Full sample of LMC stars, continued

ID[a]	α(J2000)[a]	δ(J2000)[a]	HRV	error	K_s^a	H^a	J^a	ΣEW (Å)	error	W' (Å)	[Fe/H](dex)[b]
05175662-6844494	05:17:56.620	-68:44:49.40	287.34	6.22	12.79	13.88	13.03	9.099	0.980661	7.2702	-0.340834
05383715-7005383	05:38:37.150	-70:05:38.30	256.5	6.37	11.1	12.32	11.43				
05310991-7006180	05:31:09.910	-70:06:18.00	241.46	6.34	11.88	12.79	12.1	10.168	0.48848	7.9024	-0.132208
05314440-7005498	05:31:44.400	-70:05:49.80	262.61	4.9	12.78	13.77	12.98	9.84	0.509079	8.0064	-0.097888
05403039-7009289	05:40:30.390	-70:09:28.90	288.68	5.81	11.51	12.66	11.83	9.395	0.739509	6.9518	-0.445906
05341420-7007324	05:34:14.200	-70:07:32.40	249.76	5.82	12.27	13.48	12.58	7.936	0.552588	5.8576	-0.806992
05332216-7007292	05:33:22.160	-70:07:29.20	246.82	5.25	12.83	13.77	13.02	9.585	0.495874	7.7754	-0.174118
05323921-7007340	05:32:39.210	-70:07:34.00	273.82	5.27	12.66	13.73	12.88	9.244	0.492831	7.3528	-0.313576
05350102-7009341	05:35:01.020	-70:09:34.10	257.47	5.27	11.43	12.28	11.63	8.002	0.412234	5.5204	-0.918268
05313083-7007041	05:31:30.830	-70:07:04.10	239.63	4.41	12.95	13.9	13.12	9.141	0.429345	7.389	-0.30163
05374495-7014176	05:37:44.950	-70:14:17.60	262.21	5.59	11.45	12.45	11.68	10.254	0.4878	7.782	-0.17194
05401755-7017152	05:40:17.550	-70:17:15.20	259.59	5.47	12.91	13.99	13.15	9.641	0.853344	7.8698	-0.142966
05354740-7013058	05:35:47.400	-70:13:05.80	242.7	4.7	12.25	13.3	12.48	9.67	0.564852	7.582	-0.23794
05364375-7014405	05:36:43.750	-70:14:40.50	249.05	5.74	12.85	13.86	13.05	10.137	0.714313	8.337	0.01121
05391620-7020142	05:39:16.200	-70:20:14.20	250.94	6.24	11.73	12.68	11.95	10.335	0.507587	7.9974	-0.100858
05405282-7022549	05:40:52.820	-70:22:54.90	282.88	6.72	11.81	12.87	12.09	9.856	0.782739	7.5568	-0.246256
05372744-7018023	05:37:27.440	-70:18:02.30	271.9	5.87	12.46	13.38	12.67	9.593	0.56256	7.6058	-0.230086
05364141-7018312	05:36:41.410	-70:18:31.20	261.24	5.6	12.41	13.49	12.66	9.236	0.55789	7.2248	-0.355816
05383950-7022250	05:38:39.500	-70:22:25.00	231.85	6.35	12.93	14.01	13.17	10.056	0.722549	8.2944	-0.002848
05401802-7026349	05:40:18.020	-70:26:34.90	258.11	5.68	12.52	13.63	12.76	9.615	0.791279	7.6566	-0.213322
05311018-7008437	05:31:10.180	-70:08:43.70	267.01	5.58	11.17	12.28	11.43	9.759	0.504598	7.1526	-0.379642

Table E.1: Full sample of LMC stars, continued

ID[a]	α(J2000)[a]	δ(J2000)[a]	HRV	error	K_s^a	H[a]	J[a]	ΣEW (Å)	error	W' (Å)	[Fe/H](dex)[b]
05353361-7018357	05:35:33.610	-70:18:35.70	265.01	4.75	12.72	13.76	12.94	9.088	0.556231	7.2256	-0.355552
05355800-7020328	05:35:58.000	-70:20:32.80	263.9	5.6	11.91	13.05	12.19	7.376	0.533414	5.1248	-1.048816
05375037-7025306	05:37:50.370	-70:25:30.60	287.67	5.65	11.21	12.44	11.54	8.28	0.541872	5.6928	-0.861376
05353431-7020538	05:35:34.310	-70:20:53.80	267.79	5.28	12.58	13.61	12.79	9.281	0.495589	7.3514	-0.314038
05344542-7017391	05:34:45.420	-70:17:39.10	263.89	5.71	11.8	12.95	12.09	9.174	0.482362	6.87	-0.4729
05340029-7017183	05:34:00.290	-70:17:18.30	290.92	5.17	12.7	13.79	12.96	9.761	0.506853	7.889	-0.13663
05360004-7024256	05:36:00.040	-70:24:25.60	232.22	5.31	12.48	13.54	12.71	10.006	0.578053	8.0284	-0.090628
05341107-7016270	05:34:11.070	-70:16:27.00	279.29	5.48	12.45	13.58	12.71	9.28	0.481443	7.288	-0.33496
05352472-7024161	05:35:24.720	-70:24:16.10	285.58	5.34	11.58	12.69	11.87	9.398	0.532233	6.9884	-0.433828
05383305-7034443	05:38:33.050	-70:34:44.30	284.72	5.13	12.63	13.6	12.83	7.236	0.400807	5.3304	-0.980968
05372174-7031421	05:37:21.740	-70:31:42.10	266.19	6.84	12.79	13.81	12.97	9.364	0.525742	7.5352	-0.253384
05330392-7019000	05:33:03.920	-70:19:00.00	275.01	5.36	11.76	12.95	12.07	7.866	0.476544	5.5428	-0.910876
05360543-7030314	05:36:05.430	-70:30:31.40	258.88	4.89	12.52	13.58	12.76	9.375	0.603279	7.4166	-0.292522
05333272-7021132	05:33:32.720	-70:21:13.20	241.29	4.76	12.1	12.99	12.33	6.236	0.34638	4.076	-1.39492
05305541-7013085	05:30:55.410	-70:13:08.50	300.91	4.61	12.5	13.51	12.71	8.735	0.431519	6.767	-0.50689
05301710-7008455	05:30:17.100	-70:08:45.50	307.56	6.74	11.22	12.41	11.51				
05304046-7008521	05:30:40.460	-70:08:52.10	267.18	5.21	12.69	13.78	12.97	9.523	0.525595	7.6462	-0.216754
05341245-7028458	05:34:12.450	-70:28:45.80	261.53	5.67	11.85	12.94	12.12	9.614	0.492176	7.334	-0.31978
05325099-7022101	05:32:50.990	-70:22:10.10	269.1	5.22	12.47	13.52	12.71	9.911	0.47695	7.9286	-0.123562
05312012-7015456	05:31:20.120	-70:15:45.60	251.32	13.69	12.94	13.85	13.19				
05312710-7018441	05:31:27.100	-70:18:44.10	214.38	4.72	11.85	12.98	12.12	7.637	0.522002	5.357	-0.97219

Table E.1: Full sample of LMC stars, continued

ID[a]	α(J2000)[a]	δ(J2000)[a]	HRV	error	K_s^a	H[a]	J[a]	ΣEW (Å)	error	W' (Å)	[Fe/H](dex)[b]
05364384-7048413	05:36:43.840	-70:48:41.30	250.69	5.23	12.44	13.36	12.65	10.155	0.567159	8.1582	-0.047794
05351328-7041126	05:35:13.280	-70:41:12.60	261.3	6.18	11.76	12.82	12.02	9.76	0.691499	7.4368	-0.285856
05360913-7045127	05:36:09.130	-70:45:12.70	255.23	5.23	12.76	13.84	12.97	9.591	0.542803	7.7478	-0.183226
05345721-7040537	05:34:57.210	-70:40:53.70	263.2	6.37	12.48	13.47	12.67	8.334	0.482076	6.3564	-0.642388
05315891-7020275	05:31:58.910	-70:20:27.50	186.78	4.16	12.27	13.33	12.51	8.977	0.477301	6.8986	-0.463462
05311868-7020267	05:31:18.680	-70:20:26.70	253.74	5.07	11.62	12.8	11.91	8.128	0.451719	5.7376	-0.846592
05332446-7033014	05:33:24.460	-70:33:01.40	261.58	5.72	11.98	13.08	12.26	8.346	0.45637	6.1284	-0.717628
05352207-7048461	05:35:22.070	-70:48:46.10	273.15	5.11	12.4	13.48	12.64	8.366	0.527266	6.35	-0.6445
05344563-7046020	05:34:45.630	-70:46:02.00	207.55	4.18	12.98	13.9	13.14	8.007	0.527243	6.2694	-0.671098
05333902-7039461	05:33:39.020	-70:39:46.10	243.69	5.17	12.83	13.82	13.05	9.536	0.546068	7.7264	-0.190288
05350477-7053447	05:35:04.770	-70:53:44.70	269.53	5.63	12.61	13.67	12.84	9.481	0.651682	7.5658	-0.243286
05333979-7044095	05:33:39.790	-70:44:09.50	258.35	5.61	12.14	13.15	12.36	9.339	0.482405	7.1982	-0.364594
05305303-7014211	05:30:53.030	-70:14:21.10	287.34	5.31	12.4	13.49	12.64	9.018	0.480344	7.002	-0.42934
05314421-7027360	05:31:44.210	-70:27:36.00	222.83	4.59	12.91	13.95	13.14	9.016	0.627523	7.2448	-0.349216
05312625-7027015	05:31:26.250	-70:27:01.50	262.16	4.79	12.5	13.55	12.72	9.763	0.562346	7.795	-0.16765
05330007-7047331	05:33:00.070	-70:47:33.10	334.26	5.33	12.57	13.61	12.76	8.704	0.519055	6.7696	-0.506032
05323716-7047385	05:32:37.160	-70:47:38.50	270.69	13.96	11.21	12.38	11.54				
05305706-7025239	05:30:57.060	-70:25:23.90	277.23	7.62	11.26	12.43	11.59				
05315490-7042313	05:31:54.900	-70:42:31.30	223.78	4.57	12.65	13.66	12.88	8.721	0.567856	6.825	-0.48775
05312234-7035372	05:31:22.340	-70:35:37.20	256.5	5.49	12.45	13.46	12.68	9.798	0.576706	7.806	-0.16402
05301139-7022266	05:30:11.390	-70:22:26.60	209.89	4.6	12.53	13.58	12.8	9.694	0.571864	7.7404	-0.185668

Table E.1: Full sample of LMC stars, continued

ID[a]	α(J2000)[a]	δ(J2000)[a]	HRV	error	K_s^a	H[a]	J[a]	ΣEW (Å)	error	W' (Å)	[Fe/H](dex)[b]
05310584-7031269	05:31:05.840	-70:31:26.90	250.98	5.05	12.65	13.65	12.86	9.445	0.468348	7.549	-0.24883
05312015-7045159	05:31:20.150	-70:45:15.90	253.63	5.76	12.54	13.57	12.76	9.356	0.560004	7.4072	-0.295624
05312718-7051012	05:31:27.180	-70:51:01.20	251.72	5.15	12.74	13.78	12.95	9.28	0.638405	7.4272	-0.289024
05301672-7028011	05:30:16.720	-70:28:01.10	248.66	5.96	11.15	12.31	11.48				
05304038-7049072	05:30:40.380	-70:49:07.20	226.27	4.12	12.82	13.82	13.04	9.23	0.49793	7.4156	-0.292852
05304045-7025514	05:30:40.450	-70:25:51.40	244.02	4.82	12.78	13.77	12.98	9.484	0.668216	7.6504	-0.215368
05302513-7040457	05:30:25.130	-70:40:45.70	261.42	5.48	12.65	13.59	12.85	9.47	0.43492	7.574	-0.24058
05300994-7029171	05:30:09.940	-70:29:17.10	228.37	5.01	11.82	12.72	12.04	10.128	0.486042	7.8336	-0.154912
05295637-7021170	05:29:56.370	-70:21:17.00	238.07	4.88	12.28	13.38	12.53	9.676	0.566094	7.6024	-0.231208
05293169-7037580	05:29:31.690	-70:37:58.00	245.47	5.11	11.71	12.8	11.97	9.466	0.521296	7.1188	-0.390796
05290928-7039512	05:29:09.280	-70:39:51.20	195.51	6.83	11.19	12.4	11.56	7.454	0.633257	4.8572	-1.137124
05293548-7048217	05:29:35.480	-70:48:21.70	251.17	4.22	12.72	13.7	12.92	7.684	0.414923	5.8216	-0.818872
05290527-7042002	05:29:05.270	-70:42:00.20	229.21	4.89	12.79	13.8	13	8.476	0.559805	6.6472	-0.546424
05284520-7055364	05:28:45.200	-70:55:36.40	257.67	4.52	12.81	13.84	13.04	9.507	0.635942	7.6878	-0.203026
05291172-7032265	05:29:11.720	-70:32:26.50	283.49	18.91	10.91	12.16	11.29				
05283203-7056081	05:28:32.030	-70:56:08.10	256.96	5.54	12.77	13.81	13.03	8.672	0.685137	6.8336	-0.484912
05294214-7010197	05:29:42.140	-70:10:19.70	239.12	4.7	12.72	13.75	12.93	8.88	0.499453	7.0176	-0.424192
05290562-7006253	05:29:05.620	-70:06:25.30	243.83	5.73	11.18	12.34	11.48	7.724	0.575048	5.1224	-1.049608
05281835-7046298	05:28:18.350	-70:46:29.80	234.51	19.8	10.94	13.37	12.04				
05273986-7050542	05:27:39.860	-70:50:54.20	222.4	5.43	12.51	13.56	12.72	9.009	0.536616	7.0458	-0.414886
05271996-7057033	05:27:19.960	-70:57:03.30	223.55	6.75	11.45	12.57	11.73	7.638	0.909746	5.166	-1.03522

Table E.1: Full sample of LMC stars, continued

ID[a]	α(J2000)[a]	δ(J2000)[a]	HRV	error	K_s^a	H[a]	J[a]	ΣEW (Å)	error	W' (Å)	[Fe/H](dex)[b]
05273635-7046228	05:27:36.350	-70:46:22.80	265.35	5.49	12.98	13.96	13.17	8.854	0.485965	7.1164	-0.391588
05292724-7012340	05:29:27.240	-70:12:34.00	264.02	7.41	11.31	12.46	11.57				
05281085-7032178	05:28:10.850	-70:32:17.80	234.67	5.28	12.38	13.41	12.59	9.706	0.45617	7.6804	-0.205468
05283743-7019294	05:28:37.430	-70:19:29.40	255.93	5.37	11.74	12.86	12.02	8.705	0.467615	6.3722	-0.637174
05260891-7053208	05:26:08.910	-70:53:20.80	302.36	5.66	11.41	12.53	11.67	7.932	0.454193	5.4408	-0.944536
05272007-7035290	05:27:20.070	-70:35:29.00	280.9	5.44	12.54	13.56	12.76	9.052	0.452596	7.1032	-0.395944
05273464-7034287	05:27:34.640	-70:34:28.70	279.09	6.12	12.1	13.09	12.3	9.591	0.400312	7.431	-0.28777
05261415-7046378	05:26:14.150	-70:46:37.80	268.98	5.45	11.57	12.64	11.87	7.297	0.42858	4.8826	-1.128742
05284148-7017257	05:28:41.480	-70:17:25.70	214.12	5.54	11.58	12.71	11.85	8.799	0.526666	6.3894	-0.631498
05255420-7046411	05:25:54.200	-70:46:41.10	233.13	5.03	12.55	13.61	12.79	9.915	0.605898	7.971	-0.10957
05264037-7038005	05:26:40.370	-70:38:00.50	249.89	5.67	12.58	13.58	12.77	9.07	0.418777	7.1404	-0.383668
05275402-7024370	05:27:54.020	-70:24:37.00	258.44	6.26	11.2	12.38	11.52				
05255674-7041405	05:25:56.740	-70:41:40.50	267.92	5.47	12.96	13.98	13.19	9.417	0.864125	7.6698	-0.208966
05285226-7012050	05:28:52.260	-70:12:05.00	268.53	4.81	12.66	13.63	12.86	8.103	0.39863	6.2118	-0.690106
05292936-7008172	05:29:29.360	-70:08:17.20	229.37	5	11.5	12.66	11.79	9.12	0.542043	6.672	-0.53824
05265757-7029213	05:26:57.570	-70:29:21.30	229.2	5.63	11.74	13.02	12.15	7.131	0.61518	4.7982	-1.156594
05243689-7047312	05:24:36.890	-70:47:31.20	246.29	5.3	11.33	12.38	11.54	10.22	0.503763	7.6904	-0.202168
05240589-7050375	05:24:05.890	-70:50:37.50	231.56	4.79	12.43	13.5	12.7	8.358	0.534237	6.3564	-0.642388
05250070-7042426	05:25:00.700	-70:42:42.60	247.21	5.16	11.6	12.71	11.86	9.272	0.521335	6.872	-0.47224
05283304-7013252	05:28:33.040	-70:13:25.20	273.84	4.92	12.38	13.46	12.65	8.4	0.425676	6.3744	-0.636448
05272621-7016366	05:27:26.210	-70:16:36.60	260.16	5.06	12.86	13.85	13.06	9.175	0.61991	7.3798	-0.304666

Table E.1: Full sample of LMC stars, continued

ID[a]	α(J2000)[a]	δ(J2000)[a]	HRV	error	K_s^a	H[a]	J[a]	ΣEW (Å)	error	W' (Å)	[Fe/H](dex)[b]
05262471-7024445	05:26:24.710	-70:24:44.50	262.34	6.26	12.24	13.34	12.5	9.639	0.515603	7.5462	-0.249754
05280704-7011046	05:28:07.040	-70:11:04.60	259.96	5.26	11.11	12.3	11.42	9.083	0.587882	6.4478	-0.612226
05245007-7032231	05:24:50.070	-70:32:23.10	245.7	7.58	11.09	12.31	11.45				
05270128-7018356	05:27:01.280	-70:18:35.60	278.74	5.53	12.62	13.67	12.89	9.202	0.539505	7.2916	-0.333772
05251137-7027224	05:25:11.370	-70:27:22.40	307.44	4.69	12.46	13.4	12.62	6.953	0.62937	4.9658	-1.101286
05253743-7023239	05:25:37.430	-70:23:23.90	283.36	4.73	12.58	13.62	12.8	9.316	0.796715	7.3864	-0.302488
05262564-7018439	05:26:25.640	-70:18:43.90	272.84	6.53	11.3	12.47	11.63	7.1	0.567115	4.556	-1.23652
05280295-7013083	05:28:02.950	-70:13:08.30	268.64	6.09	11.03	12.18	11.35	9.413	0.625743	6.7394	-0.515998
05230208-7033592	05:23:02.080	-70:33:59.20	202.58	5.09	12.62	13.66	12.84	9.989	0.745946	8.0786	-0.074062
05215151-7038108	05:21:51.510	-70:38:10.80	286.45	5.22	12.92	13.89	13.1	9.295	0.907946	7.5286	-0.255562
05241816-7027352	05:24:18.160	-70:27:35.20	241.76	5.38	12.35	13.39	12.58	9.495	0.621509	7.455	-0.27985
05272459-7014291	05:27:24.590	-70:14:29.10	249.86	9.66	11.25	12.49	11.63				
05230824-7028507	05:23:08.240	-70:28:50.70	295.94	5.66	12.83	13.87	13.05	9.778	0.625241	7.9684	-0.110428
05270543-7015075	05:27:05.430	-70:15:07.50	289.39	13.5	10.8	12.1	11.24				
05230476-7027008	05:23:04.760	-70:27:00.80	269.25	5.33	12.69	13.79	12.94	9.9	0.611966	8.0232	-0.092344
05210166-7032218	05:21:01.660	-70:32:21.80	292.89	5.05	12.57	13.55	12.76	9.346	0.493649	7.4116	-0.294172
05222459-7027527	05:22:24.590	-70:27:52.70	239.41	5.54	12.84	13.87	13.05	9.527	0.57699	7.7222	-0.191674
05284225-7008186	05:28:42.250	-70:08:18.60	258.37	5.87	12.76	13.65	12.95	10.326	0.591693	8.4828	0.059324
05271122-7014030	05:27:11.220	-70:14:03.00	316.33	4.35	12.85	13.68	12.98	6.932	0.410805	5.132	-1.04644
05203789-7028280	05:20:37.890	-70:28:28.00	271.95	5.97	12.85	13.82	13.04	8.887	0.895237	7.087	-0.40129
05235932-7020280	05:23:59.320	-70:20:28.00	268.09	6.29	11.56	12.67	11.87	7.395	0.571812	4.9758	-1.097986

Table E.1: Full sample of LMC stars, continued

ID[a]	α(J2000)[a]	δ(J2000)[a]	HRV	error	K_s^a	H[a]	J[a]	ΣEW (Å)	error	W' (Å)	[Fe/H](dex)[b]
05211873-7025076	05:21:18.730	-70:25:07.60	260.43	5.3	12.32	13.37	12.55	9.584	0.577403	7.5296	-0.255232
05284907-7004486	05:28:49.070	-70:04:48.60	240.94	5.09	12.34	13.38	12.56	9.184	0.492517	7.1392	-0.384064
05201020-7025279	05:20:10.200	-70:25:27.90	286.24	5.81	12.11	13.18	12.33	9.816	0.618085	7.6608	-0.211936
05272155-7010485	05:27:21.550	-70:10:48.50	291.73	6.68	11.97	13.05	12.23	9.87	0.546799	7.6476	-0.216292
05265195-7011078	05:26:51.950	-70:11:07.80	249.74	5.23	11.48	12.65	11.79	8.751	0.515219	6.2934	-0.663178
05230627-7017337	05:23:06.270	-70:17:33.70	240.73	5.42	12.14	13.23	12.38	9.106	0.627874	6.9652	-0.441484
05220852-7018149	05:22:08.520	-70:18:14.90	212.93	5.18	12.4	13.51	12.66	9.037	0.505891	7.021	-0.42307
05292437-7001462	05:29:24.370	-70:01:46.20	233.44	5.39	12.07	13.17	12.32	8.747	0.533451	6.5726	-0.571042
05234788-7015272	05:23:47.880	-70:15:27.20	254.46	4.5	12.66	13.79	12.96	8.081	0.511709	6.1898	-0.697366
05225725-7015386	05:22:57.250	-70:15:38.60	225.84	4.9	12.67	13.66	12.88	9.595	0.571015	7.7086	-0.196162
05244616-7012528	05:24:46.160	-70:12:52.80	233.48	5.52	12.66	13.69	12.88	9.285	0.477445	7.3938	-0.300046
05203162-7016287	05:20:31.620	-70:16:28.70	241.48	6.22	11.67	12.82	11.94				
05234394-7012382	05:23:43.940	-70:12:38.20	260.99	6.09	11.66	12.67	11.9	10.232	0.492728	7.8608	-0.145936
05221203-7011445	05:22:12.030	-70:11:44.50	223.81	6.55	11.81	13.05	12.18	8.657	0.858464	6.3578	-0.641926
05284089-7004218	05:28:40.890	-70:04:21.80	250.84	6.47	12.44	13.52	12.67	9.295	0.577417	7.2982	-0.331594
05261210-7007422	05:26:12.100	-70:07:42.20	232.84	4.91	11.94	13.05	12.2	8.135	0.505413	5.8982	-0.793594
05183662-7012301	05:18:36.620	-70:12:30.10	268.47	9.39	11.3	12.48	11.62				
05192192-7011080	05:19:21.920	-70:11:08.00	244.45	4.6	12.84	14.1	13.16	8.967	0.840605	7.1622	-0.376474
05215509-7009288	05:21:55.090	-70:09:28.80	198.02	4.63	11.83	12.94	12.13	8.483	0.481873	6.1934	-0.696178
05241317-7007279	05:24:13.170	-70:07:27.90	245.24	6.25	11.99	12.93	12.19	10.253	0.499035	8.0402	-0.086734
05234615-7006012	05:23:46.150	-70:06:01.20	246.18	5.36	12.5	13.56	12.74	9.342	0.568003	7.374	-0.30658

Table E.1: Full sample of LMC stars, continued

ID[a]	α(J2000)[a]	δ(J2000)[a]	HRV	error	K_s^a	H[a]	J[a]	ΣEW (Å)	error	W' (Å)	[Fe/H](dex)[b]
05192342-7005540	05:19:23.420	-70:05:54.00	254.19	9.01	10.91	12.1	11.27				
05225965-7005055	05:22:59.650	-70:05:05.50	268.29	5.56	11.97	13.09	12.25	9.524	0.551698	7.3016	-0.330472
05181978-7002594	05:18:19.780	-70:02:59.40	258.78	5.75	12.23	13.29	12.48	9.284	0.551142	7.1864	-0.368488
05194159-7002349	05:19:41.590	-70:02:34.90	293.97	3.83	12.97	13.77	13.16	5.963	0.424802	4.2206	-1.347202
05270906-7004447	05:27:09.060	-70:04:44.70	257.65	5.61	12.9	13.95	13.14	9.449	0.575929	7.673	-0.20791
05232604-7002486	05:23:26.040	-70:02:48.60	292.97	5.69	11.64	12.81	11.96	8.648	0.507257	6.2672	-0.671824
05225286-7001594	05:22:52.860	-70:01:59.40	275.41	7.21	11.25	12.42	11.6	8.838	0.681271	6.27	-0.6709
05220581-7000527	05:22:05.810	-70:00:52.70	262.49	6.67	12.19	13.36	12.48	9.24	0.591146	7.1232	-0.389344
05195960-6959011	05:19:59.600	-69:59:01.10	228.03	5.43	12.9	13.91	13.11	9.37	0.68853	7.594	-0.23398
05185636-6957131	05:18:56.360	-69:57:13.10	241.7	4.41	12.62	13.66	12.89	9.372	0.60377	7.4616	-0.277672
05252346-7002548	05:25:23.460	-70:02:54.80	277.19	5.36	11.67	12.77	11.95	8.616	0.487334	6.2496	-0.677632
05252967-7001490	05:25:29.670	-70:01:49.00	286.02	6.5	11.24	12.39	11.52				
05212739-6957169	05:21:27.390	-69:57:16.90	269.6	3.7	12.76	13.57	12.93	5.272	0.403046	3.4288	-1.608496
05252531-7000597	05:25:25.310	-70:00:59.70	255.6	5.86	12.28	13.27	12.5	8.896	0.461204	6.8224	-0.488608
05234396-6958416	05:23:43.960	-69:58:41.60	257.38	5.93	11.49	12.59	11.76	9.683	0.527277	7.2302	-0.354034
05200948-6953068	05:20:09.480	-69:53:06.80	247.33	5.16	12.43	13.5	12.66	9.002	0.537272	7.0004	-0.429868
05252509-6959375	05:25:25.090	-69:59:37.50	248.69	5.5	12.81	13.55	12.93	9.085	0.478579	7.2658	-0.342286
05200890-6951420	05:20:08.900	-69:51:42.00	218.04	5.68	11.34	12.5	11.62	9.06	0.556953	6.5352	-0.583384
05204966-6951575	05:20:49.660	-69:51:57.50	243.51	5.97	11.81	12.96	12.08	9.457	0.546301	7.1578	-0.377926
05202375-6950267	05:20:23.750	-69:50:26.70	265.42	5.94	11.49	12.66	11.78	8.437	0.572708	5.9842	-0.765214
05222712-6953011	05:22:27.120	-69:53:01.10	247.36	7	11.66	12.93	12.01				

Table E.1: Full sample of LMC stars, continued

ID[a]	α(J2000)[a]	δ(J2000)[a]	HRV	error	K_s^a	H^a	J^a	ΣEW (Å)	error	W' (Å)	[Fe/H](dex)[b]
05231665-6953203	05:23:16.650	-69:53:20.30	235.1	4.53	12.66	13.73	12.89	8.746	0.574137	6.8548	-0.477916
05291854-7004217	05:29:18.540	-70:04:21.70	229.16	11.1	11.17	12.4	11.5				
05202022-6946071	05:20:20.220	-69:46:07.10	287.82	9.42	11.24	12.48	11.56				
05213063-6948065	05:21:30.630	-69:48:06.50	205.92	8.57	11.13	12.31	11.43				
05272406-7001237	05:27:24.060	-70:01:23.70	233.2	5.98	12.98	14.11	13.23	8.694	0.640483	6.9564	-0.444388
05200670-6942355	05:20:06.700	-69:42:35.50	292.29	5.65	12.56	13.57	12.78	8.763	0.487226	6.8238	-0.488146
05234477-6950587	05:23:44.770	-69:50:58.70	297.98	5.47	12.75	13.68	12.93	8.073	0.453137	6.225	-0.68575
05240897-6951120	05:24:08.970	-69:51:12.00	245.53	5.34	12.79	13.76	13	7.256	0.448524	5.4272	-0.949024
05212471-6943169	05:21:24.710	-69:43:16.90	258.94	5.01	12.59	13.53	12.76	9.481	0.600332	7.5562	-0.246454
05194570-6937213	05:19:45.700	-69:37:21.30	223.73	5.65	12.19	13.22	12.38	8.673	0.487401	6.5562	-0.576454
05221674-6944335	05:22:16.740	-69:44:33.50	263.23	5.25	12.96	13.94	13.18	9.297	0.831171	7.5498	-0.248566
05243875-6950390	05:24:38.750	-69:50:39.00	202.49	4.78	11.22	12.35	11.53	8.76	0.541536	6.1776	-0.701392
05243498-6949203	05:24:34.980	-69:49:20.30	258.3	5.36	12.2	13.31	12.46	8.459	0.41207	6.347	-0.64549
05214345-6938590	05:21:43.450	-69:38:59.00	271.92	9.42	10.99	12.17	11.33				
05284564-7001549	05:28:45.640	-70:01:54.90	265.15	4.78	11.62	12.81	11.93				
05201720-6931496	05:20:17.200	-69:31:49.60	260.03	5.67	11.48	12.52	11.76	10.017	0.608356	7.5594	-0.245398
05215084-6936302	05:21:50.840	-69:36:30.20	273.98	6.58	11.62	12.39	11.76	10.768	0.468523	8.3776	0.024608
05251274-6949038	05:25:12.740	-69:49:03.80	217.19	5.48	11.2	12.35	11.51				
05255859-6951101	05:25:58.590	-69:51:10.10	265.41	6.78	11.06	11.99	11.24	11.299	0.55416	8.6398	0.111134
05270067-6954406	05:27:00.670	-69:54:40.60	269.22	6.35	11.3	12.47	11.59				
05281159-6958594	05:28:11.590	-69:58:59.40	203.21	5.09	12.69	13.75	12.94	9.429	0.538669	7.5522	-0.247774

Table E.1: Full sample of LMC stars, continued

ID[a]	α(J2000)[a]	δ(J2000)[a]	HRV	error	K_s^a	H[a]	J[a]	ΣEW (Å)	error	W' (Å)	[Fe/H](dex)[b]
05242640-6939353	05:24:26.400	-69:39:35.30	272.95	5.83	12.25	13.35	12.51	9.751	0.519971	7.663	-0.21121
05240179-6938347	05:24:01.790	-69:38:34.70	284.12	14.77	11.09	12.46	11.48				
05232217-6934187	05:23:22.170	-69:34:18.70	256.73	5.07	12.4	13.46	12.64	9.172	0.482038	7.156	-0.37852
05263090-6948262	05:26:30.900	-69:48:26.20	240.16	5.08	12.6	13.57	12.81	9.054	0.456361	7.134	-0.38578
05254194-6943281	05:25:41.940	-69:43:28.10	257.69	6.48	12.57	13.6	12.79	9.759	0.482165	7.8246	-0.157882
05271836-6951466	05:27:18.360	-69:51:46.60	257.54	5.6	11.47	12.57	11.73	9.525	0.544334	7.0626	-0.409342
05243144-6935046	05:24:31.440	-69:35:04.60	274.73	7.06	12.28	13.26	12.51	9.543	0.493831	7.4694	-0.275098
05241061-6930495	05:24:10.610	-69:30:49.50	181.04	4.33	12.81	13.83	13.04	9.238	0.640757	7.4188	-0.291796
05271269-6949083	05:27:12.690	-69:49:08.30	250.56	6.32	11.45	12.36	11.67	10.425	0.55903	7.953	-0.11551
05270699-6947158	05:27:06.990	-69:47:15.80	201.18	8.64	11.22	12.42	11.57				
05272369-6948300	05:27:23.690	-69:48:30.00	240.75	5.71	11.07	12.2	11.36	9.398	0.605599	6.7436	-0.514612
05280020-6952312	05:28:00.200	-69:52:31.20	236.75	6.46	12.26	13.26	12.46	9.834	0.523242	7.7508	-0.182236
05240990-6919480	05:24:09.900	-69:19:48.00	264.76	8.13	11.23	12.69	11.67				
05262585-6938181	05:26:25.850	-69:38:18.10	266.94	5.56	12.37	13.42	12.6	9.432	0.527049	7.4016	-0.297472
05252760-6923440	05:25:27.600	-69:23:44.00	268.35	6.7	11.35	12.47	11.65	6.185	0.445042	3.665	-1.53055
05271265-6938530	05:27:12.650	-69:38:53.00	235.97	5.59	12.48	13.47	12.68	9.519	0.519289	7.5414	-0.251338
05272914-6940339	05:27:29.140	-69:40:33.90	242.76	8.18	11.53	12.53	11.79	9.472	0.775237	7.0384	-0.417328
05281074-6946138	05:28:10.740	-69:46:13.80	233.26	4.92	12.52	13.6	12.77	9.698	0.47212	7.7396	-0.185932
05251702-6909025	05:25:17.020	-69:09:02.50	255.82	8.48	11.39	12.64	11.74				
05265162-6926358	05:26:51.620	-69:26:35.80	263.6	5.79	11.58	12.68	11.82	8.333	0.466705	5.9234	-0.785278
05272612-6932390	05:27:26.120	-69:32:39.00	253.34	6.3	12.11	13.23	12.39	9.625	0.556602	7.4698	-0.274966

Table E.1: Full sample of LMC stars, continued

ID[a]	α(J2000)[a]	δ(J2000)[a]	HRV	error	K_s^a	H[a]	J[a]	ΣEW (Å)	error	W' (Å)	[Fe/H](dex)[b]
05281613-6943489	05:28:16.130	-69:43:48.90	265.26	6.44	11.57	12.39	11.77	11.318	0.402076	8.9036	0.198188
05272161-6928362	05:27:21.610	-69:28:36.20	293.04	5.5	12.31	13.41	12.57	9.461	0.590474	7.4018	-0.297406
05275378-6934484	05:27:53.780	-69:34:48.40	240.16	5.36	12.27	13.38	12.55	8.84	0.570801	6.7616	-0.508672
05264685-6910203	05:26:46.850	-69:10:20.30	245.89	5.81	11.31	12.45	11.57	8.379	0.499371	5.8398	-0.812866
05282121-6939325	05:28:21.210	-69:39:32.50	252.63	5.64	12.88	13.94	13.1	9.04	0.489813	7.2544	-0.346048
05275629-6927311	05:27:56.290	-69:27:31.10	278.87	6.51	12.29	13.3	12.49	9.967	0.48421	7.8982	-0.133594
05284289-6946113	05:28:42.890	-69:46:11.30	234.86	5.65	11.58	12.68	11.86	9.307	0.476614	6.8974	-0.463858
05291009-6951480	05:29:10.090	-69:51:48.00	279.34	6.02	12.19	13.34	12.45	9.145	0.466095	7.0282	-0.420694
05283341-6931476	05:28:33.410	-69:31:47.60	241.28	5.38	11.52	12.64	11.78	9.31	0.475673	6.8716	-0.472372
05275447-6907000	05:27:54.470	-69:07:00.00	289.02	6.74	11.61	12.8	11.91	7.632	0.580904	5.2368	-1.011856
05282382-6922314	05:28:23.820	-69:22:31.40	273.36	6.01	12.58	13.66	12.86	9.566	0.563469	7.6364	-0.219988
05294179-6956034	05:29:41.790	-69:56:03.40	269.65	6.06	12.32	13.42	12.58	9.855	0.549099	7.8006	-0.165802
05291374-6946495	05:29:13.740	-69:46:49.50	276.38	6.1	11.82	12.82	12.06	10.898	0.627797	8.6036	0.099188
05284702-6910444	05:28:47.020	-69:10:44.40	250.15	4.92	11.71	12.81	12.03				
05293433-6948094	05:29:34.330	-69:48:09.40	260.55	5.56	12.28	13.41	12.54	9.784	0.538202	7.7104	-0.195568
05291309-6917361	05:29:13.090	-69:17:36.10	275.74	4.97	12.55	13.53	12.74	8.732	0.593977	6.788	-0.49996
05292777-6932123	05:29:27.770	-69:32:12.30	313.82	7.22	12.46	13.5	12.66	8.893	0.489254	6.9058	-0.461086
05293697-6938179	05:29:36.970	-69:38:17.90	221.76	4.33	12.94	13.94	13.15	8.921	0.486013	7.1642	-0.375814
05295730-6918210	05:29:57.300	-69:18:21.00	269.73	5.64	12.06	13.14	12.29	9.126	0.485737	6.9468	-0.447556
05293748-6950506	05:29:37.480	-69:50:50.60	239.25	6.33	11.61	12.54	11.82	10.334	0.482663	7.9388	-0.120196
05301079-6908236	05:30:10.790	-69:08:23.60	287.92	5.78	12.52	13.57	12.76	9.571	0.600522	7.6126	-0.227842

Table E.1: Full sample of LMC stars, continued

ID[a]	α(J2000)[a]	δ(J2000)[a]	HRV	error	K_s^a	H[a]	J[a]	ΣEW (Å)	error	W' (Å)	[Fe/H](dex)[b]
05295244-6940599	05:29:52.440	-69:40:59.90	295.28	7.2	11.33	12.59	11.66				
05300840-6947534	05:30:08.400	-69:47:53.40	223.84	9.83	11.25	12.45	11.56				
05303870-6905439	05:30:38.700	-69:05:43.90	266.76	6.54	12.56	13.66	12.81	9.804	0.611543	7.8648	-0.144616
05293652-7003138	05:29:36.520	-70:03:13.80	236.25	5	12.66	13.69	12.89	9.192	0.471878	7.3008	-0.330736
05301603-6942556	05:30:16.030	-69:42:55.60	246.97	4.76	12.22	13.3	12.48	9.479	0.453925	7.3766	-0.305722
05310654-6911452	05:31:06.540	-69:11:45.20	290.74	7.48	11.66	13.11	12.07				
05314338-6906595	05:31:43.380	-69:06:59.50	248.81	5.93	12	13.07	12.25	7.006	0.471892	4.798	-1.15666
05305277-6942150	05:30:52.770	-69:42:15.00	267.44	6.05	11.59	12.79	11.92	7.706	0.501337	5.3012	-0.990604
05320289-6918589	05:32:02.890	-69:18:58.90	297.75	6.18	12.55	13.61	12.76	9.6	1.097359	7.656	-0.21352
05320293-6922148	05:32:02.930	-69:22:14.80	277.25	6.36	12.46	13.26	12.64	9.497	0.421621	7.5098	-0.261766
05313901-6934169	05:31:39.010	-69:34:16.90	344.7	6.95	12.83	13.83	12.99	8.762	0.481047	6.9524	-0.445708
05330083-6908525	05:33:00.830	-69:08:52.50	277.34	7.03	12.5	13.71	12.82	9.71	1.002694	7.742	-0.18514
05310058-6947554	05:31:00.580	-69:47:55.40	273.83	6.14	12.78	13.59	12.94	9.491	0.533024	7.6574	-0.213058
05324002-6924335	05:32:40.020	-69:24:33.50	346.56	6.83	12.29	13.36	12.54	9.36	0.533439	7.2912	-0.333904
05314791-6938533	05:31:47.910	-69:38:53.30	269.82	5.41	12.85	13.82	13.03	8.585	0.614008	6.785	-0.50095
05333061-6918221	05:33:30.610	-69:18:22.10	252.1	5.18	11.72	12.86	12.01	8.345	0.524758	6.0026	-0.759142
05304730-6952068	05:30:47.300	-69:52:06.80	240.4	6.56	10.88	12.04	11.22				
05321228-6938164	05:32:12.280	-69:38:16.40	261.5	5.84	11.27	12.38	11.53	10.121	0.480689	7.5626	-0.244342
05325564-6931160	05:32:55.640	-69:31:16.00	265.36	5.96	12.77	13.55	12.94	9.714	0.480077	7.8756	-0.141052
05304702-6956154	05:30:47.020	-69:56:15.40	271.63	5.97	12.37	13.41	12.59	9.538	0.51937	7.5076	-0.262492
05333487-6927564	05:33:34.870	-69:27:56.40	297.14	6	12.56	13.59	12.76	8.666	0.468189	6.7268	-0.520156

Table E.1: Full sample of LMC stars, continued

ID[a]	α(J2000)[a]	δ(J2000)[a]	HRV	error	K_s^a	H^a	J^a	ΣEW (Å)	error	W' (Å)	[Fe/H](dex)[b]
05340815-6923101	05:34:08.150	-69:23:10.10	329.88	6.84	11.98	13.07	12.28	8.492	0.614199	6.2744	-0.669448
05340454-6925017	05:34:04.540	-69:25:01.70	321.26	6.27	12.2	13.25	12.46	8.391	0.531363	6.279	-0.66793
05312161-6951535	05:31:21.610	-69:51:53.50	237.07	6.13	11.53	12.73	11.85				
05322365-6946077	05:32:23.650	-69:46:07.70	258.9	5.4	12.74	13.83	12.97	9.167	0.552464	7.3142	-0.326314
05332851-6934493	05:33:28.510	-69:34:49.30	272.86	6.32	12.53	13.74	12.82	9.914	0.653	7.9604	-0.113068
05302871-6959545	05:30:28.710	-69:59:54.50	248.12	5.34	11.38	12.51	11.66	9.751	0.497177	7.2454	-0.349018
05342735-6929339	05:34:27.350	-69:29:33.90	247.31	5.68	12.23	13.35	12.5	9.207	0.502169	7.1094	-0.393898
05325208-6942372	05:32:52.080	-69:42:37.20	252.57	5.27	12.38	13.48	12.64	9.502	0.604557	7.4764	-0.272788
05350154-6927470	05:35:01.540	-69:27:47.00	248.01	4.91	12.2	13.31	12.45	9.457	0.600911	7.345	-0.31615
05321892-6947466	05:32:18.920	-69:47:46.60	281.92	5.76	12	13.2	12.31	8.512	0.485466	6.304	-0.65968
05355973-6923042	05:35:59.730	-69:23:04.20	251.36	5.81	12.17	13.32	12.47	8.842	0.626817	6.7156	-0.523852
05364036-6919014	05:36:40.360	-69:19:01.40	262.33	5.77	12.5	13.72	12.83	8.663	0.798515	6.695	-0.53065
05334728-6939487	05:33:47.280	-69:39:48.70	269.13	5.32	11.21	12.4	11.52	7.469	0.547394	4.8818	-1.129006
05335301-6937592	05:33:53.010	-69:37:59.20	300.88	8.22	11.13	12.36	11.48				
05315787-6952525	05:31:57.870	-69:52:52.50	231.77	8.56	11.64	12.82	11.98	8.899	0.840779	6.5182	-0.588994
05312908-6957168	05:31:29.080	-69:57:16.80	255.53	5.6	12.56	13.62	12.82	9.669	0.563576	7.7298	-0.189166
05333411-6946312	05:33:34.110	-69:46:31.20	251.49	5.67	12.33	13.44	12.58	9.956	0.509362	7.9064	-0.130888
05303820-7000150	05:30:38.200	-70:00:15.00	199.79	4.54	12.28	13.35	12.52	9.32	0.434895	7.2464	-0.348688
05343825-6940421	05:34:38.250	-69:40:42.10	267.79	6.11	12.23	13.35	12.48	8.61	0.57436	6.5124	-0.590908
05314812-6952266	05:31:48.120	-69:52:26.60	256.73	5.1	12.26	13.36	12.5	8.954	0.505421	6.8708	-0.472636
05332843-6949563	05:33:28.430	-69:49:56.30	256.91	5.45	12.47	13.54	12.72	9.686	0.542569	7.7036	-0.197812

Table E.1: Full sample of LMC stars, continued

ID[a]	α(J2000)[a]	δ(J2000)[a]	HRV	error	K_s^a	H[a]	J[a]	ΣEW (Å)	error	W' (Å)	[Fe/H](dex)[b]
05331551-6949417	05:33:15.510	-69:49:41.70	260.31	8.75	11.12	12.28	11.42				
05345112-6944157	05:34:51.120	-69:44:15.70	216.48	6.11	11.52	12.69	11.84				
05354286-6939213	05:35:42.860	-69:39:21.30	256.47	5.56	12.35	13.5	12.62	9.374	0.519862	7.334	-0.31978
05383176-6929110	05:38:31.760	-69:29:11.00	270.71	5.93	12.23	13.23	12.49	10.034	0.515368	7.9364	-0.120988
05390958-6927506	05:39:09.580	-69:27:50.60	318.93	18.19	11.36	12.7	11.78				
05334880-6949374	05:33:48.800	-69:49:37.40	266.74	6.22	11.21	12.35	11.48	9.619	0.465129	7.0318	-0.419506
05344361-6947026	05:34:43.610	-69:47:02.60	251.67	6.16	12.57	13.69	12.86	9.546	0.69076	7.6116	-0.228172
05312729-7002559	05:31:27.290	-70:02:55.90	269.6	9.77	11.06	12.27	11.42				
05391265-6933402	05:39:12.650	-69:33:40.20	231.85	4.81	12.79	13.89	13.04	9.593	0.663086	7.7642	-0.177814
05360267-6947265	05:36:02.670	-69:47:26.50	252.31	6.32	11.34	12.53	11.65	7.232	0.577126	4.7072	-1.186624
05322043-7000419	05:32:20.430	-70:00:41.90	186.41	3.27	12.88	13.79	13.04	6.895	0.357873	5.1094	-1.053898
05371770-6944025	05:37:17.700	-69:44:02.50	225.32	7.02	12.72	14.04	13.06	10.608	0.855694	8.7456	0.146048
05372956-6945097	05:37:29.560	-69:45:09.70	265.91	4.27	12.87	13.79	13.05	8.179	0.491539	6.3886	-0.631762
05394001-6939094	05:39:40.010	-69:39:09.40	202.92	8.77	12.73	13.84	12.99				
05331980-6956437	05:33:19.800	-69:56:43.70	245.64	6.26	11.34	12.36	11.55	10.607	0.493677	8.0822	-0.072874
05392442-6941443	05:39:24.420	-69:41:44.30	243.84	5.75	12.73	13.77	12.96	9.726	0.572745	7.8684	-0.143428
05310696-7002467	05:31:06.960	-70:02:46.70	237.9	4.99	11.35	12.53	11.69				
05334592-6957155	05:33:45.920	-69:57:15.50	259.1	5.99	12.56	13.65	12.81	9.935	0.495263	7.9958	-0.101386
05355762-6952498	05:35:57.620	-69:52:49.80	268.28	5.62	11.42	12.54	11.69	10.15	0.521332	7.6636	-0.211012
05330947-6959448	05:33:09.470	-69:59:44.80	269.84	6.2	11.79	12.89	12.04	9.882	0.479944	7.5732	-0.240844
05344085-6955488	05:34:40.850	-69:55:48.80	229.39	4.59	12.3	13.39	12.56	8.599	0.4712	6.535	-0.58345

Table E.1: Full sample of LMC stars, continued

ID[a]	α(J2000)[a]	δ(J2000)[a]	HRV	error	K_s^a	H[a]	J[a]	ΣEW (Å)	error	W' (Å)	[Fe/H](dex)[b]
05334722-6957521	05:33:47.220	-69:57:52.10	254.04	5.71	12.5	13.65	12.78	9.946	0.54463	7.978	-0.10726
05384393-6949597	05:38:43.930	-69:49:59.70	264.95	4.89	12.5	13.73	12.81	9.148	0.688506	7.18	-0.3706
05411465-6946020	05:41:14.650	-69:46:02.00	182.2	5.86	12.78	14.31	13.18				
05373485-6954086	05:37:34.850	-69:54:08.60	277.77	6.16	12.19	13.38	12.48	10.484	0.8146	8.3672	0.021176
05334816-7000081	05:33:48.160	-70:00:08.10	286.33	12.57	12.58	13.68	12.82	10.275	0.614702	8.3454	0.013982
05394207-6952130	05:39:42.070	-69:52:13.00	286.14	7.04	11.99	13.17	12.32	7.492	0.664094	5.2792	-0.997864
05350079-6958575	05:35:00.790	-69:58:57.50	249.38	7.7	12.31	13.13	12.47	10.897	0.413757	8.8378	0.176474
05392165-6954208	05:39:21.650	-69:54:20.80	254.42	5.8	12.46	13.55	12.73	9.091	0.685749	7.1038	-0.395746
05403561-6954448	05:40:35.610	-69:54:44.80	205.93	6.67	11.04	12.18	11.37				
05372056-6958406	05:37:20.560	-69:58:40.60	253.42	5.67	12.41	13.51	12.66	9.807	0.617898	7.7958	-0.167386
05394700-6957257	05:39:47.000	-69:57:25.70	278.48	6.15	12.92	13.64	13.04	9.683	0.570089	7.9166	-0.127522
05344839-7002429	05:34:48.390	-70:02:42.90	255.28	8.58	11.35	12.55	11.68				
05354465-7002232	05:35:44.650	-70:02:23.20	257.54	5.47	12.46	13.58	12.74	9.335	0.6257	7.3478	-0.315226
05405391-6958564	05:40:53.910	-69:58:56.40	256.05	6.88	12.76	13.75	12.95	10.276	0.560766	8.4328	0.042824
05335559-7003496	05:33:55.590	-70:03:49.60	238.17	5.15	12.36	13.51	12.63	9.066	0.57797	7.0308	-0.419836
05410107-7000401	05:41:01.070	-70:00:40.10	282.66	8.67	12.88	13.96	13.12	9.615	0.860382	7.8294	-0.156298

Acronyms

ΛCDM	Λ cold dark matter.
AGB	asymptotic giant branch.
CMD	colour-magnitude diagram.
dE	dwarf elliptical.
dIrr	dwarf irregular.
DM	dark matter.
dSph	dwarf spheroidal.
GASS	Galactic anti-centre stellar structure.
GC	globular cluster.
HB	horizontal branch.
HVC	high velocity clouds.
IMF	initial mass function.
ISM	interstellar medium.
LG	Local Group.
LMC	Large Magellanic Cloud.
LPV	long period variables.
LTE	local thermodynamic equilibrium.
MCMC	Markov chain Monte Carlo.

MgS	Magellanic stream.
MLE	maximum likelihood estimation.
MS	main sequence.
MW	Milky Way.
OoI	Oosterhoff Type I.
OoII	Oosterhoff Type II.
OoIII	Oosterhoff Type III.
OoInt	Oosterhoff intermediate.
PNe	planetary nebulae.
RGB	red giant branch.
RSG	red super-giant.
SFH	star formation history.
SFR	star formation rate.
Sgr	Sagittarius.
SMC	Small Magellanic Cloud.
SNe	supernovae.
SNe Ia	supernovae Type Ia.
SNe II	supernovae Type II.
SNR	signal to noise ratio.
TO	main-sequence turnoff.
TRGB	tip of the red giant branch.

ZAHB zero-age horizontal branch.